INTERFACE CHARACTERIZATION AND MODELLING OF CEMENT COMPOSITE SYSTEMS

Thesis Submitted in Partial Fulfillment of the Requirements for the Degree of Doctor of Philosophy in Civil Engineering

by

Ping Xie

University of Ottawa

*The Ph.D. Program in Civil Engineering is a joint program with Carleton University, administrated by the Ottawa-Carleton Institute for Civil Engineering

National Library of Canada
Acquisitions and Bibliographic Services Branch
395 Wellington Street
Ottawa, Ontario
K1A 0N4

Bibliothèque nationale du Canada
Direction des acquisitions et des services bibliographiques
395, rue Wellington
Ottawa (Ontario)
K1A 0N4

Your file Votre référence

Our file Notre référence

ISBN 0-315-83849-3

Canada

UNIVERSITÉ D'OTTAWA
UNIVERSITY OF OTTAWA

ABSTRACT

A detailed review of cement paste-aggregate interface phenomena in concrete is presented as a precursor to identification of the specific problems addressed in the current interface investigation. The principal deficiencies with current interface investigations described in the literature are as follows: (i). a lack of effective and simple investigative methods to quantitatively characterize interfacial microstructure; (ii). no simple and effective method of interfacial modification.

A systematic electrical conductivity theory for the interface characterization of cement composites is proposed in this study. Based on the proposed theory, a novel investigative tool, **the electrical conductivity method**, has been developed. The proposed theory indicates that the characteristics of interfacial microstructure and interfacial zone formation and development can be described uniquely by a parameter, referred to as the "θ-parameter" or "interfacial excess conductance".

The developed method was successfully applied to practical cement paste-aggregate systems. Several new findings pertaining to the nature of the aggregate-cement paste interface were obtained. Extensive experimentation indicates that the θ-parameter is a powerful interfacial microstructural descriptor. It is also a useful parameter for characterizing chemical processes at interfaces in cement-aggregate systems.

A hypothesis for interfacial microstructure formation is proposed in concert with observed features of the θ-parameter. Electrical conductivity models of both the interfacial zone and the bulk paste are developed to formulate the hypothesis. The hypothesis stresses the significance of the water film on aggregates at mixing for the interfacial microstructure formation.

A relationship between interfacial bond strength and interfacial microstructure is developed. It was deduced that reducing the thickness of the water film and using low w/c ratio are two possible methods of enhancing interfacial bond strength.

A method of enhancing interfacial microstructure, i.e. coating aggregate surfaces with silica fume, was developed. The experiments indicated that the interfacial microstructure can be effectively densified by aggregate surface treatment. The consequence of interfacial densification is that compressive strength and sulphate resistance of mortar are increased; bending strength is however increased only at later hydration times.

A new tool, an a.c. impedance spectroscopy technique, has bee utilized recently to study hydrating cement systems. Its further application was however limited due to lack of a fundamental explanation of the a.c. impedance behavior of the hydrating cement systems. A theoretical model for a.c. impedance spectroscopy of hydrating cement systems was developed. A fundamental understanding of the a.c. impedance behavior of hydrating cement systems has been obtained through application of the proposed model, and the validity of the a.c. impedance technique in investigating hydrating cement systems has, therefore, been strongly enhanced.

The established link between interface phenomena and ingress of sulphate ions into cement mortar prompted a re-examination of durability related to sulphate expansion. Sulphate expansion is an important research topic dealing with durability of concrete. The mechanism of sulphate expansion, however, remains controversial. A thermodynamic theory of sulphate expansion is proposed after a careful analysis of the physico-chemical processes concerning the sulphate expansion. The theory is validated by extensive experiments. It appears that most sulphate expansion phenomena in the previous work can be explained by the proposed theory.

ACKNOWLEDGEMENTS

I would like to express my sincere gratitude to my thesis supervisor Dr. J.J. Beaudoin for his help, encouragement, advice and kindness throughout the course of this work. It was Dr. J.J. Beaudoin who gave me the opportunity to study at the University of Ottawa to pursue my degree and to continue my research in concrete science.

Special thanks are accorded to Professor Tang Mingshu, Nanjing Institute of Chemical Technology, P.R. China. It was Professor Tang Mingshu who kindled my interest in cement and concrete science and led me into this scientific field.

Thanks to Dr. Gu Ping and Dr. Xu Zhongzi for their wonderful cooperation in my research. Thanks are also due to the staff of the Materials Laboratory, Institute for Research in Construction, National Research Council of Canada, particularly Dr. P.E. Grattan-Bellew, Dr. R. Brousseau, B. Myers, W. Lei, E. Quinn, G. Chan and R. Lacroix with their assistance on the experimental apparatus.

DEDICATED TO MY WIFE LIXIN

CONTENTS

CHAPTER ONE

REVIEW OF INTERFACE PHENOMENA IN CEMENT PASTE-AGGREGATE SYSTEMS

SUMMARY

A detailed review is presented as a precursor to identification of the specific problems addressed in the current cement paste-aggregate interface investigation. It is apparent that the principal problem with current interface investigations described in the literature is a lack of effective and simple investigative methods to quantitatively characterize interfacial microstructure and transition zone formation and development. In addition, no simple and effective method of interfacial modification has been produced. The significance and objectives of this study are addressed.

§1.1 INTRODUCTION

Interface problems in concrete science and engineering have attracted attention since they were identified as having a significant influence on concrete behavior. There are several types of interfaces in hydrated cement composites: aggregate-cement paste, reinforcement-cement paste, fiber-cement paste, hydrated cement-unhydrated cement and

even cement hydrate-cement hydrate. Aggregate(both coarse and fine)-cement paste interface problems, however, appear to be most significant since aggregate and cement paste are the two most elementary components of concrete.

A detailed review of aggregate-cement paste interface phenomena is given in the following sections of this chapter. Emphasis is placed on problems associated with previous work. The significance and objectives of this work are also addressed.

It is noted that this review does not cover research dealing with alkali-aggregate reaction though aspects of this topic belong to the domain of aggregate-cement paste interface problems. Alkali-aggregate reaction is a specific discipline of concrete science dealing with characteristics of aggregate-cement paste interaction.

§1.2 AGGREGATE-CEMENT PASTE INTERFACE PHENOMENA AND THEIR SIGNIFICANCE IN CONCRETE

A concept widely accepted for many years in concrete technology was that concrete with high quality should result from use of high quality aggregate and cement and adequate compaction. This concept, however, merited reconsideration since Farran's[11] first investigation of interface phenomena between cement paste and aggregate in concrete. The interface properties of concrete are now known to differ from those of its major constituent phases, aggregate and hydrated cement paste. For instance, both aggregate and hydrated cement paste when tested separately in uniaxial compression remain approximately elastic until fracture, whereas concrete shows inelastic behavior. Also, the ultimate strength of concrete is lower than that of either of its component phases at a given water/cement ratio and degree of hydration. Similarly, the permeability of a

concrete containing even very dense aggregate(the key to its freeze-thaw durability and chemical resistance) is higher by up to two orders of magnitude than corresponding values for cement paste[2].

Glucklich[3] described the microcrack propagation process in a concrete during loading. At a stress less than $0.3\sigma_m$(σ_m is the ultimate strength of concrete in compression), the stress vs strain curve remains essentially linear and the pre-existing cracks at aggregate-cement paste interfaces extend only slightly. At stress levels $(0.3\text{-}0.5)\sigma_m$, however, the stress vs strain curve deviates from linearity and the cracks at interfaces grow lowly and continuously. At stress levels $(0.5\text{-}0.75)\sigma_m$, the bond cracks grow with slow growth of matrix cracks, and the isolated cracks gradually form a continuous crack network. The matrix cracks grow rapidly and lead to the fracture of concrete at stress levels $>0.75\sigma_m$. It is apparent that the crack growth process in concrete under load initiates from aggregate-cement paste interfaces. This phenomenon has been confirmed by other work[4-9]. It is, therefore, suggested that the aggregate-cement paste interface is the weakest mechanical link.

Investigations employing SEM(Scanning Electron Microscopy), XRD(X-Ray Diffraction) and IR (Infrared Spectroscopy) techniques have determined that the interfacial zone between cement paste and quartz when a quartz mortar immersed in Na_2SO_4 solution becomes an accessible path for the corrosive ion, $SO_4^{=}$, to penetrate.

More gypsum, a product of sulphate attack, forms at the interfaces than in the bulk paste[10]. Hoke et al.[11,12] investigated the interfacial phase composition in a concrete placed in SO_2 and HCl environments and found that the products of some chemical reactions existed mainly in the interfacial zones. The products were identified to be the monosulphaluminate phase and silicate gel. These results would suggest that the

aggregate-cement paste interface in concrete is a potential problem source for the durability of concrete.

It is now well recognized that the interfacial zone in a concrete is a distinct phase with completely different microstructural features and mechanical properties than the bulk paste. In addition, the interfacial zone is estimated to be 40-50 μm thick(though only about the first 20 μm from the aggregate surface has significantly different mechanical properties from those of the bulk paste). The mean spacing between two aggregate particles is estimated to be around 100 μm in a normal concrete[13], and therefore most hydrated cement paste lies within the interfacial zone, and only a relatively small volume of "bulk" paste exists. Hence, the properties of the interfacial zone have a very strong influence on the mechanical behavior and durability of concrete.

§1.3 MICROSTRUCTURAL CHARACTERISTICS OF THE INTERFACIAL ZONE

The properties of a material are generally dependent on its constituents and microstructure. Interfacial characteristics are, of course, dependent on specific microstructure in this special zone. Several studies in the past two decades have determined the predominant interfacial constituents and microstructure, and a few detailed reviews have been published[14-18]. The principal characteristics of the interfacial constituent and microstructure will be briefly described in this section.

The primary features of the interfacial region are the **"duplex film"** and the **"transition zone"**.

The **duplex film** occurs immediately adjacent to the aggregate surface. It consists of a layer, approximately 0.5 μm thick, of calcium hydroxide, CH, aligned perpendicular to the c-axis in contact with the aggregate and a layer of C-S-H gel adjacent to the CH layer. The thickness of the duplex film is usually less than 1 μm. The CH in this film is crystalline but the morphology revealed by SEM appears amorphous. This is believed to be a result of early calcium hydroxide supersaturation in the mix water of the aggregate-fresh cement paste system. The C-S-H gel in the film is in the form of short fibers that extend into the cement paste. It is suggested that the duplex film may not form over all areas of aggregate surface as some researchers[19,20] have observed its existence and others not[21,22]. It is also suggested that the duplex film is not a consequence of any aggregate-cement paste reaction, but rather the normal result of nucleation on any surface in contact with a supersaturated liquid. It may deposit on aggregates of a variety of compositions, such as silica glass, alkali-resistant glass fiber, steel and polytetra-fluoroethylene ("Teflon")[16].

The **transition zone** is a larger region between the aggregate surface and the bulk cement paste; it is approximately 50 μm wide and includes the duplex film. It differs from the bulk paste in a number of respects.

There are several specific microstructural features of the transition zone:

(1). Non C-S-H phases: Application of SEM and XRD techniques indicate that crystals, of **portlandite** and **ettringite**, enrich the transition zone. The concentration gradually decreases from the aggregate surface to the bulk paste[23].

(2). Crystal size: Crystal size of both portlandite and ettringite in the transition zone is larger than that in the bulk paste. Gradually decreasing crystal size with distance from the aggregate surface has been found by using XRD techniques[24].

(3). Preferred orientation of CH crystals: The preferred orientation of portlandite crystals(determined by XRD techniques) with c-axis perpendicular to the aggregate surface was first reported by Grandet and Ollivier[25]. It has subsequently been confirmed by many other researchers[26,27]. The degree of orientation gradually decreases from maximum at the aggregate surface to random in the bulk paste.

(4). Porosity and pore size distribution: It is well recognized that the transition zone is a more porous region than the bulk paste. This result has been confirmed by several methods, e.g. SEM, BEI(Backscattered Electron Imaging) combined with QIA(Quantitative Image Analysis)[28,29], computer modelling[30] and electrical conductivity methods[31]. In addition, some larger size pores concentrate in the transition zone. Tognon[32], using the mercury intrusion method, found a high concentration of 300 Å pores at the quartz-cement paste interface.

It is apparent that the above microstructural characteristics influence the mechanical behavior and durability of the interfacial zone. It is believed that large size portlandite crystals with preferred orientation and large pores in the interfacial zone act as regions for crack initiation in stressed concrete. The interfacial zone provides an open path for aggressive ions to penetrate into concrete due to high porosity and large pore size.

The mechanism of the interfacial zone formation has not been fully resolved. The precipitation of portlandite in the interfacial zone has been attributed to heterogeneous

nucleation of CH on the aggregate surface. For example, Chen and Wang[33] concluded that the CH portion of the duplex film results from heterogeneous nucleation and subsequent growth of CH from an supersaturated solution. Their analysis based on interfacial energy considerations indicated that CH is more likely to nucleate and grow on an aggregate surface than in the bulk paste.

The process of heterogeneous nucleation may explain the occurrence of a duplex film containing CH, but does not provide an explanation for other microstructural features of the transition zone, such as the higher porosity and larger size crystals behind the duplex film. Scrivener et al.[28,29] by using BEI/QIA techniques found that the interfacial zone contains much less unhydrated cement particles compared with the bulk paste. The number of unhydrated cement particles increases with increasing distance from the aggregate surface where there are no cement particles. Porosity, however, has the opposite tendency. Similar results were obtained through a computer simulation of interfacial zone formation[30], where the interfacial zone is assumed to form by a "through-solution" mechanism. These appear to support Maso's hypothesis described as follows[15]: The aggregates become coated by a water film several microns thick when mixed with fresh cement paste. In the water film, anhydrous cement grains, if any, can be found only in very limited numbers. The concentration of anhydrous cement is zero in the vicinity of aggregates and progressively increases with the distance from the aggregate surface. After dissolution of anhydrous components, the most mobile ions are the first to diffuse in the water film. For the portland cements, the order of diffusion is as follows: sodium and potassium, sulphate ions, aluminate ions, calcium ions and silicate ions. If the aggregates are insoluble, the ions in the water film come only from cement. In the water film the first nuclei to form are those of the hydrated components

corresponding to the most mobile ions, portlandite and ettringite in the case of portland cement. As a result of a larger space for crystal growth in the water film, the products in the vicinity of the aggregate consist of relatively larger crystals, and therefore form a more porous framework than in the bulk cement paste.

§1.4 INTERFACIAL BONDING AND ITS EFFECT ON CONCRETE PROPERTIES

There is no exact definition in the literature for the term "interfacial bonding"; a general understanding is, however, that it is a measure of the adhesion of interfacial products to the aggregate surface. It should be emphasized that the interface in question is not a mathematically geometric surface but an interfacial region; therefore inherent in the definition of interfacial bonding is a consideration of the cohesion of the interfacial zone itself.

It is suggested that interfacial bonding originates from two possible sources, i.e. mechanical interlocking between aggregate and cement paste, and chemical reactions at the interface. Their relative importance is unknown.

Mechanical interlocking results from the roughness of aggregate surface, and it is believed that it plays a major role in the behavior of porous and non-reactive aggregate-cement interfaces, e.g. in the case of lightweight concrete[34]. It has been found that the roughness of aggregate surface influences the permeability and freeze-thaw resistance of concrete[35].

Several cases of chemical reaction at aggregate-cement paste interfaces that could possibly enhance interfacial bonding have been reported. For calcareous aggregates, e.g. limestone, marble, it has been observed that the chemical reaction between $CaCO_3$ and C_3A in cement occur at normal temperature; the products are carboaluminate hydrate, $C_3A \cdot CaCO_3 \cdot 11H_2O$[36-38]. In addition, $CaCO_3$ can react with $Ca(OH)_2$ to form a basic calcium carbonate responsible for the strengthening of the transition zone[39]. For siliceous aggregate, e.g. quartz, there is no evidence of aggregate-cement paste chemical reactions at room temperature. However, these can occur under hydrothermal conditions. Quartz, for example, reacts under autoclave condition at 190°C with the cement paste to form a tobermorite crystal layer at the interface; it grows topochemically on the aggregate. This reaction enhances the interfacial bonding and hence mechanical behavior of concrete[40-42].

The nature of interfacial enhancement due to chemical reactions between aggregates and cement paste is unclear. For calcareous or siliceous aggregate-portland cement paste system, there is no convincing evidence of the occurrence of chemical bonds between aggregate and the products at the interface. The direct consequence of these chemical reactions appears to be densification of the transition zone due to formation of new products.

§1.5 CHARACTERIZATION OF INTERFACIAL MICROSTRUCTURE

Several interface characterization methods have been developed based on different techniques. The most widely used methods are SEM and XRD techniques.

1.5.1. SEM Techniques:

SEM techniques can directly reveal the morphological characteristics of hydrated products in the interfacial zone. Crystalline and non-crystalline microstructural features can be observed. The principal limitation is that SEM techniques generally can not quantitatively characterize interfacial microstructure. Although some quantitative information can be obtained using "quantitative image analysis" in conjunction with SEM(principally "backscattered electron imaging") , a large number of sampling points must be processed to validate conclusions.

1.5.2. XRD Techniques:

XRD techniques are principally used for determining the degree of orientation of portlandite and the crystal size in the interfacial zone. The method of determining the degree of orientation of portlandite was developed by Grandet and Ollivier[25]. In this method, an orientation index, I, was defined by the following expression:

$$I = \frac{I_{(001)} / I_{(101)}}{0.74} \qquad (1\text{-}1)$$

where, $I_{(001)}$ is the intensity of X-ray beam at d=4.90 Å of the (001) planes of portlandite, $I_{(101)}$ is that of (101) planes at d=2.682 Å, and 0.74 is $I_{(001)} / I_{(101)}$ ratio when there is no preferred orientation of portlandite. Published results indicate that the value of index I is generally much greater in the interfacial zone than in the bulk paste where I=1. Based on the curve of I value vs distance from aggregate surface, the thickness of region in which CH has preferred orientation can be estimated. This thickness, δ_o , is generally thought of as the thickness of the interfacial zone.

This method has been widely adopted by researchers. Chen et al.[43], however, analyzed theoretically the limitations of equation (1-1) and pointed out that it can be used only for qualitative analysis. They proposed an improved method of determining the degree of orientation of CH, based on the "rocking curve of the diffraction line". It appears, however, that the improved method does not reveal any new information even though the expression for the orientation index is theoretically more rigorous.

Comment: The XRD technique, as a method for interface investigation, is quite effective and therefore widely adopted by researchers. There are, however, some intrinsic limitations with this technique. Microstructural features relating only to crystalline compounds can be revealed(non-crystalline compounds are not discriminated). In addition, complex sample preparation procedures are also required.

§1.6 MODIFICATION OF INTERFACIAL MICROSTRUCTURE

The interfacial zone is a unique region controlling many important properties of concrete. The modification of interfacial microstructure has the general objective of enhancing interfacial bond for the production of high quality concrete. There are two major methods of interfacial modification:

1.6.1. Modification of Aggregate Surfaces before Mixing

Coating aggregate surfaces by application of chemical reagents or polymers appears to be an excellent idea[44-47]. The purpose is to increase interfacial bonding and reduce the crystal size and the degree of orientation of portlandite. It appears, however, that neither highly effective coating materials nor coating methods have been found.

It has been reported that by using clinkers as aggregates the mechanical properties and chemical resistance of concrete have been significantly enhanced[31, 48-50]. The reason is that these concretes or mortars have very dense interfacial microstructure due to the hydration of clinker itself and the compatibility between clinker and cement paste. These results suggest that producing a layer of clinker-like product on a general aggregate surface may be beneficial. This concept has been validated by calcining corundum particles with calcium carbonate powder at high temperature[51]. It was found that the interfacial microstructure and hence the mechanical properties and durability of mortar were enhanced in a manner similar to that of the clinker-cement paste system[51,52]. The major problem with this method is that high temperature treatment of aggregate is a complicated process and may not pass the scrutiny of economical considerations for practical application in industry.

1.6.2. Addition of Mineral Admixtures such as Silica Fume, Fly Ash, Blast Furnace Slag etc. as Partial Replacement of Cement

Most research indicates that silica fume is a highly effective admixture for improvement of concrete properties due to the enhancement of the transition zone[53,54]. It is argued that very fine silica fume particles behave as nucleation sites for crystallization of hydration products, leading to formation of small crystals of calcium hydroxide and a reduced tendency for preferred orientation[55,56]. In addition, pozzolanic reaction between silica fume and calcium hydroxide reduces calcium hydroxide content and increases transition zone density. The amount of silica fume addition to cement is often greater than ten per cent and up to thirty per cent of cement by weight has been used. It is not clear whether property enhancement is due principally to the improvement of the transition zone or to the bulk paste itself. Some researchers have suggested that the

increase of the compressive strength of mortar blended with silica fume is primarily due to the increase of the strength of the cement paste matrix[57]. It was further stated that the bond strength of the interface may even be reduced by adding silica fume to cement.

§1.7 PROGRAM OBJECTIVES

The review process described above was a precursor for identification of the specific problems addressed in the current investigation. This research program was designed to provide a clearer understanding of questions raised by the following aspects of previous investigations:

1. Methodology: There has been a lack of innovation in studying interface phenomena in concrete. Determination of the degree of CH crystal orientation constitutes only a relatively minor advance. This resulted in several papers by various authors which were repetitive and unoriginal. Detailed characteristics of formation and development of the interfacial zone have not been provided due to ineffective investigative methods. XRD and SEM techniques alone have been insufficient to result in a significant advance.

2. Modification of interfacial microstructure: No effective and simple method of interfacial modification has been produced by other researchers.

The principal objectives of this program are as follows:

(1). To develop a new and effective method for interfacial characterization in cement composites including concrete.

(2). Establish time-dependent parameters that can be used as descriptors of interface microstructure. Apply conductivity modelling techniques for evaluating effects of interface modification on durability.

(3). Develop new and effective methods of interfacial modification to enhance interfacial density, bonding and mechanical properties of concrete.

(4). Determine the effectiveness of "A.C. impedance spectroscopy" as a tool for microstructural investigation and delineation of the quality of cement paste-aggregate interfaces.

New Electrical Conductivity Methods will be developed for interface investigation. Compared with techniques such as, XRD and SEM, the new methods have the following advantages:

(i). Interfacial microstructure can be characterized quantitatively.

(ii). The process of interfacial microstructure development can be rationalized.

(iii). The experimental procedure, including calculation of final results, is easily computerized.

(iv). Preparation of samples is extremely simple and no special pre-treatment of the sample is needed. XRD and SEM techniques require the sample to be dried.

(v). Specimens containing either flat aggregate or granular aggregate can be analyzed.

CHAPTER TWO

INTERFACE CHARACTERIZATION OF CEMENT COMPOSITES –ELECTRICAL CONDUCTIVITY THEORY

SUMMARY

A general formula for the electrical conductivity of a composite material consisting of multi-phase components is advanced. Emphasis is given to the development and determination of an interfacial microstructure descriptor, θ-parameter. The relationship between the θ-parameter and the microstructural features of the interfacial zone is described in detail.

Two types of aggregate-cement paste systems, flat aggregate-cement paste and granular aggregate-cement paste, are used to model coarse aggregate and fine aggregate-cement paste interfaces in concrete.

§2.1 INTRODUCTION

It is well known that the hardened cement paste is a micro-porous material. Generally, dry hardened cement paste is an excellent insulator. It becomes a conductor, however, when saturated with pore solution. The electrical conductivity of a cement paste sample

actually reflects pore structure information, such as porosity and pore connectivity, since the electrical conduction in the saturated cement paste, mortar and concrete can only be carried out through the motion of ions in the pore solution, e.g. OH^-, Ca^{2+}, K^+, Na^+, and $SO_4^=$.

The electrical conductivity, σ, of a porous material saturated with an electrolytic solution is controlled by two factors: microstructure and the electrical conductivity of the pore solution. This can be expressed as follows:

$$\sigma = \sigma(\text{ Microstructure}, \sigma_l)$$

where, σ_l is the electrical conductivity of pore solution. The influence of microstructural features of a porous material can be obtained by measuring its electrical conductivity for a specific value of σ_l . The development of the electrical conductivity method for characterizing microstructure of a porous material begins with this premise.

The proposed electrical conductivity method for the interface investigation is based on an understanding that the cement paste-aggregate interface in mortar or concrete has a different microstructure than the bulk paste, especially porosity, pore size and pore size distribution. It follows that the interface should have different electrical properties than the bulk paste, e.g. electrical conductivity.

The principle and methodology of the "electrical conductivity method" for characterization of interfacial microstructure are described in detail in the following sections. Emphasis is given to the development and determination of an interfacial microstructure parameter, $\theta=\delta(\sigma_f-\sigma_p)$, referred to as "interfacial excess conductance"; δ is

the thickness of the interfacial zone, and σ_f ,σ_p are the electrical conductivities of the interfacial zone and the bulk paste, respectively.

§2.2 PRINCIPLES OF INTERFACIAL CHARACTERIZATION BY ELECTRICAL CONDUCTIVITY METHODS

2.2.1. General Equation of Electrical Conductivity of Cement Composites

Consider a cement composite specimen as an element in an electrical circuit, as shown in figure 2.1(a). Suppose that the specimen consists of m-phase components with different electrical conductivity. The specimen can be regarded as consisting of a series of electrical elements connected in series in the direction of the electrical field, as shown by figure 2.1(b). All elements are physically the same if all the phases have statistically uniform distributions in the specimen. Each element, therefore, consists of m-sub-elements equivalently connected in parallel, figure 2.1(c) and 2-1(d). The apparent electrical conductivity of the specimen, σ, can be calculated by the following equation:

$$\sigma = \frac{L}{S}\frac{1}{R} \qquad (2\text{-}1)$$

where, L is the thickness of the specimen in the direction of the electrical field, and S is the area of the specimen normal to the electrical field. R is the electrical resistance and can be obtained from the expression:

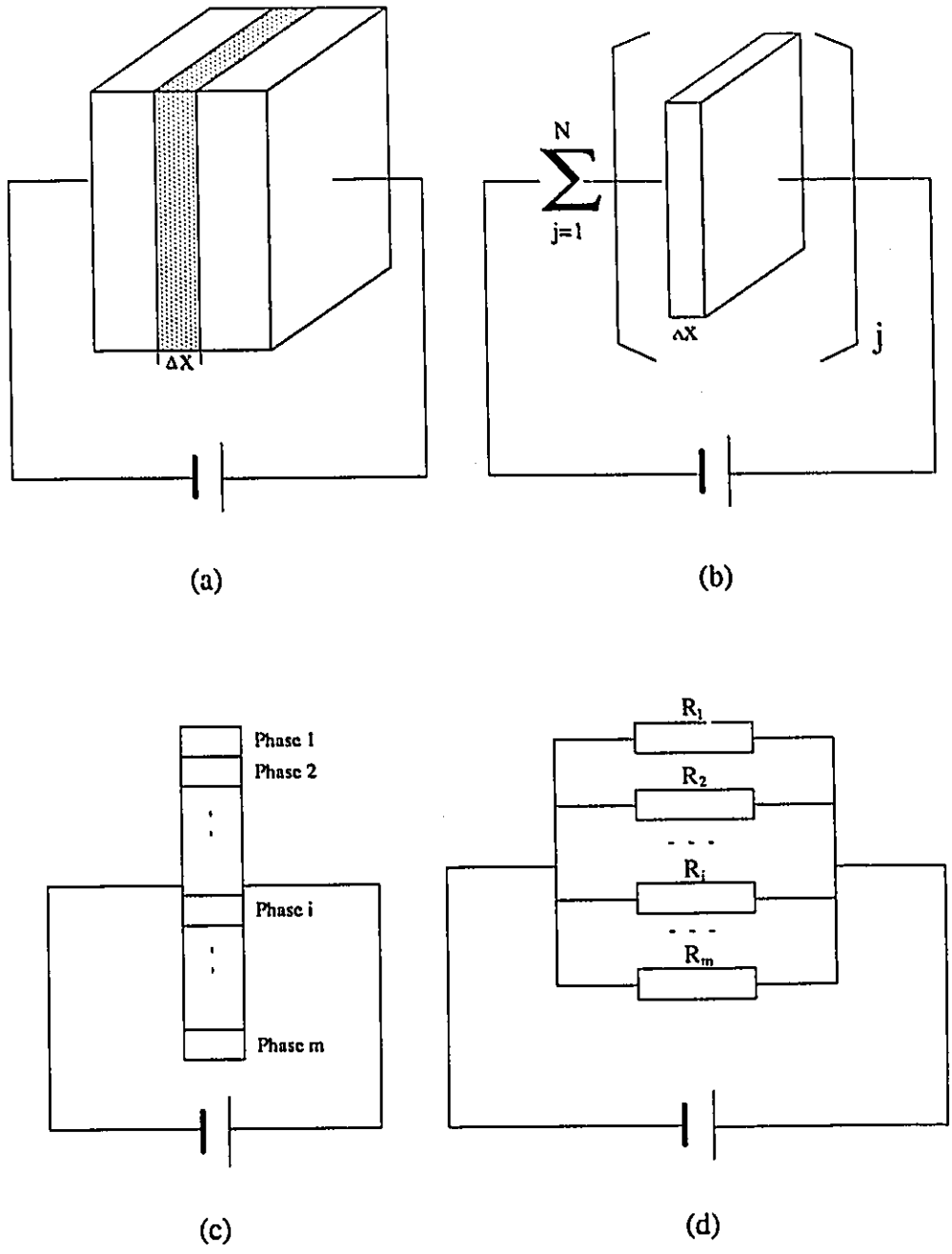

Figure 2.1. Electrical conduction model of m-phase composition material

$$R = \sum_{j=1}^{N} \left(\frac{1}{\sum_{i=1}^{m} \frac{1}{R_i}} \right)_j = \frac{N}{\sum_{i=1}^{m} \frac{1}{R_i}} = \frac{N}{\sum_{i=1}^{m} \frac{S_i}{\Delta x} \sigma_i} = \frac{N \Delta x}{\sum_{i=1}^{m} S_i \sigma_i}$$

$$= \frac{L}{\sum_{i=1}^{m} S_i \sigma_i} = \frac{L}{S} \frac{1}{\sum_{i=1}^{m} (\frac{S_i}{S}) \sigma_i} = \frac{L}{S} \frac{1}{\sum_{i=1}^{m} \psi_i \sigma_i} \qquad (2\text{-}2)$$

where, σ_i is the electrical conductivity of the ith component. S_i is the area of ith component normal to the electrical field, and $\psi_i = S_i / S$ is the corresponding area fraction and

$$\sum_{i=1}^{m} \psi_i = 1 \qquad (2\text{-}3)$$

Substituting equation (2-2) into equation (2-1) yields:

$$\boxed{\sigma = \sum_{i=1}^{m} \psi_i \sigma_i} \qquad (2\text{-}4)$$

Equation (2-4) is a general expression of the electrical conductivity of an m-phase composite.

For a saturated cement paste, the system can be considered to consist of two phases, i.e. solid products(insulator) and pore solution(conductor). Its electrical conductivity can, therefore, be expressed as follows:

$$\sigma = \psi_s \sigma_s + (1-\psi_s)\sigma_l \approx (1-\psi_s)\sigma_l \qquad (2\text{-}5)$$

where, the subscripts "s" and "l" represent solid and liquid, respectively.

2.2.2. Development of the θ Parameter for Interfacial Characterization

Consider a concrete specimen connected in an electrical circuit similar to that in figure 2.1. According to Ohm's law, the average current intensity, I, through the specimen is as follows:

$$I = (\sigma \cdot S)\, E \quad \text{or} \quad \frac{I}{E} = \sigma\, S \qquad (2\text{-}6)$$

where, E is the intensity of electrical field, S is the area of specimen section normal to the electrical field, and σ is the apparent electrical conductivity of the specimen.

Consider further a particular situation where there is no interfacial effect, i.e. the specimen consists of two components, aggregate and cement paste, figure 2.2(a). In this case, the apparent electrical conductivity, σ , is

$$\sigma = \sigma_a \psi_a + \sigma_p \psi_p = \sigma_a \psi_a + \sigma_p(1 - \psi_a) \qquad (2\text{-}7)$$

where, σ_a , σ_p are electrical conductivities of aggregate and cement paste, respectively, and ψ_a, ψ_p are corresponding area fractions. Since $\sigma_a \approx 0$ compared with σ_p , (2-7) becomes

$$\sigma = \sigma_p(1 - \psi_a) \qquad (2\text{-}8)$$

Hence

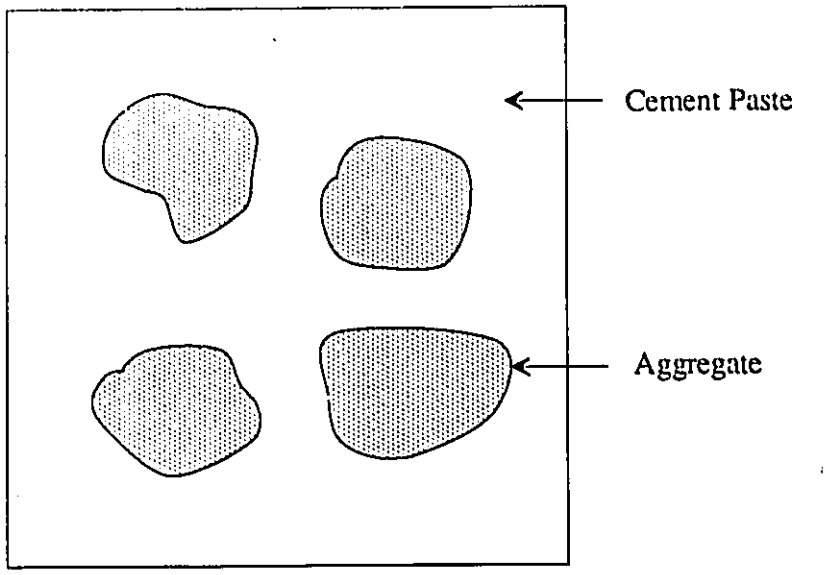

(a)

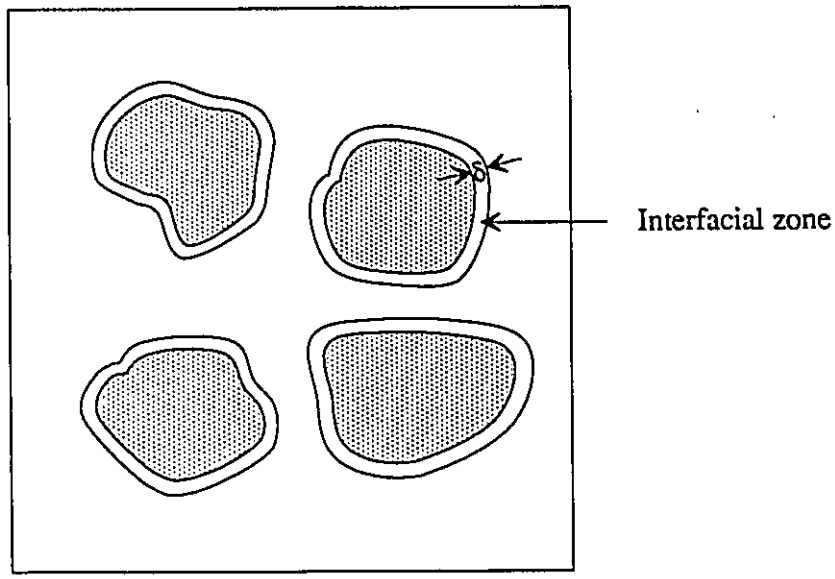

(b)

Figure 2.2. A sketch of a typical concrete section (a). without interface effect (b). with interface effect

$$\frac{I}{E} = \sigma_p(1 - \psi_a)S$$

$$= \sigma_p(S - S_a) \qquad (2\text{-}9)$$

where, S_a is the area of aggregate in the section. Equation (2-9) indicates that the contribution to the current intensity through the specimen only comes from cement paste.

For a general situation including the interfacial effect, where the specimen consists of three phases, aggregate, cement paste and interfacial zone, as shown in figure 2.2(b), the apparent electrical conductivity of the specimen is expressed as follows:

$$\sigma = \sigma_a \psi_a + \sigma_p \psi_p + \sigma_f \psi_f$$

$$= \sigma_a \psi_a + \sigma_p(1 - \psi_a - \psi_f) + \sigma_f \psi_f$$

$$\approx \sigma_p(1 - \psi_a - \psi_f) + \sigma_f \psi_f$$

$$= \sigma_p(1 - \psi_a) + (\sigma_f - \sigma_p)\psi_f \qquad (2\text{-}10)$$

where, σ_f ,ψ_f are the electrical conductivity and area fraction of interfacial zone.

Substituting equation (2-10) into (2-6) yields

$$\frac{I}{E} = [\sigma_p(1 - \psi_a) + (\sigma_f - \sigma_p)\psi_f]\, S$$

$$= \sigma_p(S - S_a) + (\sigma_f - \sigma_p)S_f$$

$$= \sigma_p(S - S_a) + \delta(\sigma_f - \sigma_p)\left(\frac{S_f}{\delta}\right) \qquad (2\text{-}11)$$

In equation (2-11), δ and S_f are interfacial thickness and area respectively. Since δ is a very small quantity compared with the size of aggregate, S_f / δ is, therefore, thought of as the "length" of the interfacial zone and it is approximately equal to the total perimeter of aggregates in the section, denoted by L_f. Hence equation (2-11) becomes

$$\frac{I}{E} = \sigma_p(S - S_a) + \delta(\sigma_f - \sigma_p)L_f \qquad (2\text{-}12)$$

A parameter θ is defined as

$$\theta=\delta(\sigma_f - \sigma_p)$$

and is referred to as "interfacial excess conductance". Let $S_p^*=S-S_a$, area of cement paste, in the case of no interfacial effect. Equation (2-12) can then be expressed as

$$\boxed{\frac{I}{E} = \sigma_p S_p^* + \theta L_f} \qquad (2\text{-}13)$$

It can be easily seen by comparing equation (2-13) with (2-9) that the first term on the right side of equation (2-12) is the contribution of cement paste in the case of no interfacial effect and the second term is an extra contribution resulting from the interfacial effect. It is also noted that all interfacial effects are reflected in the second term which is determined by the θ parameter and L_f, "length of interfacial zone". L_f is a measure of the "quantity" of interfacial zone. θ, however, carries important information relating to interfacial microstructure. This is the physical basis underlying the use of θ parameter and the electrical conductivity method for interfacial characterization.

The parameter, θ, is hence equal to the thickness of the interfacial zone multiplied by the difference between interface conductivity and bulk paste conductivity. The quantity ($\sigma_i - \sigma_p$) can be thought of as the electrical conductivity of the interfacial zone in excess of that ascribed to the bulk paste. θ has the dimension of conductance. This is why it is referred to as "interfacial excess conductance".

2.2.3. θ–Parameter as a Microstructural Descriptor

It has been demonstrated in the preceding discussion that θ is a unique descriptor of interfacial microstructure in cement mortar or concrete systems. Further details on the significance of θ follow.

The electrical conductivity of a saturated porous material composed of insulator components can generally be expressed by equation (2-5). In equation (2-5) ψ_s is a quantity directly related to material microstructure, and can be expressed as:

$$\psi_s = \psi_s \text{ (porosity, pore size, number and geometry of solid components etc.)}$$

Hence, ψ_s is a function of the density of the material.

Utilizing similar expression for the interfacial zone and the bulk paste in concrete, we have

$$\left.\begin{aligned} \sigma_p &= (1 - \psi_{ps})\,\sigma_{pl} \\ \sigma_f &= (1 - \psi_{fs})\,\sigma_{fl} \end{aligned}\right\} \qquad (2\text{-}14)$$

Combining the expression for θ and equation (2-14), we have

$$\theta = \delta(\sigma_{fl} - \sigma_{pl}) + \delta(\psi_{ps}\,\sigma_{pl} - \psi_{fs}\,\sigma_{fl}) \qquad (2\text{-}15)$$

Generally, it can be considered that $\sigma_{fl} = \sigma_{pl} = \sigma_l$ for an inert aggregate-cement paste system, hence

$$\theta = \delta(\psi_{ps} - \psi_{fs})\sigma_l \qquad (2\text{-}16)$$

Basic criteria for identifying interfacial microstructural features can be obtained from equation (2-16):

(i). $\theta > 0$, or $\sigma_f > \sigma_p$, or $\psi_{ps} > \psi_{fs}$: Physically, this implies a less dense interfacial microstructure than that of bulk paste.

(ii). $\theta < 0$, or $\sigma_f < \sigma_p$, or $\psi_{ps} < \psi_{fs}$: This implies a more dense interfacial microstructure than that of bulk paste.

The following information can be inferred for a practical cement paste-aggregate system by determining the values of θ at different hydration times:

(1). Microstructural features of the interfacial zone.

(2). Occurrence of chemical reactions, if any, between aggregate and cement paste for a reactive aggregate-cement paste system.

(3). Kinetic features of the process controlling the formation and development of the interfacial zone.

§2.3 DETERMINATION OF THE θ-PARAMETER

Two types of aggregate, coarse aggregate and fine aggregate, are generally employed in most concrete formulation. The difference often lies in aggregate size. It is suggested that aggregate size affects the characteristics of the interfacial zone. Two types of aggregate systems will, therefore, be used to model interfacial microstructure corresponding to the two types of aggregate.

(1). Flat aggregate-cement paste system: Flat aggregate-cement paste interfaces can be used to represent coarse aggregate-cement paste interfaces in concrete since the aggregate size is sufficiently large, relative to the thickness of the interfacial zone, to neglect any effect of surface curvature on interfacial features.

(2). Granular aggregate-cement paste system: This system is for the characterization of fine aggregate-cement paste interface in concrete.

2.3.1. Flat Aggregate-Cement Paste Interface

A specimen composed of alternate layers of cement paste and flat aggregate with thickness "a" is depicted in figure 2.3(a). The electrical conductivity of the specimen can be calculated as follows:

$$\sigma = \sigma_a \psi_a + \sigma_p \psi_p + \sigma_f \psi_f$$

$$\approx \sigma_p(1 - \psi_a) + (\sigma_f - \sigma_p)\psi_f \quad (\sigma_a \approx 0, \text{ compared with } \sigma_p \text{ and } \sigma_f)$$

It can be readily shown for the specimen in figure 2.3(a) that

$$\psi_a = \frac{Nab}{S}, \quad \text{and} \quad \psi_f = \frac{2N\delta b}{S}$$

hence

$$\psi_f = 2(\frac{\delta}{a})\,\psi_a \tag{2-17}$$

where N, b are the number and length of aggregate plates, respectively and S is the total area of the specimen.

Hence, the electrical conductivity of the specimen at hydration time "t" is readily formulated by

$$\left.\begin{aligned} \sigma(t) &= A(t)\,\psi_a + B(t) \\ A(t) &= 2(\frac{\delta}{a})[\sigma_f(t) - \sigma_p(t)] - \sigma_p(t) \\ B(t) &= \sigma_p(t) \end{aligned}\right\} \tag{2-18}$$

The following expression for θ can be readily derived from equation (2-18)

$$\theta(t) = \frac{a}{2}\,[A(t) + B(t)] \tag{2-19}$$

The straight line plot of $\sigma(t)$ vs ψ_a is obtained by experiment. The slope A(t) and intercept B(t) can be readily obtained and the θ parameter calculated using equation (2-19).

It should be pointed out that equation (2-19) theoretically holds only under the following condition:

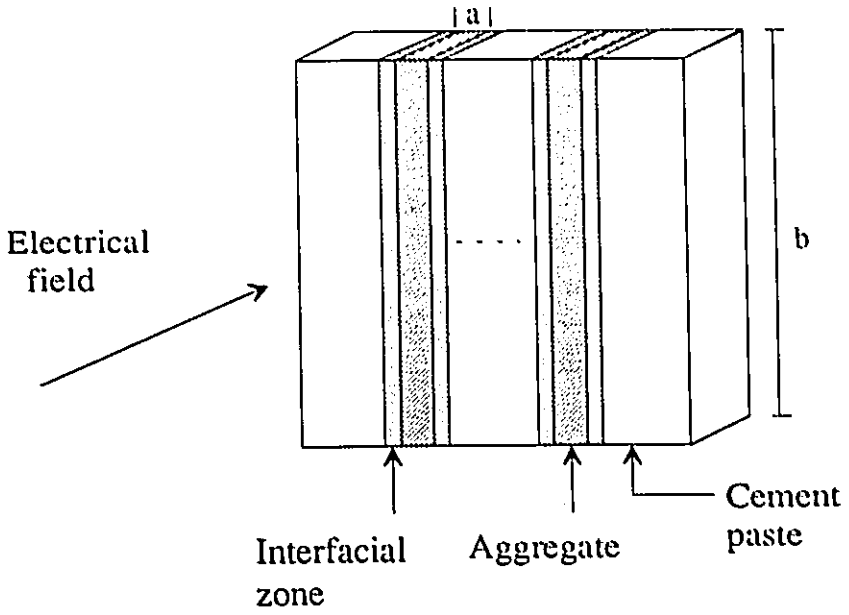

(a)

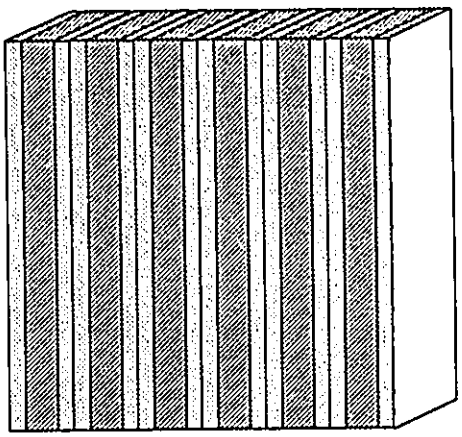

(b)

Figure 2.3. A sketch of specimen containing flat aggregates
(a). normal situation (b). limiting situation

$$\psi_a < \psi_{a,max} = \frac{1}{1 + 2(\frac{\delta}{a})} \qquad (2\text{-}20)$$

$\psi_{a,max}$ corresponds to the case where the interfacial zones of two adjacent aggregates will meet each other, as shown by figure 2.3(b).

2.3.2. Granular Aggregate-Cement Paste Interface

The electrical conductivity of a mortar specimen containing spherical aggregate particles with radii "r" can be expressed as a function of hydration time "t" as follows[31]

$$\left.\begin{aligned} \sigma(t) &= k(t)\,\varphi_a + b(t) \\ k(t) &= 3(\frac{\delta}{r})(1 + \frac{\delta}{2r})[\sigma_f(t) - \sigma_p(t)] - \frac{3}{2}\sigma_p(t) \\ b(t) &= \sigma_p(t) \end{aligned}\right\} \qquad (2\text{-}21)$$

where, φ_a is the volumetric fraction of aggregate in the mortar specimen.

Since $\delta << 2r$, by the definition of θ and equation (2-21), we have

$$\theta(t) = \delta\,[\sigma_f(t) - \sigma_p(t)] = r\,[\frac{k(t)}{3} + \frac{b(t)}{2}] \qquad (2\text{-}22)$$

$\theta(t)$ can be easily obtained after determining the slope k(t) and intercept b(t) of the $\sigma(t)$ vs φ_a line.

The condition for the validity of equation (2-21) can be obtained by considering a limiting situation, i.e. the spheres with $(r+\delta)$ radii pack at maximum density(face-centered cubic structure), figure 2.4, where the interfacial zone meet each other:

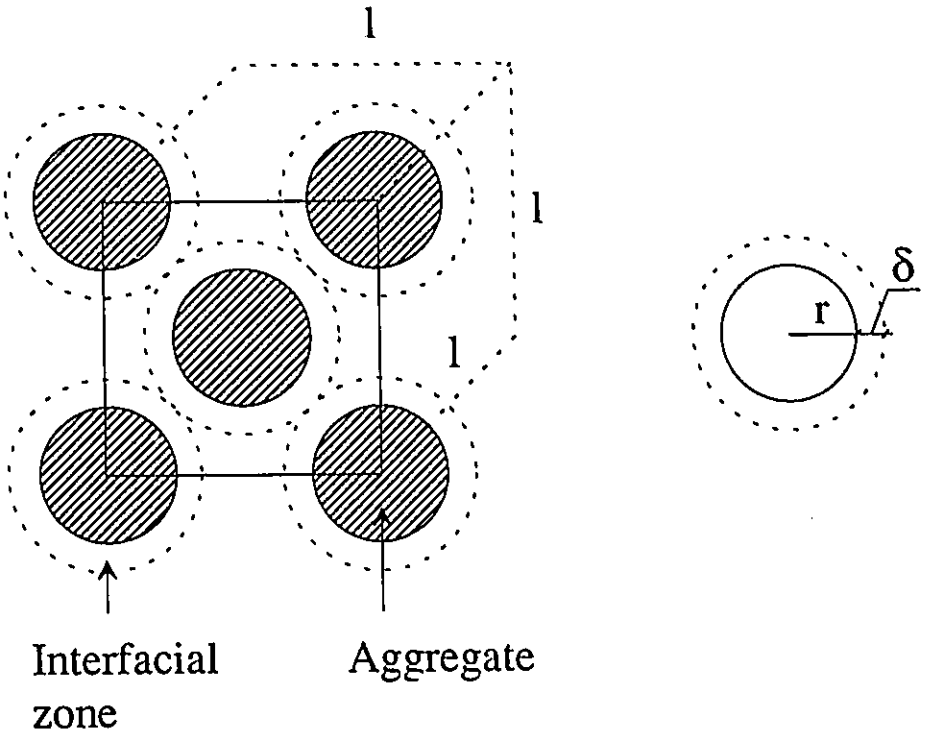

Figure 2.4. A sketch of a limiting situation in mortar where aggregate-interfacical zones pack at maximum density(Face-Centred Cubic Structure)

Since $\frac{4 \cdot \frac{4}{3}\pi (r+\delta)^3}{l^3} = \frac{\pi}{3\sqrt{2}} \approx 0.74$ from the geometry in figure 2.4,

hence

$$\varphi_{a,max} = \frac{4 \cdot \frac{4}{3}\pi r^3}{l^3} = \frac{0.74}{(1 + \frac{\delta}{r})^3}$$

The condition for the validity of equation (2-21) can be, therefore, expressed by the following inequality:

$$\varphi_a < \varphi_{a,max} = \frac{0.74}{(1 + \frac{\delta}{r})^3} \qquad (2\text{-}23)$$

CHAPTER THREE

ELECTRICAL CONDUCTIVITY OF CEMENT SYSTEMS – EXPERIMENTAL DESIGN

SUMMARY

The principles and methods of determining the electrical conductivity for both flat and granular aggregate-cement paste systems are described in detail. Emphasis is given to the steps of determining θ-parameter.

§3.1 INTRODUCTION

The principal experiment, determination of electrical conductivity, and the apparatus and materials concerned are described in detail in this chapter. The emphasis is given to the former. The philosophy of the analysis of experimental results is also described.

Other relevant experiments, including those pertaining to the determination of mechanical properties and sulphate resistance of mortar, modification of interfacial

microstructure and a.c. impedance behavior of hydrating cement system, will be described in subsequent chapters.

§3.2 PRINCIPLES OF ELECTRICAL CONDUCTIVITY DETERMINATION

3.2.1. Flat Aggregate-Cement Paste System

3.2.1.1. Principle

A sketch of the electrical conduction cell employed in these studies is given in figure 3.1(a), 1(b). The cell is filled with saturated $Ca(OH)_2$ solution, and the sample is located in the middle of the cell. The resistances of the cell with and without the sample and the temperature of the solution are measured and recorded.

The resistance of the sample at temperature T, $R_s(T)$, can be obtained from the following equation:

$$R_s(T) = R_a(T) - R_b(T) + R_l(T) \qquad (3\text{-}1)$$

Let $$R'(T) = R_a(T) - R_b(T) \qquad (3\text{-}1')$$

then $$R_s(T) = R'(T) + R_l(T) \qquad (3\text{-}2)$$

where, $R_a(T)$ is the resistance of the cell with sample, $R_b(T)$ is that without sample, and $R_l(T)$ is the resistance of the solution at the position at which the sample is placed. The electrical conductivity of the sample at T_o can be, therefore, calculated by the following equation:

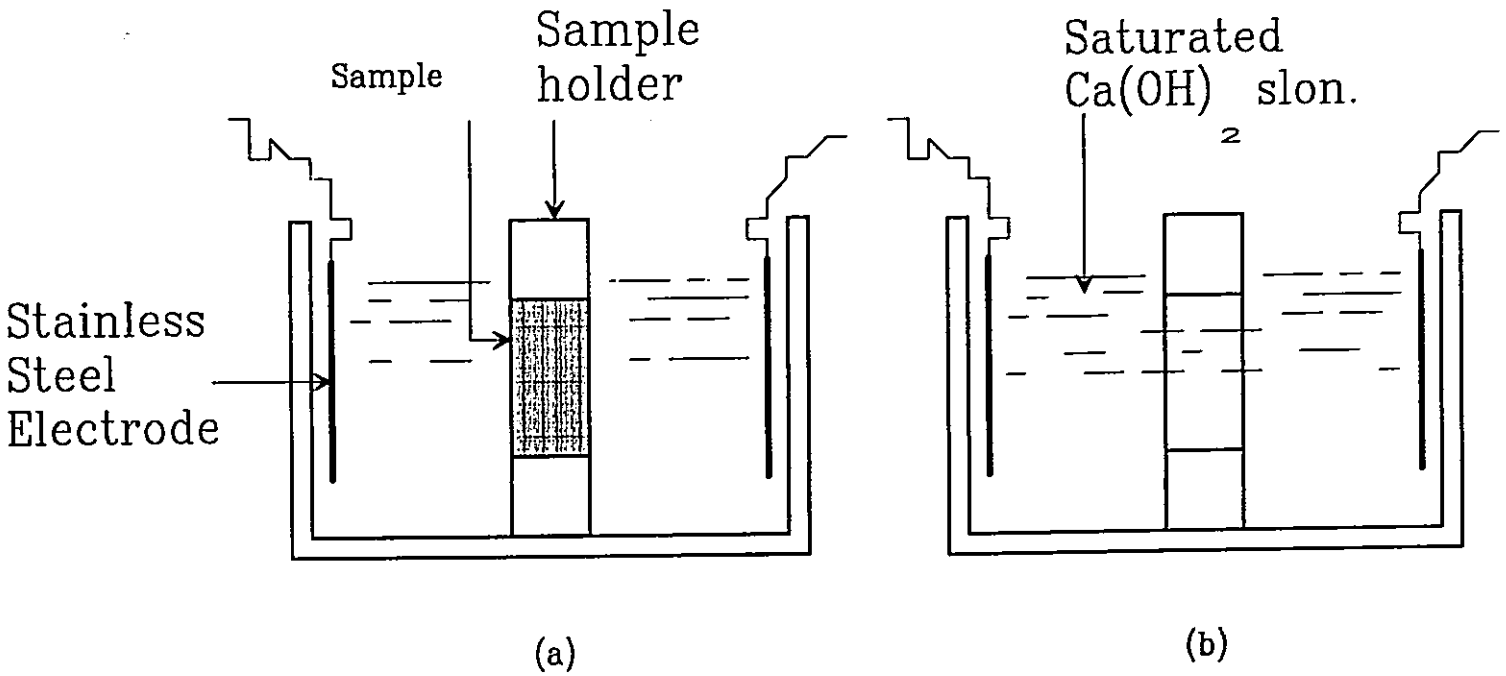

Figure 3.1. A sketch of the conduction cell used for resistance determination of the flat aggregate-cement paste system (a). with specimen (b). without specimen

$$\sigma_s(T_o) = \frac{L}{S}\frac{1 + \alpha_s(T_o - T)}{R_s(T)}$$

$$= \frac{L}{S}\frac{1 + \alpha_s(T_o - T)}{R'(T) + R_l(T)} \qquad (3\text{-}3)$$

where, L and S are the thickness and area of the sample, respectively, and α_s is the temperature coefficient of the resistance of the sample at T_o, defined as follows:

$$\alpha_s = -\frac{1}{R_s(T_o)}\left[\frac{dR_s(T)}{dT}\right]_{T_o} \qquad (3\text{-}4)$$

or

$$\alpha_s = \frac{1}{\sigma_s(T_o)}\left[\frac{d\sigma_s(T)}{dT}\right]_{T_o} \qquad (3\text{-}4')$$

For portland cement paste at approximately 20°C, $\alpha_s = 0.025$[58].

After considering the temperature correction for the electrical conductivity of the $Ca(OH)_2$ solution, equation (3-3) can be expressed as follows:

$$\frac{1}{\sigma_s(T_o)} = \frac{1}{\sigma'(T_o)} + \frac{1 + \alpha_l(T_o - T)}{1 + \alpha_s(T_o - T)}\frac{1}{\sigma_l(T_o)} \qquad (3\text{-}5)$$

where,

$$\sigma'(T_o) = \frac{L}{S}\frac{1 + \alpha_s(T_o - T)}{R'(T)} \qquad (3\text{-}5')$$

and $\sigma_l(T_o)$ is the electrical conductivity of the liquid in the conduction cell at T_o, and α_l is the corresponding temperature coefficient.

In this research program, T_o=20°C, and for saturated $Ca(OH)_2$ solution, σ_l(20°C) and the corresponding value of α_l are determined using the following experimentally obtained values of the electrical conductivity of saturated $Ca(OH)_2$ solution:

Table 2.1. Electrical conductivity of saturated $Ca(OH)_2$ solution

T (°C)	17.8	18.8	20.0	20.3	20.8	21.8
σ_l ($\Omega^{-1}m^{-1}$)	0.7101	0.7211	0.7340	0.7389	0.7459	0.7643

From the values in table 2.1, α_l was found to be 0.018 at 15.5°C - 23.5°C.

It can be seen that the electrical conductivity of the sample at 20°C can be readily obtained by equation (3-5) when $R_a(T)$, $R_b(T)$ and T are measured. It is noted that the effect of any error of $Ca(OH)_2$ solution conductivity measurement due to a small temperature change or non-equilibrium condition on the conductivity of the specimen would be negligible.

3.2.1.2. Specimen preparation

Rectangular aggregate pieces were prepared by cutting limestone slices from a block using a precision saw with diamond tipped blade; glass plate was also cut into rectangular slices. The size of the slice is 0.14cm x 1.25cm x 6.5cm for limestone and 0.25cm x 1.25cm x 6.5cm for glass.

The aggregate slices were inserted into a hollow plexi-glass mould(sample holder) in which the two parallel edges of the square hole contain several grooves for aligning the aggregate slices. The fresh cement paste with specified w/c ratio was cast into the remaining space. The sample was cured in a moist room at 20°C for about 6 hours. The

sample together with the mould was then taken from the curing room, and the surface of sample was treated very carefully with a scraper to make the surface smooth. The specimen was then inserted in the middle of the conduction cell for test.

Seven to eight specimens each containing a different number of aggregate slices were made. Each specimen was put in its own conduction cell. All cells were placed in a larger container filled with N_2 to minimize carbonation of the $Ca(OH)_2$ solution.

3.2.2. Granular Aggregate-Cement Paste Systems

An apparatus for determining the electrical conductivity of mortar is shown in figure 3.2. The fresh mortar is placed in the cell(8.0cm x 8.0cm x3.0cm), and its electrical conductivity at 20°C obtained using the following equation after the temperature, T, and the resistance, R(T), are measured:

$$\sigma(20°C) = \frac{L}{S}\frac{1 + 0.025(20 - T)}{R(T)} \qquad (3\text{-}6)$$

where, L/S is referred to as the cell constant(obtained by calibration with 0.1 N KCl solution). It is noted that in practical measurements the specimen contains a "tissue wick" connected to a water source to keep the specimen continuously saturated with water. The conduction cell was placed in a temperature controlled water bath at 20±2°C to minimize specimen temperature fluctuations.

3.2.3. Experimental Principle of Resistance Measurement

The equivalent circuit for the measurement of the cell resistance is given in figure 3.3. R_o is a standard resistor. An a.c. signal was used to avoid polarization of the electrodes. The

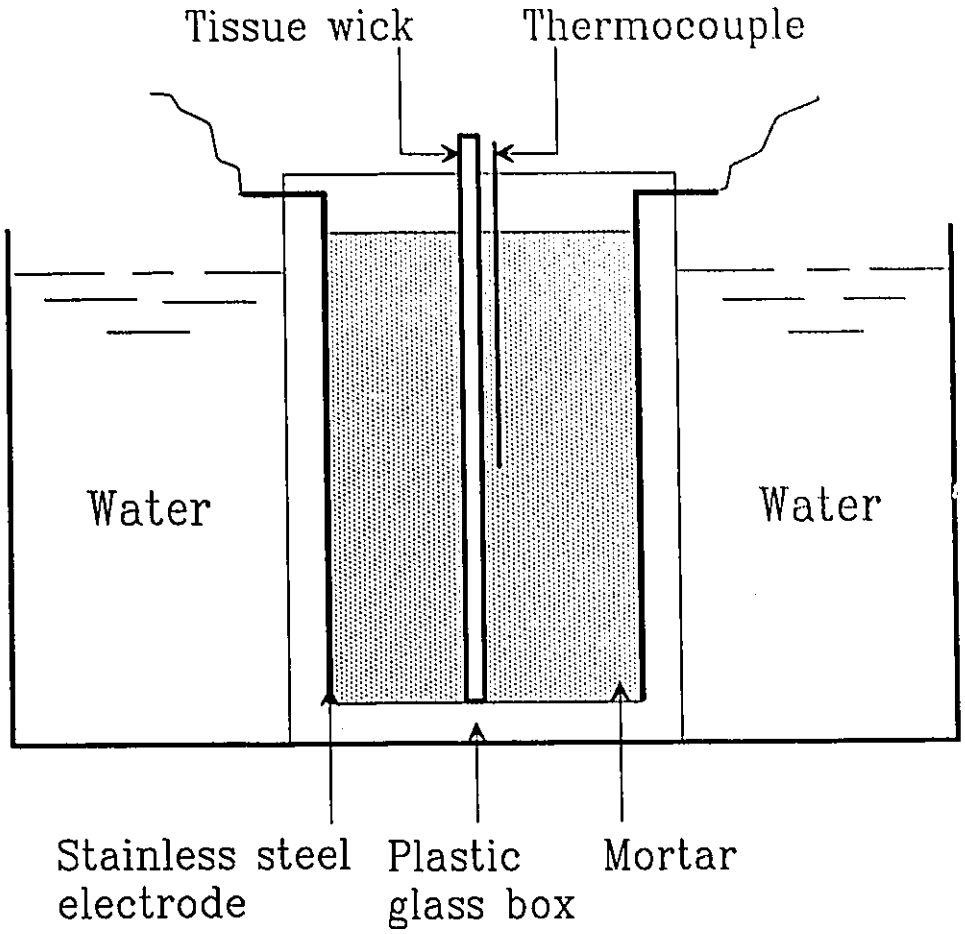

Figure 3.2. A apparatus for determining the electrical resistance of mortar

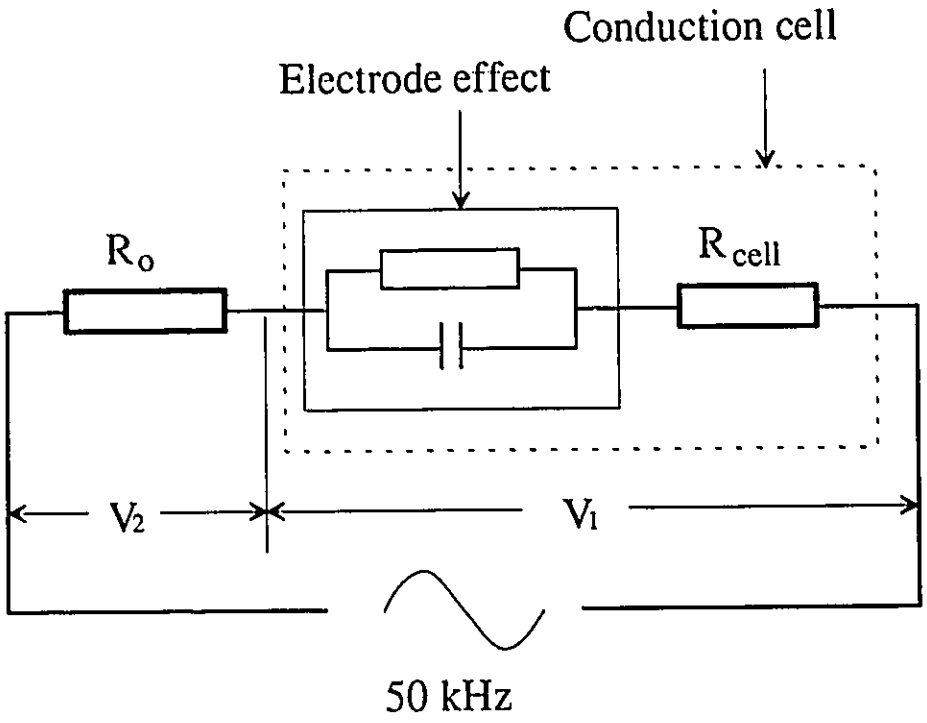

Figure 3.3. An electric circuit for determining resistance of specimen

equivalent circuit of the electrode effects under the a.c. signal is given in the sketch. It consists of a parallel circuit with an equivalent resistor and capacitor. Electrode effects can be neglected by using high frequency of a.c. signals. A frequency of 50 KHz was used. Measuring the voltages V_1 and V_2 for the given current intensity yields the cell resistance, R_{cell}:

$$R_{cell} = \frac{V_1}{V_2} R_o \qquad (3\text{-}7)$$

A computer controlled data acquisition system was used to record the measurements of V_1 and V_2 and to make the calculations of R_{cell}.

3.2.4. Determination of the θ-Parameter

Steps in the procedure to determine the θ-parameter included the following:

(1). Selection of raw materials: aggregates, cements etc.

(2). Mixing and moulding samples containing different amount of aggregates(i.e. different values of ψ_a (or φ_a)).

(3).Determining the electrical resistance of the samples using the computer data acquisition system; simultaneously recording sample temperature.

(4). Calculating the electrical conductivity of the specimens using equation (3-5) or (3-6); establishing the σ vs ψ_a (or φ_a) straight line relationships and calculating the slope and intercept using regression analysis.

(5). Calculating the θ-parameter using equation (2-19) or (2-22).

(6). Analysis of results.

3.2.5. Analysis of Results

Analysis of the results involved:

(1). Interpretation of new experimental phenomena based on fundamental scientific principles and development of new hypotheses.

(2). A combination of deductive and inductive reasoning. Emphasis on the former was given as the basic theory of the electrical conductivity method was developed prior to experiment.

§3.3 APPARATUS AND MATERIALS

3.3.1. Apparatus

(1). Computer-controlled data acquisition system for determination of electrical resistance: This system was designed and constructed at the Material Laboratory, IRC/NRC (Institute for Research in Construction/National Research Council of Canada). It consists of the following elements:

(i). EG&G Princeton Applied Research 5208 Two Phase Lock-in Analyzer.

(ii). KEITHLEY, 706 Scanner.

(iii). KEITHLEY, 175 Autoranging Multimeter.

(iv). Model 9350, Monitor Labs Inc.

(2). Electrical conduction cells: Conduction cells required for resistance determination were fabricated in the laboratory.

(3). Other equipment for microstructural examination and materials characterization:

(i). Scanning Electron Microscope(SEM): Cambridge Stereoscan S250.

(ii). X-Ray Diffraction Equipment(XRD): Wide Angle Goniometer by Regaku.

(iii). Materials Testing System(MTS): MTS Model 810.

(iv). Compressive strength testing machine: UBJ(Upton Bradeen & James Ltd.), 60,000 lb. capacity.

(v). SI 1260 Impedance Gain-Phase Analyzer by Schlumberger.

3.3.2. Materials

(1). Cement: Several portland cements from different sources were used. The chemical compositions are listed in Table 3.2:

(2). Aggregate: Limestone, silica glass, quartz, opal, Spratt aggregate* , cement clinker and blast furnace slag were used as aggregates.

(3). Mineral admixtures: Silica fume, fly ash and blast furnace slag were used. The chemical compositions are listed in Table 3.3:

(4). Reagent grade chemicals e.g. salts concerned with the research.

Table 3.2. Chemical Composition of Portland Cement(wt. %)

	CaO	SiO_2	Al_2O_3	Fe_2O_3	MgO	SO_3	K_2O	Na_2O	LOI
LA	64.83	20.78	6.20	2.22	1.84	3.17	0.40	0.05	
HA	61.85	20.35	6.20	2.04	2.38	2.98	1.06	0.19	2.95
WP	66.32	21.21	5.03	0.24	0.85	2.99	0.12	0.03	
PC	61.21	19.83	4.18	3.20	4.09	3.93	0.82	0.45	

LA - Low alkali; HA - Hight alkali from St. Lawrence Cement Co.; WP - White portland cement from Federal White Cement Ltd.; PC - Portland cement from St. Marys Cement Co.

Table 3.3. Chemical Composition of Mineral Admixture(wt. %)

	CaO	SiO_2	Al_2O_3	Fe_2O_3	MgO	SO_3	K_2O	Na_2O
SF	0.23	95.17	0.21	0.13	0.15	0.12	0.27	0.10
FA	1.63	45.20	20.70	24.83	0.97		2.40	0.59
BFS	36.94	35.30	10.62	0.58	13.32	1.41		

* A type of limestone from Ottawa area. It contains about 5% reactive silica.

CHAPTER FOUR

NATURE OF NON-POROUS AGGREGATE-CEMENT PASTE INTERFACES

SUMMARY

The theory of electrical conductivity methods for interfacial characterization of cement-aggregate systems has been validated by extensive experiments. Several new findings pertaining to the nature of aggregate-cement paste interfaces have been obtained. Details of the θ-parameter of both flat and granular aggregate-cement paste systems are described and discussed. A hypothesis for interfacial microstructure formation is proposed in concert with observed features of θ-parameter. Electrical conductivity models of both the interfacial zone and the bulk paste are developed to formulate the hypothesis. A relationship between interfacial bond strength and interfacial microstructure is advanced. Some possible methods of enhancing interfacial bond strength are suggested.

§4.1 INTRODUCTION

The objectives of the work described in this chapter are to explore the nature of aggregate-portland cement paste interfaces using the electrical conductivity theory

developed by the author and to develop the relationship between interfacial microstructure and mechanical properties of the interfacial zone. This chapter contains the following:

(1). A section outlining the validation of the theory for cement paste-aggregate interface development based on electrical conductivity methods.

(2). A section demonstrating features of the θ-parameter revealed by experiment.

(3). A section containing a proposed hypothesis of interfacial microstructure formation and the development of electrical conductivity models for the interfacial zone and the bulk paste in cement-aggregate systems. The physical meaning of the θ-parameter and related microstructural information are discussed.

(4). A section describing the effects of aggregate size on the interfacial microstructure.

(5). A section describing the development of a relationship between interfacial microstructure and interfacial bond strength.

(6). Conclusions.

§4.2 CHARACTERISTICS OF THE θ-PARAMETER FOR FLAT AGGREGATE-CEMENT PASTE SYSTEMS

4.2.1. Validation of an Electrical Conductivity Model

The electrical conductivity of the specimen containing flat aggregates was measured

using the methods described in chapter three to validate the electrical conductivity model expressed by equation (2-18).

Limestone and silica glass* were used as aggregates. Type 10 low alkali portland cement(LA in Table 3.2) was used.

Cement pastes were prepared at w/c ratios 0.30, .040 and 0.50.

A plot of the electrical conductivity of the specimen, σ, vs the area fraction of aggregate, ψ_a, is given in figure 4.1(a) and 1(b). The curves are linear as predicted by equation (2-18). This relationship also hold for other w/c ratios, and is evidence of the validity of the model developed.

Figure 4.2 shows the changes of the slope and intercept of the straight line σ vs ψ_a with hydration time. It can be seen that the slope, A, increases but the intercept, B, decreases with hydration time. From equation (2-18), the intercept B is the electrical conductivity of the bulk paste, and its decrease with hydration time is due to the increase in volume of solid phases in the system.

4.2.2. Characteristics of the θ-Parameter

Values of θ-parameter, interfacial excess conductance, for the above systems are plotted versus hydration time in figure 4.3. Values for the limestone and glass samples with different w/c ratios are given.

---

* The possibility of alkali-glass reaction at early hydration times was ruled out by SEM observation on glass surface immersed in 0.1 N NaOH solution for 24 hours.

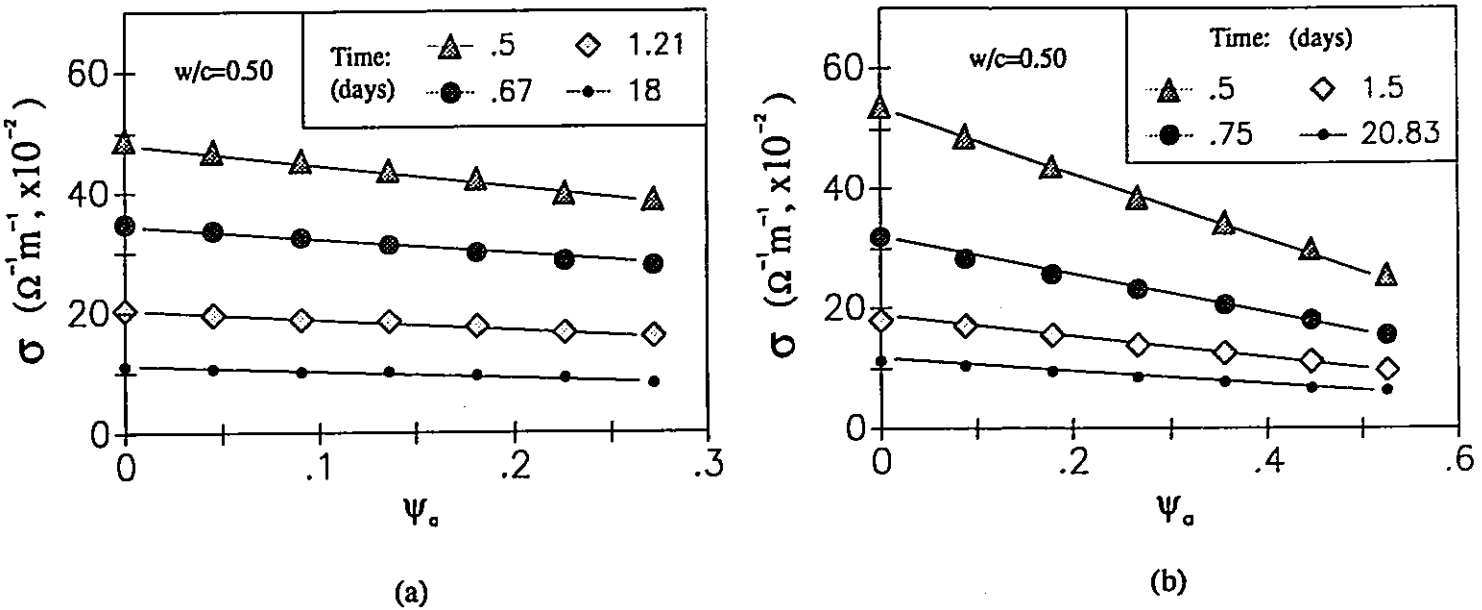

Figure 4.1. Electrical conductivity of cement paste-aggregate specimen vs area fraction of aggregate (a). limestone (b). glass

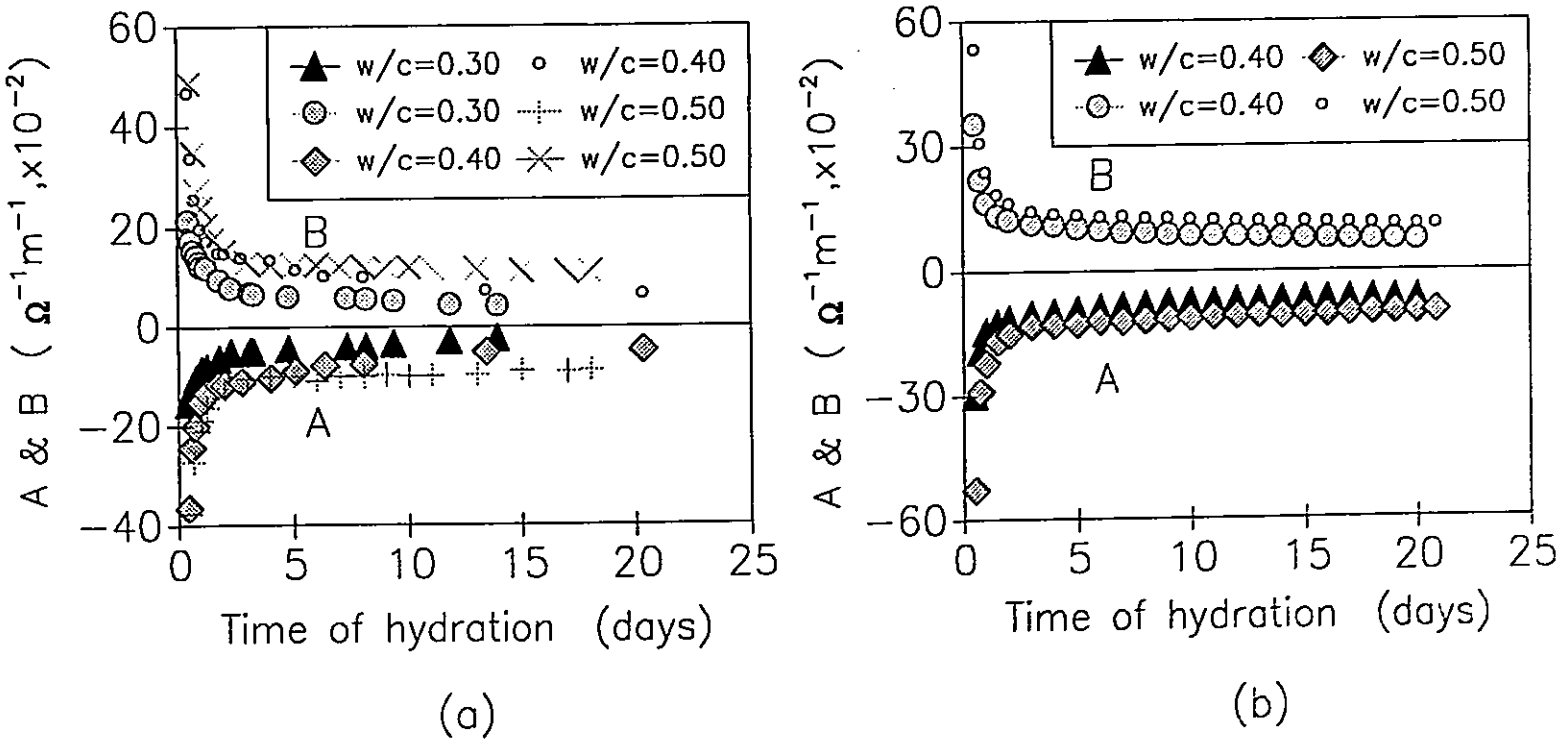

Figure 4.2. Slope and intercept in equation (2-18)
(a). limestone (b). glass

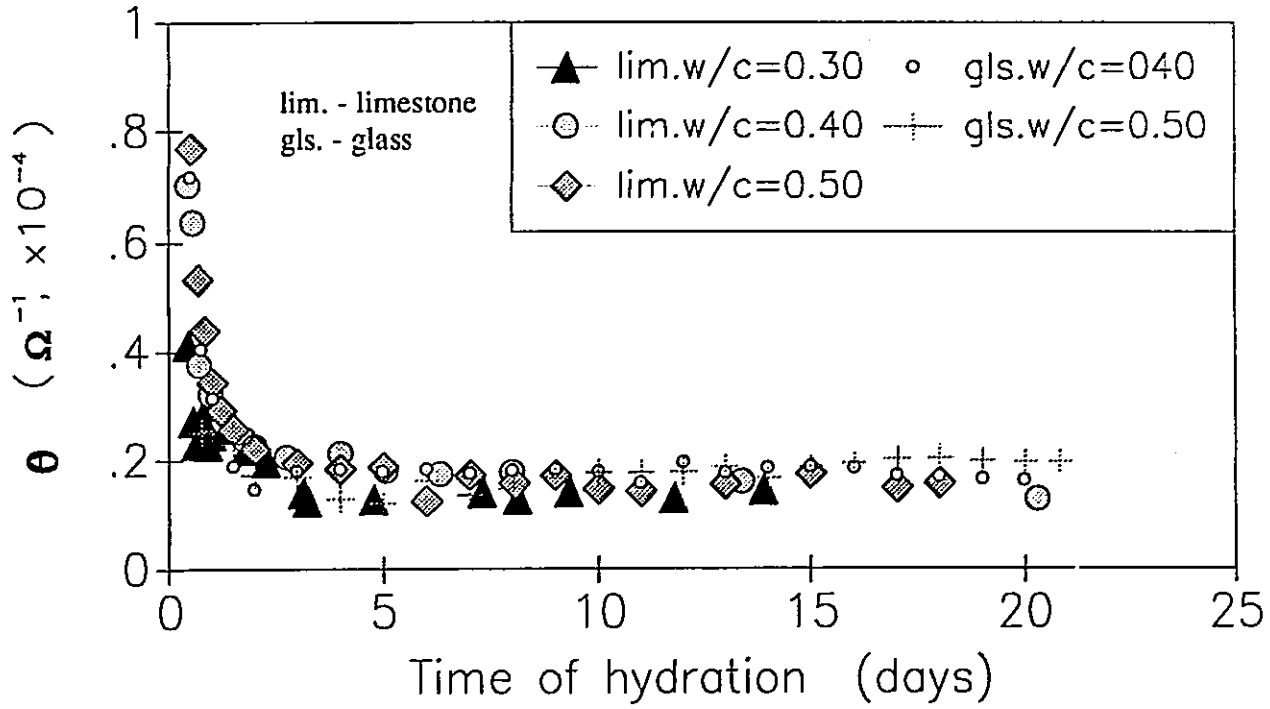

Figure 4.3. Interfacial excess conductance, θ, vs hydration time

From figure 4.3, the main characteristics of θ are as follows:

(1). $\theta > 0$.

This result implies a less dense interfacial microstructure than the bulk paste, as indicated in chapter two.

(2). θ is to a first approximation independent of w/c ratio.

(3). θ appears to be independent of the type of the aggregate used in the investigation.

(4). $\frac{d\theta}{dt} < 0$, $\frac{d^2\theta}{dt^2} > 0$, and θ decreases quickly during the early hydration followed by a slow change; θ approaches a constant value after about one week hydration.

Further analysis results in a hypothesis for the microstructural formation of the interfacial zone described in the following section.

§4.3 HYPOTHESIS FOR INTERFACIAL ZONE FORMATION

4.3.1. Hypothesis

Maso has postulated that after initial mixing of aggregate and fresh cement paste, there is a water film on the non-porous aggregate that contains no cement particles[15]. The formation of solid structure in the film occurs by a "through-solution" mechanism. The thickness of the water film is estimated to be a couple of microns compared to the whole interfacial zone which is about 40-50 μm. This raises a question as to the role of the

water film in the formation of the whole transition zone.

A hypothesis is rationalized as follows. The structure of the surface region of the solid substances is distorted due to the unbalanced force field acting on the surface atoms, e.g. the distance between adjacent two atoms in surface region is less than that in the bulk phase[59]. This distorted surface structure causes the solid to have some particular surface properties, surface energy for example.

A similar situation is considered to occur in a region containing a few layers of cement particles close to the water film on the aggregate at the beginning of mixing. The cement particles in this region are in a different environment from that of the bulk cement particles. This environmental difference causes the structural difference between this region and bulk paste as well as between the water film region and bulk paste. It is suggested that a few layers of cement particles close the water film are the sources of hydrates for structural formation and development in the water film as well as for that in this region itself. The cement particles in the bulk phase do not act in this way. Therefore, this region containing a few layers of cement particles is considered to be a part of the whole interfacial zone from the beginning of hydration to the complete formation of the internal structure of the paste system. This region will be referred to "effect region".

In summary the elements for formation of the interfacial zone are as follows:

(1). Formation of a water film on the non-porous aggregate surface at the beginning of the mixing of aggregate and fresh cement paste. No cement particles are contained within this layer.

(2). The interfacial zone includes a region containing a few layers of cement particles close to the water film. These cement particles are the sources of the hydrates for the formation and development of solid structure in the water film as well as in the remainder of this region itself.

4.3.2. Electrical Conductivity Models of the Interfacial Zone and Bulk Paste

The above hypothesis can be readily formalized by developing the electrical conductivity models of the interfacial zone and the bulk paste.

A model of the initial structure of the interfacial zone is sketched in figure 4.4. The electrical conductivities of the transition zone, σ_f, and the bulk paste, σ_p, at any given hydration time can be expressed by equation (2-14), or

$$\left.\begin{aligned} \frac{\sigma_f}{\sigma_l} &= (1 - \psi_{fs}) \\ \frac{\sigma_p}{\sigma_l} &= (1 - \psi_{ps}) \end{aligned}\right\} \qquad (4\text{-}1)$$

where, ψ_{fs}, ψ_{ps} are area fractions of the solid phases in the interfacial zone and the bulk paste, respectively. In the hydrating cement system, the solid phases come from the hydrates, "h", and unhydrated cement particles, "c". Hence,

$$\left.\begin{aligned} \psi_{fs} &= \psi_{fc} + \sum_h \psi_{fh} \\ \psi_{ps} &= \psi_{pc} + \sum_h \psi_{ph} \end{aligned}\right\} \qquad (4\text{-}2)$$

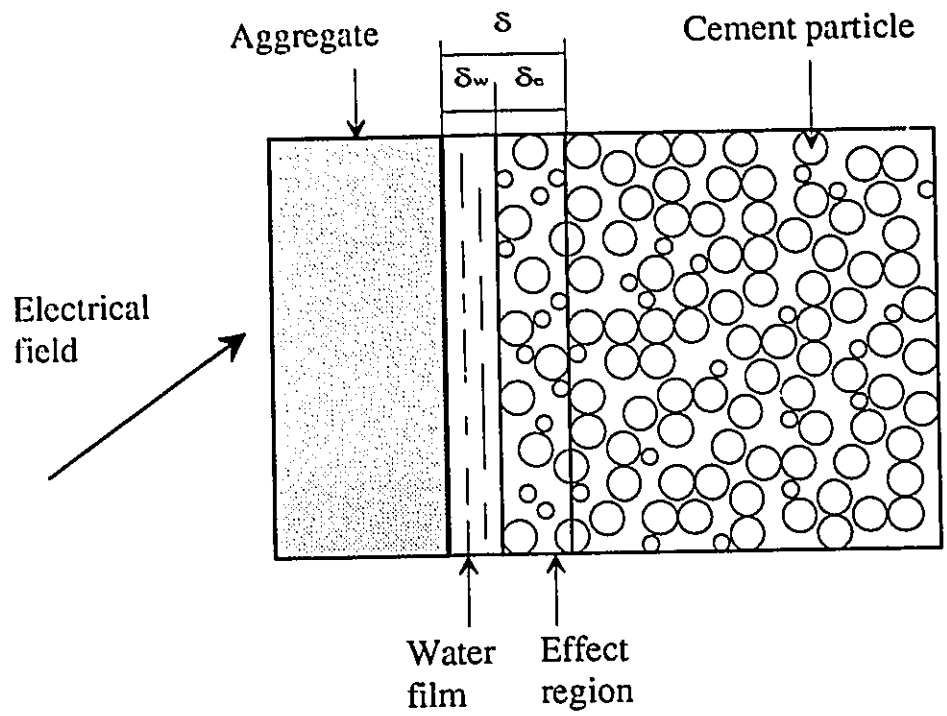

Figure 4.4. A sketch of the initial structure of the interfacial zone

C-S-H gel and CH are the major hydrates in the hydrating portland cement system. In addition there are small amounts of aluminate hydrates and sulpho-aluminates, e.g. AFt and AFm. The structural developments of the interfacial zone and the bulk paste therefore mainly rely on the production of C-S-H gel and CH. Hence, equation (4-2) can be written as follows:

$$\left.\begin{aligned} \psi_{fs} &= \psi_{fc} + \psi_{fo} + \psi_{f.gel} + \psi_{f.ch} \\ \psi_{ps} &= \psi_{pc} + \psi_{po} + \psi_{p.gel} + \psi_{p.ch} \end{aligned}\right\} \qquad (4\text{-}3)$$

where, the subscripts "gel" and "CH" represent C-S-H gel and CH, respectively, and "o" represents hydrates other than C-S-H gel and CH.

Substituting equation (4-3) into (4-1) yields:

$$\left.\begin{aligned} \frac{\sigma_f}{\sigma_l} &= (1 - \psi_{fo}) - \psi_{fc} - \psi_{f.gel} - \psi_{f.ch} \\ \frac{\sigma_p}{\sigma_l} &= (1 - \psi_{po}) - \psi_{pc} - \psi_{p.gel} - \psi_{p.ch} \end{aligned}\right\} \qquad (4\text{-}4)$$

Assuming the area fraction of each solid, ψ_i, is proportional to its volumetric fraction, φ_i, viz.

$$\psi_i = \lambda_i \varphi_i \ , \qquad (i = c, \text{ gel and CH}) \qquad (4\text{-}5)$$

equation (4-4) becomes

$$\left.\begin{aligned} \frac{\sigma_f}{\sigma_l} &= (1 - \psi_{fo}) - \lambda_c \varphi_{fc} - \lambda_{gel} \varphi_{f.gel} - \lambda_{CH} \varphi_{f.CH} \\ \frac{\sigma_p}{\sigma_l} &= (1 - \psi_{po}) - \lambda_c \varphi_{pc} - \lambda_{gel} \varphi_{p.gel} - \lambda_{CH} \varphi_{p.CH} \end{aligned}\right\} \quad (4\text{-}6)$$

Employing the definition of volumetric fraction and regions described in figure 4.4,

$$\varphi_{fi} = \frac{V_{fi}}{V_f} = \frac{V_{fi}}{V_w + V_e} = \frac{V_{fi}}{(1 + V_w/V_e)\, V_e}$$

$$= \frac{1}{(1 + \delta_w/\delta_e)} \frac{V_{fi}}{V_e} = \left(\frac{\delta_e}{\delta}\right) \frac{V_{fi}}{V_e} \quad , \qquad (4\text{-}7)$$

and

$$\varphi_{pi} = \frac{V_{pi}}{V_p} \qquad (4\text{-}7')$$

(i = c, gel and CH)

where, V_{fi}, V_{pi} are the volumes of i-solid in the interfacial zone and the bulk paste, respectively, V_f , V_p are the total volumes of the interfacial zone and the bulk paste, V_w , V_e are the volumes of the water film and the "effect region", and δ_w , δ_e are their thicknesses.

Hence, at any degree of hydration, m, we have

$$\left.\begin{aligned}
\varphi_{fc} &= \left(\frac{\delta_e}{\delta}\right)(1-m)\left(\frac{V_{fc}^{\circ}}{V_e}\right) = \left(\frac{\delta_e}{\delta}\right)(1-m)\,\varphi_c^{\circ} \\
\varphi_{f,gel} &= \left(\frac{\delta_e}{\delta}\right)\eta_{gel}\,m\left(\frac{V_{fc}^{\circ}}{V_e}\right) = \left(\frac{\delta_e}{\delta}\right)\eta_{gel}\,m\,\varphi_c^{\circ} \\
\varphi_{f,CH} &= \left(\frac{\delta_e}{\delta}\right)\eta_{CH}\,m\left(\frac{V_{fc}^{\circ}}{V_e}\right) = \left(\frac{\delta_e}{\delta}\right)\eta_{CH}\,m\,\varphi_c^{\circ}
\end{aligned}\right\} \qquad (4\text{-}8)$$

and

$$\left.\begin{aligned}
\varphi_{pc} &= (1-m)\,\varphi_c^{\circ} \\
\varphi_{p,gel} &= \eta_{gel}\,m\,\varphi_c^{\circ} \\
\varphi_{p,CH} &= \eta_{CH}\,m\,\varphi_c^{\circ}
\end{aligned}\right\} \qquad (4\text{-}8')$$

where, η_i, i = gel, CH, is the volume ratio of i-hydrate to the cement it comes from, and V_{fc}° is the volume of initial cement in the effect region. φ_c° is the volumetric fraction of initial cement to the volume of fresh cement paste in the effect region, and it can be considered to be that in the bulk paste.

Substituting equations (4-8) and (4-8') into equation (4-6) yields

$$\frac{\sigma_f}{\sigma_l} = A_f\,\varphi_c^{\circ} + B_f \qquad (4\text{-}9)$$

where,

$$\left.\begin{aligned} A_f &= -\left(\frac{\delta_e}{\delta}\right)\left[\lambda_c\,(1-m) + \lambda_{gel}\,\eta_{gel}\,m + \lambda_{ca}\,\eta_{ca}\,m\right] \\ B_f &= 1 - \psi_{fo} \end{aligned}\right\} \qquad (4\text{-}9')$$

and

$$\frac{\sigma_p}{\sigma_l} = A_p\,\varphi_c^{\circ} + B_p \qquad (4\text{-}10)$$

where,

$$\left.\begin{aligned} A_p &= -\left[\lambda_c\,(1-m) + \lambda_{gel}\,\eta_{gel}\,m + \lambda_{ca}\,\eta_{ca}\,m\right] \\ B_p &= 1 - \psi_{po} \end{aligned}\right\} \qquad (4\text{-}10')$$

herein, φ_c° can be related to the initial w/c ratio of the system:

$$\varphi_c^{\circ} = \frac{1}{1 + (w/c)\,(\rho_c/\rho_w)} \qquad (4\text{-}11)$$

where, ρ_c , ρ_w are the densities of cement and water.

From equations (4-9) and (4-10), we can see that the electrical conductivities of both the interfacial zone and the bulk paste are directly proportional to the negative initial volumetric fraction of cement, or inversely proportional to the negative initial w/c ratio. For a specific w/c ratio, σ_f/σ_l (or σ_p/σ_l) depends on the degree of hydration.

The relationship described by equation (4-10) has been validated by experiment. Electrical conductivity measurements were made on a series of cement pastes with w/c ratio from 0.25 to 0.50 at times ranging from 25 hours to 10 days. The cement used was

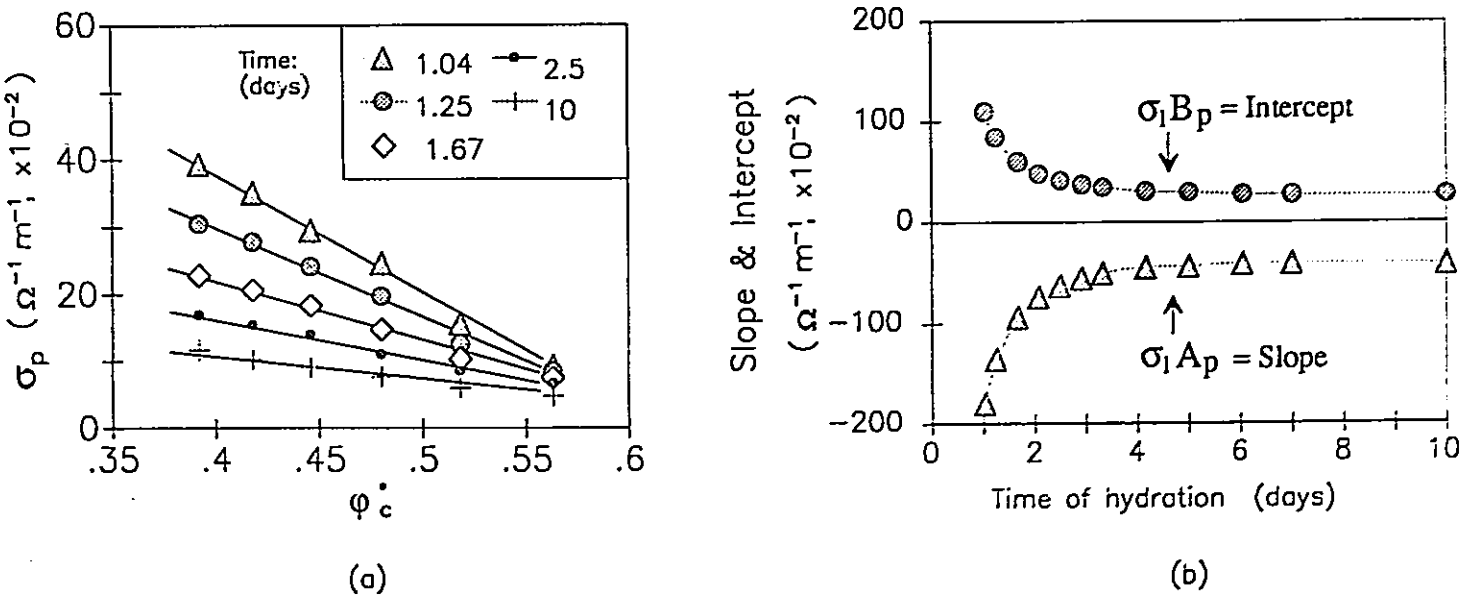

Figure 4.5. Experimental testing of equation (4-10)

the low alkali portland cement(LA in Table 3.2). The results are shown in figure 4.5.

4.3.3. Explanation of θ-Parameter Characteristics

According to equations (4-9) and (4-10), we have

$$\theta = \delta\,(\sigma_f - \sigma_p)$$

$$= \delta\,(\psi_{po} - \psi_{fo}) + \delta_w\,[\lambda_c\,(1\text{-}m) + \lambda_{gel}\,\eta_{gel}\,m + \lambda_{ca}\,\eta_{ca}\,m]\,\varphi_c^{\circ}\,\sigma_l \qquad (4\text{-}12)$$

Generally, $\psi_{po} \approx \psi_{fo}$, hence

$$\boxed{\theta = \delta_w\,[\lambda_c\,(1\text{-}m) + \lambda_{gel}\,\eta_{gel}\,m + \lambda_{ca}\,\eta_{ca}\,m]\,\varphi_c^{\circ}\,\sigma_l} \qquad (4\text{-}13)$$

or

$$\boxed{\theta = \frac{\delta_w\,\sigma_l}{1 + (w/c)\,(\rho_c/\rho_w)}\,[\lambda_c\,(1\text{-}m) + \lambda_{gel}\,\eta_{gel}\,m + \lambda_{ca}\,\eta_{ca}\,m]} \qquad (4\text{-}13')$$

All the features of θ-parameter described in the previous section can be explained in terms of the electrical conductivity models developed.

(1). $\theta > 0$.

This is the natural deduction of equation (4-13). It is apparent that the reason why $\theta > 0$ is due to the occurrence of the water film on the aggregate surface at mixing.

(2). θ is to a first approximation independent of w/c ratio.

This result readily leads to a deduction in terms of equation (4-13') by considering

$$\delta_w \propto 1 + (w/c)\,(\rho_c/\rho_w)\,,$$

which means that the thickness of the water film is directly proportional to the w/c ratio. In addition, the thickness of the effect region is also directly proportional to the w/c ratio since the volume of fresh cement paste is directly proportional to the w/c ratio. The total thickness of the interfacial zone is, therefore, directly proportional to the w/c ratio.

(3). θ appears to be independent of the type of the aggregate used in the investigation, i.e. limestone and silica glass.

This result can be explained by equation (4-13'). In equation (4-13'), only δ_w may have something to do with the properties of the aggregate, but non-porous and inert or slightly reactive aggregates, like limestone and silica glass, are not likely to affect δ_w significantly. Therefore it would be expected that the two aggregates would have almost the same θ values.

(4). $\frac{d\theta}{dt} < 0$, $\frac{d^2\theta}{dt^2} > 0$, and θ decreases quickly during the early hydration period followed by slow change approaching a constant value after about one week hydration.

From equation (4-13),

$$\frac{d\theta}{dt} = -\,\delta_w\,[\lambda_c - \lambda_{gel}\,\eta_{gel} - \lambda_{CH}\,\eta_{CH}\,m]\,\varphi_c^o\,\sigma_l\,(\frac{dm}{dt})\,, \quad (4\text{-}14)$$

from equation (4-10'),

$$[\lambda_c - \lambda_{gel}\,\eta_{gel} - \lambda_{ca}\,\eta_{ca}\,m]\left(\frac{dm}{dt}\right) = \left(\frac{dA_p}{dt}\right) \qquad (4\text{-}15)$$

As $\frac{dm}{dt} > 0$, hydration degree increases with time, and $\frac{dA_p}{dt} > 0$ from figure 4.5(b), it follows that

$$[\lambda_c - \lambda_{gel}\,\eta_{gel} - \lambda_{ca}\,\eta_{ca}\,m] > 0 \qquad (4\text{-}16)$$

Combing equation (4-14) and inequality (4-16) yields $\frac{d\theta}{dt} < 0$.

Also, from equation (4-14),

$$\frac{d^2\theta}{dt^2} = -\,\delta_w\,[\lambda_c - \lambda_{gel}\,\eta_{gel} - \lambda_{ca}\,\eta_{ca}\,m]\,\varphi_c^{\circ}\,\sigma_l\left(\frac{d^2m}{dt^2}\right) \qquad (4\text{-}17)$$

Since $\frac{d^2m}{dt^2} < 0$, the rate of hydration decreases with time, hence $\frac{d^2\theta}{dt^2} > 0$, which means that the θ vs t curve is concave.

The fact that θ changes very quickly during early hydration and then slowly is consistent with the hydration characteristic of cement.

4.3.4. Kinetic Features of the Interfacial Microstructure Formation

The formation of microstructure both in the interfacial zone and the bulk paste is a process in which the density of the system increases with hydration. According to the electrical conductivity theory, the density of the system can be measured by the area fraction of the solid phases. For the interfacial zone and the bulk paste, equation (4-1) becomes

$$\left.\begin{aligned} \psi_{fs} &= 1 - \frac{\sigma_f}{\sigma_l} \\ \psi_{ps} &= 1 - \frac{\sigma_p}{\sigma_l} \end{aligned}\right\} \qquad (4\text{–}18)$$

Microstructure formation rates can be determined using the following expressions

$$\left.\begin{aligned} \frac{d\psi_{fs}}{dt} &= -\frac{1}{\sigma_l}\frac{d\sigma_f}{dt} \\ \frac{d\psi_{ps}}{dt} &= -\frac{1}{\sigma_l}\frac{d\sigma_p}{dt} \end{aligned}\right\} \qquad (4\text{-}19)$$

Since

$$\frac{d\theta}{dt} < 0, \qquad \text{or} \qquad \frac{d\sigma_f}{dt} < \frac{d\sigma_p}{dt},$$

$$\text{or} \qquad \frac{\left(\frac{d\sigma_f}{dt}\right)}{\left(\frac{d\sigma_p}{dt}\right)} > 1, \ (\text{since } \frac{d\sigma_f}{dt} < 0 \text{ and } \frac{d\sigma_p}{dt} < 0)$$

from equation (4-19), we have

$$\frac{\left(\frac{d\psi_{fs}}{dt}\right)}{\left(\frac{d\psi_{ps}}{dt}\right)} = \frac{\left(\frac{d\sigma_f}{dt}\right)}{\left(\frac{d\sigma_p}{dt}\right)} > 1$$

or

$$\frac{d\psi_{fs}}{dt} > \frac{d\psi_{ps}}{dt} \qquad (4\text{-}20)$$

Inequality (4-20) indicates that the formation rate of the interfacial zone is higher than that of the bulk paste.

It is not intended to discuss in this work specific details about the microstructural features of the interfacial zone, such as enrichment with crystals like portlandite and ettringite, the preferred orientation of CH, the formation of the duplex film etc. It should be stressed, however, that these structural features mainly depend on crystal morphology and the crystal growth environment. The significance of the inert aggregate lies in its action as a low-barrier crystallization center. The existence of the water film is a decisive factor causing the porosity of the interfacial zone.

§4.4 FEATURES OF THE θ-PARAMETER DETERMINED FOR GRANULAR AGGREGATE-CEMENT PASTE SYSTEMS

The values of θ-parameter for granular aggregate-cement paste systems have been determined. The effects of aggregate size on the properties of the interfacial zone will be elucidated in this section.

Table 4.1. Particle size of aggregate

Limestone		Quartz	
US No. of Sieve	Mean radii of particles(mm)	US No. of Sieve	Mean radii of particles(mm)
#16 - #20	0.506	#14 - #20	0.561
#20 - #30	0.356	#20 - #30	0.356
#30 - #35	0.273	#30 - #35	0.273
#35 - #50	0.199	#35 - #50	0.199
#50 - #60	0.136	#50 - #60	0.136
#60 - #100	0.099	#60 - #100	0.099

Type 10 white portland cement was used. The chemical composition is given in Table 3.2. Two types of aggregate, limestone and quartz sand, were used. The limestone particles were obtained by crushing larger pieces. The particles were sieved to obtain different particle sizes, as shown in Table 4.1.

4.4.1. Quartz Particle-Portland Cement Paste Interface

The θ-parameter of the quartz mortar vs time of hydration is plotted in figure 4.6. It can be seen that θ has the following features:

(1). $\theta > 0$ for all aggregate sizes.

(2). $\frac{d\theta}{dt} > 0$ up to about 3 hours hydration; $\frac{d\theta}{dt} < 0$ and $\frac{d^2\theta}{dt^2} > 0$ after 3 hours.

(3). θ decreases with decreasing aggregate size.

The experimental results indicate that the first and second features of θ described above are completely consistent with that in the flat aggregate-cement system. This suggests that the hypothesis for the formation of the interfacial zone in the flat aggregate-cement paste system is applicable to the granular aggregate-cement system. The initial structure of the transition zone for the granular aggregate-cement system according to the hypothesis is depicted in figure 4.7. The water film around the aggregate particle and the "effect region" around the water film constitute the whole transition zone. The first and second features of θ can, therefore, be explained in a manner similar to that in the previous section.

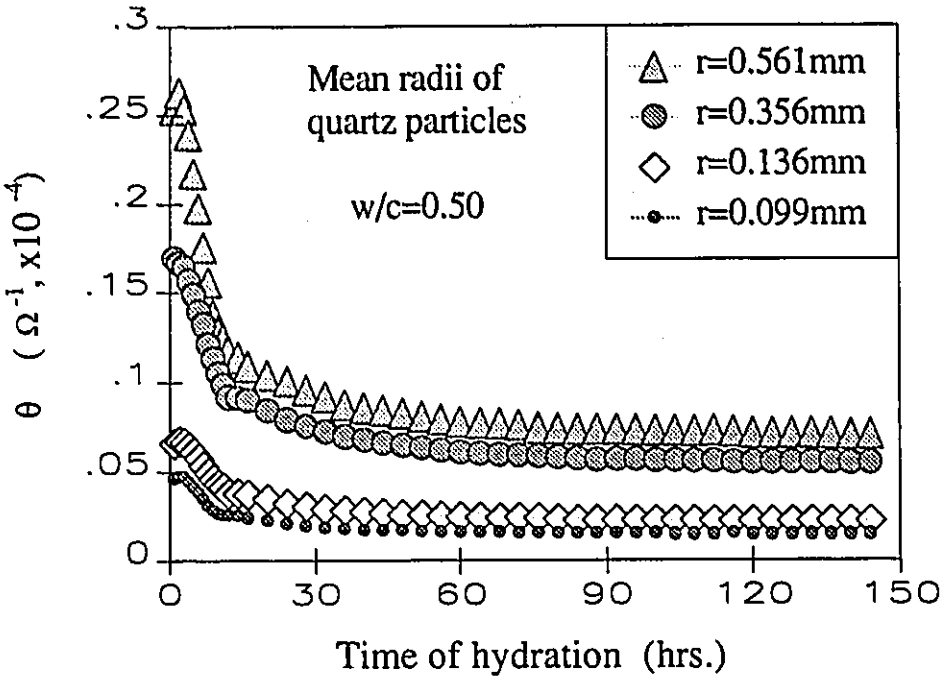

Figure 4.6. θ-parameter of quartz mortar vs hydration time

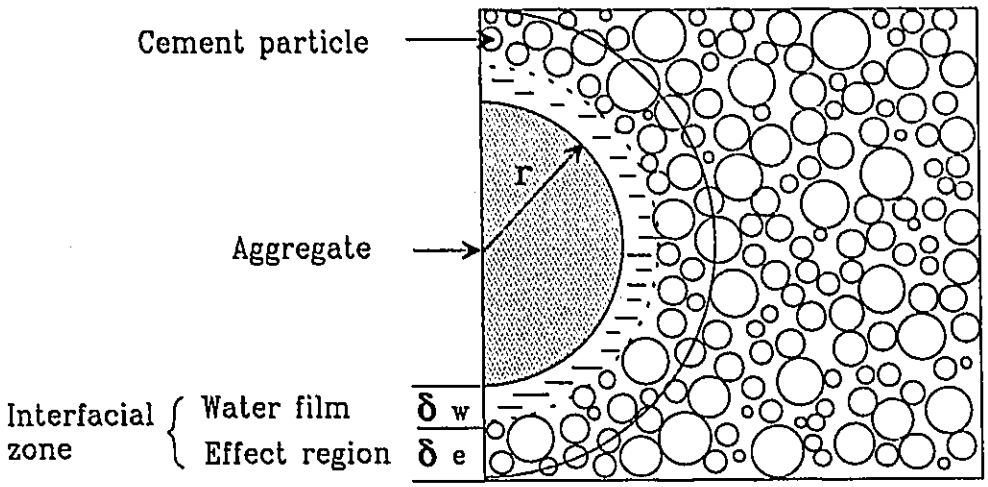

Figure 4.7. A sketch of the intical structure of the interfacial zone for mortar system

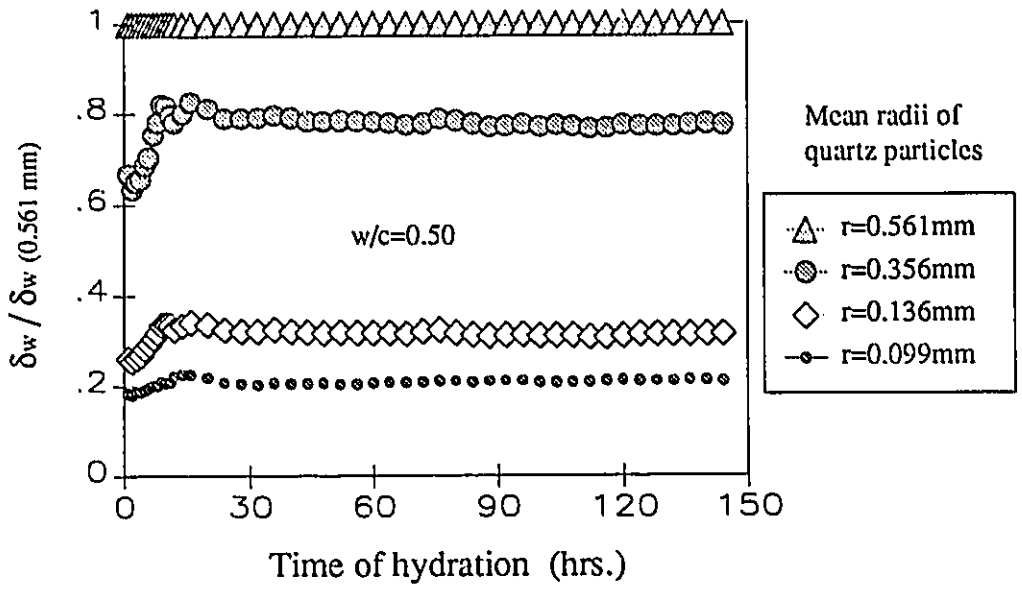

Figure 4.8. Relative thickness of the water film vs hydration time

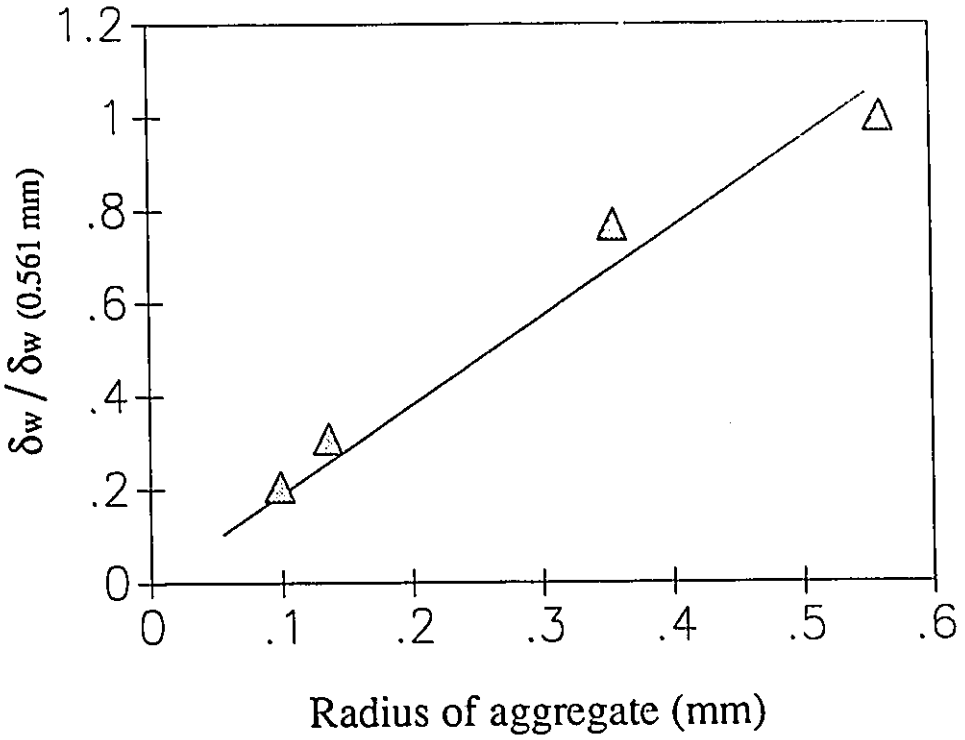

Figure 4.9. Relative thickness of the water film vs aggregate size

A new deduction can be obtained from the observation that θ decreases with decreasing aggregate size, i.e. the thickness of the water film on the aggregate surface at mixing decreases with decreasing aggregate size. This can be seen from equation (4-13). The relative thickness of the water film for the four aggregate sizes, relative to that for the aggregate with r=0.561 mm, can be calculated from figure 4.6 and equation (4-13).

$$\frac{\delta_w(r)}{\delta_w(0.561\ mm)} = \frac{\theta(r)}{\theta(0.561\ mm)}$$

Figure 4.8 is a plot of $\delta_w(r)/\delta_w(0.561mm)$ vs hydration time. It can be seen that $\delta_w(r)/\delta_w(0.561mm)$ is relatively constant after about 24 hours hydration. A plot of $\delta_w(r)/\delta_w(0.561mm)$ vs mean radii of aggregate particles reveals a linear dependence of the water film thickness ratio on aggregate size, figure 4.9. This result indicates that the water film thickness decreased linearly with decreasing aggregate size.

The thickness of the "effect region" also decreases with decreasing aggregate size since the distance the effects of the aggregate and the water film can reach decreases with decreasing aggregate size. The total effect is, therefore, that the interfacial zone thickness decreases with decreasing aggregate size.

4.4.2. Limestone Particle-Portland Cement Paste Interface

Figure 4.10 is a plot of the θ value of the limestone mortar vs hydration time.

A new feature of θ for the limestone mortar is observed. θ<0 when aggregate size is less than a critical value, r=0.199 mm. The features of θ are the same for the limestone particle-portland cement system as those for quartz mortar only when r>0.199 mm, viz

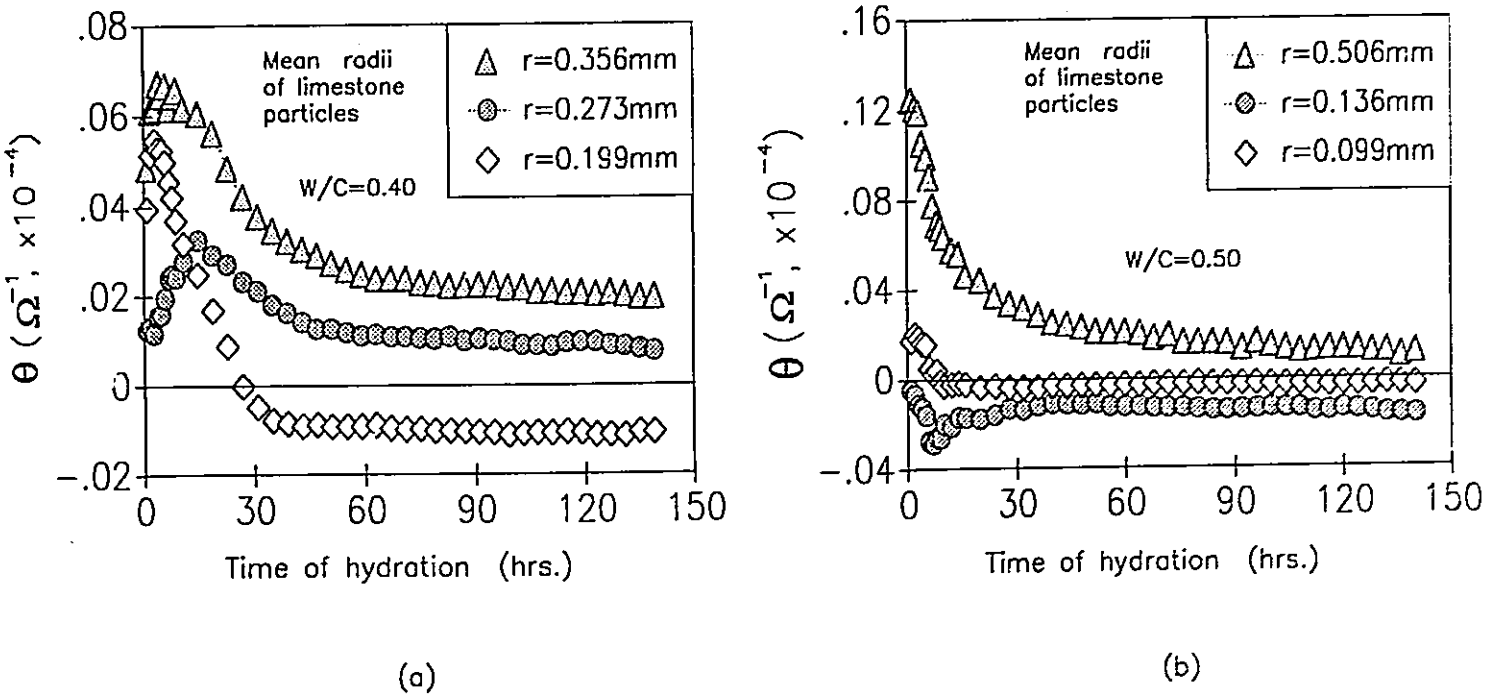

Figure 4.10. θ-parameter of limestone mortar vs hydation time
(a). w/c=0.40 (b). w/c=0.50

$\theta>0$ and the interfacial zone thickness decreases with decreasing aggregate size. The case is opposite as $r\leq 0.199$ mm, i.e. $\theta<0$. Physically the interfacial zone is structurally denser than the bulk paste.

This new feature of θ, $\theta<0$, can not be explained by the proposed hypothesis. A reasonable explanation for this phenomenon is that it likely results from chemical interaction between the limestone surface and portland cement paste. Reaction products are reported to contain carboaluminate hydrate[60,61]. Carbonate reactions affect hydration and microstructure of cement paste. Monteiro, et.al.[39] investigated the interaction between carbonate rock and portland cement paste and confirmed that carbonate rock reacts with calcium hydroxide at the interface. They reported etching of aggregate surfaces and the subsequent precipitation of much smaller crystals than calcium hydroxide. The author considers that chemical reactions between limestone particles and portland cement may result in $\theta<0$ for $r\leq 0.199$mm. The results indicate that the effects of these interactions on the structural features of the interfacial zone are significant only when $r\leq 0.199$ mm. This is understandable since the total surface area of aggregate for the reaction increases with the decreasing of the aggregate particle size.

The derivative $\frac{d\theta}{dt} > 0$ only at early hydration time. This is likely a result of increasing electrical conductivity of the pore solution in the sample with time during this period.

4.4.3. Effect of the Electrical Conductivity of Pore Solution on θ-Parameter

It can be seen from equation (4-13') that the value of θ-parameter is dependent on two principal factors, interfacial microstructure and the electrical conductivity of the pore

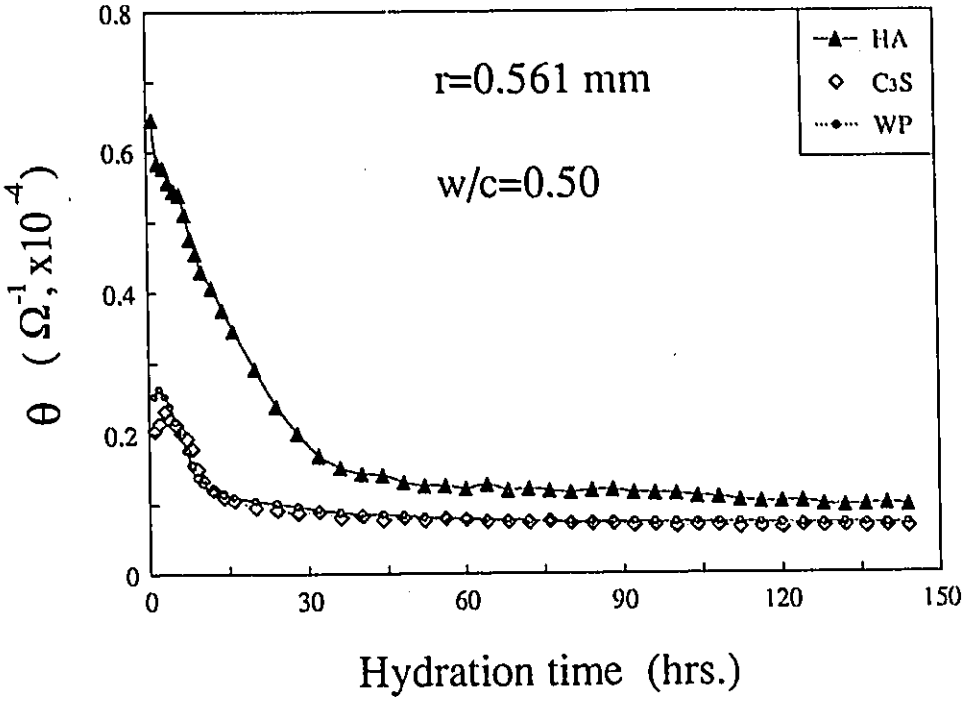

Figure 4.11. Effect of chemical composition of cement on θ-parameter

solution. It is suggested that the latter is dependent on the ionic concentrations of the pore solution.

Three types of cement were used to demonstrate the effect of the pore solution, high alkali portland cement(HA in Table 3), white portland cement(WP) and pure C_3S. The aggregate is quartz sand.

The plot of θ vs hydration time is shown in figure 4.11. The highest value of θ for high alkali cement is obtained, and the other two have the almost same value. It is suggested that the three systems have approximately the same microstructures at the same hydration age. The experimental results indicate, therefore, that the electrical conductivity of the pore solution depends principally on the concentration of alkali in the solution; the alkali increases with increasing alkali content of cement, since the white portland cement used contains little and the C_3S essentially none.

§4.5 EFFECT OF INTERFACIAL ZONE MICROSTRUCTURE ON BOND STRENGTH OF AGGREGATE-CEMENT PASTE INTERFACES

It is well recognized that the bond strength of the aggregate-cement paste interface is dependent on interfacial microstructure. The previous sections have described microstructural features and the formation process of the interfacial zone between non-porous aggregate and portland cement paste using an electrical conductivity model. The same approach can be used to relate interfacial bond strength to microstructural features of the interfacial zone.

This section describes the development of a relationship between interfacial bond

strength and interfacial zone microstructure. Microstructural factors affecting the bond strength will be elucidated.

4.5.1. General Equation

No current strength theory has been applied directly to the interface between aggregate and cement paste due to the complexity of the microstructure. As a first approximation, interfacial bond strength can be considered to be directly proportional to the total area fraction of solid phases associated with the fracture surface in the interfacial zone, i.e.

$$P_f \propto \psi_{fs}$$

or

$$P_f = P_{fo}\,\psi_{fs} \qquad (4\text{–}21)$$

where, P_f is the interfacial bond strength, and ψ_{fs} is the total area fraction of solid phases along the fracture surface in the interfacial zone, and P_{fo} is the interfacial bond strength in the case, $\psi_{fs}=1$, or zero-porosity bond strength. P_{fo}, however, can not be conceptually considered as the "intrinsic strength" of the interface since both composition and development of microstructure in the interfacial zone are time-dependent.

Since $\psi_{fs} = 1 - \frac{\sigma_f}{\sigma_i}$, equation (4-21) can be expressed as

$$P_f = P_{fo}\left(1 - \frac{\sigma_f}{\sigma_i}\right) \qquad (4\text{-}22)$$

Equation (4-22) relates bond strength and electrical conductivity of the aggregate-cement

paste interface, viz. the interfacial bond strength is linearly dependent on the ratio of interface and pore solution conductivity.

4.5.2. Interfacial Bond Strength of Non-Porous Aggregate-Portland Cement Paste Systems

Equation (4-22) is a general equation expected to hold for any aggregate-cement paste interface. For non-porous aggregate-portland cement paste system, substituting equation (4-9) into equation (4-22) yields:

$$P_f = P_{fo} [\psi_{fo} + (\frac{\delta_c}{\delta}) \Phi \varphi_c^\circ]$$

$$= P_{fo} [\psi_{fo} + (1 - \frac{\delta_w}{\delta}) \Phi \varphi_c^\circ]$$

$$= P_{fo} \left[\psi_{fo} + \frac{(1 - \frac{\delta_w}{\delta})}{1 + (w/c)(\rho_c/\rho_w)} \Phi \right] \qquad (4\text{-}23)$$

where, $\Phi = [\lambda_c (1-m) + \lambda_{gel} \eta_{gel} m + \lambda_{ca} \eta_{ca} m]$.

It can be inferred from equation (4-23) that there are two microstructural factors that affect the interfacial bond strength:

(1). Interfacial structure factor, δ_w/δ (or δ_c/δ): interfacial bond strength decreases with δ_w/δ, the thickness of the water layer relative to the thickness of the interfacial zone.

(2). Bulk paste structure factor,φ_c° (or w/c ratio): increasing φ_c° (or decreasing w/c ratio)

will increase the bond strength.

4.5.3. Validation of the Theoretical Relationship

Experimental results obtained by Liu et al.[62] were used to validate the relationship given by equation (4-23).

Plots of both tensile strength and shear strength of limestone- and quartz-portland cement paste interfaces vs φ_c^o are given in figure 4.12 and figure 4.13, respectively. It can be seen that interfacial bond strength(tensile and shear), is directly proportional to φ_c^o or inversely proportional to w/c ratio.

Interpretation as equation (4-23) and the experimental results, suggests that there are two possible ways to increase the interfacial bond strength. One is to decrease the thickness of the water film on the aggregate surface at the beginning of mixing. An excellent example is given by R. Zimbelmann[63]. It was shown that the bond strength was increased by 100 to 180% by adding some tensides into the mixing water to reduce the thickness of the water film. The other way to increase the bond strength is to use low w/c ratio. It is well known that w/c ratio determines the initial porosity of cement paste and a low w/c ratio is an essential prerequisite for preparing high strength concrete. Equation (4-23) indicates that low w/c ratio is also a necessary condition to enhance the interface between non-porous aggregate and portland cement paste.

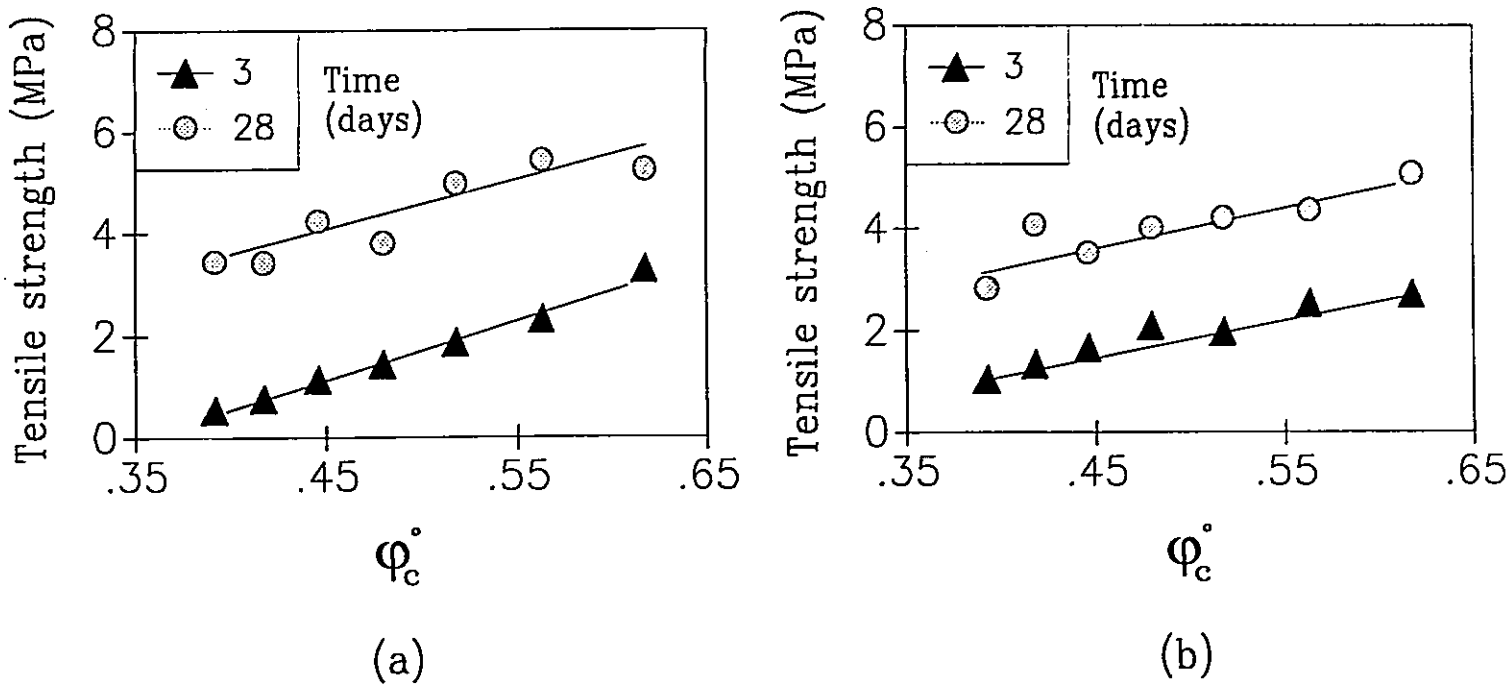

Figure 4.12. Interfacial tensile strength vs initial volume fraction of cement
(a). limestone (b). quartz

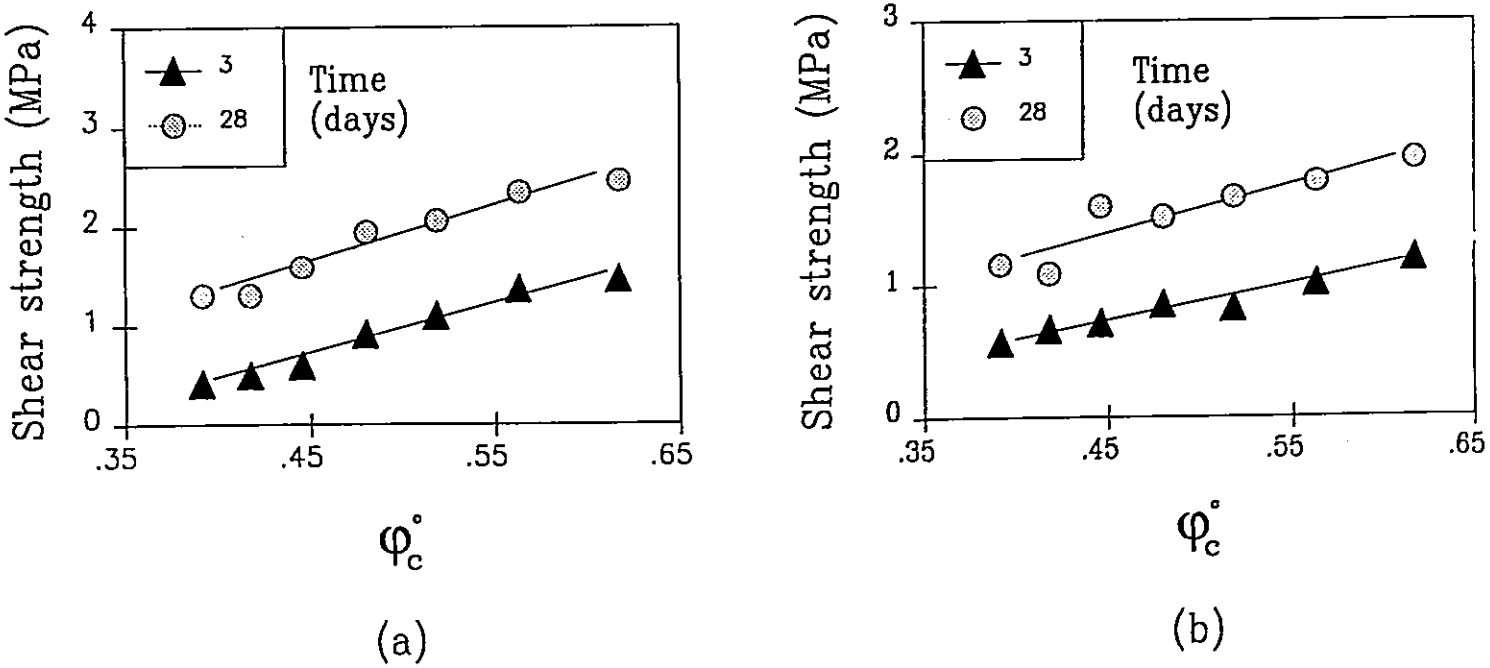

Figure 4.13. Interfacial shear strength vs initial volume fraction of cement
(a). limestone (b). quartz

§4.6 CONCLUSIONS

In summary the following conclusions appear warranted:

(1). The theory based on electrical conductivity methods presented in this chapter has been validated by an extensive number experiments. The θ-parameter, referred to as interfacial excess conductance, has been demonstrated to be a powerful microstructural descriptor of the interfacial zone.

(2). The following new findings pertaining to the nature of non-porous aggregate-cement paste interfaces have been obtained through application of the methods developed:

(i). The interfacial zone is generally less dense than the bulk paste.

(ii). The rate of formation of interfacial microstructure is greater than that of the bulk paste.

(iii). The thickness of the interfacial zone decreases with decreasing aggregate size.

(iv). The thicknesses of the water film on the aggregate surface at mixing and the whole interfacial zone increase with w/c ratio.

(3). A hypothesis for interfacial zone formation was validated by development and application of the electrical conductivity models of the interfacial zone and the bulk paste. The hypothesis emphasizes two elements for the interfacial zone formation: (i). the existence of the water film on the aggregate surface at the beginning of mixing; (ii). the "effect region" containing a few layers of cement particles close to the water film as a

source of the hydrates for formation and development of the interfacial microstructure. The existence of the water film is a decisive factor causing the porosity of the interfacial zone.

(4). The chemical reaction between the aggregate and the cement paste for limestone-portland cement system can be detected by determining the value of θ-parameter if aggregate size is reduced to a critical value.

(5). The electrical conductivity of the pore solution depends principally on the concentration of alkali in the solution.

(6). A relationship between the interfacial microstructure and the interfacial bond strength has been developed and validated. There are two principal microstructural factors influencing bond strength, i.e. the thickness of the water film on the aggregate surface at mixing and w/c ratio. It is suggested that decreasing the thickness of the water film and w/c ratio are two possible ways to increase the bond strength.

CHAPTER FIVE

MODIFICATION OF INTERFACIAL MICROSTRUCTURE–SILICA FUME COATING OF AGGREGATE SURFACES

SUMMARY

A new method of enhancing interfacial microstructure, coating aggregate surfaces with silica fume, is developed. Electrical conductivity experiments and SEM/EDXA indicate that the interfacial microstructure can be effectively densified by aggregate surface treatment. The mechanism of interfacial densification lies in the pozzolanic reaction between silica fume and calcium hydroxide. The consequence of interfacial densification is that compressive strength and sulphate resistance of mortar are increased; bending strength is however increased only at later ages.

§5.1 INTRODUCTION

The previous work concerning interfacial modification and its attendant problems were presented in chapter one. The following sections will describe a simple and effective

method of interfacial modification and its effects on mechanical properties and durability of mortar specimen.

The proposed method is based on the concept of coating aggregate surfaces with an effective material before mixing. Important consideration are that the coating procedure should be simple and the coating material should be effective in reducing the amount of CH in the interfacial zone.

Emphasis will be given to the coating method and testing its efficiency.

§5.2 SILICA FUME COATING OF AGGREGATE SURFACES

5.2.1. Design of Silica Fume Coating on the Aggregate Surface

idea of coating aggregate surfaces with silica fume to enhance the interfacial microstructure results from the following facts:

(1). There are a large number of CH particles in the interfacial zone.

(2). Silica fume is a highly reactive pozzolanic material. It can quickly react with CH to form C-S-H products, the principal source of strength of portland cement-based materials.

Therefore, the principal purpose for coating aggregate surfaces with silica fume is to reduce the amount of CH in the interfacial zone, to increase the amount of C-S-H gel and to densify the interfacial microstructure.

The silica fume coated aggregate-cement system is illustrated in figure 5.1.

The principal design index for the silica fume coating is the thickness of the coating layer on the aggregate surface, δ. The amount of silica fume needed for a specific thickness of the coating layer can be calculated using the following equation:

$$\alpha = \left[(1 + \frac{\delta}{r})^3 - 1 \right] \frac{\rho_{SF}}{\rho_a} \qquad (5\text{-}1)$$

where, α is the weight ratio of silica fume to the aggregate weight, δ is the design thickness of the silica fume coating, r is the radius of aggregate and ρ_{SF} , ρ_a are the densities of silica fume and aggregate, respectively. It can be seen from equation (5-1) that the value of α is dependent on the design thickness of the coating, δ, and the size of aggregate, r.

5.2.2. Coating Procedure

The coating procedure is briefly described as follows:

(1). A water film surrounding the aggregate particles is formed by mixing the aggregate with a small amount of water. The amount of water depends on the amount and size of aggregate and is generally 1-3% by weight of aggregate.

(2). The wet aggregate particles are then mixed with silica fume and a layer of silica fume slurry forms on the aggregate surfaces. The amount of silica fume used depends on the design thickness of the coating and aggregate size, as indicated by equation (5-1).

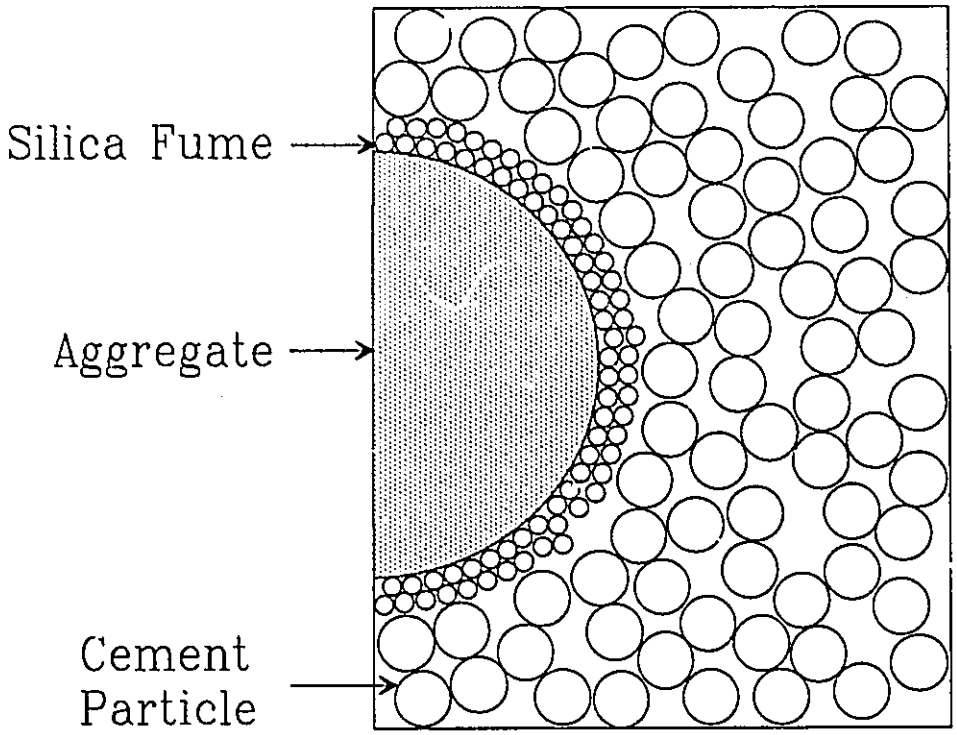

Figure 5.1. A schematic illustrating interfacial microstructure of the silica fume coated aggregate-cement paste system

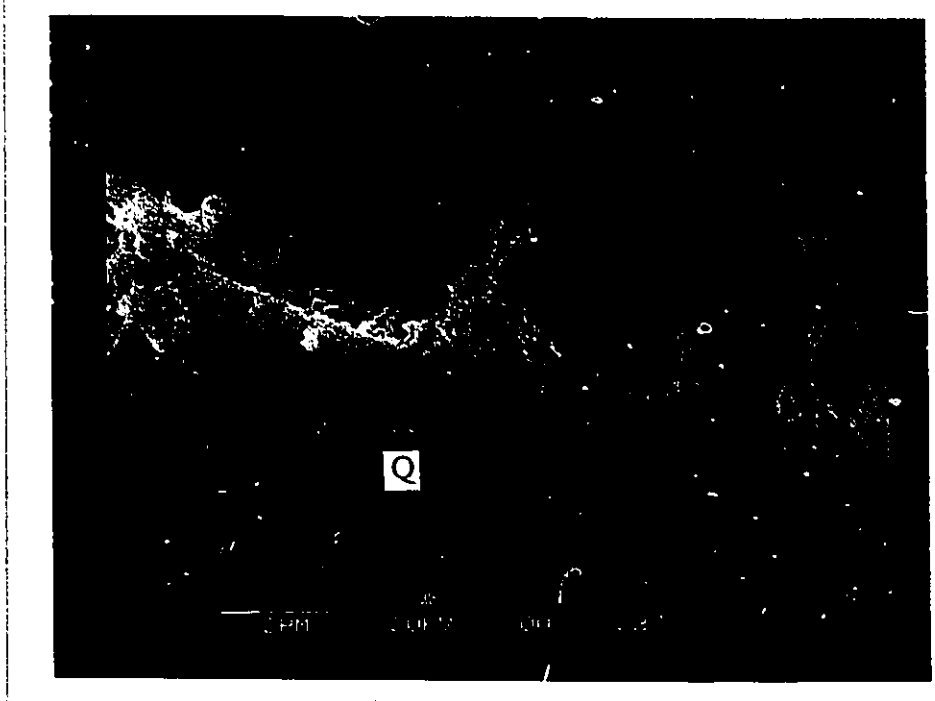

Figure 5.2. Micrograph of silica fume coating layer on quartz surface
Q - Quartz, SF - Silica Fume

(3). The aggregate-silica fume slurry system is then oven-dried to obtain particles coated with a densely consolidated layer of silica fume.

5.2.3. Mechanism of the Stability of the Silica Fume Layer

Figure 5.2 shows the appearance of quartz-silica fume coating interfacial region after treatment using the above procedure. It can be seen that the silica fume coating layer is physically stable and remains intact subsequent to the fracture of the aggregate particle itself. This raises a question as to the formation mechanism of the silica fume layer. The possible mechanisms are described as follows:

(1). Cohesion of the silica fume particle system.

Silica fume particle has a very small particle size, with the diameter generally being about 0.1-0.2 μm. The specific surface area of silica fume is typically about 21×10^3 m^2/kg. The silica fume system is, therefore, a porous system with a huge internal surface area. This would be expected to produce some capillary effects when silica fume slurry is being dried. Figure 5.3 illustrates the capillary effect. When the silica fume slurry is partially dried, a meniscus forms between two particles, as shown in figure 5.3(a). This results in a tensile stress in the water, which pulls the particles toward one another. The whole system, therefore, will shrink under this tensile stress. When the system is completely dried, the silica fume particles stick together and the cohesive force of the system is the sum of the Van de Waal's force between particles.

The maximum tensile stress, P, can be estimated by applying the following equation[64]:

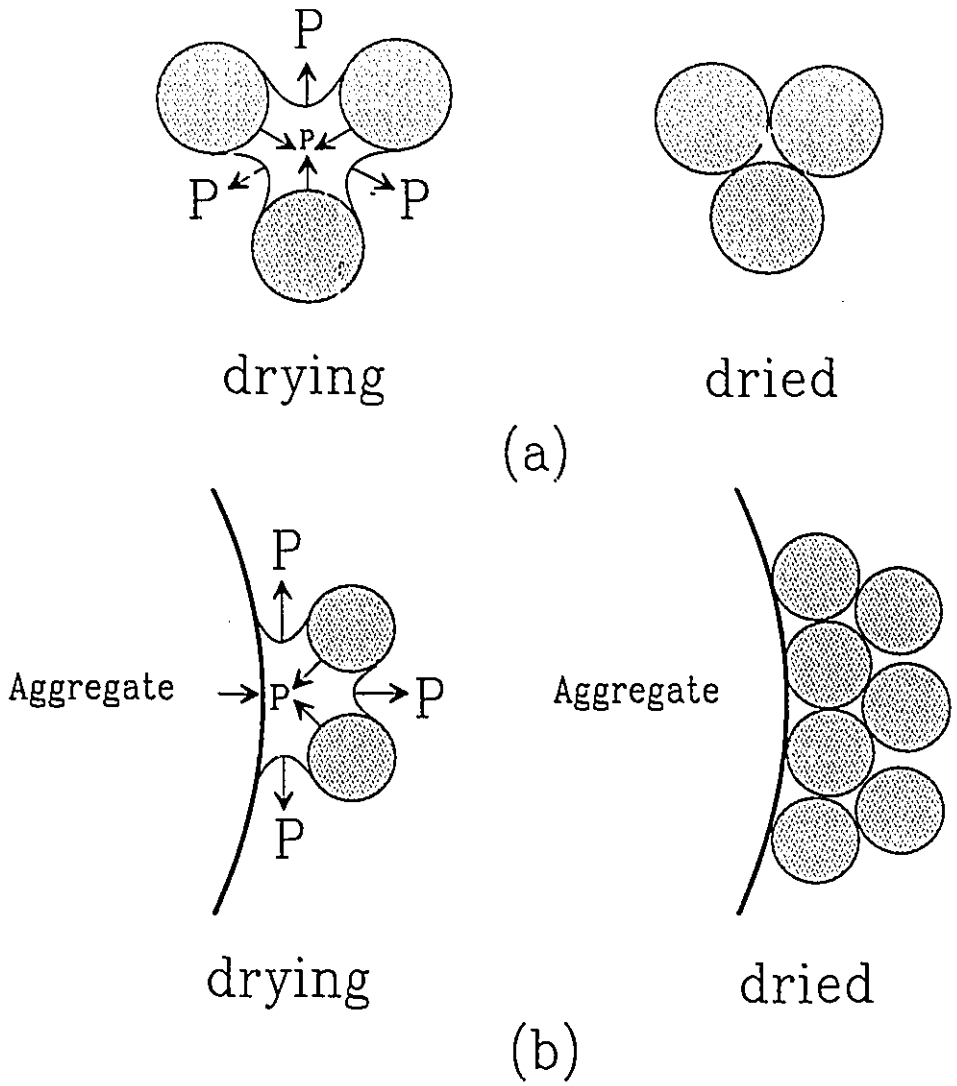

Figure 5.3. Sketch of the formation mechanism of silica fume coatings on aggregate surfaces

$$P = 2.6 \times 10^{-7} \gamma S_{SF} \rho_{SF} \qquad \text{(MPa)} \qquad (5\text{-}2)$$

where, ρ_{SF} (kg/m^3), S_{SF} (m^2/kg) are the density and specific surface area of silica fume, respectively, γ is the surface tension of water, ie. 7.3 x 10^{-2} N/m, and 2.6 x 10^{-7} is a dimensionless constant. The value of P for the silica fume used is estimated to be about 0.9 MPa.

(2). Adhesion of silica fume layer on the aggregate surface.

It is suggested that adhesion of silica fume on aggregate surface is due to the same reason as that described above, as shown in figure 5.3(b).

§5.3 MICROSTRUCTURAL FEATURES OF SILICA FUME COATED AGGREGATE-CEMENT PASTE INTERFACES

5.3.1. Assessment of Interface Modification by Electrical Conductivity Methods

Experiments were conducted to test the efficiency of the coated aggregates in improving the interfacial zone.

White portland cement was used. Limestone and quartz sand with average radii 0.506 mm and 0.561 mm respectively were used as aggregates. Silica fume coated aggregates were prepared with the design thickness of the silica fume layer about 10-30 μm. The microstructural features of coated aggregate-cement paste interfaces revealed by the electrical conductivity methods are demonstrated as follows.

5.3.1.1. Effects of silica fume coated aggregate on interfacial microstructure

Values of the interface microstructural parame ", θ, for mortar containing aggregate with and without silica fume coatings are plotted in figure 5.4 against hydration time for both limestone and quartz containing mortar.

The following observations are made from an analysis of data in figure 5.4. The θ parameter is always positive for mortar without silica fume coating, indicating a more porous interfacial zone than bulk paste, as discussed previous chapters. The θ parameter for aggregate with a silica fume coating, however, changes from positive to negative at about three to four days of hydration. This result indicates that the electrical conductivity of the interfacial zone is greater than that corresponding to the bulk paste during the first few days of hydration but rapidly decreases to a value less than that for bulk paste thereafter. Two possible causes for the above phenomenon are suggested. A water film may still exist around the coating layer when coated aggregate is mixed with fresh cement paste. The porosity of this region, therefore, is higher than that of matrix. The coating consisting of silica fume particles, however, is reactive unlike an inert aggregate surface and it reacts with calcium hydroxide to produce C-S-H product. This eliminates the effect of the water film eventually and gradually enhances the microstructure of interfacial zone. It has been shown that such a chemical (pozzolanic) reaction can begin at early hydration times[65]. The other possible effect that could result in change of θ from positive to negative is a decrease in electrical conductivity of the pore solution in the interfacial zone. Electrical conduction in saturated concrete is assisted by ions in the pore solution and electrical conductivity of the pore solution is dependent on ionic concentration. Some researchers have reported that the concentrations of both cations and anions in the pore solution would substantially decrease in the case of silica fume

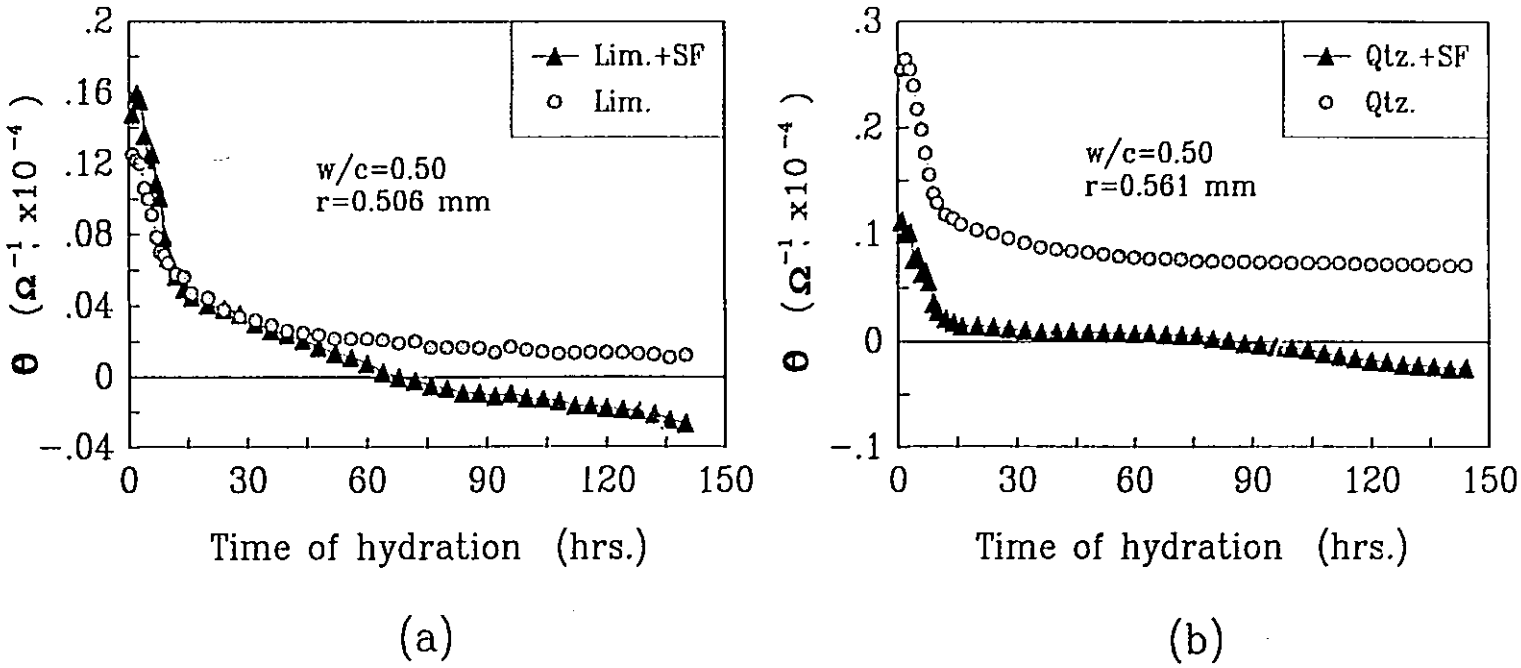

Figure 5.4. Effect of silica fume coated aggregate on θ-parameter
(a). limestone mortar (b). quartz mortar

addition[66]. The above two effects can both be attributed to pozzolanic reaction of silica fume with calcium hydroxide.

It is instructive to compare the value of θ for the coated quartz-cement paste system with paste made from a blend of silica fume added to the bulk paste in an amount equivalent to that required to coat the aggregates. The results are plotted in figure 5.5. It can be seen from figure 5.5 that $\theta > 0$ for this system, which implies that the interfacial zone is less dense than the bulk paste. This is obvious since the principal effect of this silica fume lies in the densification of the bulk paste instead of the interfacial zone. This result indicates that the partial replacement of cement by silica fume in most previous work enhances principally the bulk paste microstructure, and only marginally the interfacial microstructure.

5.3.1.2. Effects of aggregate type on interfacial zone development in presence of silica fume coatings

θ parameters for both limestone and quartz mortars, both containing aggregates coated with silica fume, are plotted against time in figure 5.6. The results show that the θ-parameter for both mortars has almost the same value when θ is negative. It is apparent that chemical composition and microstructure of the interfacial zone for the two mortars are similar after pozzolanic reaction takes place even though the aggregates used are completely different. θ values during early hydration for the two mortars are however quite different. Values for quartz mortar are greater than the limestone mortar. It is suggested that this is due to the effects of a water film around the silica fume coating at mixing and the particle size of aggregate. As described in chapter three, a larger aggregate size is associated with a thicker water film and a greater θ value. The above

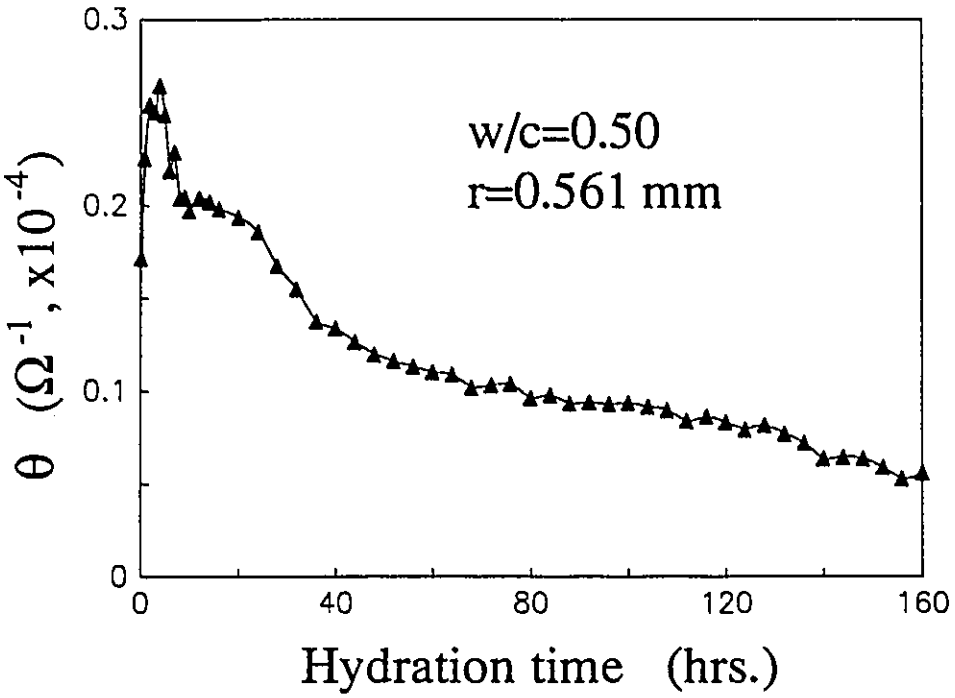

Figure 5.5. θ-parameter of the quartz-cement paste system made with a cement blend containing an amound of silica fume equivalent to that used in coating the aggregate

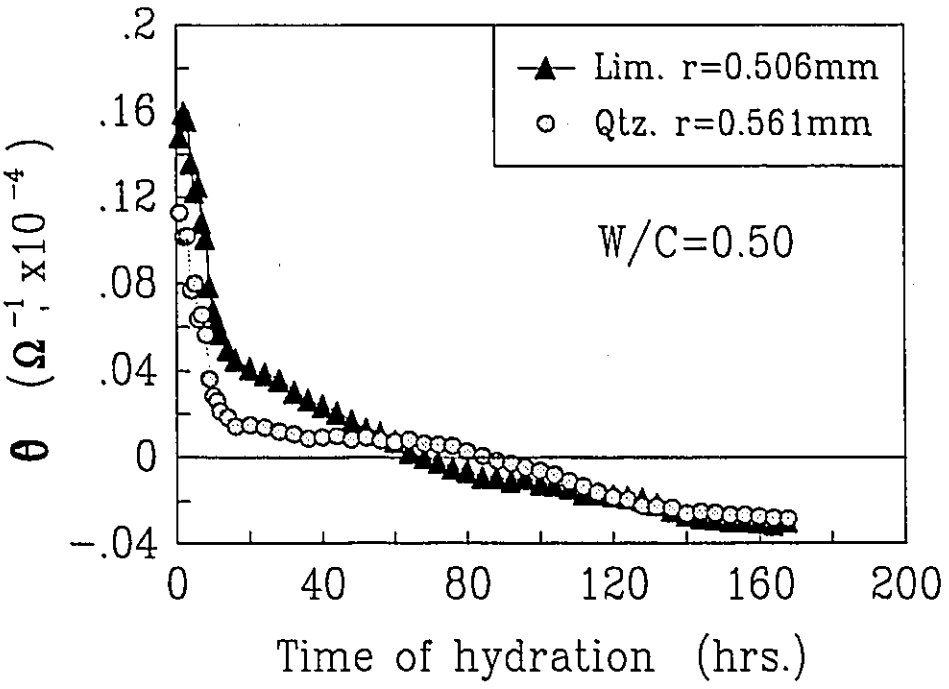

Figure 5.6. Effect of aggregate type on θ-parameter of mortar containing silica fume coated aggregate

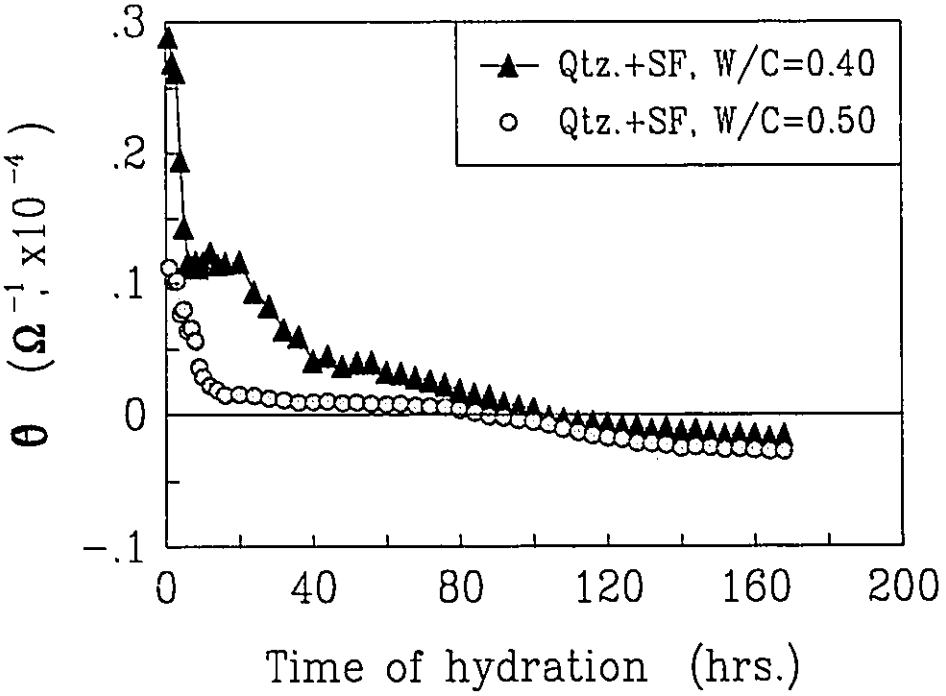

Figure 5.7. Effect of w/c ratio on θ-parameterof quartz mortar containing silica fume coated aggregate

results indicate that the effect of a water film can be gradually eliminated with the hydration process.

5.3.1.3. Effect of w/c ratio on microstructure of the interfacial zone

The effect of w/c ratio on the θ parameter for quartz mortar containing silica fume coated aggregate is illustrated in figure 5.7.

The results in figure 5.7 indicate that the lower the w/c ratio is, the greater is the θ value. It is noted however that this result does not imply any direct relationship between w/c ratio and microstructure of the interfacial zone principally composed of silica fume and products of pozzolanic reaction. It is known that the effect of w/c ratio on microstructure of cement paste lies in its determining the initial porosity of the paste. Obviously, the initial porosity of such an interfacial zone is not influenced by w/c ratio. This situation is quite different from the case with no silica fume coating, where the thickness of water film and whole transition zone increases with increasing w/c ratio. The w/c ratio does however affect the microstructure of bulk paste. Therefore, the effect of w/c ratio on the θ parameter for mortar containing silica fume coated aggregate lies in its influencing the electrical conductivity of the bulk cement paste instead of interfacial zone conductivity. The lower w/c ratio, the lower the electrical conductivity of cement paste and hence the greater θ value.

5.3.2. Observations by SEM/EDXA Techniques

The morphology of the aggregate-silica fume layer-cement paste region was directly observed by SEM, and the Ca/Si ratio in the silica fume layer was determined by

EDXA(Energy Dispersive X-ray Analysis) technique. The microstructural features of this region and changes with hydration time are described as follows.

Figure 5.8 and figure 5.9 illustrate the morphology of the aggregate-silica fume layer-cement paste region at 1 day hydration time in quartz and limestone mortars respectively. The principal characteristics at this time is that the aggregate-SF(silica fume) interface and SF layer itself are apparently less porous than SF-cement paste interface.

The morphology at 3 days hydration is shown in figure 5.10 and figure 5.11. It can be seen that a large number of CH(portlandite) particles, up to 10 μm thick for quartz mortar, form at SF-paste layer and layered CH has preferred orientation with the c-axis normal to aggregate surface. This is consistent with electrical conductivity methods indicating that a water film forms around the silica fume layer when coated aggregate is mixed with fresh cement paste.

The silica fume layer appears to be more dense at 7 days hydration, figure 5.12 and figure 5.13. The CH layer can still be observed. The thickness, however, seems to be less than that at 3 days, ie. 4-5 μm thick. The reason is probably that more CH is consumed by the chemical(pozzolanic) reaction between silica fume and CH with hydration.

The presence of layered CH at SF-paste interface is not easily detected at 14 days hydration, figure 5.14 and figure 5.15. The quartz-SF interface appears very intimate and tight. The SF layer itself appears to be more dense than the bulk paste.

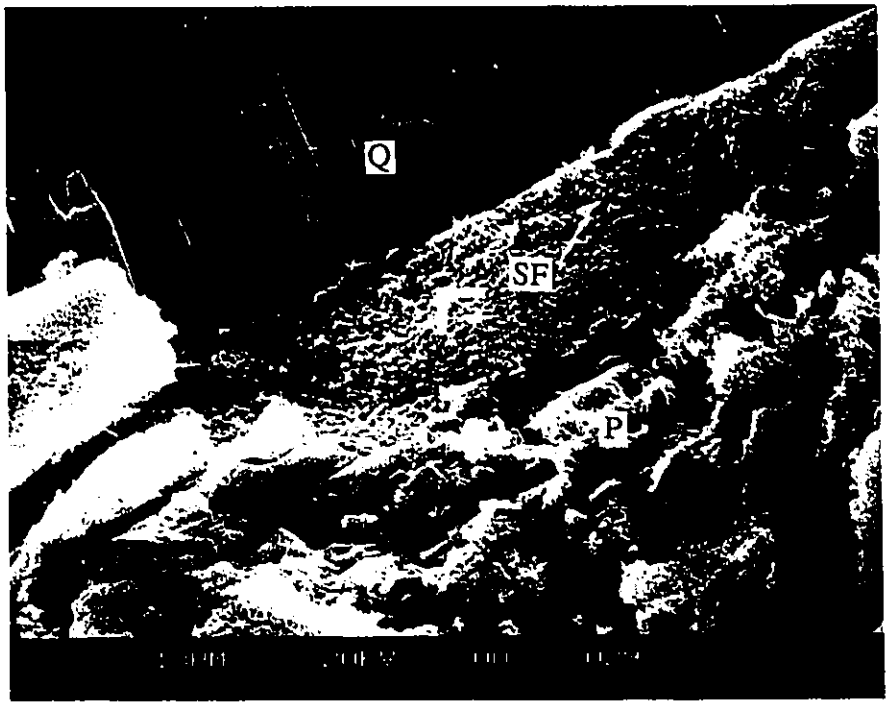

Figure 5.8. Micrograph of SF coated quartz-cement paste interface at 1 day hydration
Q - Quartz, SF - Silica Fume, P - Paste

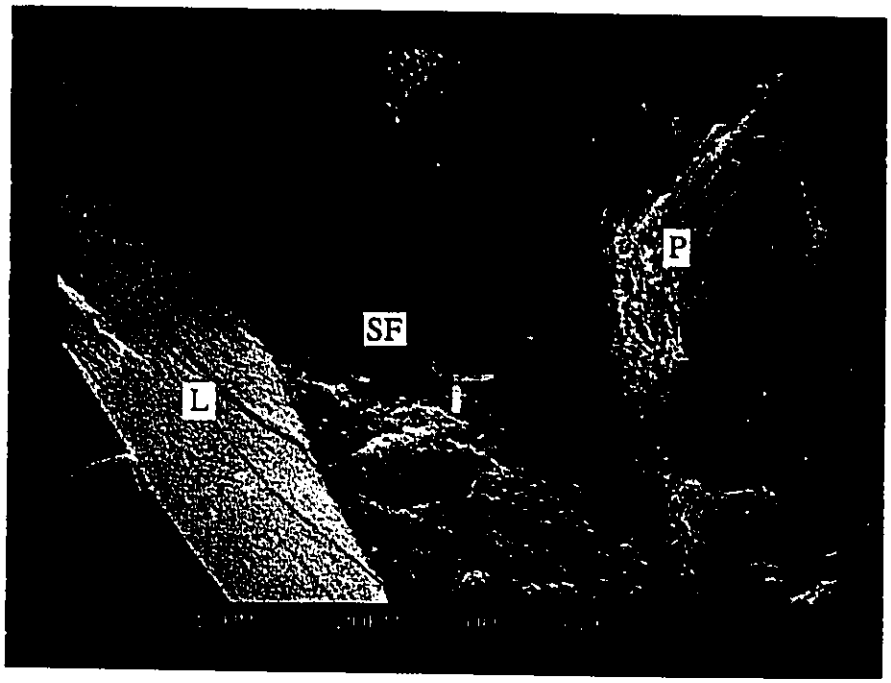

Figure 5.9. Micrograph of SF coated limestone-cement paste interface at 1 day hydration
L - Limestone, SF - Silica Fume, P - Paste

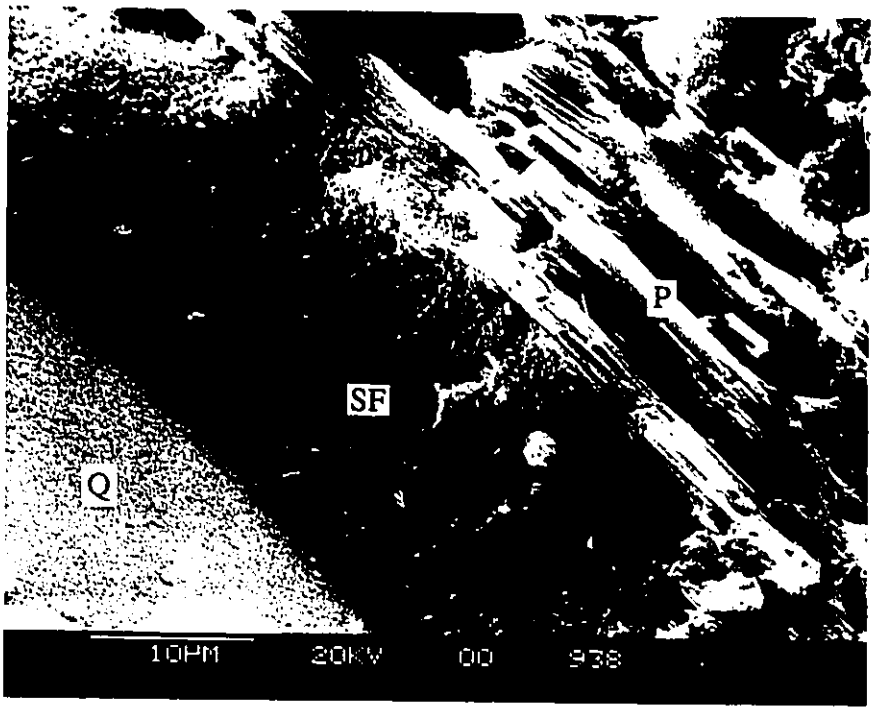

Figure 5.10. Micrograph of SF coated quartz-cement paste interface at 3 days hydration

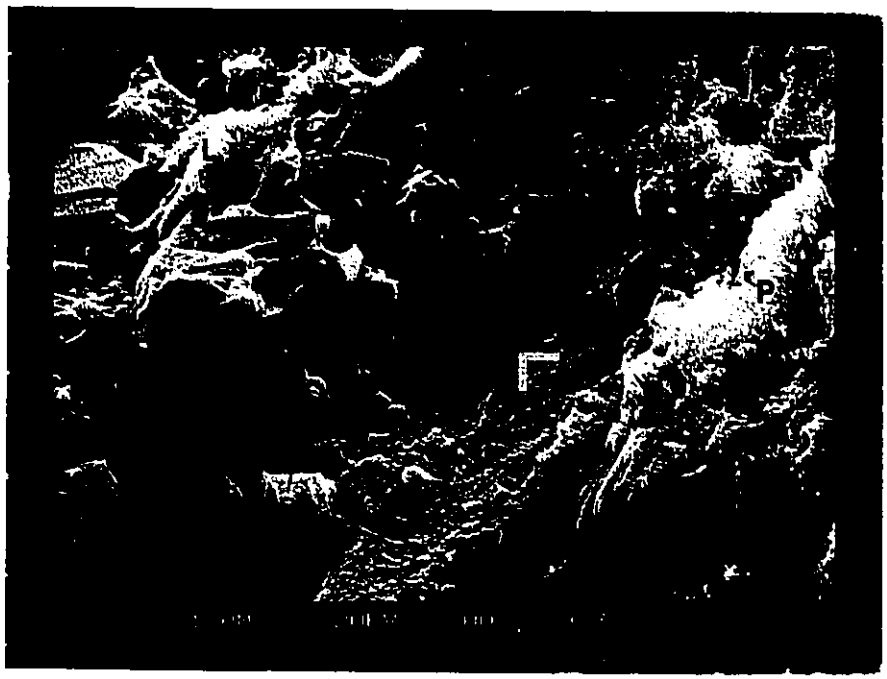

Figure 5.11. Micrograph of SF coated limestone-cement paste interface at 3 days hydration

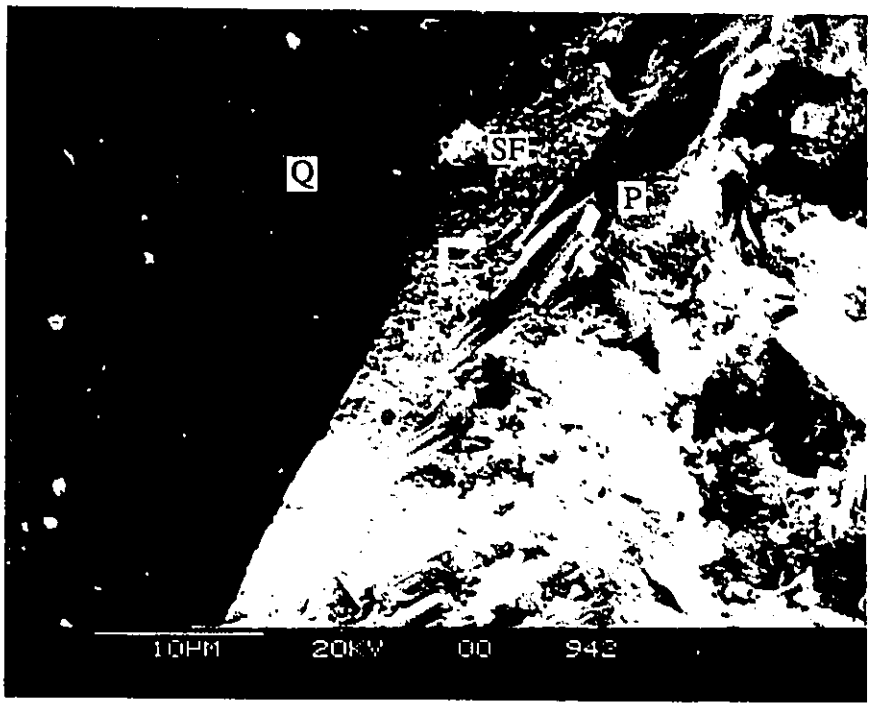

Figure 5.12. Micrograph of SF coated quartz-cement paste interface at 7 days hydration

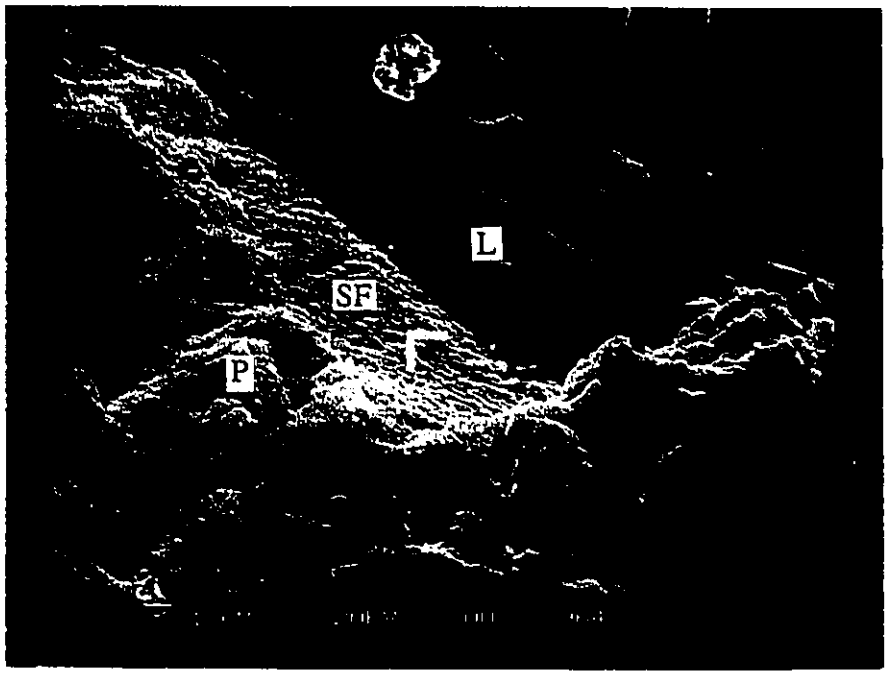

Figure 5.13. Micrograph of SF coated limestone-cement paste interface at 7 days hydration

Figure 5.14. Micrograph of SF coated quartz-cement paste interface at 14 days hydration

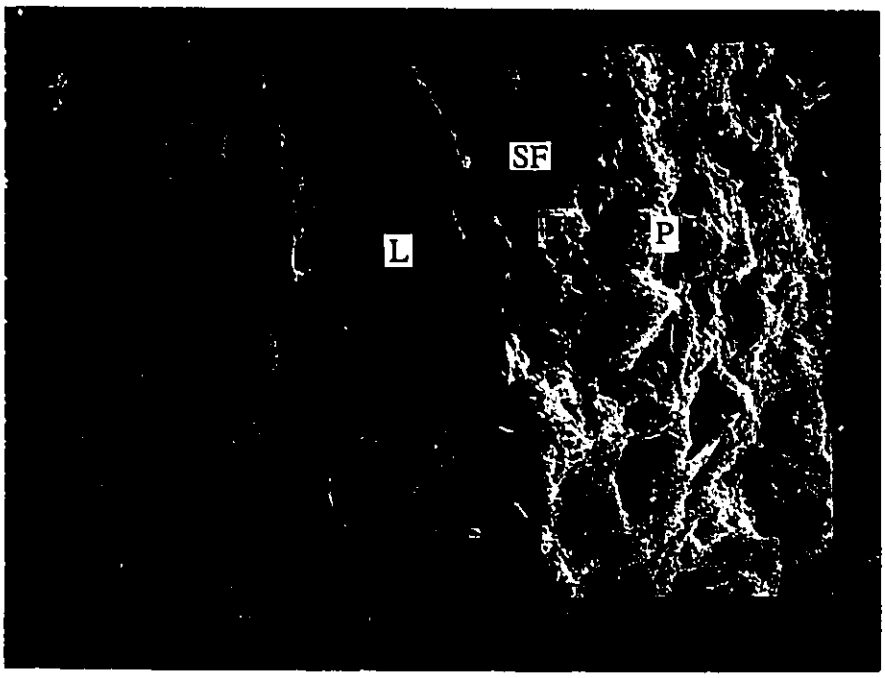

Figure 5.15. Micrograph of SF coated limestone-cement paste interface at 14 days hydration

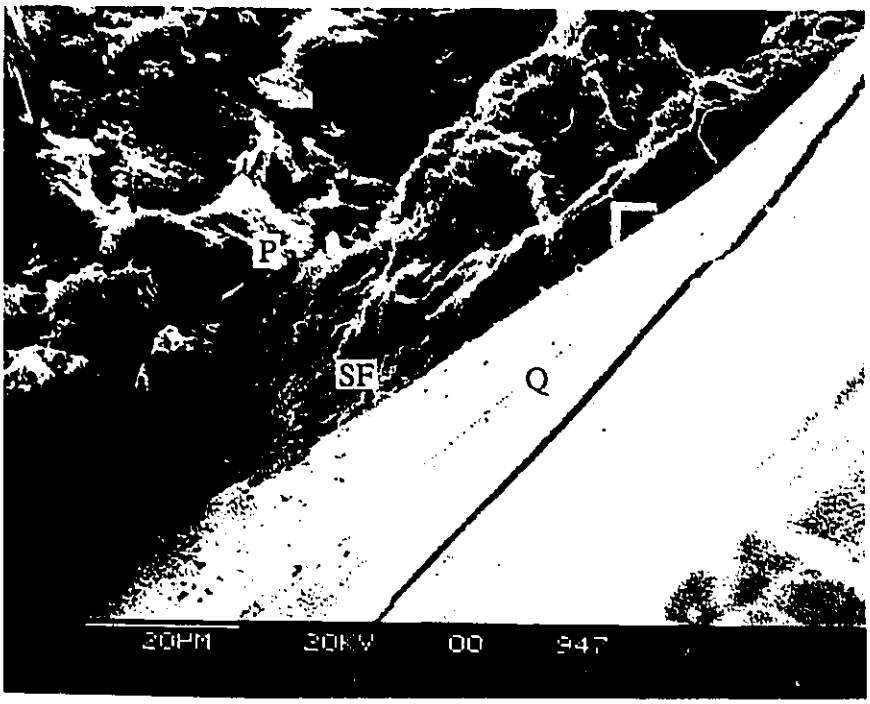

Figure 5.16. Micrograph of SF coated quartz-cement paste interface at 42 days hydration

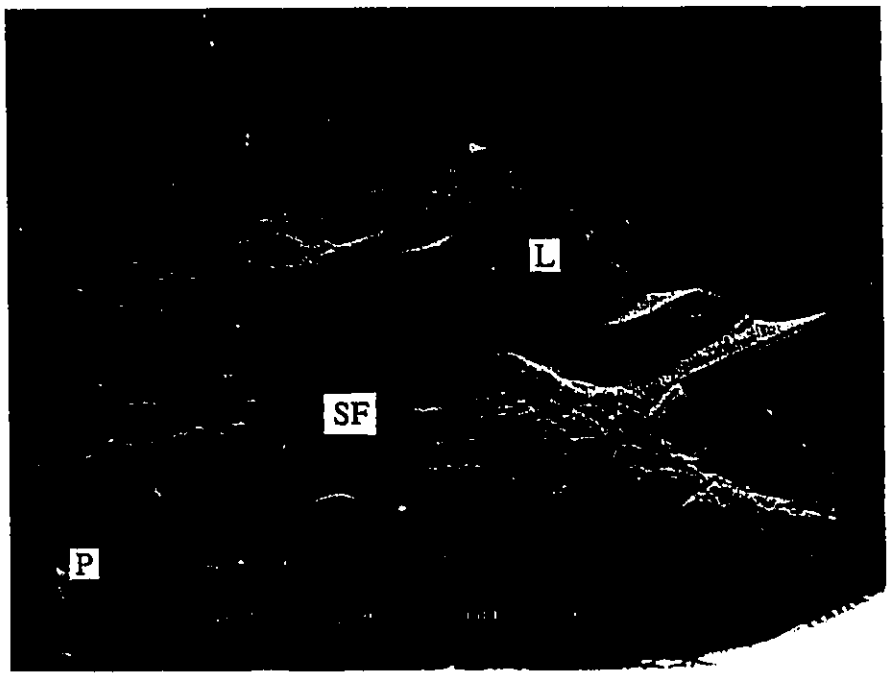

Figure 5.17. Micrograph of SF coated limestone-cement paste interface at 42 days hydration

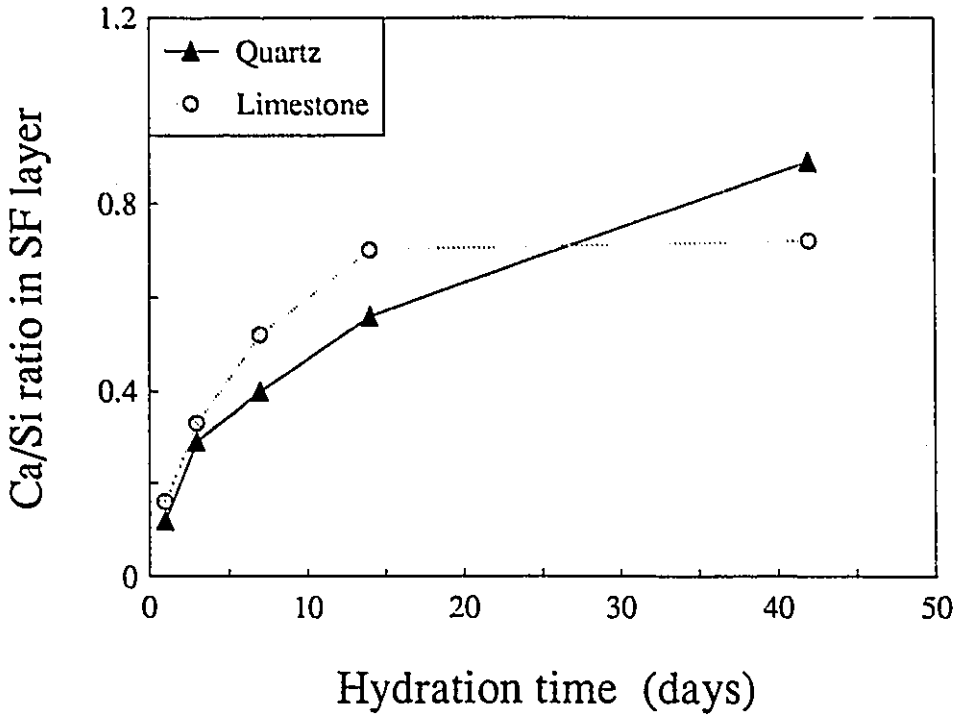

Figure 5.18. Ca/Si ratio in the silica fume coating adhered to aggregate surfaces vs hydration time

At 7 weeks hydration the whole aggregate-SF-paste region appears very dense, figure 5.16 and figure 5.17. Although some CH can still be detected, it seems to be combined with the SF layer very tightly.

The occurrence of pozzolanic reaction between the silica fume coating layer and calcium hydroxide is confirmed by the determination of Ca/Si ratio in the SF layer with hydration. The values of Ca/Si ratio in SF layer for quartz and limestone mortars are plotted vs hydration time in figure 5.18. Obviously, Ca/Si ratio increases with hydration. It is suggested from the obtained results that the increasing content of Ca with hydration is due to the diffusion of calcium ions from the bulk paste into the SF layer. With increasing amounts of diffusing calcium ions into SF layer, the amount of C-S-H product is increased and the SF layer is densified; its cohesion is strengthened.

§5.4 EFFECT OF SILICA FUME COATING ON PROPERTIES OF MORTAR

Preliminary studies on the effect of silica fume coated aggregate on the mechanical properties and sulphate resistance of mortar specimen were conducted. The experimental procedures and the results are as follows.

5.4.1. Effect of Silica Fume Coating on Mechanical Properties

Bending and compressive strength of mortar specimen containing coated and uncoated aggregates were determined. The bending test was conducted by the "three-point method", illustrated in figure 5.19, and the bending strength of the sample, f_b, is calculated by the following equation:

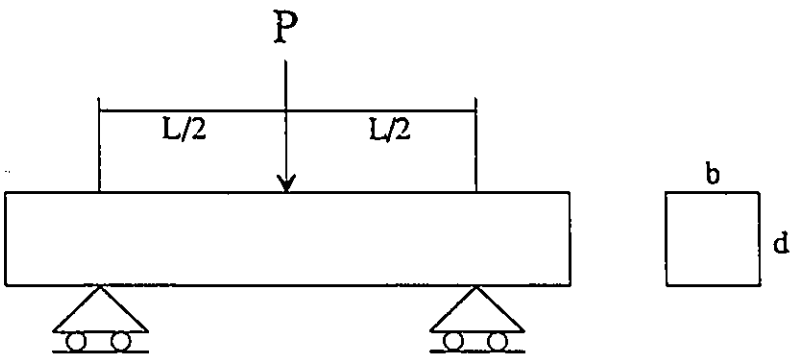

L = 4.0 cm
b = 3.5 mm
d = 4.1 mm

Figure 5.19. Three-point bending test

$$f_b = \frac{3}{2}\frac{P_m L}{b d^2} \qquad (5\text{-}3)$$

where, P_m is the maximum load.

Type 10 portland cement(PC in Table 3.2) was used. Quartz sand was used as aggregate. Some experimental parameters are listed in Table 5.1. All the samples were cured in a fog room at 20°C for 24 hours after moulding, and then placed in saturated calcium hydroxide solution at room temperature until tested.

The experimental results are listed in Table 5.2 and Table 5.3 respectively. Each value is the average from three samples.

Table 5.1. Experimental parameters

	Bending Test	Compression Test
Sample size	6.0cm x 0.35cm x 4.1cm	2.54cm x 2.54cm x 2.54cm
water/cement ratio	0.35	0.40
aggregate/cement	1.5	2.0
Designing thickness of SF layer (μm)	5	10
Aggregate size (US No. of sieve)	#35 - #50	#14 - #20

Table 5.2. Bending strength of mortar (MPa)

Hydration time (days)	3	7	14	21	28
Uncoated sample	9.78	10.61	9.89	9.71	10.68
Coated sample	9.90	8.78	7.25	9.77	11.40

Table 5.3. Compressive strength of mortar (MPa)

Hydration time (days)	1	3	7	14	21	28
Uncoated sample	25.68	38.74	42.71	49.99	51.11	56.54
Coated sample	33.96	45.25	56.11	62.40	63.86	69.08

It can be seen from Table 5.2 and Table 5.3 that the compressive strength is apparently increased by coating the aggregate; the bending strength however decreased up to 14

days hydration. This raises a question as to the function of the silica fume coating. It is suggested that the principal function of the silica fume coating is to increase the interfacial density and not necessarily interfacial bond. The results suggest that the cohesion of the silica fume coating layer itself is lower than that of uncoated aggregate-cement paste interfacial zone during early hydration. It is apparent, however, that interfacial bond continuously increases with hydration due to the pozzolanic reaction between silica fume and calcium hydroxide.

5.4.2. Effect of Silica Fume Coating on Sulphate Resistance of Mortar

The sulphate resistance of mortar was measured by the linear expansion of mortar bars in Na_2SO_4 solution. White portland cement and quartz sand were used to make mortar bars, 6.0 cm x 1.0 cm x 1.0 cm. the w/c ratio was 0.50 and the volumetric fraction of aggregate 0.40. The mortar bars were cured in a saturated solution of calcium hydroxide at room temperature for 27 days after 24 hours-moist curing at 20°C; then they were immersed in 5% and 10% (by weight) Na_2SO_4 solutions respectively. The linear expansion is calculated by the following equation:

$$\text{Expansion } (\%) = \frac{L - L_o}{L_o} \times 100 \qquad (5\text{-}4)$$

where, L is the length of the mortar bar at a specified time of corrosion, and L_o is that before the corrosion.

The results are plotted in figure 5.20. It can be seen that the expansion caused by sulphate corrosion is apparently reduced by the coated aggregate surfaces. The principal reason is that the permeability of the system is reduced and the concentration of Ca^{2+} and OH^-

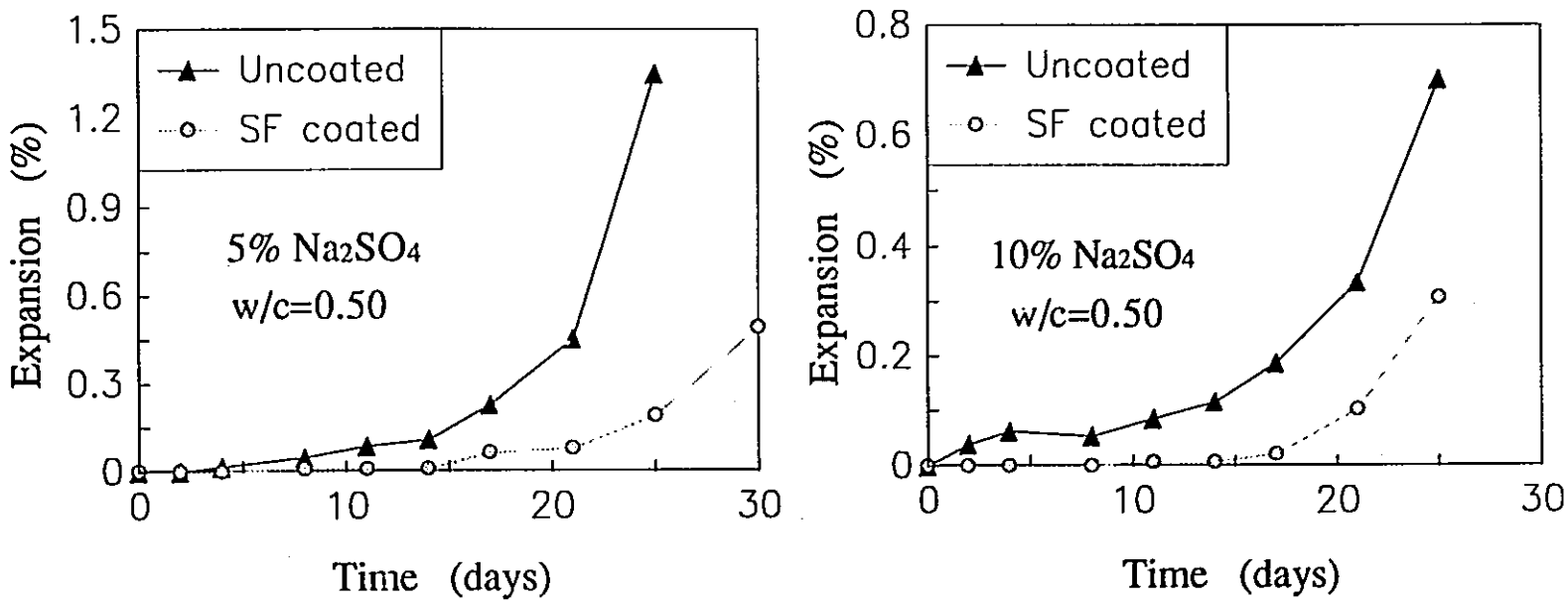

Figure 5.20. Mortar bar expansion in Na_2SO_4 solution

ions in the pore solution within the interfacial zone are decreased by the silica fume coating. These two causes result in the decrease of "crystallization pressure" causing sulphate expansion. A theory concerning "crystallization pressure" of sulphate expansion will be discussed in detail in chapter eight.

The above results indicate that coating aggregate surfaces is an effective method of enhancing interfacial microstructure and hence the properties of concrete.

It should be pointed out, however, that further research is needed to make the new method more effective. It is suggested that emphasis should be given to development of methods to accelerate the pozzolanic reaction between the silica fume layer and calcium hydroxide during early hydration. Increase of the early bending strength of concrete is also desirable. In addition, optimization of the design thickness of the silica fume layer for a specified system appears warranted.

§5.5 CONCLUSIONS

(1). A physically stable silica fume layer on aggregate surfaces can be produced by the method described in this chapter. The mechanism of formation of the silica fume layer is considered to involve capillary effects during the coating procedure.

(2). The microstructure of the interfacial zone at an aggregate-binder interface can be improved by application of a layer of silica fume to aggregate surfaces before mixing. The interfacial zone initially composed of silica fume gradually densifies with the hydration process due to pozzolanic reaction. It becomes more dense than bulk paste

after 3 to 4 days of hydration. The occurrence of the pozzolanic reaction is through the diffusion of calcium ions into the silica fume layer.

(3). The microstructure of the interfacial zone in mortar containing silica fume coated aggregate is apparently not affected by aggregate type used after pozzolanic reaction takes place. These interface reactions lead to interfacial zone enhancement which eliminate the effect of a water film around silica fume coatings.

(4). Microstructure of the interfacial zone in mortar containing silica fume coated aggregate is not influenced by w/c ratio. This is not the case for non-coated aggregate-cement paste interfaces. The thickness of the water film outside the silica fume coating during mixing is probably affected by w/c ratio.

(5). The compressive strength and sulphate resistance of mortar are apparently increased by coating aggregate surfaces with silica fume. The bending strength however is decreased at early hydration. It is suggested that further research is necessary to make the proposed method more effective.

CHAPTER SIX

APPLICATION OF ELECTRICAL CONDUCTIVITY METHODS IN INTERFACIAL CEMENT CHEMISTRY

SUMMARY

The potential application of electrical conductivity methods in areas dealing with chemical reaction at interfaces is discussed. Attention is given to the alkali-aggregate reaction, a specific discipline dealing with interfacial phenomena in concrete science. The approach is also applied to a specific solid-liquid chemical reaction, ie. pozzolanic reaction between silica fume and calcium hydroxide solution. New findings are helpful in understanding the chemical reaction processes occurring in these systems.

§6.1 INTRODUCTION

The electrical conductivity method for interfacial characterization of cement systems has been developed and validated in the previous chapters. The results suggest that the new method may be extended to other areas of interface science. A direct application of the new method is its use for investigations of interfacial chemistry since for systems

containing liquid phase the electrical conductivity of the system usually carries some important information about chemical processes occurring in the system.

The principal objective of this chapter is to test the validity of the electrical conductivity method in the investigation of interfacial chemical reactions. Emphasis will be given to a specific system involving interfacial chemistry, ie. alkali-aggregate reaction.

It is noted that the studies presented in this chapter are preliminary. Further research is recommended.

§6.2 PRINCIPLES

It has been established in the previous chapters that θ is an important parameter characterizing interfacial microstructure in the aggregate-cement paste systems. It can be generally expressed by equation (2-15), or

$$\theta = \delta(\sigma_{fl} - \sigma_{pl}) + \delta(\psi_{ps}\,\sigma_{pl} - \psi_{fs}\,\sigma_{fl})$$

where, σ_{fl} , σ_{pl} are the electrical conductivities of the pore solutions in the interface zone and the bulk paste, and ψ_{fs} , ψ_{ps} are the area fractions of the two regions.

θ is dependent on two principal factors. These are microstructural features of the interfacial zone and bulk paste and the electrical conductivity of pore solution in both regions. It is noted that the θ-parameter is a quantity reflecting the difference between the interfacial zone and the bulk cement paste for both microstructure features and liquid phase conductivity. Any chemical process affecting these differences is expected to produce changes in the values of θ-parameter.

The electrical conductivity of the pore solution is mainly dependent on ionic concentration determined by the chemical processes concerned. Therefore, the electrical conductivity of the interfacial pore solution, σ_{fl} , can reveal some important information about the chemical reactions between aggregate and cement paste since the chemical composition of the interfacial pore solution will be changed by the reactions. The other possible consequence of the interfacial reaction is that the interfacial microstructural features, for example ψ_{fs} , may be changed; these can also be detected by changes to the θ-parameter. The changes in microstructure and pore solution conductivity due to the interfacial reactions form the basis for the application of the electrical conductivity method in interfacial chemistry.

§6.3 ALKALI-AGGREGATE REACTION

Alkali-aggregate reaction(AAR) is a specific discipline of concrete science dealing with characteristics of aggregate-cement paste interfaces. In this type of interfacial phenomenon, the aggregates are alkali reactive, i.e. the aggregates can react with alkali in the pore solution and under certain conditions result in the deterioration of concrete. It is apparent that an understanding of the process of chemical reaction involved in AAR is necessary for the development of some effective measures of preventing AAR from occurring. However, the interfacial reactions involved in AAR are far from fully understood due to the complexity of the problem although investigations of AAR have been conducted for more than five decades.

The electrical conductivity method is used in the study of AAR to obtain some new and useful information about the chemical reactions at alkali-reactive aggregate-cement paste interfaces.

There are at least two well recognized types of AAR, i.e. alkali-silica reaction and alkali-carbonate reaction depending on the type of aggregate. Only the former is considered in this investigation.

Three well known alkali-reactive aggregates were used, i.e. opal, Spratt(a reactive carbonate from Ottawa area) and obsidian. High alkali portland cement was used. The θ-parameter for these three aggregate-cement systems was determined and results are discussed as follows.

6.3.1. Opal-High Alkali Cement System

The θ value vs hydration time for this system is plotted in figure 6.1. It can be seen that unlike any θ - t curve obtained previously, the θ - t curve for the opal-high alkali cement system has some particular features as follows:

(1). $\theta < 0$ from the beginning of the measurement(one hour of hydration). This implies that the interfacial conductivity is less than that of the bulk paste.

(2). $\frac{d\theta}{dt} > 0$ during first 10 days hydration, or θ increases with time during this period.

(3). The value of θ remains about zero after about 10 days hydration. This implies that the interfacial zone and the bulk paste have the same electrical conductivity.

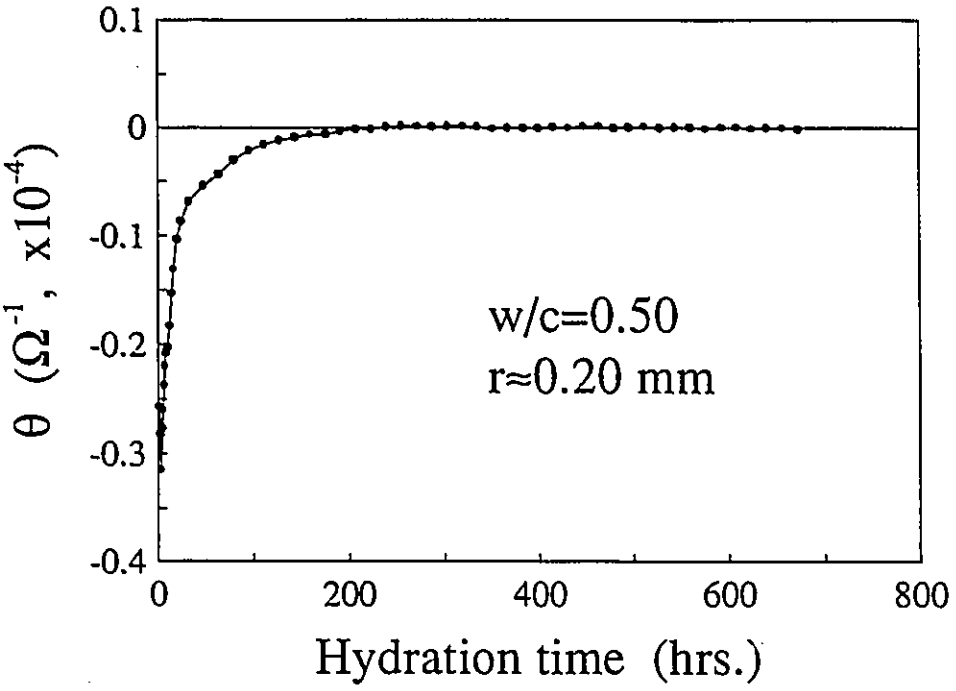

Figure 6.1. θ-parameter of the opal-high alkali cement system

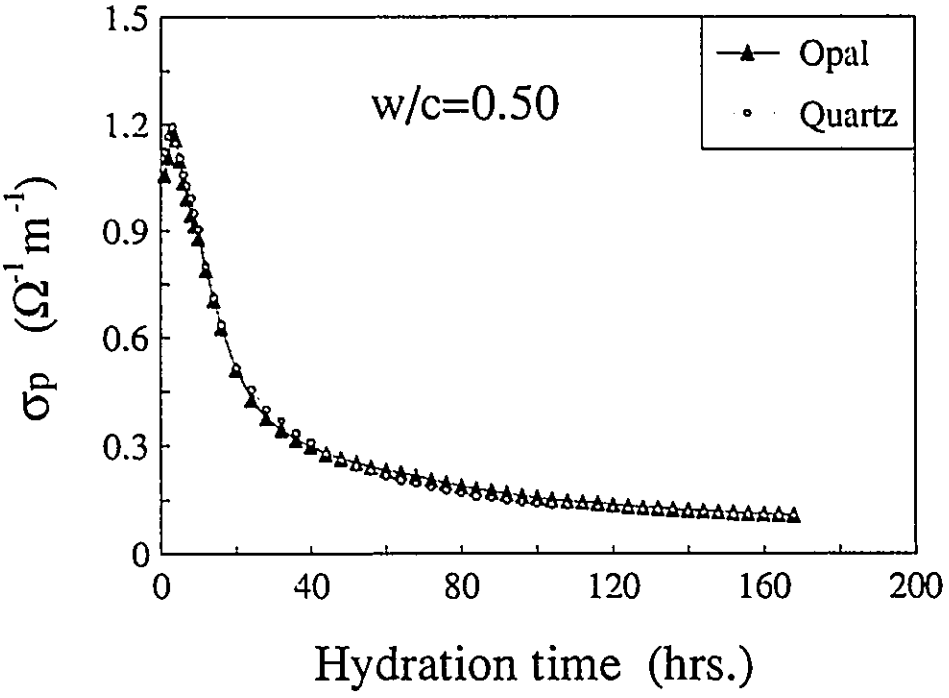

Figure 6.2. Effect of aggregate type on the electrical conductivity of the bulk paste

It is believed that the above features of θ result from the particular chemical reaction between opal and alkali solution. Chemically, opal is a type of amorphous silica, and it is very alkali reactive. When opal is in contact with an alkali solution, for example NaOH solution, the alkali-silica reaction will occur at once on the opal surface. The reaction is reported to consist of the following processes[67]:

(i). The absorption of Na^+, OH^- ions to the opal surface.

(ii). OH^- ions hydrolyse siloxane bonds at the opal surface in contact with the alkali solution according to the following equation:

$$\equiv Si\text{-}O\text{-}Si\equiv + OH^- = \equiv Si\text{-}OH + \equiv Si\text{-}O- \qquad (6\text{-}1)$$

and the unsaturated silanol group, ≡Si-O-, will be neutralized by cations in the solution, for example Na^+ , i.e.

$$\equiv Si\text{-}O- + Na^+ = \equiv Si\text{-}O\text{-}Na \qquad (6\text{-}2)$$

(iii). Diffusion of silica out of the opal particle. This is consequence of the above chemical reactions. The chemical reactions represented by equations (6-1) and (6-2) are the processes by which Si-O bonds at opal surface are broken and the silanol group gets rid of the opal surface and diffuses into the liquid phase.

These processes will continue as long as opal remains in contact with alkali solution.

An attempt to explain the observed features of θ is as follows.

It is suggested that the much lower interfacial conductivity relative to that of the bulk paste at early hydration is probably due to the absorption of Na^+, OH^- ions on the opal surface, resulting in the lower ionic concentration in the interfacial region and hence lower electrical conductivity of interfacial pore solution. Since opal is a very reactive material, this effect is believed to be very quick. The interfacial conductivity of liquid is then reduced quickly once opal and fresh paste is mixed together. With the progress of interfacial reaction between opal and alkali solution, however, more silanol groups are dissolved into the solution in the interfacial zone. These charged groups are expected to make contributions to the electrical conduction. The interfacial conductivity will, therefore, increase with time.

The reason why the value of θ remains about zero after about 10 days hydration is unclear. Further study is required.

The above results raise a question as to whether the opal-alkali reaction affects the electrical conductivity of the bulk paste, σ_p . Figure 6.2 shows the values of the bulk paste conductivities(the intercept of straight line σ vs φ_a) for opal- and quartz-high alkali cement paste systems. It is apparent from figure 6.2 that the two systems have the same σ_p. This indicates that alkali-opal reaction affects only the interfacial zone.

6.3.2. Spratt Aggregate-High Alkali Cement System

The θ value vs hydration time for this system is plotted in figure 6.3. There is a different type of θ - t curve than that for the opal system, i.e. $\theta > 0$ during the first 24 hours hydration and it thereafter decreases to a negative value and continues to decrease until

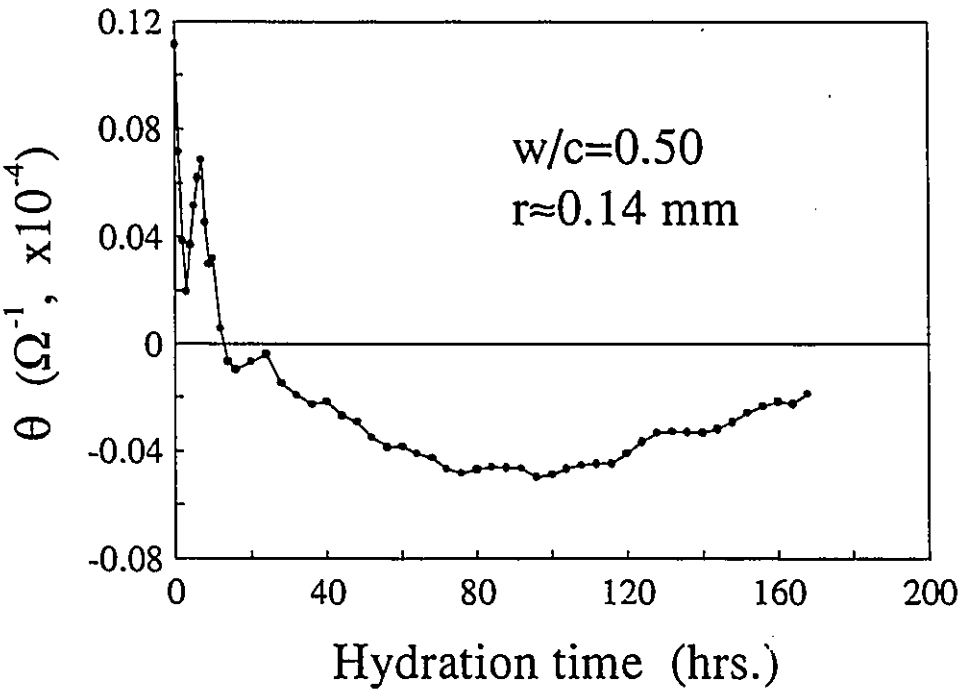

Figure 6.3. θ-parameter of Spratt aggregate-high alkali cement system

about 4 days hydration. After 4 days hydration, however, it increases with time and has the same change tendency as in the opal system.

It is suggested that the above features is determined by the particular properties of Spratt aggregate. The principal alkali-reactive component in Spratt aggregate is chalcedony. Chalcedony is a type of microcrystaline quartz with numerous defects in the crystal structure. Unlike opal, Spratt aggregate contains only a small amount of chalcedony, about 5%, and its alkali-reactivity is obviously less than that of opal. When Spratt aggregate is mixed with fresh cement paste, the effect of the water film still dominates as in the case of the inert aggregate-cement paste system; a positive value of θ results due to the less dense interfacial microstructure. With hydration time, however, the alkali-silica reaction between chalcedony and alkali solution occurs, and the reaction process is similar to that described in the opal system. The negative value of θ is considered to result from the decrease of ionic concentration of the interfacial pore solution due to the adsorption of Na^+, OH^- ions to the chalcedony surface. With the chemical processes continuing, more charged silanol groups are dissolved into the interfacial pore solution resulting in the increase of the interfacial liquid conductivity. This is probably the reason why the θ - t curve rises upward after 4 days hydration.

6.3.3. Obsidian-High Alkali Cement System

Obsidian is a type of volcanic glass. It is a well recognized alkali-reactive aggregate. The θ - t curve for the obsidian-high alkali cement system, figure 6.4, indicates that no differences can be observed compared with that of inert aggregate-cement paste systems. The reason is unclear. Further studies are, therefore, necessary.

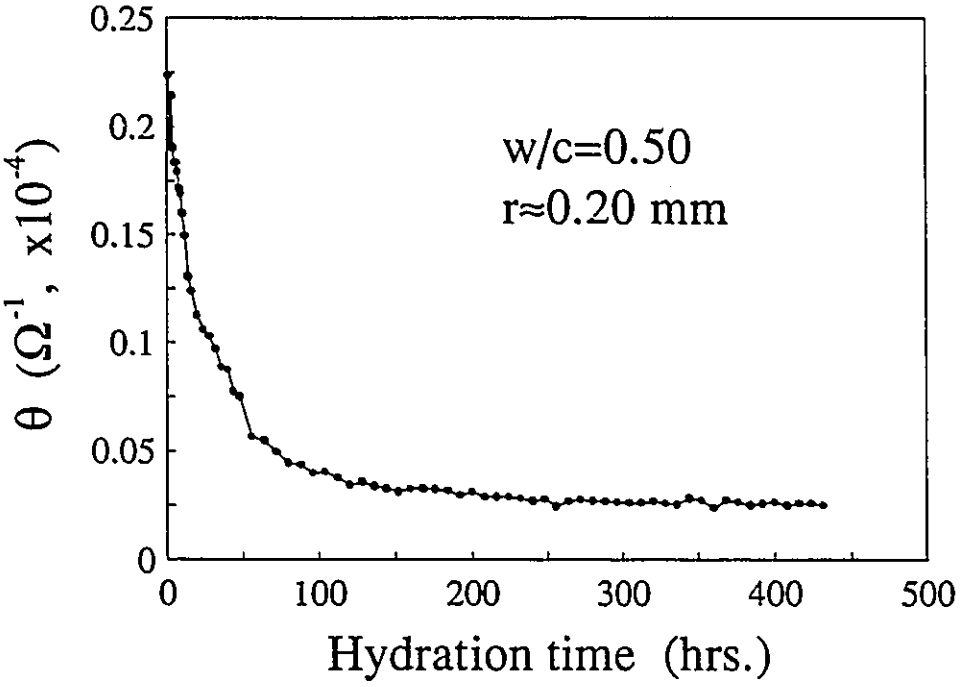

Figure 6.4. θ-parameter of obsidian-high alkali cement system

§6.4 OTHER INTERFACIAL REACTIONS IN AGGREGATE-CEMENT SYSTEMS

6.4.1. Clinker-Cement Paste System

Portland cement clinker was used as a specific type of aggregate. The θ value vs hydration time for the clinker-high alkali portland cement system is plotted in figure 6.5. The θ - t curve shows a feature common to the reactive aggregate-cement systems, i.e. the θ value becomes negative at a certain hydration age.

The negative value of θ for this system is apparently caused by the hydration of clinker itself. It should be pointed out that for this particular system, a negative value of θ indicates a more dense interfacial microstructure relative to that for the bulk paste since the interfacial liquid conductivity is equal to that in the bulk paste, or $\sigma_{fl} = \sigma_{pl}$.

6.4.2. Limestone-Cement Paste System

Limestone is a slightly reactive aggregate consisting mainly of carbonate. Carbonate can react with aluminate and alkali solution in cement paste. The features of θ for this system have been described in detail in chapter 4. A negative value of θ was obtained when the aggregate size was decreased beyond a certain value.

6.4.3. Silica Fume Coated Aggregate-Cement Paste Systems

From a chemical point of view, coating aggregate surfaces with silica fume is intended to activate the aggregate. The pozzolanic reaction of the silica fume coating layer and

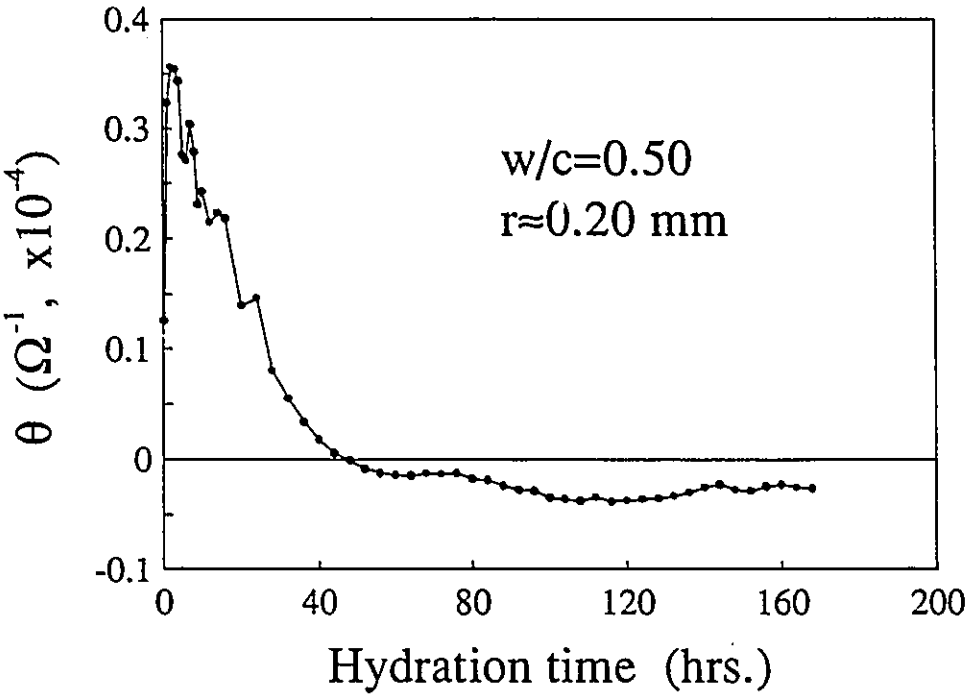

Figure 6.5. θ-parameter of portland cement clinker-high alkali cement system

calcium hydroxide in the interfacial region can also be detected by determining the θ value of this system. This has been discussed in detail in chapter 5, where a negative value of θ was also obtained.

From the above discussion, an important concept emerges: a negative value of θ-parameter will be obtained under certain conditions if chemical reactions between aggregate and cement paste exist.

§6.5 SOLID-LIQUID REACTION

Generally, solid-liquid reactions take place at the solid-liquid interface. The electrical conductivity method may, therefore, find application in characterizing solid-liquid chemical reactions in general, analogous to the aggregate-cement paste interaction. Some information about the mechanism of the reaction may be obtained.

As an example, the electrical conductivity of silica fume-saturated calcium hydroxide solution systems with different relative amounts of silica fume added to the solution were determined. The electrical conductivity of the system is plotted vs time in figure 6.6 and vs volumetric fraction of silica fume, φ_{sf}, in figure 6.7. The following findings were obtained:

(1). At early times, the conductivity of the systems containing a small amount of silica fume decreases with time more quickly than for those systems containing a relatively large amount of silica fume.

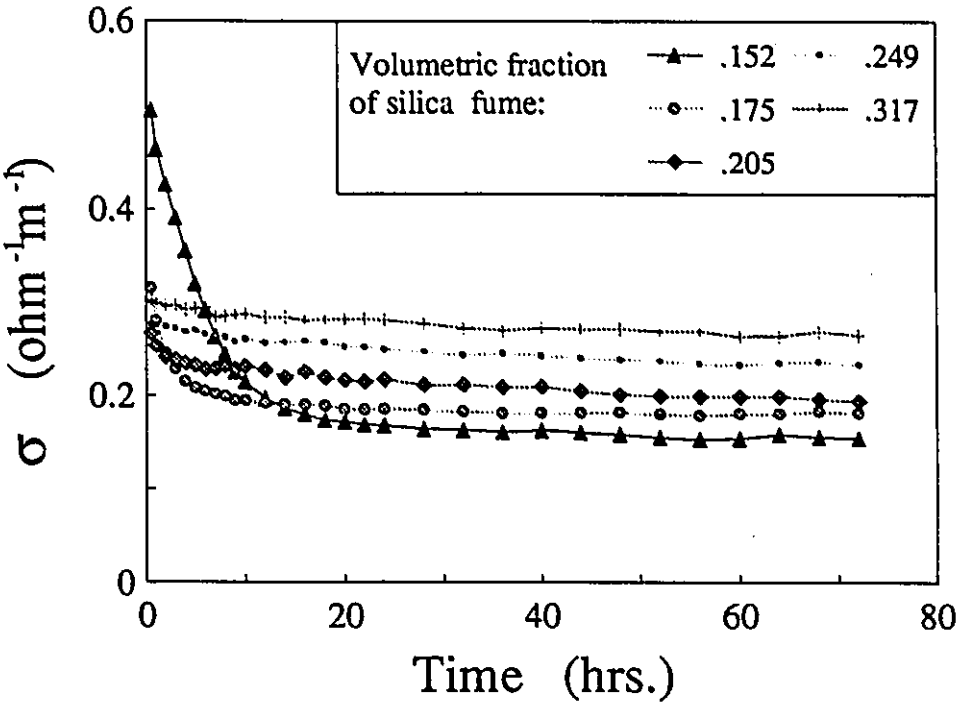

Figure 6.6. Electrical conductivity of silica fume-saturated $Ca(OH)_2$ solution system

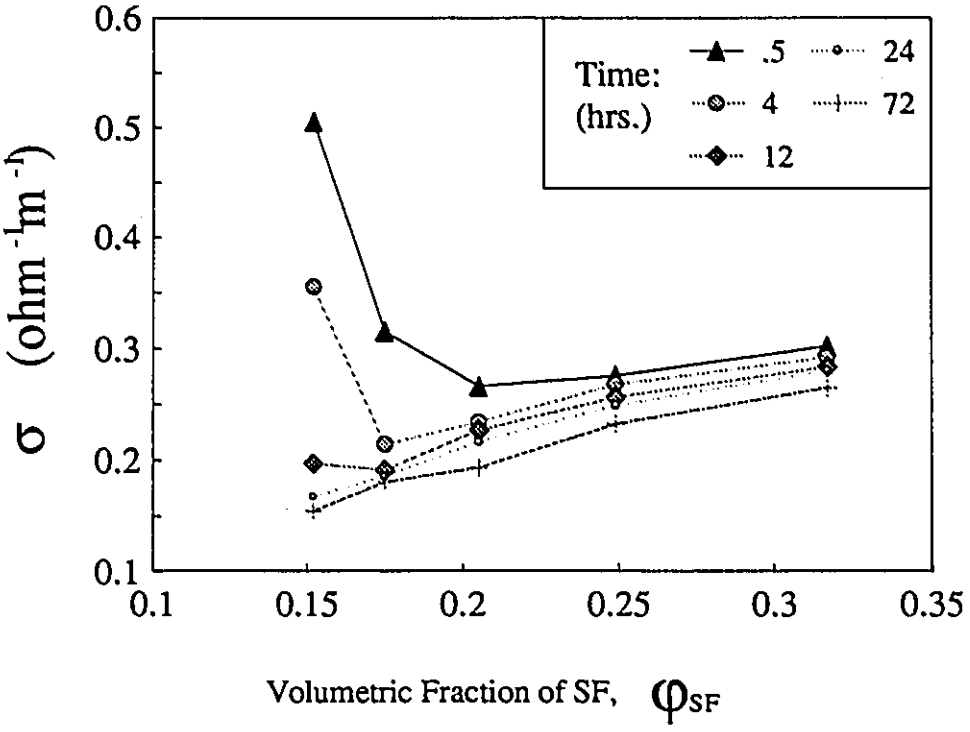

Figure 6.7. Electrical conductivity of SF-$Ca(OH)_2$ solution system vs φ_{SF}

(2). At early times, the conductivity decreases first and then increases with φ_{SF}. At later times, however, the conductivity increases with the amount of silica fume in the system.

The results indicate that the composition and hence the electrical conductivity of the liquid phase in the system must change with time and the amount of silica fume since there would not be a minimum value in the σ - φ_{SF} curve without change of liquid composition. The composition change of the liquid phase results from the pozzolanic reaction between silica fume and calcium hydroxide. It is suggested that the chemical precess is similar to that described in the opal-cement paste system. The results of the reaction lie in the consumption of OH^-, Ca^{2+} ions in the solution and dissolution of silanol groups into the liquid phase.

For the system with less silica fume, it is believed that the liquid conductivity is controlled by the concentration of ions such as OH^-, Ca^{2+} at early reaction times since there are not enough charged silanol groups in the solution. The concentration of OH^-, Ca^{2+} ions will be consumed quickly with the reaction and the concentrations of these ions decreases with silica fume content. This is why the conductivity of the system with less silica fume changes quickly with time and decreases with φ_{SF} at early time. With more charged silanol groups entering the solution, the liquid conductivity will be controlled by the concentration of silanol group ions. As silica fume content increases the concentration of these ions in the solution increases. This is the reason why σ increases with φ_{SF} at later reaction times.

§6.6 CONCLUSIONS

(1). Preliminary experimental results indicate that the electrical conductivity method is effective for investigations of interfacial cement chemistry; the method is very helpful in understanding the mechanism of the reactions.

(2). It is suggested that the interfacial chemical reaction in aggregate-cement systems usually results in a negative value of θ-parameter. This has potential as a criteria to determine if there is a chemical reaction at the interface or not.

(3). A new feature of the θ value for systems undergoing alkali-silica reaction was obtained, i.e. $\frac{d\theta}{dt} > 0$. It is suggested that this is due to the dissolution of charged silanol groups from aggregate surfaces into the pore solution in the interfacial region.

(4). The effect of the opal-alkali reaction on the electrical conductivity of the liquid phase seems to exist only in the interfacial region, and not in the bulk paste.

CHAPTER SEVEN

A.C. IMPEDANCE TECHNIQUES AND THEIR APPLICATION IN HYDRATING CEMENT SYSTEMS

SUMMARY

The validity of a new tool, an a.c. impedance spectroscopy technique, in investigating hydrating cement systems has been strongly enhanced by development of a theoretical model for a.c. impedance spectroscopy of hydrating cement systems. A fundamental understanding of the a.c. impedance behavior of hydrating cement systems has been obtained through application of the proposed model. The theory emphasizes that the a.c. impedance behavior of hydrating cement systems results from solid-liquid interfacial phenomena.

It is indicated by theory and experiment that there are two principal factors influencing the a.c. impedance behavior: (i). microstructure of the system, e.g. number, size, distribution and geometry of solid products in the system; (ii). solid-liquid interaction.

It is therefore suggested that the a.c. impedance technique is an effective tool for characterizing microstructure and investigating solid-liquid interaction in porous materials.

§7.1 INTRODUCTION

The a.c. impedance technique has been applied recently to investigate the behavior of hydrating cement systems[68-73]. New information related to the microstructure of the system and the hydration process of cement has been obtained. The significance of a.c. impedance spectroscopy for characterizing hydrating cement systems is based on a finding that a high frequency semicircle exists in the real-imaginary impedance plane of the specimen subjected to an a.c. signal with variable frequency. The typical a.c. impedance spectrum for the hydrating cement system is illustrated in figure 7.1(a), and figure 7.1(b) is the corresponding equivalent circuit, ie. a simple R-C circuit. It is recognized that the semicircle at high frequency is related to the microstructure of the system and the arc at low frequency results from the electrode effects.

It is noted that most previous work was limited solely to the detection of the semicircle and description of the phenomena relating to its change. This was due primarily to lack of a fundamental explanation of the origin of the semicircle and the physical meanings of the elements in the equivalent circuit with respect to the microstructure or properties of the system. It appears, therefore, that further application of a.c. impedance techniques in cement systems would be difficult unless relationships between the parameters from the a.c. impedance spectra and the microstructural factors of the system are developed.

The objective of this chapter is to propose a rationalized electrical conduction model for hydrating cement systems based on a.c. impedance methods and to formulate a physical model and obtain a fundamental understanding of the a.c. impedance behavior of hydrating cement systems. The a.c. impedance behavior of silica fume cement pastes and

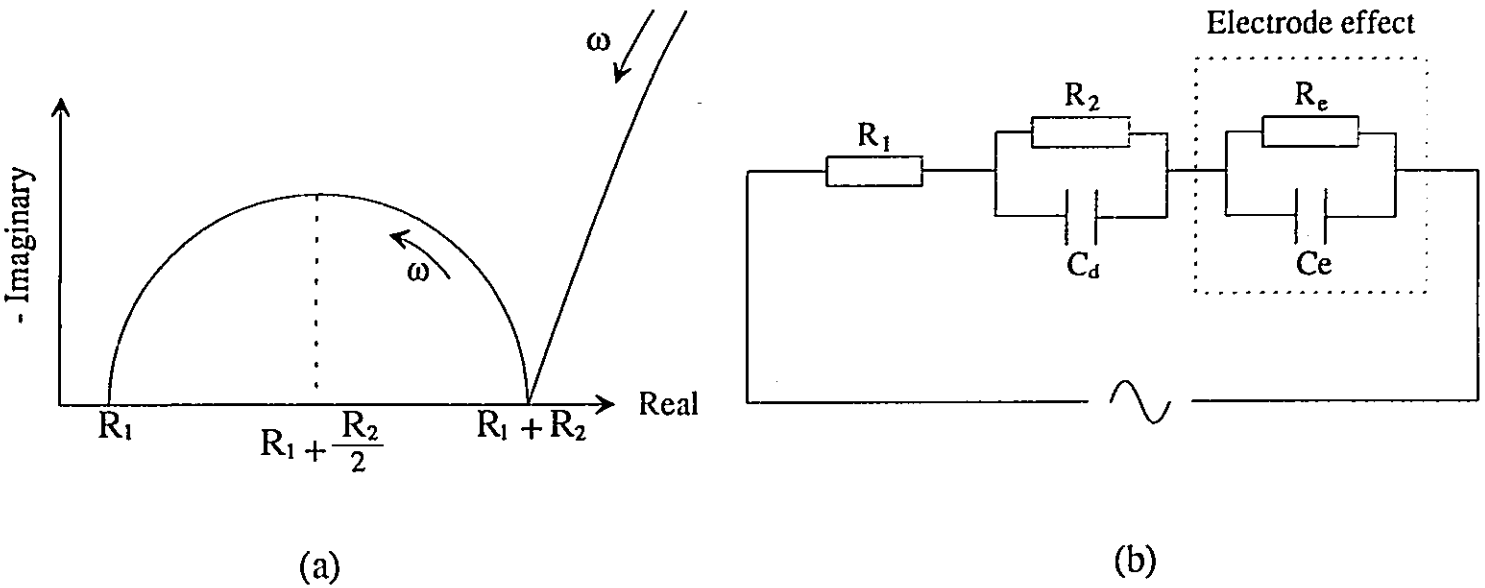

Figure 7.1. A typical a.c. impedance spectrum for hydrating cement system, (a), and the corresponding equivalent circuit, (b).

cement paste systems containing mineral admixtures, fly ash and blast furnace slag and coated aggregate will be discussed in terms of the proposed model.

§7.2 AN ELECTRICAL CONDUCTION MODEL FOR THE HYDRATING CEMENT SYSTEM

7.2.1. Physical Model

Consider a saturated hydrating cement specimen subjected to an applied a.c. signal. The specimen can be described by a circuit consisting of N electric elements connected in series, as shown by figure 7.2(a) and 7.2(b). All the elements are the same physically and consist of three sub-elements, ie. solid, pore(liquid) and solid-liquid interface normal to the electrical field, figure 7.2(c). It is emphasized that in any solid-electrolyte system there is a specific liquid region in contact with the solid surface, referred to as the double layer or diffuse layer. The double layer has different ionic composition and microstructure than the bulk liquid due to surface adsorption on the solid. It contains opposite charges to that on the solid surface. It is suggested that under an a.c signal the separation of opposite charges in the solid and double layer results in capacitance behavior and the specific ionic composition and microstructure of the double layer results in a different electrical resistance than the bulk liquid. The sub-element in figure 1(c) can, therefore, be modelled by an equivalent circuit, figure 7.2(d). The equivalent circuit for the whole specimen is a summation of the sub-circuit, figure 7.2(d), shown in figure 7.2(e).

The physical model can be formulated through the following mathematical analysis:

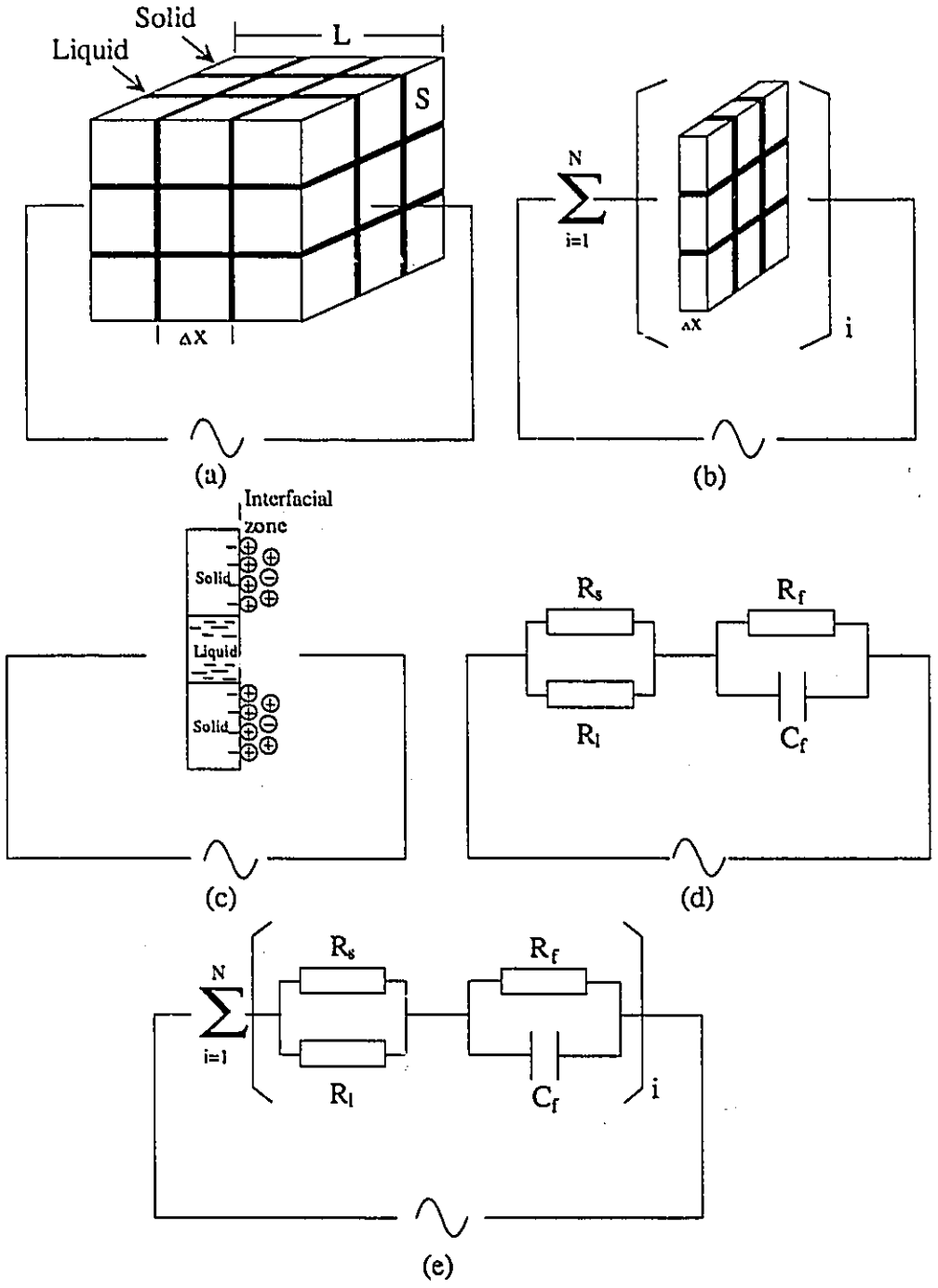

Figure 7.2. Electrical conduction model for the hydrating cement system

7.2.2. Mathematical Analysis

The total impedance, Z, of the specimen can be calculated as follows:

$$Z = Z_1 + Z_2 \tag{7-1}$$

and

$$Z_1 = \sum_{i=1}^{N} \left[\frac{1}{\frac{1}{R_s} + \frac{1}{R_l}} \right]_i$$

$$\approx \sum_{i=1}^{N} [R_l]_i \qquad \text{(Since } R_s >> R_l \text{)}$$

$$= \sum_{i=1}^{N} \left[\frac{\Delta x}{S_l} \frac{1}{\sigma_l} \right]_i = \frac{L}{S_l} \frac{1}{\sigma_l}$$

$$= \frac{L}{S} \frac{1}{\psi_l} \frac{1}{\sigma_l} = \frac{L}{S} \frac{1}{(1 - \psi_s)} \frac{1}{\sigma_l} \tag{7-2}$$

where, L is thickness of the specimen in the direction of the electrical field, S is its area normal to the electrical field. S_l (= ψ_l S) is the area of liquid phase, ψ_l is the corresponding area fraction and ψ_s is the area fraction of solid phase. σ_l is the electrical conductivity of liquid phase.

$$Z_2 = \sum_{i=1}^{N} \left[\frac{1}{\frac{1}{R_f} + j\,\omega C_f} \right]_i = \sum_{i=1}^{N} \left[\frac{R_f}{1 + (\omega C_f R_f)^2} - j \frac{\omega C_f R_f^2}{1 + (\omega C_f R_f)^2} \right]_i$$

$$= \frac{N R_f}{1 + (\omega C_f R_f)^2} - j \frac{N \omega C_f R_f^2}{1 + (\omega C_f R_f)^2} \qquad (7\text{-}3)$$

where, ω is the angular frequency of the a.c. signal and R_f , C_f are the electrical resistance and capacitance of the solid-liquid interfacial zone or double layer, respectively. N is total number of solid-liquid interfaces within the specimen in the direction of the electrical field.

Substituting equations (7-2) and (7-3) into equation (7-1) yields:

$$Z = \frac{L}{S} \frac{1}{(1 - \psi_s)} \frac{1}{\sigma_l} + \frac{N R_f}{1 + (\omega C_f R_f)^2} - j \frac{N \omega C_f R_f^2}{1 + (\omega C_f R_f)^2} \qquad (7\text{-}4)$$

Let

$$R_1 = \frac{L}{S} \frac{1}{(1 - \psi_s)} \frac{1}{\sigma_l} , \qquad \text{and} \quad \left.\begin{array}{l} R_2 = N R_f \\ C_d = C_f / N \end{array}\right\} \qquad (7\text{-}5)$$

Hence,

$$Z = R_1 + \frac{R_2}{1 + (\omega C_d R_2)^2} - j \frac{\omega C_d R_2^2}{1 + (\omega C_d R_2)^2} \qquad (7\text{-}6)$$

If $X = R_1 + \frac{R_2}{1 + (\omega C_d R_2)^2}$, $Y = \frac{\omega C_d R_2^2}{1 + (\omega C_d R_2)^2}$, it can be readily proven that the following equation holds:

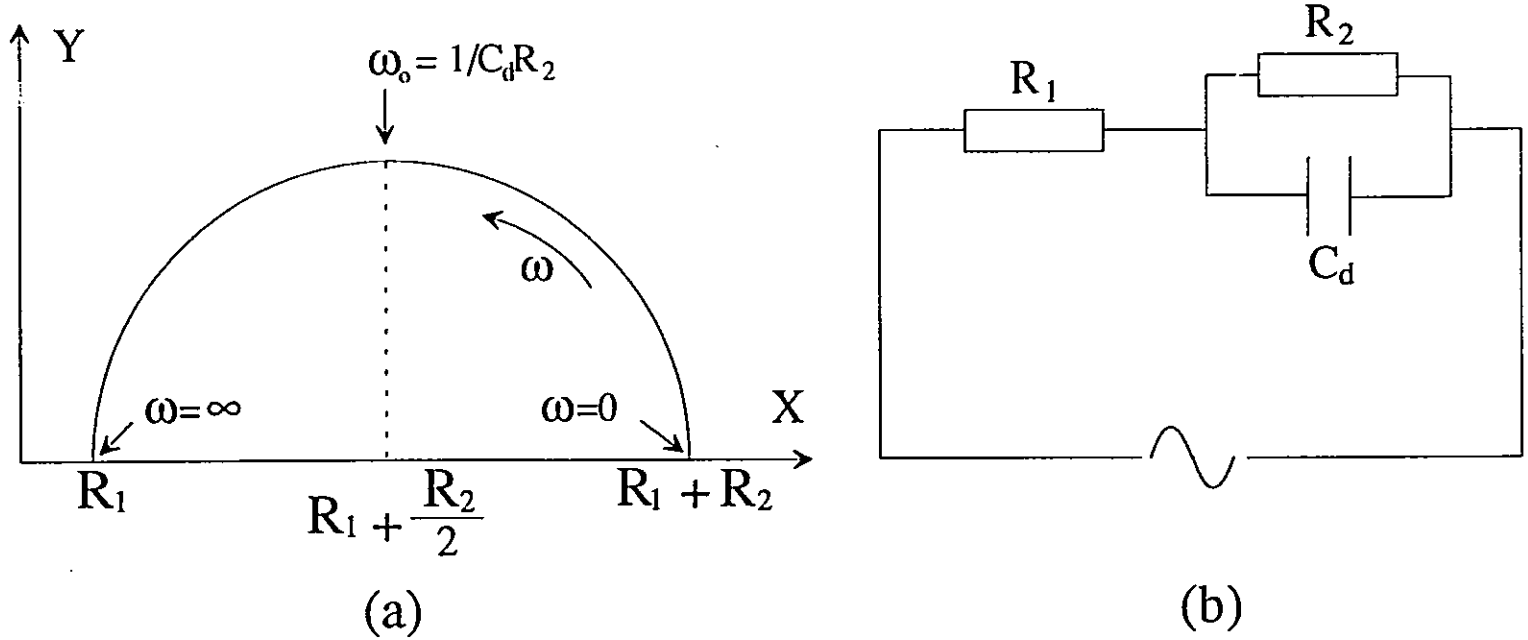

Figure 7.3. The equivalent circuit and the corresponding semicircle

$$\left[X - (R_1 + \frac{R_2}{2})\right]^2 + Y^2 = \left[\frac{R_2}{2}\right]^2 \qquad (7\text{-}7)$$

This is the equation of a circle with radius $R_2/2$ and center $(R_1+R_2/2, 0)$ in the X-Y plane(Real-Imaginary plane of Z), as shown in figure 7.3(a). Figure 7.3(b) is the corresponding electrical circuit represented by the circle in figure 7.3(a).

A useful relationship between the angular frequency at the top of the semicircle, ω_o, and C_d , R_2 can be obtained by setting $Y=R_2/2$:

$$\omega_o C_d R_2 = 1 \quad \text{or} \quad \omega_o = \frac{1}{C_d R_2} \qquad (7\text{-}8)$$

ω_o, and R_2 can be determined by experiment. C_d , therefore, can be readily calculated from equation (7-8).

Substituting equation (7-5) into (7-8) yields:

$$\omega_o C_f R_f = 1 \quad \text{or} \quad \omega_o = \frac{1}{C_f R_f} \qquad (7\text{-}9)$$

It will be seen in the following section that ω_o has a special function in characterizing solid-liquid interaction.

§7.3 APPLICATION OF A.C. IMPEDANCE TECHNIQUES IN THE INVESTIGATION OF SOLID-LIQUID INTERFACES

The proposed model indicates that the a.c. impedance behavior of the hydrating cement system is controlled by the solid-liquid interfacial zone in the system. Some

characteristics of the interfacial zone can be, therefore, revealed by this technique. For example, the electrical conductivity of the solid-liquid interfacial zone and the solid-liquid interaction will be discussed as follows.

The microstructure of the charged solid-electrolyte interfacial zone can be modelled as illustrated by figure 7.4. The solid-liquid interfacial zone consists of two parts, the "Stern layer" and a "diffuse layer"[59]. The Stern layer is a layer of counter-ions strongly adsorbed to the solid surface. The ions in the Stern layer are difficult to move due to the attraction of the solid surface. A diffuse layer exists behind the Stern layer. The diffuse layer contains a net excess of counter-ions compared with the neutral bulk liquid. It is apparent that the interfacial zone has a different electrical conductivity than the bulk liquid.

The interfacial electrical resistance, R_f, in the proposed model can be expressed as follows:

$$R_f = \frac{\delta_{st}}{S_{sl}}\frac{1}{\sigma_{st}} + \frac{\delta-\delta_{st}}{S_{sl}}\frac{1}{\sigma_d}$$

$$= \frac{\delta}{S_{sl}}\left[\frac{1}{\sigma_d} + \left(\frac{\delta_{st}}{\delta}\right)\left(\frac{1}{\sigma_{st}} - \frac{1}{\sigma_d}\right)\right]$$

$$= \frac{\delta}{S_{sl}}\frac{1}{\sigma_f} \qquad (7\text{-}10)$$

where, σ_{st} , σ_d are electrical conductivities of the Stern layer and diffuse layer, respectively. δ_{st} is the thickness of Stern layer and δ is the total thickness of the

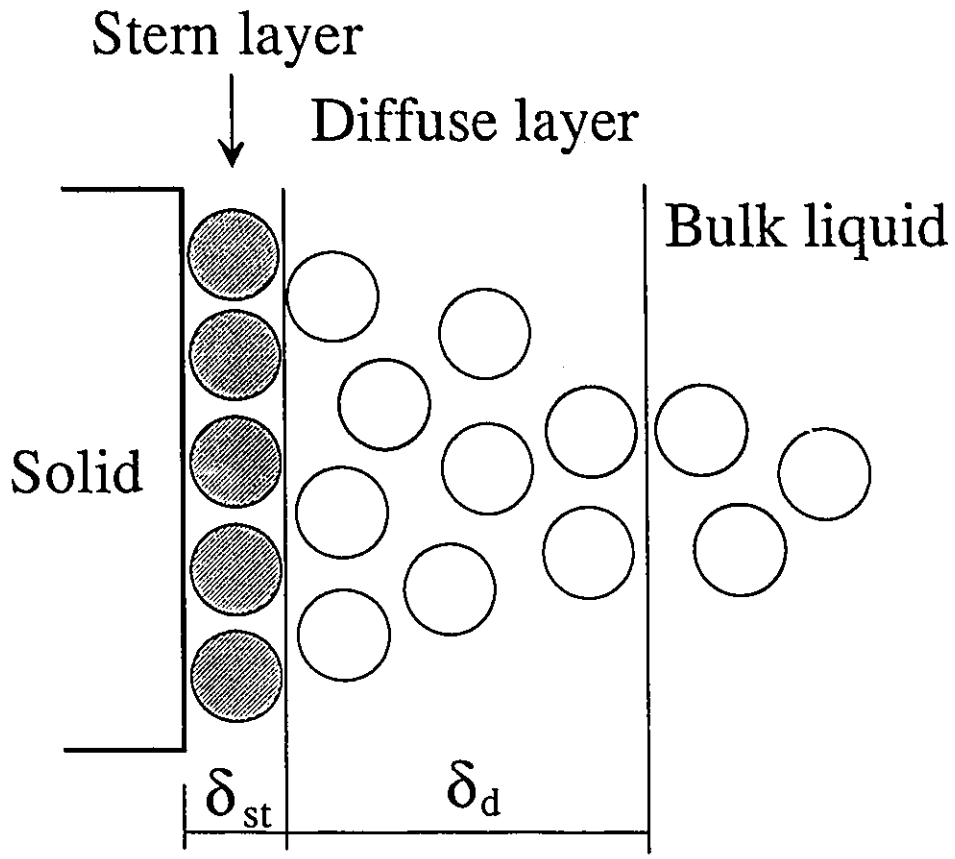

Figure 7.4. The Stern model of the solid-liquid interface

interfacial zone. S_{sl} is the area of solid-liquid interface in the section. σ_f is an apparent electrical conductivity of the interfacial zone, i.e.

$$\frac{1}{\sigma_f} = \frac{1}{\sigma_d} + \left(\frac{\delta_{st}}{\delta}\right)\left(\frac{1}{\sigma_{st}} - \frac{1}{\sigma_d}\right) \tag{7-11}$$

The interfacial capacitance, C_f, can be expressed as follows:

$$\begin{aligned}
\frac{1}{C_f} &= \frac{1}{C_{st}} + \frac{1}{C_{df}} \\
&= \frac{\delta_{st}}{\varepsilon_{st}\,\varepsilon_o\,S_{sl}} + \frac{\delta_d}{\varepsilon_d\,\varepsilon_o\,S_{sl}} \\
&= \frac{\delta_{st}}{\varepsilon_{st}\,\varepsilon_o\,S_{sl}} + \frac{\delta - \delta_{st}}{\varepsilon_d\,\varepsilon_o\,S_{sl}} \\
&= \frac{\delta}{\varepsilon_o\,S_{sl}}\left[\frac{(\delta_{st}/\delta)}{\varepsilon_{st}} + \frac{1 - (\delta_{st}/\delta)}{\varepsilon_d}\right] \\
&= \frac{\delta}{\varepsilon_o\,S_{sl}}\left[\frac{1}{\varepsilon_d} + \frac{\delta_{st}}{\delta}\left(\frac{1}{\varepsilon_{st}} - \frac{1}{\varepsilon_d}\right)\right] \\
&= \frac{\delta}{\varepsilon_o\,S_{sl}}\,\frac{1}{\varepsilon_f}
\end{aligned} \tag{7-12}$$

where, C_{st} and C_{df} are capacitances of the Stern layer and diffuse layer, respectively. ε_{st}, ε_d are dielectric constants of the media in the two layers, respectively. $\varepsilon_o = 8.854 \times 10^{-12}$ C^2/Nm^2 is the permittivity of a vacuum. ε_f is referred to as the apparent dielectric constant in the interfacial zone, and

$$\frac{1}{\varepsilon_f} = \frac{1}{\varepsilon_d} + \frac{\delta_{st}}{\delta}\left(\frac{1}{\varepsilon_{st}} - \frac{1}{\varepsilon_d}\right) \qquad (7\text{-}13)$$

From equations (7-10) and (7-12), we have

$$C_f R_f = \frac{\varepsilon_f \varepsilon_o}{\sigma_f} \qquad (7\text{-}14)$$

Combining equations (7-14) and (7-9) yields:

$$\boxed{\sigma_f = \omega_o \varepsilon_f \varepsilon_o = 2\pi f_o \varepsilon_f \varepsilon_o} \qquad (7\text{-}15)$$

or

$$\boxed{f_o = \frac{\sigma_f}{2\pi \varepsilon_f \varepsilon_o}} \qquad (7\text{-}15')$$

It can be seen that the apparent electrical conductivity of the solid-liquid interfacial zone can estimated by equation (7-15) if ω_o (or f_o) is obtained from the a.c. impedance spectrum. In addition, equation (7-15') indicates that the value of f_o in the a.c. impedance spectrum reflects the electrical conductivity of the interfacial zone. Experiment indicates that f_o for hydrating cement system is in the order of MHz. Equation (7-15') may lead to discussion of the cause of the occurrence of the semicircle at a frequency around the order of MHz for hydrating cement systems as follows:

It is estimated that $\varepsilon_{st} \approx 20$ and $\varepsilon_d \approx 81$ for water[74]; $\delta_{st} \approx 5$ Å and $\delta_d \approx 20$ Å. Generally, the electrical conductivity of the pore solution extracted from hydrated portland cement paste

ranges from 2.8 to 4 $\Omega^{-1}m^{-1}$[75]. If there were no solid-liquid interaction in the interfacial zone, the value of σ_f would be considered to be in this range, and the corresponding value of f_o would, therefore, be in the order of GHz from equation (7-15'). This result indicates that the semicircle should occur at the frequency around the order of GHz if the features of the interfacial zone are the same as the bulk liquid phase. The actual finding is, however, that it occurs around MHz. In the practical system, there are strong interactions between a solid surface and the ions near the surface and between the ions themselves. These result in less mobility of the ions in the interfacial zone, especially in the Stern layer, leading to a much lower electrical conductivity of the interfacial zone than in the bulk liquid and hence the lower value of f_o . Obviously, the occurrence of the semicircle at a frequency around the order of MHz instead of GHz is a consequence of the solid-ion and ion-ion interactions. It can be estimated from equation (7-15) that the electrical conductivity of the solid-liquid interfacial zone is less than that of the bulk liquid by three orders of magnitude.

The above discussion suggests that a.c. impedance techniques can potentially be used for the investigation of solid-liquid interaction in the porous materials.

§7.4 EXPLANATION OF A.C. IMPEDANCE BEHAVIOR OF HYDRATING CEMENT SYSTEMS

Extensive experiments for several hydrating systems were conducted. Canadian Standard Type 10 portland cement(PC in Table 3.2) was used. The details of the experiment have been described in reference[72]. Impedance data was collected using a 1260 impedance gain-phase analyzer from Schlumberger Technologies. Measurements were made

logarithmically down in frequency range from 21 MHz to 1 Hz with 10 readings per decade. The principal results and analyses are as follows.

7.4.1. Hydrating Portland Cement System

The a.c. impedance data for this system at hydration time from 48 to 380 hours is plotted in the complex plane(Real vs -Imaginary), as shown in figure 7.5. The parameters corresponding to the elements in an equivalent circuit(see figure 7.1) are listed in Table 7.1, where the term f_o is the frequency at the apex of the semicircle.

Table 7.1 The parameters in the equivalent circuit

Hydration Time (hrs.)	R_1 (Ω)	R_2 (Ω)	C_d (nF)	f_o (MHz)
48	80	---	---	---
68	87	---	---	---
169	99	13.5	12.0	0.978
194	104	15.0	10.8	0.978
283	111	25.0	4.2	1.506
380	113	30.0	3.5	1.506

Data in figure 7.5 and Table 7.1 demonstrate some typical features of the a.c. impedance spectra of hydrating cement paste:

(1). The diameter of the high frequency circle, R_2, increases dramatically with hydration time.

Reference is made to the rationalized equivalent circuit for hydrating cement, figure 7.2 and figure 7.3. The diameter of the high frequency semicircle, denoted by D_{AC} , a principal parameter directly obtained from a.c. impedance experiment, can be expressed as

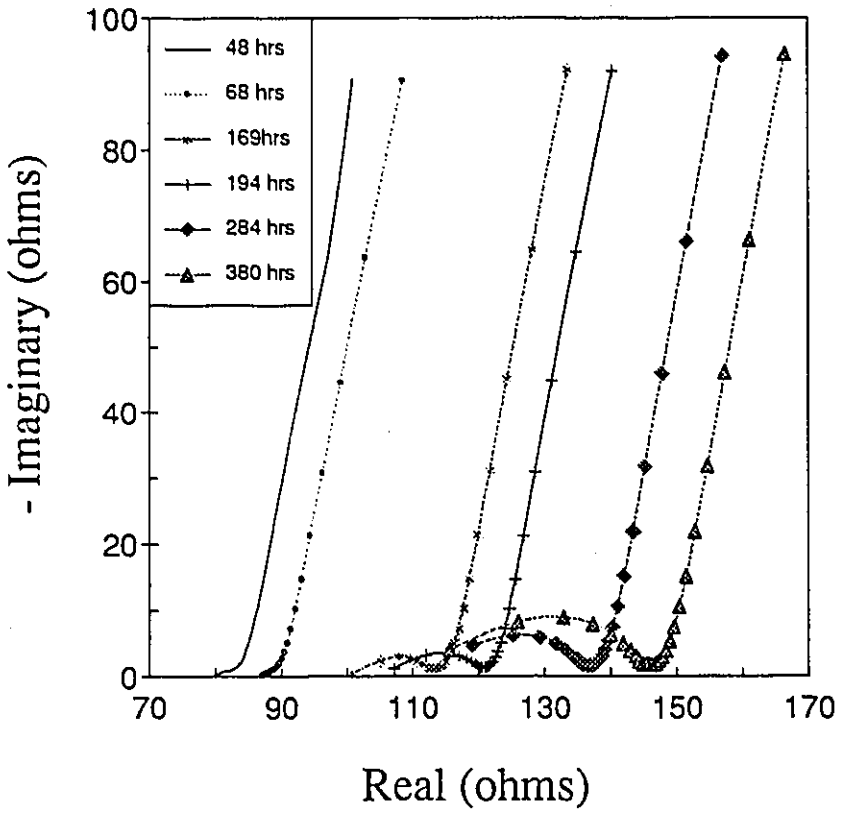

Figure 7.5. The a.c. impedance spectra of hydrating portland cement paste, w/c=0.35

$$D_{AC} = R_2 = N R_f \qquad (7\text{-}16)$$

N is the number of solid-liquid interfaces between two electrodes in contact with the specimen. This is a microstructural parameter dependent on the number, size and distribution of solid products, including hydrates and unhydrated cement. For the hydrating portland cement system, the principal solid product is C-S-H gel which has a large specific surface area. Hydration is actually a process in which C-S-H gel and hence the number of solid-liquid interfaces rapidly increases. The increase of D_{AC} with hydration time is actually due to the rapid increase of N with time.

(2). The capacitance C_d decreases with hydration time.

For certain systems, C_f will not change dramatically with time. Since N increases with hydration time, C_d will decrease with time according to equation (7-5).

(3). R_1 increases with hydration time marginally and only during the early stage of hydration.

R_1 is dependent on ψ_s and σ_l according equation (7-5). Apparently ψ_s and σ_l change with time only during the early hydration stage, generally a few days, and the changes do not exceed one order of magnitude. Therefore, R_1 changes marginally during early hydration period.

(4). The high frequency circle does not occur until a critical hydration time has been reached.

No circle occurs at the early hydration stage due to a low value of N between the two electrodes. The value of NR_f is not large enough to be detected by the equipment. The significance of N to the D_{AC} can also be seen by another experiment. The high frequency semicircle completely disappears for a mortar specimen hydrated for about one year, when the thickness of the specimen is decreased to a limiting value.

(5). There is a necessary condition for the measurement of a.c. impedance behavior, i.e. no semicircle can be obtained for dried cement systems.

This is obvious since no solid-liquid interfaces exist in the system and hence no corresponding a.c. impedance behavior can be determined.

7.4.2. Hydrating Portland Cement-Silica Fume Systems

The a.c. impedance spectra for the systems with the partial replacement of cement by silica fume, 5, 10 and 15% based on the weight of cement, are plotted in figure 7.6 - figure 7.11. The results indicate that addition of silica fume significantly changes the impedance behavior of the hydrating system. The principal features compared with the neat cement paste system are as follows:

(1). The diameter of the semicircle increases linearly with the amount of added silica fume at the same hydration time. The critical hydration time for the occurrence of the semicircle is shortened dramatically.

It is suggested that there are two principle causes for the increased diameter of the semicircle. The first is that N can be dramatically increased when silica fume is added to

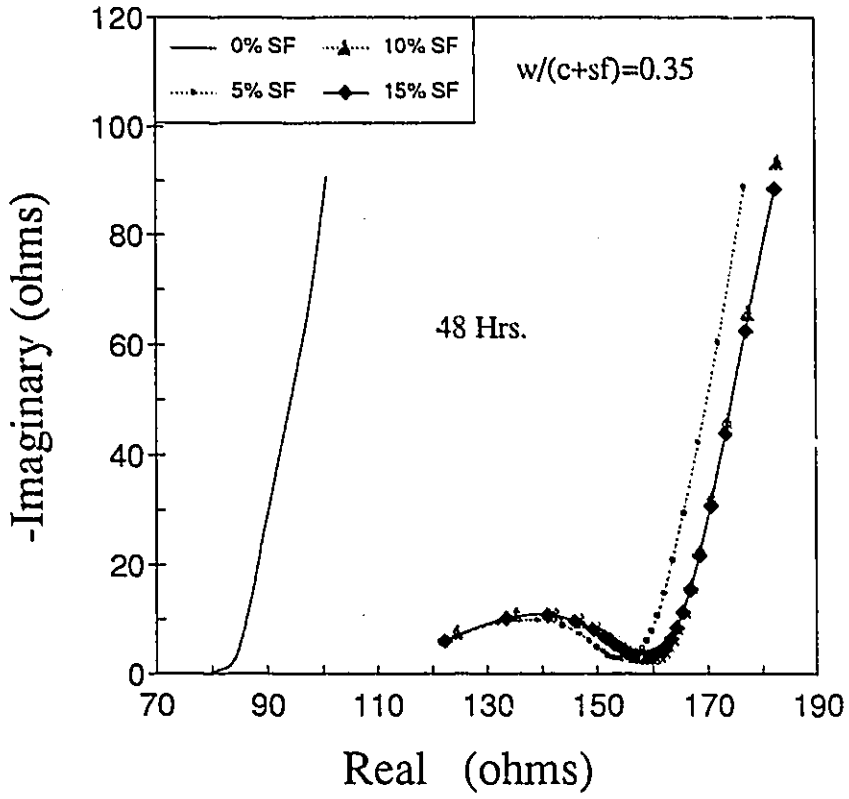

Figure 7.6. The a.c. impedance spectra of silica fume-cement paste systems at 48 hrs. hydration

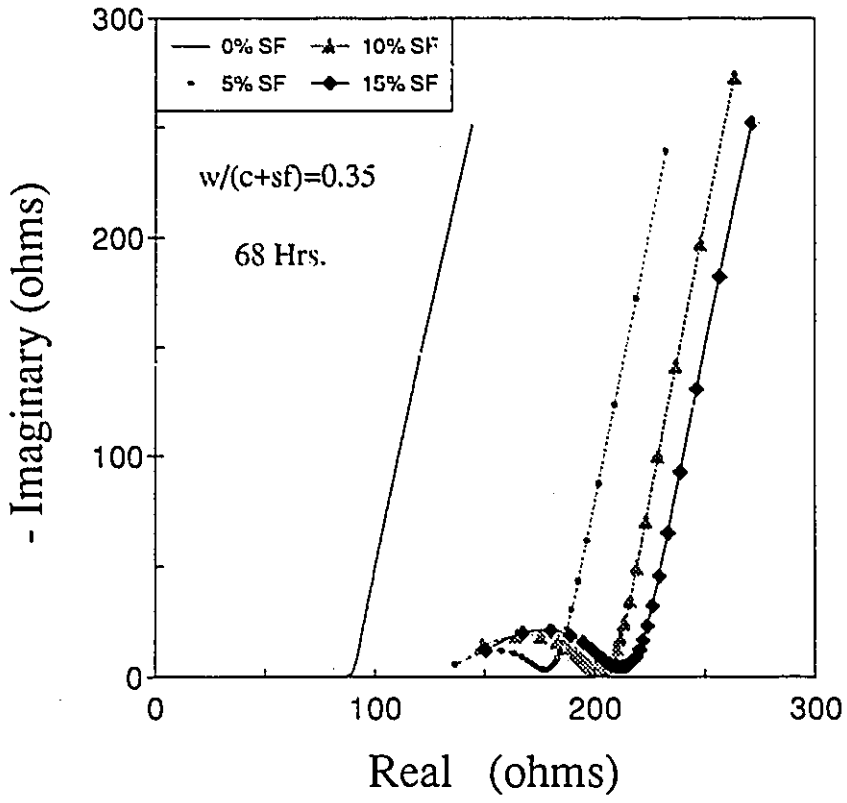

Figure 7.7. The a.c. impedance spectra of silica fume-cement paste systems at 68 hrs. hydration

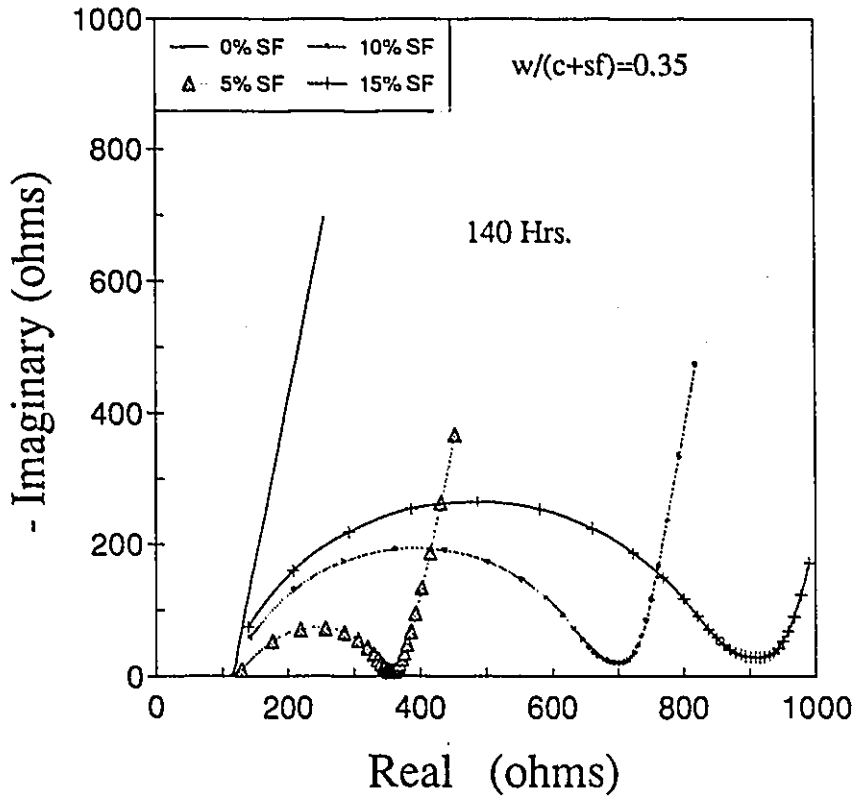

Figure 7.8. The a.c. impedance spectra of silica fume-cement paste systems at 140 hrs. hydration

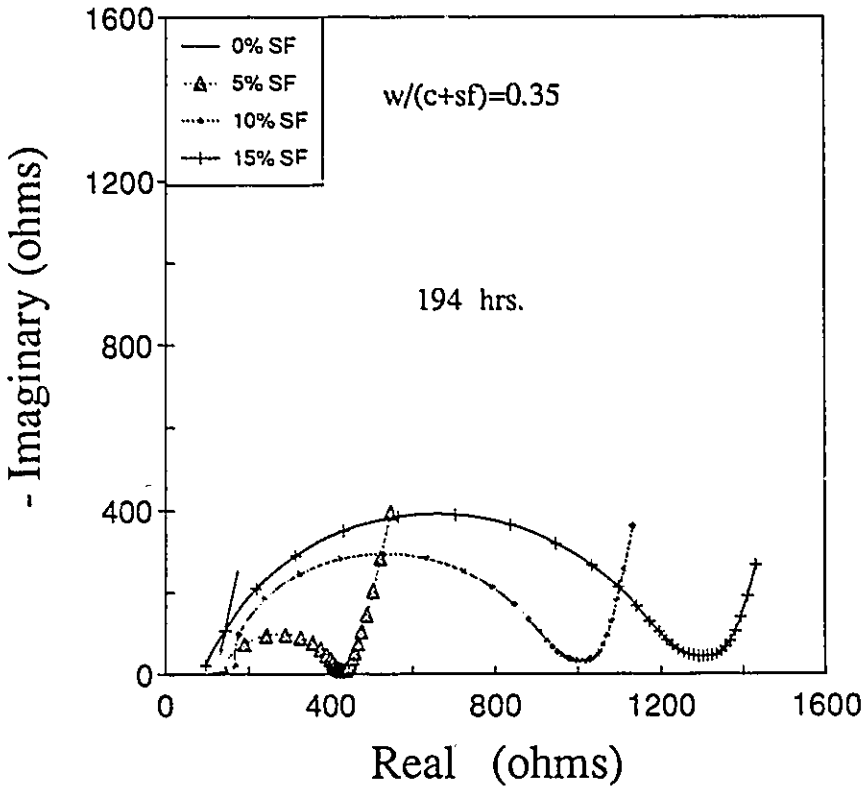

Figure 7.9. The a.c. impedance spectra of silica fume-cement paste systems at 194 hrs. hydration

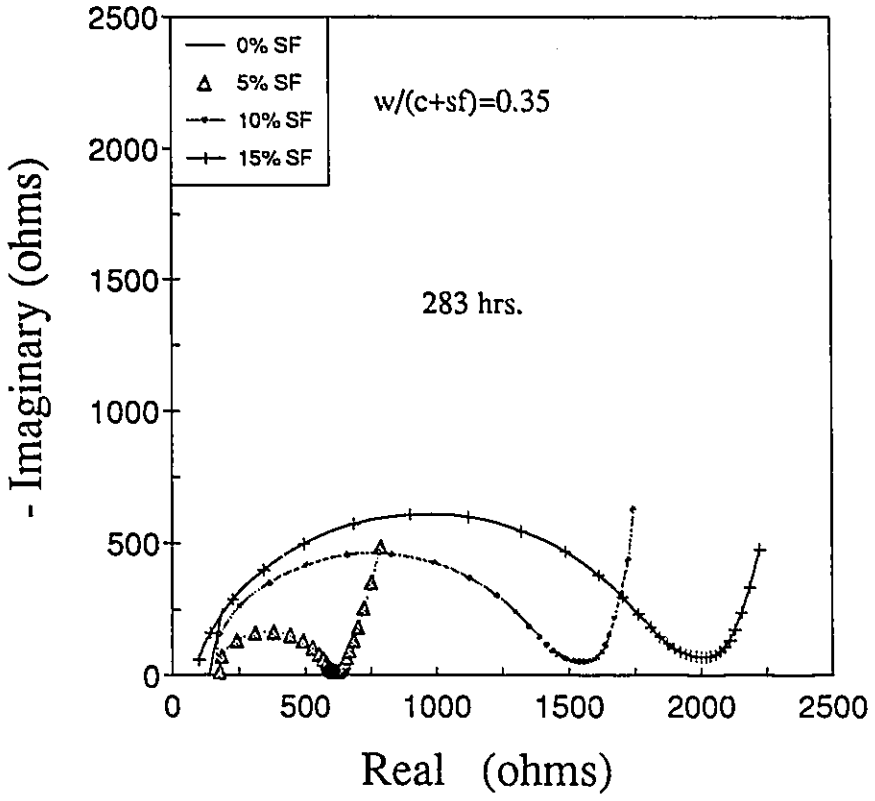

Figure 7.10. The a.c. impedance spectra of silica fume-cement paste systems at 283 hrs. hydration

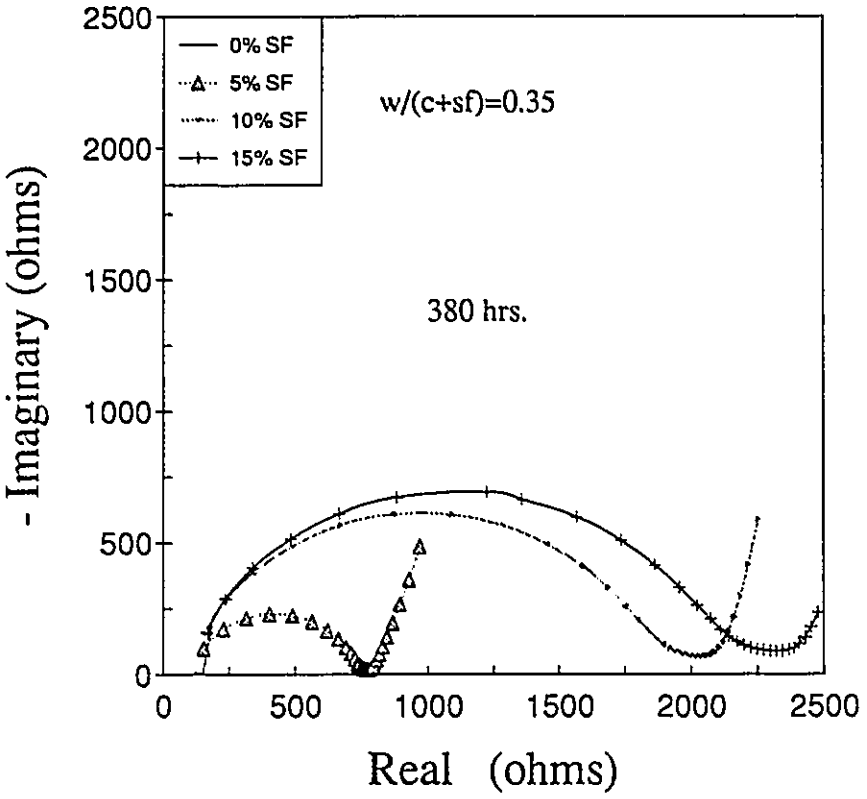

Figure 7.11. The a.c. impedance spectra of silica fume-cement paste systems at 380 hrs. hydration

the portland cement system due to the much smaller size of silica fume than that of cement particles. Secondly, due to the pozzolanic reaction in the system containing silica fume, the concentrations of ions in the pore solution is decreased. R_f will, therefore, be increased due to the decrease of σ_f. This can be seen from the values of f_o for these systems, Table 7.2. It can be seen from Table 7.2 that f_o for the silica fume paste decreases with increasing amount of silica fume after 194 hrs. hydration and has approximately the same value before that time. Lower values of f_o imply a lower interfacial conductivity, σ_f, (equation (7-15)), or higher value of R_f.

A larger value of D_{AC}($=NR_f$) for silica fume added systems than for neat cement systems at the same hydration time is apparently a result of the two factors discussed above.

Table 7.2. The values of f_o for silica fume-cement paste systems (MHz)

t (hrs.)	PC	5% SF	10% SF	15% SF
48	---	1.506	1.506	1.506
68	---	1.506	1.506	1.506
140	---	2.317	2.317	1.506
194	0.978	2.317	1.506	0.978
283	1.506	2.317	0.978	0.978
380	1.506	2.317	0.978	0 636

It is apparent that the shortened critical hydration time for the occurrence of the semicircle can be explained by the arguments presented above. The minimum D_{AC} value that can detected by the equipment occurs earlier than the corresponding value for the neat cement paste system.

Figure 7.12 indicated that there is a linear relationship between the diameter, D_{AC}, and the amount of silica fume added to the cement system, β_{SF}, i.e.

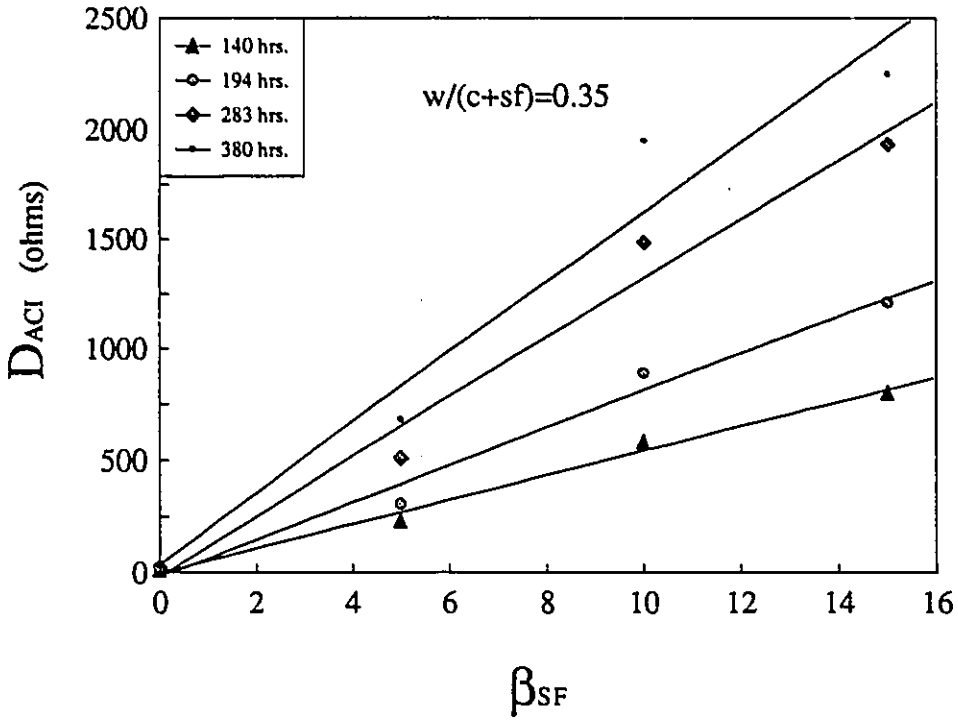

Figure 7.12. The diameter of the semicircle, D_{ACI}, vs the amount of silica fume, β_{SF}

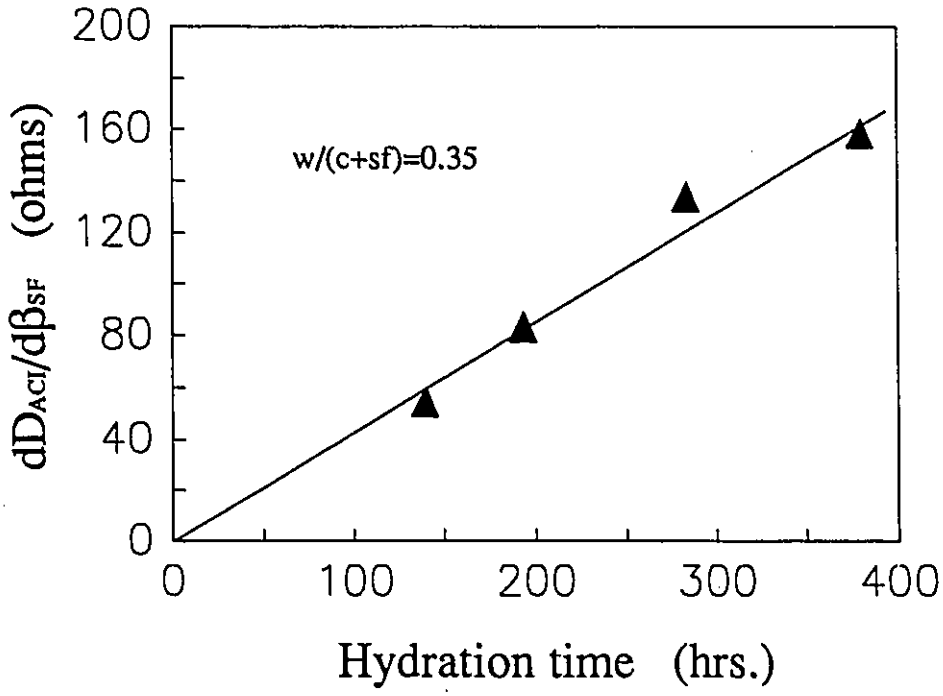

Figure 7.13. $dD_{ACI}/d\beta_{SF}$ vs the hydration time

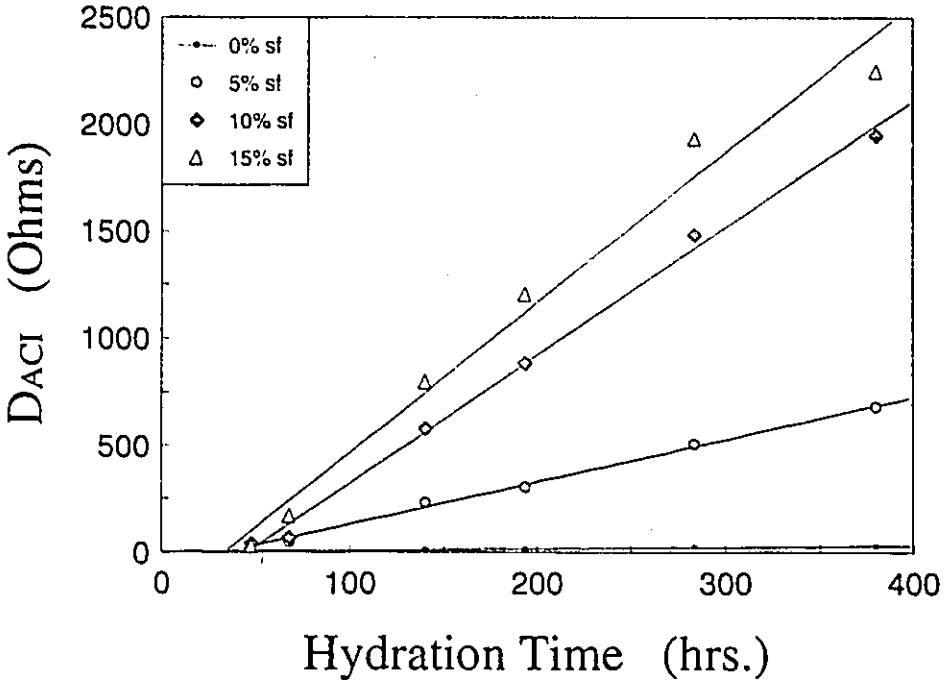

Figure 7.14. The diameter of the semicircle for silica fume-cement paste systems vs hydration time

$$D_{ACI} = K(t)\,\beta_{SF} + C \qquad (7\text{-}17)$$

where, $K(t)=\left(\frac{dD_{ACI}}{d\beta_{SF}}\right)_t$ is a coefficient dependent on the hydration time and C is a constant.

A plot of K(t) against hydration time, t, is given in figure 7.13. It can be seen from figure 7.13 that K(t) is a linear function of t, i.e.

$$K(t) = K_0\,t, \qquad (7\text{-}18)$$

where, K_0 is a constant.

Substituting equation (7-18) into equation (7-17) yields:

$$D_{ACI} = K_0\,\beta_{SF}\,t + C \qquad (7\text{-}19)$$

Equation (7-19) is an empirical equation correlating the diameter of the semicircle to silica fume content and hydration time for silica fume-cement paste systems.

(2). The rate of growth of the diameter increases with the amount of added silica fume at the same hydration time.

The diameters of the semicircles of the systems are plotted vs hydration time in figure 7.14. It can be seen that the diameter increases at a constant rate with hydration and the rate increases with the amount of silica fume. This result is obviously a natural deduction of equation (7-19).

§7.5 MICROSTRUCTURAL CHARACTERIZATION OF THE AGGREGATE-CEMENT PASTE INTERFACE BYA.C. IMPEDANCE TECHNIQUES

It has been demonstrated in the preceding discussions that the diameter of the semicircle, $D_{AC}=NR_f$, is a parameter very sensitive to the microstructure of the system. It can be used for the characterization of the density of the system since N, the number of solid-liquid interfaces between two electrodes, is a parameter dependent on the number, size and distribution of solid products in the system.

In this section, an attempt is given to characterize the microstructure of aggregate-cement paste interfaces by this technique. Different interfaces were made by coating quartz sand with silica fume(SF), blast furnace slag(BFS), fly ash(FA) and latex(EVA, a type of emulsion) by the method described in chapter five. The chemical composition of the mineral admixtures is listed in Table 3.3. The thickness of the coating layer is about 40-80 μm for the mineral admixture coated systems and 5 μm for the latex coated system. All the specimens were prepared with w/c=0.35 and aggregate/cement=0.50.

The a.c. impedance data are plotted in Real-Imaginary plane, as shown in figure 7.15 to figure 7.17, and the corresponding values of f_0 are listed in Table 7.3.

Table 7.3 The values of f_0 for aggregate-cement paste systems (MHz)

t (days)	SF	FA	BFS	EVA	PC
2	2.317	1.506	2.317	0.636	0.987
15	3.566	2.317	3.566	2.317	3.566
27	3.566	3.566	3.566	2.317	3.566

Apparent differences occur among these systems. Silica fume and slag coated systems have maximum semicircle diameters, and the latex coated system has the minimum diameter. All mineral admixture coated systems have a larger diameter than uncoated

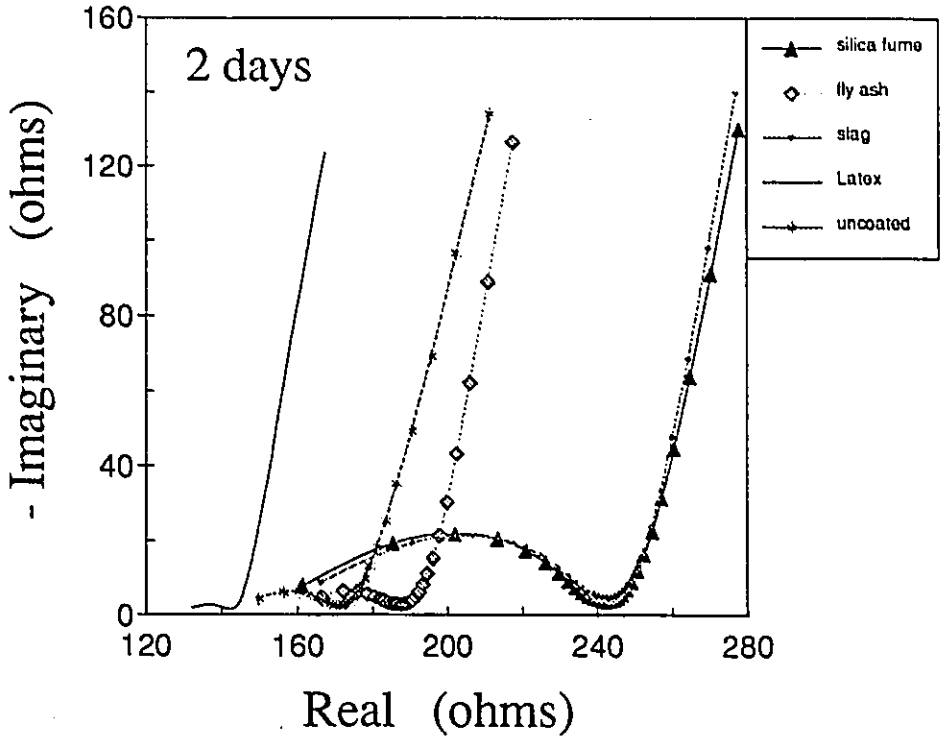

Figure 7.15. The a.c. impedance spectra of coated aggregate-cement paste systems at 2 days hydration

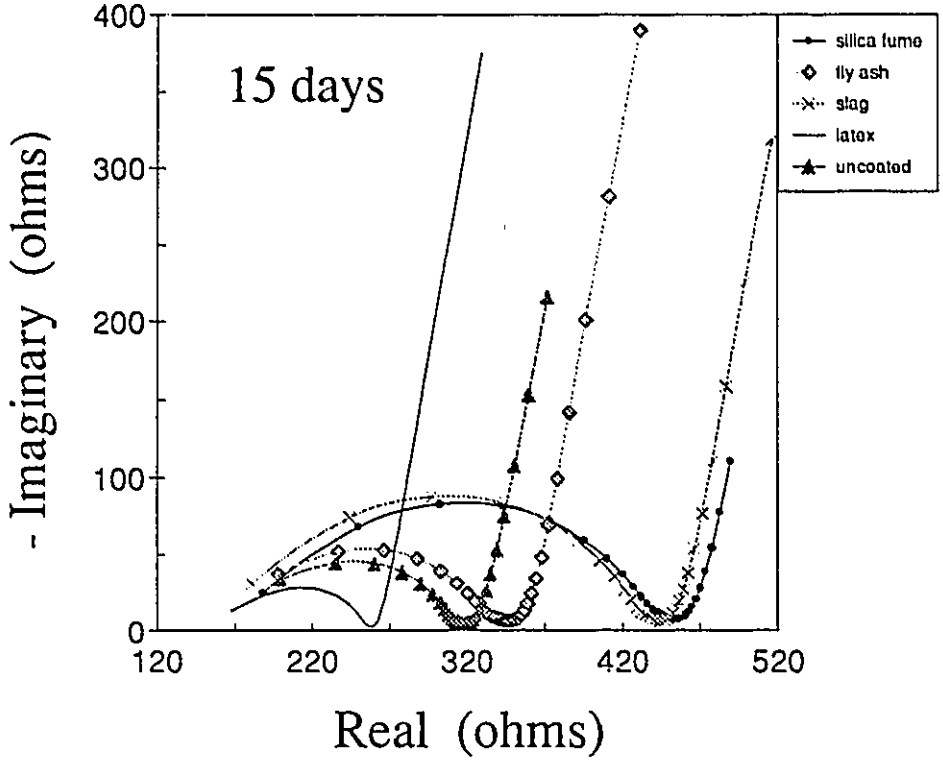

Figure 7.16. The a.c. impedance spectra for coated aggregate-cement systems at 15 days hydration

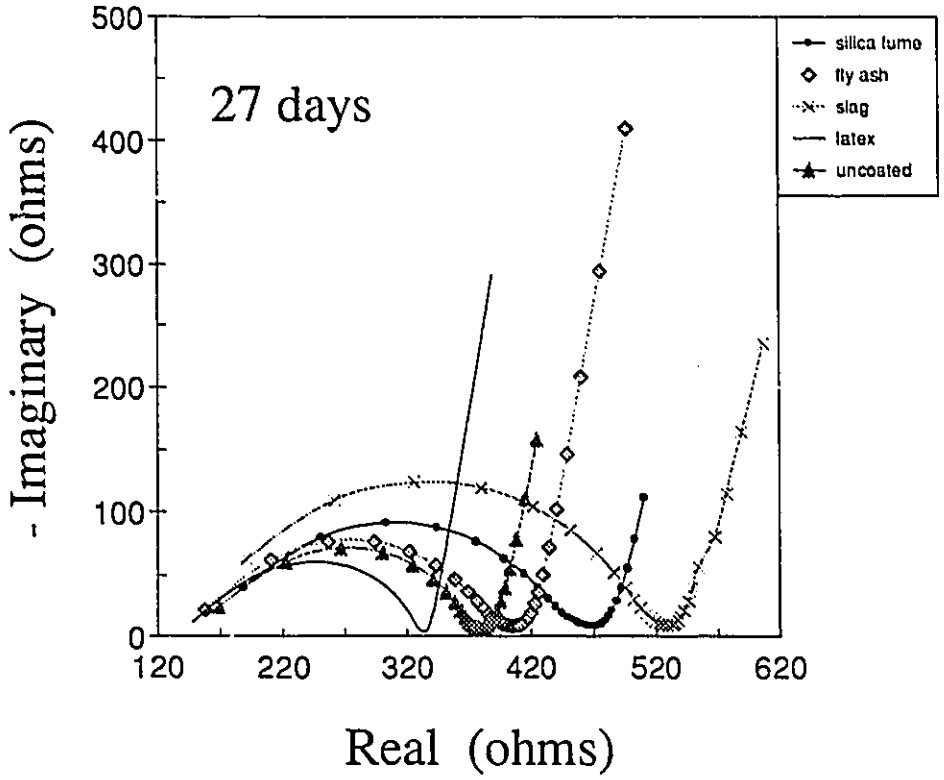

Figure 7.17. The a.c. impedance spectra for coated aggregate-cement paste systems at 27 days hydration

system; the diameter of the latex coated system is smaller. These results are completely consistent with the interfacial microstructure in those systems. Mineral admixture coated systems have more and the latex coated system less solid-liquid interfaces in the region between the aggregate and cement paste than the uncoated system. In addition, it is noted from Table 7.3 that all systems have the same solid-liquid interfacial conductivity at later hydration times except the latex coated system which has a lower value. Therefore, it is considered that the difference in the diameter of the semicircle is due principally to microstructural differences.

§7.6 CONCLUSIONS

(1). A theoretical model based on a.c. impedance spectroscopy for hydrating cement systems has been proposed. A fundamental understanding of the a.c. impedance behavior of hydrating cement systems has been obtained.

(2). The a.c. impedance behavior of hydrating cement systems results from solid-liquid interface phenomena and it is affected strongly by the microstructure of the system. It is suggested that a.c. impedance spectroscopy is an effective technique for characterizing microstructure of porous materials and investigating solid-liquid interfacial interaction.

(3). Two useful parameters for characterizing hydration of cement systems can be obtained from the a.c. impedance spectra: (i). the frequency at the top of the semicircle; (ii). diameter of the semicircle. The former can be used for characterizing solid-liquid interactions in the interfacial zone by relating it to the interfacial electrical conductivity. The latter is useful for characterizing the microstructure of the system.

(4). The electrical conductivity of the pore solution in the solid-liquid interfacial region is less than the conductivity of the pore solution extracted from hydrated cement paste by about three orders of magnitude. The solid-liquid interaction reduces the mobility of ions in the interfacial region and hence the electrical conductivity.

(5). The diameter of the semicircle for the hydrating portland cement system increases rapidly with hydration time. This is due mainly to the rapid increase of C-S-H gel and hence the number of solid-liquid interfaces with hydration.

(6). The addition of silica fume to the portland cement system generally results in a larger semicircle diameter and lower frequency at the circle apex than that of neat portland cement paste. The reason is that the number of solid-liquid interfaces is increased and the interfacial conductivity reduced by adding silica fume to the system. During the early hydration the diameter of the semicircle is directly proportional to the amount of silica fume and hydration time.

(7). Different a.c. impedance spectra for the systems containing different aggregate-cement paste interfaces were obtained. The difference is due principally to the different interfacial microstructure.

CHAPTER EIGHT

MECHANISM OF SULPHATE EXPANSION

SUMMARY

A re-examination of the theories of sulphate expansion was prompted by the conclusion drawn in the previous chapters that the quality of the interface in cement systems controls the ingress of sulphate ions. A theory concerning sulphate expansion phenomena in cement and concrete systems based on the principles of chemical-thermodynamics is presented. It suggests that sulphate expansion is a process in which chemical energy is being converted into mechanical work to overcome the cohesion of system. The expansive force results from "crystallization pressure" which is a result of the interaction between the solid product of a chemical reaction, e.g. ettringite, and the cement paste.

Two conditions are necessary for the occurrence of crystallization pressure:

(1). Confined crystal growth of the solid product.

(2). "Activity product" of reactants in the pore solution is greater than the "solubility product" of the solid product under atmospheric pressure.

The proposed theory has been validated by extensive experiments.

§8.1 INTRODUCTION

The effect of silica fume coated aggregate surfaces on sulphate resistance of mortar was discussed in chapter five. The mechanism of sulphate expansion was inferred but not discussed in detail. It is apparent that interface quality is related to the ingress of sulphate anions into mortar and concrete. This effect would not be complete without discussion of the mechanism of sulphate expansion. It also prompted a new look at current theories and development of new arguments in support of the crystallization pressure concept.

A detailed discussion concerning sulphate expansion will be given in the following sections. Sulphate expansion(a Canadian problem) is an important research topic cognate to interface studies.

There are two principal sources of sulphate expansion phenomenon in practice, i.e. reactions involving Type K and Type M expansive cements and those resulting from sulphate attack of concrete in water containing sulphates. The mechanism of sulphate expansion remains controversial.

The origin of sulphate expansion is not fully understood. Two principal theories of sulphate expansion, the Crystal Growth Theory and the Swelling Theory, have coexisted for decades. A detailed review of these theories is given by Cohen[76]. Expansion associated with formation of some crystals, especially ettringite and gypsum is common to both theories. The essential differences between them however lie in two principal areas:

(1). Mechanism of chemical reaction: According to the first theory, the chemical reaction concerned is by "topochemical" mode[77-79]. A "through-solution" mechanism characterizes the second theory[80-82].

(2). Mechanism of expansion: The first theory attributes the expansion to an anisotropic growth of crystals[83-86]; the second theory postulates that expansion occurs as a result of uptake of water and swelling of colloidal ettringite[80,81,87-89].

The intent of this chapter is not to comment explicitly on existing theories of sulphate expansion. It is noted, however, that any interpretation of experimental results or phenomena should be based on sound scientific principles. A general theory should be able to explain experimental phenomena and enable predictions. It should also be able to explain as many experimental phenomena as possible with minimum assumptions. The objectives of this chapter are to examine sulphate expansion phenomena from a chemical-thermodynamic point of view, and to advance a new explanation for sulphate expansion. The purpose is to also address possible methods of enhancing sulphate resistance of concrete, including those related to interface enhancement.

§8.2 THERMODYNAMIC PRINCIPLE OF CRYSTALLIZATION PRESSURE

The principle of crystallization pressure is advanced as follows.

Consider a hardened cement paste system immersed in a sulphate solution or the expansive cement/water system. Experience indicates that such systems are unstable. The state of these systems changes with time, and is normally accompanied by two principal events: microscopic formation of a new phase, e.g. ettringite, due to a chemical reaction

in the system, and macroscopic expansion of the hardened cement paste. The energetics of this system irrespective of the operative phenomena is a process in which chemical energy is converted into mechanical work to overcome the cohesion of system itself. The system in question is a chemical-thermodynamic system, and the sulphate expansion issue can be dealt with on the basis of chemical-thermodynamic theories and principles.

There are two important questions to be addressed in considering sulphate expansion as a process in which a new phase forms and chemical energy is converted into mechanical work:

(1). Chemically, what is the nature of the reactions concerned ?

(2). Thermodynamically, what is the origin of the expansion force ?

8.2.1. Mechanism of Chemical Reaction Concerning Ettringite Formation

There are two different postulates for ettringite formation associated with expansion. These involve topochemical formation and through-solution precipitation mechanisms.

The formation of ettringite through topochemical reaction is by in-situ conversion of alumina-bearing solid, e.g. C_3A, C_4AH_{19} etc., in contact with solution[78]. It is the rearrangement and movement of atoms or ions in the solid phase which cause a new phase, ettringite, to form. There is however a lack of convincing experimental evidence. It was considered that ettringite formation by this solid-solid conversion was most unlikely due to large differences in the structure of ettringite and C_4AH_{19}[81]. The rate and occurrence of a chemical reaction is dependent on kinetic factors if possible

thermodynamically. The solid-solid conversion is kinetically difficult at room temperature although possible thermodynamically. This type of solid phase reaction is more likely to occur at high temperature or in very low porosity system[90]. The structural symmetry of ettringite is completely different from some alumina-bearing solids, such as C_3A, C_4AF, $C_{12}A_7$ C_4AH_{13} etc.. The space group of ettringite structure is $C\bar{3}1c$, and those of C_3A, C_4AH_{13} are Pa3 and P2, respectively[91]. Ettringite formation by solid-solid conversion at room temperature is not normally expected.

The through-solution mechanism of ettringite formation has been confirmed by experiment[82]. The following equations for ettringite and gypsum formation are usually encountered in the literature concerning sulphate expansion:

$C_4A_3\bar{S} + 8\,C\bar{S} + 96H \longrightarrow 3C_6\,A\bar{S}_3H_{32}$ (ettringite)[76]

$C_3A + C\bar{S} + 32H \longrightarrow C_6\,A\bar{S}_3H_{32}$ (ettringite)[76]

$Ca(OH)_2 + Na_2SO_4 + H_2O \longrightarrow CaSO_4.2H_2O + 2NaOH$ gypsum)[92]

$C_3AH_6 + 3\,C\bar{S} + 26H \longrightarrow C_6\,A\bar{S}_3H_{32}$ (ettringite)[92]

It is stressed that a mechanistic explanation for expansion is not implicit in these expressions. They give the stoichiometric quantities of reactants concerned, and sometimes give rise to a misunderstanding that the substances on the left side of equations can directly react to form the products on the right side. This is not true.

The chemical equation concerning a solid phase formation from solution can be expressed in the following general form:

$$\gamma_1 R_1 + \gamma_2 R_2 + \cdots\cdots + \gamma_N R_N \rightleftharpoons S \qquad (8\text{-}1)$$

where, R_i i=1,2, ... N, is i^{th} reactant in the solution, and it can be an ion or a molecule. γ_i is called the stoichiometric coefficient of R_i . S is the solid product of the reaction. This expression has at least two meanings. First, it shows all the elements constituting a chemical reaction. This is important since from the equation we can know the factors affecting product formation. Secondly, this expression reflects a most important characteristic of chemical reactions, i.e. under a definite condition the reaction will reach an equilibrium state. It is noteworthy that this equilibrium is a dynamic equilibrium. This means that the rate of solid product formation equals its decomposition rate. From this standpoint, the reaction can be equivalently expressed as follows:

$$S \rightleftharpoons \gamma_1 R_1 + \gamma_2 R_2 + \cdots\cdots + \gamma_N R_N \qquad (8\text{-}1')$$

8.2.2. Thermodynamic Principle of Crystallization Pressure

The sulphate expansion phenomenon is always associated with the formation of a solid product, i.e. ettringite or gypsum. The expansion is therefore the result of interaction between cement paste and this solid product.

The hardened portland cement paste system exposed to sulphate solution will be considered and the process of solid product formation and the origin of internal expansive force analyzed.

When cement paste is exposed to sulphate solution a series of physico-chemical processes follows, e.g. the dissociation of hydrates in the paste to produce cations and anions in the pore solution, migration of the aggressive ion in the sulphate solution into the paste, etc.. A new solid phase, ettringite for example, spontaneously forms as the

concentrations of ions in the pore solution are supersaturated with respect to it. This is expressed by the chemical equation:

$$\gamma_1 R_1 + \gamma_2 R_2 + \cdots\cdots + \gamma_N R_N \overset{\Delta G<0}{\rightleftharpoons} S \qquad (8\text{-}2)$$

This chemical reaction can carry on spontaneously from the left to the right as long as Gibbs free energy difference of this reaction is negative, i.e. $\Delta G < 0$, or

$$A = \sum_{i=1}^{N} \gamma_i \mu_i - \mu_s > 0 \qquad (8\text{-}3)$$

where, μ_i , i=1,2, ... N, is the chemical potential of reactant R_i in the pore solution, and μ_s is that of solid product, S. A is defined as "chemical affinity" of the reaction.

At constant temperature and pressure, the chemical potential of the reactants in the pore solution is a function of their activity or concentration ie. the higher concentration, the larger chemical potential. In the above reaction, μ_i i=1,2, ... N, will be reduced due to the consumption of the reactants to form the solid product. Therefore, if there is no external reactant source available, the reaction will soon reach an equilibrium state and there will be no additional formation of the solid product. The system is trying to reach an equilibrium state by producing a solid product to reduce the chemical potential of the reactants. At equilibrium , the following condition is met:

$$A = \sum_{i=1}^{N} \gamma_i \mu_i - \mu_s = 0$$

or

$$\mu_s = \sum_{i=1}^{N} \gamma_i \mu_i \qquad (8\text{-}4)$$

The reaction (8-2) can continue for the cement paste immersed in sulphate solution since the reactants consumed by the reaction can be supplied by some hydrates in the paste and the external sulphate solution. Chemical equilibrium, if any, would be disturbed and additional solid product formed due to continuous migration of aggressive ion into the paste.

The process described above is applicable to the early stage of sulphate attack of cement paste. During the first few days, there is almost no expansion, accompanying increase of solid product. The solid products are formed in the capillary pores, reducing the porosity of cement paste.

It is suggested that the formation of solid product is by two processes: nucleation and crystal growth. The former determines the number of nuclei and the latter determines their size.

A relevant question concerns what happens when the size and quantity of the solid product increases to such an extent that further crystal growth is confined due to limited capillary space and aggressive ions are still penetrating into the paste.

Under this circumstance the chemical equation (8-2) becomes:

$$\gamma_1 R_1 + \gamma_2 R_2 + \cdots\cdots + \gamma_N R_N \rightleftharpoons S_{confined} \qquad (8\text{-}2')$$

Further formation of the product must result in an interaction between the product and the paste when crystal growth of solid product, S, is confined by a capillary boundary. In

the early stage of the process solid product formation is freely carried out and the system approaches equilibrium through reduction in chemical potential of the reactants. At more advanced stages the system approaches the equilibrium state differently due to the restriction of capillary wall. The only way the system can approach an equilibrium state is to increase the chemical potential of the product, μ_s , if μ_i , i=1,2, ... N, has been increased(equation 8-4), or the following equation must therefore be satisfied according to equation(8-4):

$$d\mu_s = \sum_{i=1}^{N} \gamma_i \, d\mu_i \qquad (8\text{-}5)$$

Equation (8-5) indicates that as chemical potentials of reactants increase due to any cause, the chemical potential of confined solid product will increase.

Generally, for a pure solid μ_s is a function of temperature and pressure, i.e.

$$\mu_s = \mu_s (T, P_s) \qquad (8\text{-}6)$$

where, T is absolute temperature, and P_s is pressure of solid product. Hence,

$$d\mu_s = (\frac{\partial \mu_s}{\partial T})_{P_s} dT + (\frac{\partial \mu_s}{\partial P_s})_T dP_s$$

$$= -\bar{s}_s \, dT + \bar{v}_s \, dP_s \qquad (8\text{-}7)$$

where, $\bar{s}_s = -(\frac{\partial \mu_s}{\partial T})_{P_s}$, $\bar{v}_s = (\frac{\partial \mu_s}{\partial P_s})_T$ are molar entropy and molar volume of solid product.

Chemical potentials of reactants in solution, μ_i , i=1,2, ... N, can be generally expressed as follows[93]:

$$\mu_i = \mu_i^{\circ}(T, P_l) + RT \ln a_i \qquad (8\text{-}3)$$

where, R is universal gas constant, and μ_i° is chemical potential of R_i at the "standard state", a function of temperature and pressure of liquid phase, and a_i is activity of R_i in the solution. From (8-8), it follows:

$$d\mu_i = d\mu_i^{\circ}(T, P_l) + (R \ln a_i)\, dT + RT\, d\ln a_i \qquad (8\text{-}9)$$

Substituting (8-7), (8-9) into (8-5) yields:

$$\bar{v}_s\, dP_s = \sum_{i=1}^{N} \gamma_i\ d\mu_i^{\circ}(T, P_l) + (\bar{s}_s + R \sum_{i=1}^{N} \gamma_i \ln a_i)\, dT + RT \sum_{i=1}^{N} \gamma_i\, d\ln a_i \qquad (8\text{-}10)$$

Generally speaking, the cement paste system is under atmospheric pressure and constant temperature, and the pore solution in the paste or the sulphate solution is open to the atmosphere. P_l, T in equation (8-10) can, therefore, be considered as constants, and (8-10) can be simplified as follows:

$$dP_s = \frac{RT}{\bar{v}_s} \sum_{i=1}^{N} \gamma_i\, d\ln a_i \qquad (8\text{-}11)$$

Equation (8-11) indicates that the activity increase of any reactant in the pore solution will increase the pressure of corresponding confined solid product. Apparently the increase of solid product pressure is through the interaction of the product and the capillary wall.

Integrating equation (8-11) referred to a reference state where there is no solid product-cement paste interaction yields:

$$\int_{P_s^o}^{P_s} dP_s = \frac{RT}{\bar{V}_s} \sum_{i=1}^{N} \gamma_i \int_{a_i^o}^{a_i} d\ln a_i$$

or

$$P_s - P_s^o = \frac{RT}{\bar{V}_s} \sum_{i=1}^{N} \gamma_i \ln\left(\frac{a_i}{a_i^o}\right)$$

$$= \frac{RT}{\bar{V}_s} \ln \prod_{i=1}^{N} \left(\frac{a_i}{a_i^o}\right)^{\gamma_i}$$

$$= \frac{RT}{\bar{V}_s} \ln \left(\frac{K_{sp}}{K_{sp}^o}\right) = \frac{RT}{\bar{V}_s} \ln \Omega \qquad (8\text{-}12)$$

where, $K_{sp} = \prod_{i=1}^{N} (a_i)^{\gamma_i}$, $K_{sp}^o = \prod_{i=1}^{N} (a_i^o)^{\gamma_i}$ are terms referred to as the "solubility product" of the solid product,S, at pressure P_s, P_s^o, respectively, and $\Omega = K_{sp}/K_{sp}^o$ is the "solubility product ratio". P_s^o is the pressure of the solid product without pore-wall interaction and is generally considered to be equal to atmospheric pressure.

Let $\quad P_c = P_s - P_s^o$

then $\quad P_c = \frac{RT}{\bar{V}_s} \ln \Omega \qquad (8\text{-}13)$

P_c results from solid product-cement paste interaction due to increase in activity of the reactants in the pore solution and the restriction of product crystal growth; it is exerted simultaneously on both the solid product and the cement paste. It is apparent that P_c is the

major cause of sulphate expansion. Therefore, it is referred to as **"crystallization pressure"**.

Since $\bar{v}_s = M_s/\rho_s$, where M_s , ρ_s are molecular weight and density of the product, S, the equation (8-13) can be expressed as

$$P_c = \frac{RT\rho_s}{M_s} \ln \Omega \qquad (8\text{-}13')$$

Equations (8-13) and (8-13') can also be expressed in the derivative form:

$$\left(\frac{\partial P_c}{\partial \ln\Omega}\right)_T = \left(\frac{\partial P_c}{\partial \ln K_{sp}}\right)_T = \frac{RT}{\bar{v}_s} = \frac{RT\rho_s}{M_s} \qquad (8\text{-}14)$$

or

$$\left(\frac{\partial P_c}{\partial \Omega}\right)_T = \frac{1}{\Omega}\frac{RT}{\bar{v}_s} \quad ; \quad \left(\frac{\partial P_c}{\partial K_{sp}}\right)_T = \frac{1}{K_{sp}}\frac{RT}{\bar{v}_s} \qquad (8\text{-}14')$$

The values of $RT/\bar{v}_s$ for some cement compounds at 25°C are given in Table 8.1.

Table 8.1. Values of $RT/\bar{v}_s$ at 25°C for some cement compounds

Materials	M_s (g/mol)	ρ_s (g/cm³)	$\bar{v}_s$ (cm³/mol)	$RT/\bar{v}_s$ (MPa)
$C_6A\bar{S}_3H_{32}$ (Ettringite)	1255	1.73	725	3.42
$CaSO_4.2H_2O$ (Gypsum)	172	2.32	74.2	33.4
$Ca(OH)_2$ (Portlandite)	74.1	2.23	33.2	74.6
$Mg(OH)_2$ (Brucite)	58.3	2.38	24.5	101

8.2.3. Discussion

Sulphate expansion phenomena in cement paste and concrete related to ettringite are discussed in terms of a "crystallization pressure" concept as follows.

In the cement-water system, some of the principal aqueous species and possible chemical reactions are given in Table 8.2 and Table 8.3.

From Table 8.3, ettringite formation in the cement/water system can be expressed by

$$6\,Ca^{2+} + 2\,Al(OH)_4^- + 3\,SO_4^{=} + 4\,OH^- + 26\,H_2O \rightleftharpoons 3CaO{\cdot}Al_2O_3{\cdot}3CaSO_4{\cdot}32H_2O \qquad (8\text{-}15)$$

(Ettringite)

with $K_{sp}^{o} = 10^{-43.13}$ at 25°C.

Table 8.2. Principal aqueous species in the cement-water system[94]

Cations	Anions	Neutral Species
Ca^{2+}	$SO_4^{=}$	$H_4SiO_4^{\circ}$
Mg^{2+}	HCO_3^-	$H_2CO_3^{\circ}$
Na^+	$Fe(OH)_4^-$	
K^+	$Al(OH)_4^-$	
H^+	$H_3SiO_4^-$	
$MgOH^+$	$H_2SiO_4^{=}$	
	$CO_3^{=}$	
	OH^-	
	Cl^-	

$Al(OH)_4^-$ is used on the left of equation (8-15) since it is a principal form of aluminium ion at pH>8.0 although it can hydrolyze to form a wide variety of products in water[94] .

Table 8.3. Some reactions and corresponding values of K_{sp}^{o} at 25°C[94]

Mineral	Reaction	log K_{sp}^{o}
H_2O	$H_2O \rightleftharpoons H^+ + OH^-$	-14.00
Brucite	$Mg(OH)_2 \rightleftharpoons Mg^{2+} + 2OH^-$	-10.89
Portlandite	$Ca(OH)_2 \rightleftharpoons Ca^{2+} + 2OH^-$	-5.19
Ettringite	$6Ca^{2+}+2Al(OH)_4^-+3SO_4^{=}+4OH^-+26H_2O \rightleftharpoons 3CaO{\cdot}Al_2O_3{\cdot}3CaSO_4{\cdot}32H_2O$	-43.13
Gibbsite	$Al(OH)_3 + OH^- \rightleftharpoons Al(OH)_4^-$	-1.01
Calcite	$CaCO3 \rightleftharpoons Ca^{2+} + CO_3^{=}$	-8.41
Gypsum	$CaSO_4{\cdot}2H_2O \rightleftharpoons Ca^{2+} + SO_4^{=} + 2H_2O$	-4.58

It can be seen from the above thermodynamic analysis that the occurrence of the "crystallization pressure" requires two necessary conditions:

(1). Confined crystal growth;

(2). $\Omega > 1$ or $K_{sp} > K_{sp}^{o}$ after condition (1) is met.

Condition (1) leads to a deduction that for the expansive cement/water system or portland cement paste/sulphate solution system, there is no expansion during the early stage of ettringite formation even though most of the total amount of ettringite may be formed during this period. This has been confirmed by experiment[81, 95]. Condition (2) can be readily met for practical expansive cement/water and portland cement paste/sulphate solution systems since ettringite has a very low value of K_{sp}^{o} . This is why observed

sulphate expansion is usually associated with ettringite. It is noted, however, that theoretically any solid product, not only ettringite, may produce "crystallization pressure" and cause expansion phenomena as long as the above two conditions are met. For example, formation of gypsum is one of principal causes of the expansion of portland cement paste in contact with sulphate solution[81, 10, 96].

The theory also indicates that increased expansion does not require formation of larger amounts of ettringite after "crystallization pressure" begins, as indicated by experiment[81], since the expansive pressure comes from the increase of reactant activity in the liquid phase. This is a thermodynamic effect, i.e. conversion of chemical energy into mechanical work. It is emphasized, however, that since the system does expand under the crystallization pressure, the space available to ettringite formation would increase and the quantity of ettringite formed during the expansion would marginally increase.

It is indicated from equation (8-15) that one of the significant factors affecting the crystallization pressure of ettringite is the concentration of Ca^{2+} in the pore solution. In a practical system, Ca^{2+} is supplied principally by solid $Ca(OH)_2$. Solid $Ca(OH)_2$ in the system results in a higher concentration of Ca^{2+} in the solution since $Ca(OH)_2$ has a larger K°_{sp} value, $10^{-5.19}$ (Table 8.3). This is a basic assurance for the crystallization pressure of ettringite. This is also the reason ettringite can cause expansion for the system containing lime but can not for that without lime[76, 84, 87, 97].

§8.3 RELATIONSHIP BETWEEN CRYSTALLIZATION PRESSURE AND EXPANSION

Generally, the linear strain of a material depends on two principal factors, i.e. the stress resulting from an external load and the deformation behaviour of the material. A general relation can be expressed as follows:

$$\varepsilon = \sigma / E \qquad (8\text{-}16)$$

where, ε is strain, σ is stress and $E=(\partial\sigma/\partial\varepsilon)_{\text{other conditions}}$ is the deformation modulus of the material and equals Young's modulus for an elastic material.

It is noted that the crystallization pressure, P_c, is actually not equal to the stress, σ, in equation (8-16) since the interaction between the solid product and cement paste takes place only in a limited space within the specimen. The average stress, σ, caused by P_c, therefore, should be calculated by

$$\sigma = \psi_s P_c \qquad (8\text{-}17)$$

where, ψ_s is the fraction of contacting area between the solid product and cement paste with respect to total specimen section area. It is suggested that ψ_s is a function of following factors:

$\psi_s = \psi_s$ (Porosity of specimen; Number, size and geometry of solid product particulates).

Substituting (8-13), (8-17) into (8-16) yields:

$$\varepsilon = \frac{\psi_s}{E} P_c = \frac{\psi_s}{E} \frac{RT}{\overline{v}_s} \ln \Omega$$

$$= \frac{\Psi_s}{E} \frac{RT}{\bar{v}_-} \ln \frac{K_{sp}}{K^o_{sp}}$$

$$= \frac{\Psi_s}{E} \frac{RT}{\bar{v}_s} \ln \prod_{i=1}^{N} \left(\frac{a_i}{a^o_i}\right)^{\gamma_i} \qquad (8\text{-}18)$$

Equation (8-18) yields a relationship between the linear expansion of specimen and the crystallization pressure. From equation (8-18), a comprehensive analysis of the factors affecting expansion of cement, mortar and concrete subjected to a sulphate solution is as follows:

8.3.1. Effect of Activity or Concentration of the Reactants on Expansion

From equation (8-18), any reactant activity increase leading to the increase of K_{sp} will increase the value of Ω and hence the value of ε. It is apparent that reactant activity in the pore solution is a most direct factor affecting the expansion since it controls the value of the crystallization pressure.

Consider chemical reactions for the formation of ettringite and gypsum which are usually associated with sulphate expansion:

$$6\,Ca^{2+} + 2\,Al(OH)_4^- + 3\,SO_4^{=} + 4\,OH^- + 26\,H_2O \rightleftharpoons 3CaO{\cdot}Al_2O_3{\cdot}3CaSO_4{\cdot}32H_2O$$

(Ettringite)

$$Ca^{2+} + SO_4^{=} + 2\,H_2O \rightleftharpoons CaSO_4{\cdot}2H_2O$$

(Gypsum)

For an ordinary portland cement paste in contact with sulphate solution, $Al(OH)_4^-$ in the pore solution comes from the hydration of C_3A, and its concentration is believed to be

determined indirectly by the content of C_3A in cement. The concentration of Ca^{2+} is controlled principally by the dissociation of portlandite, i.e.

$$Ca(OH)_2 \rightleftharpoons Ca^{2+} + 2\,OH^- \qquad (8\text{-}19)$$

The concentration of OH^-, however, is directly affected by the content of alkali in cement. $SO_4^=$ in the pore solution comes mainly from the external sulphate solution, and its concentration continuously increases with time, which leads to a continuous increase of the crystallization pressure and the expansion.

As described previously, a higher concentration of Ca^{2+} ion in the pore solution is a basic assurance for activation of crystallization pressure from ettringite or gypsum. According to equation (8-19), the concentration of Ca^{2+} would be strongly affected by the concentration of OH^- in the presence of portlandite. It can be readily shown that the value of Ω or the crystallization pressure of ettringite or gypsum decreases with the increase of OH^- concentration:

$$\text{By definition} \quad \ln\Omega = \ln K_{sp} - \ln K^{\circ}_{sp}$$

$$\therefore \qquad d\ln\Omega = d\ln K_{sp} = d\Big(\sum_{i=1}^{N} \gamma_i \ln a_i\Big) = \sum_{i=1}^{N} \gamma_i \, d\ln a_i \qquad (8\text{-}20)$$

For ettringite, when the OH^- concentration in the pore solution is changed, we have

$$d\ln\Omega_{ettringite} = 6\, d\ln[Ca^{2+}] + 4\, d\ln[OH^-] + 2\, d\ln[Al(OH)_4^-] + 3\, d\ln[SO_4^=] + 26\, d\ln[H_2O]$$

$$\approx 6\, d\ln[Ca^{2+}] + 4\, d\ln[OH^-] \qquad (8\text{-}21)$$

where, $[R_i]$ is the activity of R_i .

Since $[Ca^{2+}]\,[OH^-]^2 = K^o_{sp.\ portlandite}$ (a constant at a certain temperature)

$$\therefore \quad d\ln[Ca^{2+}] = -2\, d\ln[OH^-] \tag{8-22}$$

Substituting (8-22) into (8-21) yields:

$$\left(\frac{d\ln\Omega_{ettringite}}{d\ln[OH^-]}\right)_T = -8 < 0 \tag{8-23}$$

Similarly,

$$\left(\frac{d\ln\Omega_{gypsum}}{d\ln[OH^-]}\right)_T = -2 < 0 \tag{8-24}$$

Equations (8-23) and (8-24) indicate that the crystallization pressure of ettringite or gypsum decreases with an increase in the concentration of OH^- in the pore solution if the system contains portlandite. This is why the sulphate expansion is suppressed when cement or the sulphate solution concerned contains a higher content of alkali[91,98]. It should be noted, however, that if the system contains no portlandite the crystallization pressure of ettringite or gypsum is expected to increase with an increase in the concentration of OH^- in the pore solution.

A practical application of the above theoretical analyses is that the sulphate resistance of concrete may be enhanced by reducing the concentrations of reactants, especially Ca^{2+} and $SO_4^{=}$, in the pore solution as much as possible. The addition of mineral admixtures to concrete is an effective way for this propose because of the pozzolanic reaction, and it can be expected that condensed silica fume is most effective since both cations and

anions in the pore solution can be significantly reduced by the addition of silica fume[66].

8.3.2. Effect of Temperature on Expansion

The temperature effect on expansion is complex. In equation (8-18), the values of E and K^{o}_{sp} are temperature dependent, with E decreasing and K^{o}_{sp} generally increasing with the increase of temperature. In addition increasing temperature reduces the solubility of portlandite, and hence the value of K_{sp} for ettringite or gypsum would change with temperature. It can be expected from equation (8-18), however, that the principal effect of temperature on expansion comes from T in the equation, i.e. the value of expansion will be proportional to temperature, as will be shown by experiment.

8.3.3. Effect of Young's Modulus on Expansion

It is apparent that the lower the value of E, the larger the expansion. In the process of sulphate attack on concrete, the value of E gradually decreases with time and the occurrence of microcracks, generally accelerates expansion.

8.3.4. Effect of the Value of ψ_s on Expansion

Since the solid product forms in the pores of the specimen, ψ_s is obviously dependent of the porosity of the specimen and the number, size and geometry of the solid product particulates. The greater the porosity of the specimen and the greater the amount of solid product, the greater is the value of ψ_s . Moreover, a smaller particulate size of solid product generates a larger specific surface area, which would result in a larger probability

of the solid product-cement paste contact, viz. a greater value of ψ_s . This is probably why a larger expansion is associated with a smaller particulate size of ettringite[76].

§8.4 VALIDATION OF THE THERMODYNAMIC THEORY

8.4.1. Experimental

Experiments were designed to validate the theory and arguments advanced in the preceding sections.

White portland cement, WP, was used. The chemical composition is shown in Table 3.2. Quartz sand with size ranging from #14 - #20 U.S. mesh was used as aggregate.

The following experiments were conducted to validate the crystallization pressure theory:

(1). Effect of the activity of reactant on expansion.

Linear expansion was measured for the mortar bars cured in water for 7 days at 20°C. The bars had w/c=0.50 and aggregate/cement=2/1 and were immersed in 5% Na_2SO_4 solution. All samples were removed from the Na_2SO_4 solution at an expansion value of about 0.4 - 0.5 % and immediately placed in the following solutions:

(i). Saturated $Ca(OH)_2$ solution;

(ii). 0.35 N NaOH solution;

(iii). 0.05 N $Ba(OH)_2$ solution;

(iv). Pure water.

The length changes of the mortar bars in the above solutions were continuously measured.

(2). Efficiency of silica fume addition for enhancing resistance to sulphate attack of mortar.

The sulphate resistance of mortars with and without silica fume addition were evaluated by determining the linear expansion of the mortar bars in 5% Na_2SO_4 solution.

(3). Effect of temperature on expansion.

Mortar bars cured in water for 7 days at 20°C(w/c=0.50 and aggregate/cement=2/1) were immersed in a 5% Na_2SO_4 solution at 4°C, 23°C, 38°C, 64°C, respectively. The linear expansion was determined for these mortars at specified ages.

All samples had dimensions: 6.0 cm x 1.0 cm x 1.0 cm. The linear expansion of mortar is calculated by application of equation (5-4).

8.4.2. Results and Discussion

The expansion of mortar bars exposed to 5% Na_2SO_4 solution and then immersed in $Ca(OH)_2$, NaOH solutions and water is plotted vs time in figure 8.1.

The specimen shrinks slightly after immersion in NaOH solution but expands in saturated $Ca(OH)_2$ solution and water. These phenomena are predicted from the theory. Na^+, OH^-

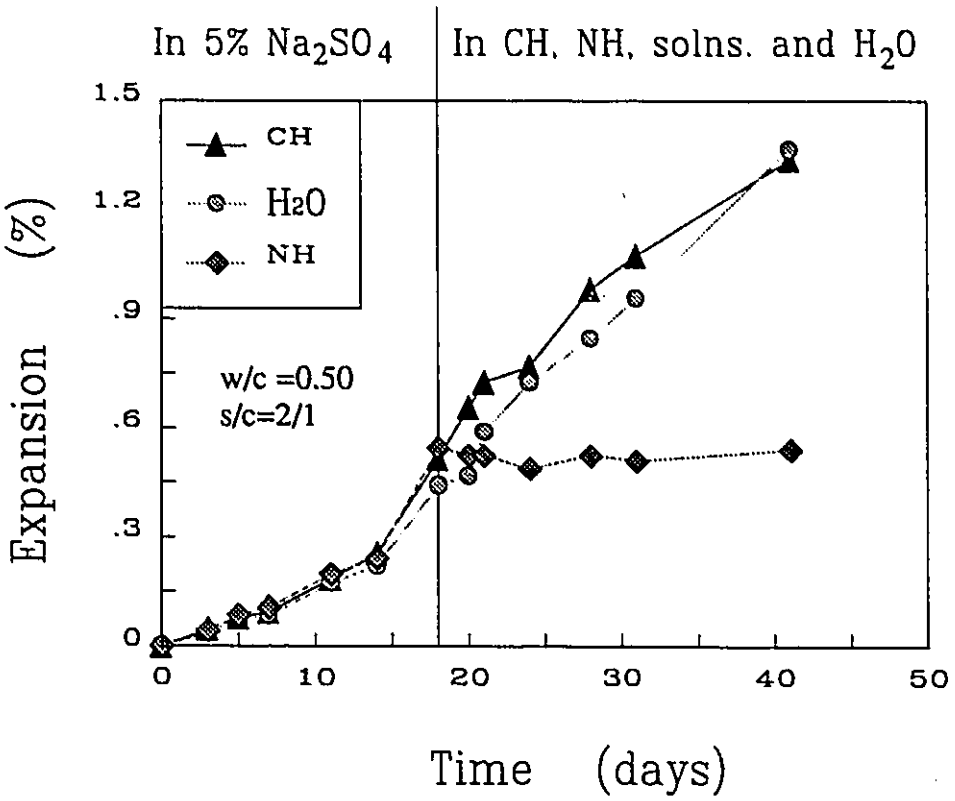

Figure 8.1. Quartz mortar expansion vs time, 20°C

ions will penetrate into the specimen pre-corroded by sulphate solution(characterized by ettringite formation and surface cracks) and placed in NaOH solution. The concentration or activity of OH^- in the pore solution will increase. The crystallization pressure of ettringite or gypsum consequently decreases according to the theoretical analysis. The crystallization pressure will dramatically increase due to the increase of Ca^{2+} concentration in the pore solution when the specimen is put in saturated $Ca(OH)_2$ solution. Of interest is that the expansion of the sample put in water also increases. According to the theory proposed and equation (8-15), this is associated with the increase of the activity of H_2O molecule in the pore solution although the concentrations of other ions may be diluted by the penetration of the H_2O molecule into the sample. The result appears to suggest an argument that the continuous expansion of the sample put in water is caused by the swelling effect due to uptake of water by colloidal ettringite[87-89]. It is emphasized, however, that since the sample is saturated by the aqueous solution during the course of the entire experiment, the uptake of water by ettringite, if any, would have been complete soon after formation of ettringite. Therefore, the result obtained would not be due to the swelling effect. It is apparent that the above results are due to the activity effect since there is not likely to be more ettringite formation after the samples are removed from the Na_2SO_4 solution.

The above results warrant the conclusion that when formation of the solid product is confined the activity of the reactant concerned in the liquid phase is a decisive factor determining the magnitude of the crystallization pressure and hence expansion.

The expansion of a mortar bar pre-corroded in 5% Na_2SO_4 solution then put in 0.05 N $Ba(OH)_2$ solution is plotted against time in figure 8.2.

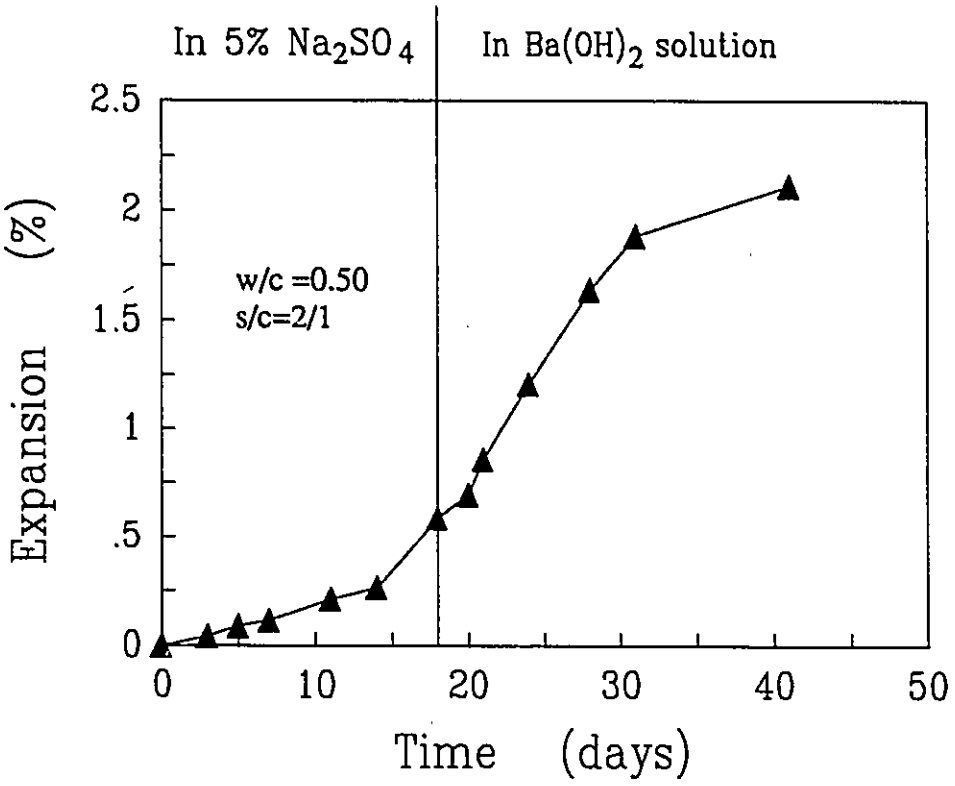

Figure 8.2. Quartz mortar expansion vs time, 20°C

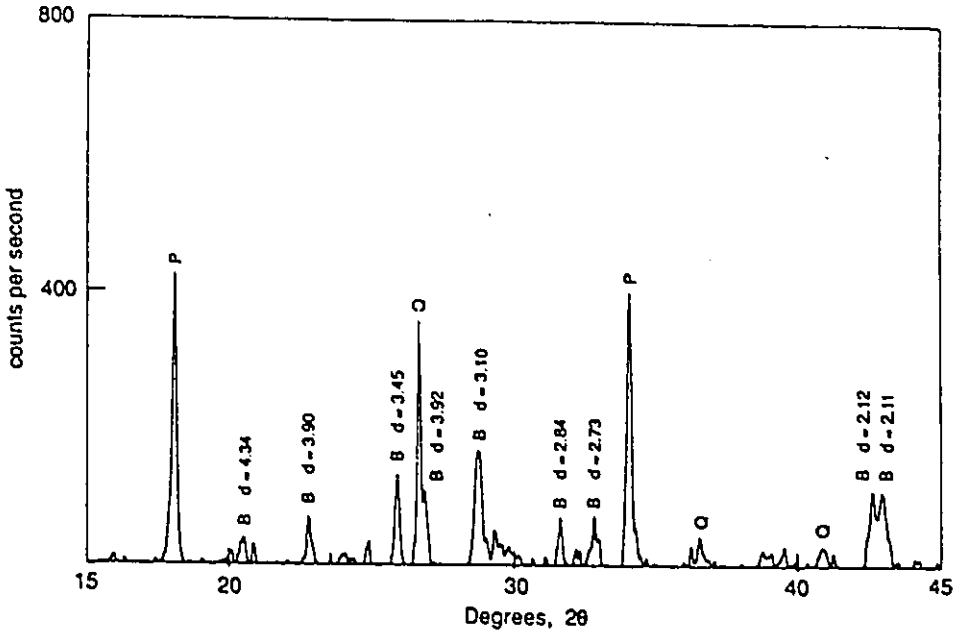

Figure 8.3. XRD spectrum of the mortar specimen immersed in $Ba(OH)_2$ solution for two weeks
B - Barite, P - Portlandite, Q - Quartz

The specimen expands dramatically after immersion in $Ba(OH)_2$ solution in a similar manner to the specimen in figure 8.1. The difference, however, is that this expansion is caused by the formation of barite instead of ettringite. The XRD spectrum of the sample immersed in $Ba(OH)_2$ solution for two weeks is given in figure 8.3. Barite is a principal reaction product.

The formation of barite is expressed by the following chemical equation:

$$Ba^{2+} + SO_4^{=} \rightleftharpoons BaSO_4 \quad \text{(Barite)} \qquad (8\text{-}25)$$

It can be calculated from thermodynamic data for $BaSO_4$, Ba^{2+} and $SO_4^{=}$ [99] that the value of K_{sp}^{o} for barite at 25°C is $10^{-9.98}$. K_{sp}^{o} is relatively small. Therefore, the two conditions for the occurrence of the crystallization pressure of barite are easily met in the experiment.

This result confirms that expansion associated with solid formation from a liquid phase is a universal phenomenon, as revealed by the theory, as long as the two necessary conditions are satisfied. The expansion associated with ettringite is one that is usually encountered in cement and concrete systems. Other direct evidence is provided by Deng, et al's work concerning the expansion mechanism of magnesia as an additive to cement[100]. It was found that expansion is caused in confined space by formation of $Mg(OH)_2$ from the pore solution; it is affected by pore solution alkalinity. Tang et al. discussed the effect of pore solution pH on the expansion caused by the alkali-carbonate reaction in concrete[101]; it is considered to be due to the crystallization pressure of brucite ie. $Mg(OH)_2$, at dolomite particle-matrix(soil network) interfaces in the

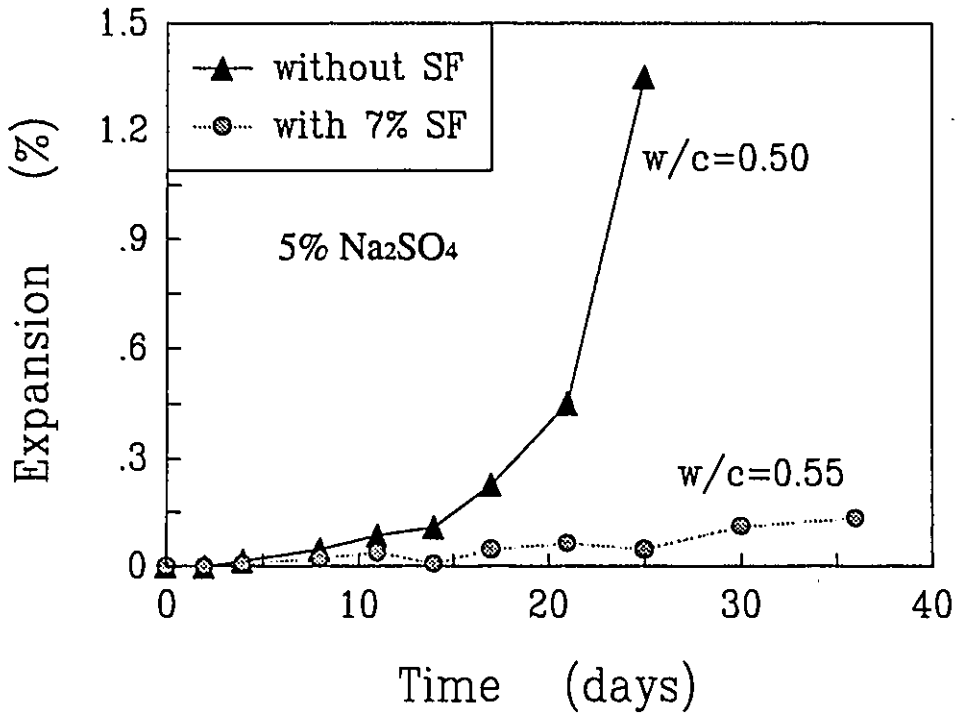

Figure 8.4. Effect of a silica fume addition on mortar expansion in sulphate solution

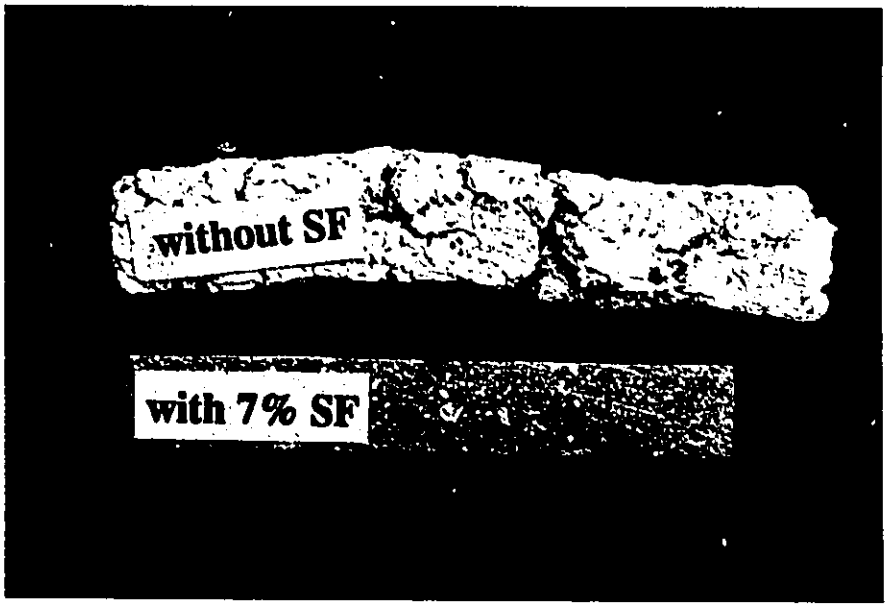

Figure 8.5. Appearance of mortar in 10% sodium sulphate solution for 4 months
(The two mortars have the same volumetric fraction of aggregate: 0.40)

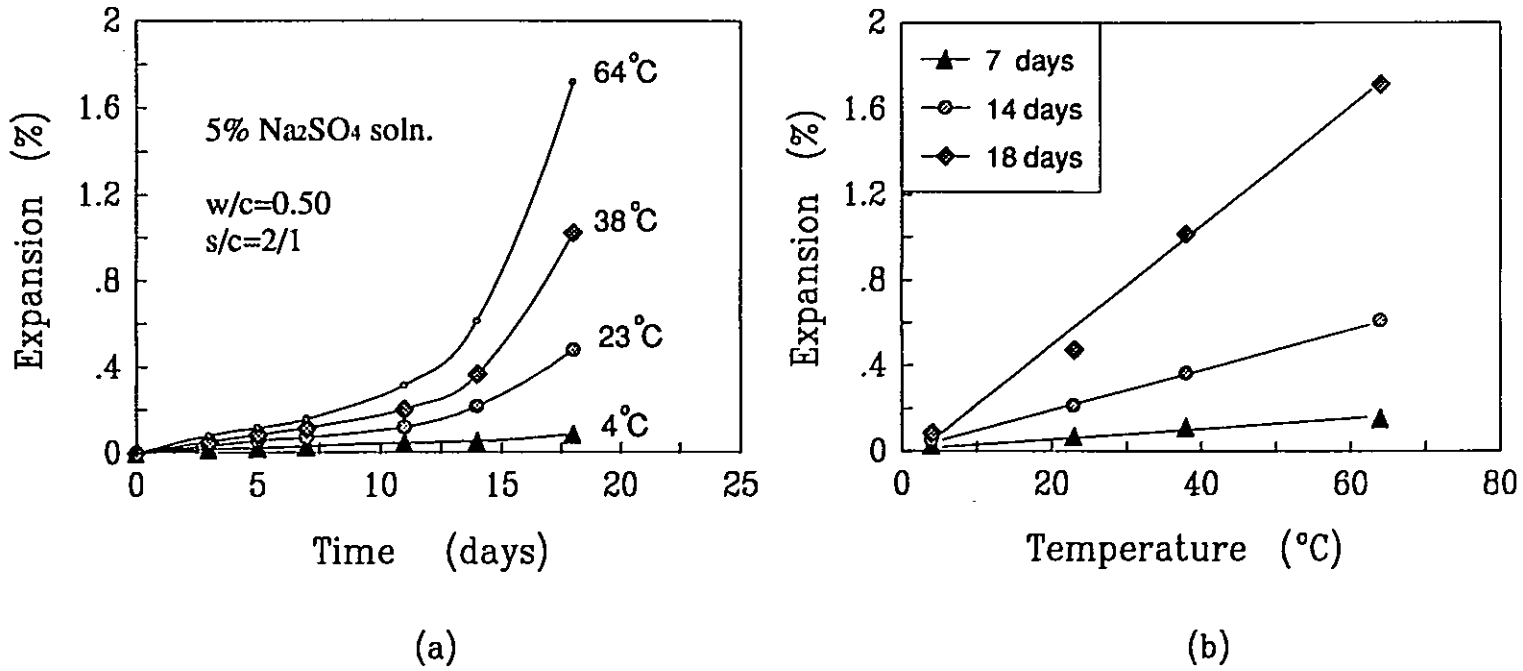

Figure 8.6. Effect of temperature on sulphate expansion
(a). Expansion vs time
(b). Expansion vs temperature

aggregate. It was indicated that the expansion increases with increasing pH value of the pore solution.

Figures 8.4 and 8.5 demonstrate the difference in sulphate resistance of mortars with and without 7% silica fume by the weight of cement. The mortars were cured in water for 28 days at 20°C before being immersed in sodium sulphate solution. Two mortars were prepared with the same initial porosity to minimize the effect of permeability difference. It can be seen that the sulphate resistance of mortar can be significantly enhanced by silica fume addition, as predicted previously. This is primarily attributed to the reduction in the concentrations of the reactants involved in ettringite formation due to the addition of silica fume resulting in reduced crystallization pressure.

The effect of temperature on sulphate expansion is shown in figure 8.6. As mentioned previously, the expansion increases linearly with the increase of temperature. A similar result for expansive cement was given by Ish-Shalom et al[95].

§8.5 CONCLUSIONS

(1). Sulphate expansion of cement and concrete is a process in which chemical energy is converted into mechanical work to overcome the cohesion of the system.

(2). Expansive force results from "crystallization pressure" which is a result of interaction between cement paste and the solid products of the chemical reaction concerned.

(3). Two conditions are necessary for the occurrence of crystallization pressure: (i). confined crystal growth of the solid product, and (ii). a value of "solubility product ratio" greater than one, i.e. $\Omega>1$, or $K_{sp} > K^{o}_{sp}$.

(4). Expansion associated with the formation of a solid product from a liquid phase is a universal phenomenon as long as the two necessary conditions for the generation of crystallization pressure are met. The expansion phenomena associated with ettringite formation are usually encountered in cement paste, mortar and concrete systems contacting sulphate solution as the two conditions for crystallization pressure induced by ettringite formation are easily met.

(5). Theory and experiment indicate that the most important factor affecting sulphate expansion in cement and concrete systems is the activity or concentration of the reactant concerned in the pore solution. Temperature is also a very important factor affecting sulphate expansion.

(6). It is always beneficial for sulphate resistance of concrete to reduce the concentration of the ions in the pore solution with respect to the formation of ettringite or gypsum, especially Ca^{2+} and $SO_4^{=}$ ions. Suppressing the concentration of the ions related to formation of ettringite or gypsum and decreasing the permeability of concrete are probably the most effective ways to improve the sulphate resistance of concrete.

(7). The sulphate resistance of concrete can be significantly enhanced by the addition of silica fume to the system. The reason is that the concentration of cations and anions like Ca^{2+} and OH^{-} etc. in the pore solution are decreased by the addition of silica fume.

CHAPTER NINE

SUMMARY OF CONCLUSIONS

1. A systematic electrical conductivity theory for the interface characterization of cement composites is proposed in this study. Based on the proposed theory, a novel investigative method, **the electrical conductivity method**, has been developed. The proposed theory indicates that the characteristics of interfacial microstructure and interfacial zone formation and development can be described uniquely by a parameter, referred to as the "θ-parameter" or "interfacial excess conductance".

2. Extensive experimentation indicates that the θ-parameter is a powerful interfacial microstructural descriptor. Several new findings pertaining to the nature of the non-porous inert aggregate-cement paste interface were obtained:

   (i). The interfacial zone is generally less dense than the bulk paste.

   (ii). The rate of formation of interfacial microstructure is greater than that of the bulk paste.

   (iii). The thickness of the interfacial zone decreases with decreasing aggregate size.

(iv). The thicknesses of the water film on the aggregate surface at mixing and the whole interfacial zone increase with w/c ratio.

3. A hypothesis for interfacial zone formation was validated by development and application of the electrical conductivity models of the interfacial zone and the bulk paste. The hypothesis emphasizes two elements for the interfacial zone formation: (i). the existence of the water film on the aggregate surface at the beginning of mixing; (ii). the "effect region" containing a few layers of cement particles close to the water film as a source of the hydrates for formation and development of the interfacial microstructure. The existence of the water film is a decisive factor causing the porosity of the interfacial zone.

4. A relationship between interfacial bond strength and interfacial microstructure is developed. It was suggested that reducing the thickness of the water film and using low w/c ratio are two possible methods of enhancing interfacial bond strength.

5. A method of enhancing interfacial microstructure, i.e. coating aggregate surfaces with silica fume, was developed. The experiments indicated that the interfacial microstructure can be effectively densified by aggregate surface treatment. The consequence of interfacial densification is that compressive strength and sulphate resistance of mortar are increased; bending strength is however increased only at later hydration times.

6. The electrical conductivity method is useful in studying interfacial cement chemistry, especially in understanding the mechanism of alkali-aggregate. It is suggested that the interfacial chemical reaction in aggregate-cement systems usually results in a negative value of θ-parameter. This has potential as a criteria to determine if there is a chemical reaction at the interface or not.

7. A theoretical model for a.c. impedance spectroscopy of hydrating cement systems was developed. A fundamental understanding of the a.c. impedance behavior of hydrating cement systems has been obtained through application of the proposed model. It is suggested that a.c. impedance technique is very effective for characterizing microstructure of cement paste and aggregate-cement paste interface.

8. A thermodynamic theory of sulphate expansion is proposed after a careful analysis of the physico-chemical processes concerning the sulphate expansion. The theory is validated by extensive experiments. It is indicated from the theory that expansive force results from "crystallization pressure" which is a result of interaction between cement paste and the solid products of the chemical reaction concerned. Two conditions are necessary for the occurrence of crystallization pressure: (i). confined crystal growth of the solid product, and (ii). a value of "solubility product ratio" greater than one, i.e. $\Omega>1$. Expansion associated with the formation of a solid product from a liquid phase is a universal phenomenon as long as the two necessary conditions for the generation of crystallization pressure are met. The theory and experiment suggest that it is always beneficial for sulphate resistance of concrete to reduce the concentration of the ions in the pore solution with respect to the formation of ettringite or gypsum, especially Ca^{2+} and SO_4^{2-} ions. Suppressing the concentration of the ions related to formation of ettringite or gypsum and decreasing the permeability of concrete are probably the most effective ways to improve the sulphate resistance of concrete.

REFERENCES

[1] J. Farran, Doctorat ès Sciences, Universite de Toulouse, Revue des Matériaux de Construction, No. 490-491 et 492 (1956).

[2] P. Kumar Mehta, "Concrete: Structure, Properties, and Materials", by Prentice-Hall, Inc., Englewood Cliffs, New Jersey 07632, 113 (1986).

[3] J. Glucklich, International Conference on the Structure of Concrete, Cement and Concrete Association, Landon, 82 (1968).

[4] S. Mindess, S. Diamond, Materiaux et Constructions, 15(86), 107 (1982).

[5] S. Mindess, S. Diamond, Cem. Concr. Res., 12, 569 (1982).

[6] T.T.C. Hsu, F.O. Slate, G.M. Sturman, G. Winter, J. Amer. Concr. Inst., 60, 209 (1963).

[7] H. Hornain, M. Regourd, 8th Inter. Congre. on the Chem. of Cem., Rio de Janeiro, Vol. V, 53 (1986).

[8] A.K. Maji, S.P. Shah, Report for the Center for Concrete and Geomaterials, Northwestern University, (1987).

[9] M. Saito, M. Kawamura, Cem. Concr. Res. 16, 653 (1986).

[10] Xie Ping, M. Sc. thesis, "Interfacial Characteristics and Its Effects on Electrical Conductivity, Chemical Corrosion Resistance and Ionic Diffusivity of Mortar", Nanjing Institute of Chemical Technology, Nanjing, Jiangsu, P.R. China, (1986).

[11] E. Hoke, P. Wilhartitz, M. Grasserbauer, G. Eder, Mikrochim. Acta. Suppl., (10), 307 (1983).

[12] E. Hoke, P. Wilhartitz, M. Grasserbauer, G. Eder, Fresenius Zeitshrift für Analytische Chemie, 318(2), 124 (1984).

[13] S. Mindess, Symposium Proc. Mater. Res. Soc., "Bonding in Cementitious Composites", Eds. S.Mindess & S.P. Shah, Pittsburgh, Vol. 114, 3 (1988).

[14] L. Struble, J. Skalny, S. Mindess, Cem. Concr. Res., 10(2), 279 (1980).

[15] J.C. Maso, 7th Inter. Congre. on the Chem. of Cem., Paris, Vol. 1, VII -1/3 (1980).

[16] S. Diamond, 8th Inter. Congre. on the Chem. of Cem., Rio de Janeiro, Vol. I, 122 (1986).

[17] F. Massazza, U. Costa, 8th Inter. Congre. on the Chem. of Cem., Rio de Janeiro, Vol.I, 158 (1986).

[18] L. Struble, Symposium Proc. Mater. Res. Soc., "Bonding in Cementitious Composites", Eds. S.Mindess & S.P. Shah, Pittsburgh, Vol. 114, 11 (1988).

[19] B.D. Barnes, S. Diamond, W.L. Dolch, Cem. Concr. Res. 8(2), 233 (1978).

[20] Z.Y. Chen, I. Odler, Cem. Concr. Res. 17, 784 (1987)

[21] L. Struble, S. Mindess, Inter. Jour. of Cem. Compos. and Lightweight Concr., 5(2), 79 (1983).

[22] K.L. Scrivener, P.L. Pratt, 8th Inter. Congre. on the Chem. of Cem., Rio de Janeiro, Vol. III, 466 (1986).

[23] P.J.M. Monteiro, P.K. Mehta, Cem. Concr. Res., 15(2), 378 (1985).

[24] J. Wang, B.Y. Liu, S.S. Xie, Z.W. Wu, 8th Inter. Congre. on the Chem. of Cem., Rio de Janeiro, Vol. III, 461 (1986).

[25] J. Grandet, J. Ollivier, 7th Inter. Congre. on the Chem. of Cem., Paris, Vol. III, VII-63 (1980).

[26] P.J.M. Monteiro, Ph.D. Thesis, University of California, Berkeley, (1985).

[27] Z.Y. Chen, I. Odler, Cem. Concr. Res., 17, 784 (1987).

[28] K.L. Scrivener, E.M. Gartner, Symposium Proc. Mater. Res. Soc., "Bonding in Cementitious Composites", Eds. S.Mindess & S.P. Shah, Pittsburgh, Vol. 114, 77 (1988).

[29] K.L. Scrivener, A. K. Crumbie, P.L. Pratt, Symposium Proc. Mater. Res. Soc., "Bonding in Cementitious Composites", Eds. S.Mindess & S.P. Shah, Pittsburgh, Vol. 114, 87 (1988).

[30] E.J. Garbocze, D.P. Bentz, J. Mater. Res., 6(1), 196 (1991).

[31] Xie Ping, Tang Mingshu, Il Cemento, 85(1), 33 (1988).

[32] G.P. Tognon, D. Cangiano, 7th Inter. Congre. on the Chem. of Cem., Paris, Vol. III, VII-133 (1980).

[33] Z.Y. Chen, J.G. Wang, Cem. Concr. Res., 17, 544 (1987).

[34] M.H. Zhang, O.E. Gjϕrv, Cem. Concr. Res., 20(4), 610 (1990).

[35] O. Valenta, "Durability of Concrete", Czechoslovadia, 53 (1961).

[36] L. Cussino, A. Negri, 7th Inter. Congre. on the Chem. of Cem., Paris, Vol. IV, V-62 (1980).

[37] A. Bachiorrini, Murat, A. Negro, Proc. of Inter. Symp. on Bond between Cement Pastes and Other Mater., 17-19th, INSA, Toulouse, France, Nov. (1982).

[38] J. Grandet, J.P. Ollivier, Cem. Concr. Res., 10(6), 759 (1980).

[39] P.J.M. Monteiro, P.K. Mehta, Cem. Concr. Res., 16(2), 127 (1986)

[40] F. Massazza, M. Pezzuoli, 7th Inter. Congre. on the Chem. of Cem., Paris, Vol. III, VII-16 (1980).

[41] G.P. Tognon, Pursella, 7th Inter. Congre. on the Chem. of Cem., Paris, Vol. III, VII-75 (1980).

[42] H. Yoshikazu, H. Michiaki, Semento Gijutsu Nenpo, (36), 124 (1982).

[43] Z.Y. Chen, W.M. Zhao, J. Lin, Materials and Structures, 21, 329 (1988).

[44]. X.Q. Wu, S.F. Han, Q.H. Bian, M.S. Tang, Proc. 8th Inter. Congress on the Chem. of Cem., Brazil, Vol. III, 454 (1986).

[45]. X.Q. Wu, D.X. Li, Q.H. Bian, L.Q. Guo, M.S. Tang, Cem. Concr. Res. 17, 709 (1987).

[46]. X.Q. Wu, D.X. Li, X. Wu, M.S. Tang, Symposia Proc. Mater. Res. Soc., "Bonding in Cementitious Composites", Eds. S.Mindess & S.P. Shah, Pittsburgh, Vol.114, 35 (1988).

[47]. S. Popovics, Materials and Structures, 20, 32 (1987)

[48] M. Conjeaud, A. Bonin, C.M. Geoge, R. Montgomery, F.P. Sorrentino, Proc. of Inter. Symp. on Bond between Cement Pastes and Other Mater., 17-19th, INSA, Toulouse, France, Nov. C12 (1982).

[49] C.M. Geoge, F.P. Sorrentino, Silicates Industrials, (3), 77 (1982).

[50] R.L. Berger, Cem. Concr. Res., 4(1), 99 (1974).

[51] Shen Yang, Zu Zhongzi, Xie Ping, Tang Mingshu, "A NEW METHOD OF ENHANCING CEMENT-AGGREGATE INTERFACES, I. IDEAL AGGREGATE AND ITS EFFECTS ON INTERFACIAL MICROSTRUCTURES', Cem. Concr. Res., In press (1992).

[52] Shen Yang, Zu Zhongzi, Xie Ping, Tang Mingshu, "A NEW METHOD OF ENHANCING CEMENT-AGGREGATE INTERFACES, II. MECHANICAL PROPERTIES AND SULPHATE ATTACK RESISTANCES OF MORTARS", Cem. Concr. Res., In press (1992).

[53] C.Y. Huang, R.F. Feldman, Cem. Concr. Res., 15, 285 (1985).

[54] A. Bentur, A. Goldman, M.K. Cohen, Symposia Proc. Mater. Res. Soc., "Bonding in Cementitious Composites", Eds. S.Mindess & S.P. Shah, Pittsburgh, Vol.114, 97 (1988).

[55] P.K. Mehta, P.J.M. Monteiro, Symposia Proc. Mater. Res. Soc., "Bonding in Cementitious Composites", Eds. S.Mindess & S.P. Shah, Pittsburgh, Vol. 114, 65 (1988).

[56] J. Wang, Symposia Proc. Mater. Res. Soc., "Bonding in Cementitious Composites", Eds. S.Mindess & S.P. Shah, Pittsburgh, Vol. 114, 127 (1988).

[57] D. Darwin, Z.J. Shen, S. Harsh, Symposia Proc. Mater. Res. Soc., "Bonding in Cementitious Composites", Eds. S.Mindess & S.P. Shah, Pittsburgh, Vol. 114, 105 (1988).

[58] N.R. Buenfeld, J.B. Newman, Magaz. Concre. Res., 36(127), 67 (1984).

[59] A. W. Adamson, "Physical Chemistry of Surfaces", 4th Ed., John Wiley & Sons, Toronto, 272, 185 (1982).

[60] L. Cussino, M. Murat, A. Negro, Il Cemento, 73(2), 77 (1976).

[61] V.S. Ramachandran, C.M. Zhang, Thermochemica Acta, 106, 273 (1986).

[62] Y.Z. Liu, P.Y. Yang, C.Y. Zhang, M.S. Tang, "Interfacial Bond Strength between Cement Paste and Aggregate", Journal of Chinese Ceramic Society, 16(4), 289 (1988). (in Chinese, with English abstract)

[63] R. Zimbelmann, Cem. Concr. Res., 17(4), 651 (1987).

[64] M.D. Cohen, J. Olek, W.L. Dolch, Cem. Concr. Res., 20(1), 103 (1990).

[65] J.A. Larbi, A.L.A. Fraay, J.M.J.M. Bijen, Cem. Concr. Res., 20, 506 (1990).

[66] V.M. Malhotra, V.S. Ramachandran, R.F. Feldman, Pierre-Claude Aitcin, "Condensed Silica fume in Concrete", CRC Press, Inc., Boca Raton, Florida, 46 (1987).

[67] S. Chatterji, "8th Inter. Confer. on Alkali-Aggregate Reaction", Eds. K. Okada, et al., Japan, 101 (1989).

[68] W.J. McCarter, S. Garvin, N. Bouzid, J. Mater. Sci. Lett., 7(10), 1056 (1988).

[69] W.J. McCarter, R. Brousseau, Cem. Concr. Res., 20 ,891 (1990).

[70] K.Brantervik, G.A. Niklasson, Cem. Concr. Res., 21,,469 (1991).

[71] C.A. Scuderi, T.O. Mason, H.M. J.Jennings, Mater. Sci. Lett., 26 ,349 (1991).

[72] Ping Gu, Ping Xie, J.J Beaudoin and R. Brousseau, " A.C. Impedance Spectroscopy (I): A New Equivalent Circuit Model for Hydrated Portland Cement Paste", Cem. Concr. Res. In Press, (1992).

[73] Ping Gu, Ping Xie, J.J Beaudoin, R. Brousseau, " A.C. Impedance Spectroscopy (II): Microstructural Characterization of Hydrating Cement-Silica Fume Systems", Cem. Concr. Res. In Press, (1992).

[74] G.H. Neale, "Interfacial Phenomena in Engineering", Lectures in the Department of Chemical Engineering, University of Ottawa, unpublished, (1990).

[75] N.R. Buenfeld, J.B. Newman, Magaz. Concr. Res., 36(127), 67 (1984).

[76] M.D. Cohen, Cem. Concr. Res., 13(6), 809 (1983).

[77] W.C. Hansen, Highway Res. Rec., 113, 1 (1966).

[78] B. Mather, Cem. Concr. Res., 3(5), 651 (1973).

[79] W.C. Hansen, Cem. Concr. Res., 3(5), 655 (1973).

[80] P.K. Mehta, Cem. Concr. Res., 3(5), 653 (1973).

[81] P.K. Mehta, Cem. Concr. Res., 13(3), 401 (1983).

[82] P.K. Mehta, Cem. Concr. Res., 6(2), 169 (1976).

[83] P.P. Budnikov, I.V. Kravchenko, 5th. Inter. Symp. Chem. Cem., Tokyo, Vol. 4, 319 (1968).

[84] M. Okushima, R. Kondo, H. Muguruma, Y. Ono, 5th. Inter. Symp. Chem. Cem., Tokyo, Vol. 4, 419 (1968).

[85] K. Ogawa, D. M. Roy, Cem. Concr. Res., 12(1), 101 (1982).

[86] G.L. Kalousek, E. Benton, J. Am. Concr. Inst., 67(2), 187 (1970).

[87] P.K. Mehta, Cem. Concr. Res., 3(1), 1 (1973).

[88] P.K. Mehta, F. Hu, J. American Ceramic Society, 61(3-4), 179 (1978).

[89] P.K. Mehta, S. Wang, Cem. Concr. Res., 12(1), 121 (1982).

[90] V.S. Ramachandran, J.J. Beaudoin, R.F. Feldman, J. Mater. Sci., 11, 1893 (1976).

[91] F.M. Lea, "The Chemistry of Cement and Concrete", 3rd edition, Edward Arnold Ltd., Glasgow, 325, 349 (1970).

[92] U. Schneider, J. Piasta, E. Nagelek W. Piasta, Materials and Structures, 23, 110 (1990).

[93] R.S. Berry, S.A. Rice, J. Ross, "Physical Chemistry", John Wiley & Sons. Inc., Toronto, (1980).

[94] E.J. Reardon, Cem. Concr. Res., 20(2), 175 (1990).

[95] M. Ish-Shalom, A. Bentur, Cem. Concr. Res., 4(4), 519 (1974).

[96] R. Kondo, 5th. Inter. Symp. Chem. Cem., Tokyo, Vol. 4, 881 (1968).

[97] L.R.Blair, Julie Chi-Sun Yang, 5th. Inter. Symp. Chem. Cem., Tokyo, Vol. 4, 849 (1968).

[98] L. Heller, M. Ben-Yair, J. Appl. Chem., 14, 20 (1964).

[99] R.C. Weast, "Handbook of Chemistry and Physics", 64th Edition, CRC Press, D51 (1983-1984).

[100] Deng Min, Cui Xuehau, Tang Mingshu, Il Cemento, 87(3), 161 (1990).

[101] Mingshu Tang, Zheng Liu, Yinong Lu, Sufen Han, Il Cemento, 88(3), 141 (1991).

APPENDIX A

ELECTRICAL CONDUCTIVITY DATA

I. FLAT AGGREGATE-CEMENT PASTE SYSTEMS

Cement : Low alkali portland cement.

Units : (i). Electrical conductivity: ohm-1 m-1; (ii). Excess interfacial conductance: ohm-1

Temperature : 20°C.

1. Limestone as aggregate

(1). w/c=0.30

Time	Area Fraction of Aggregates								A	B	Correlation Coefficient | r |	θ
(days)	0	0.0452	0.0902	0.136	0.182	0.227	0.273	0.317				(x10 -4)
0.44	0.213	0.206	0.2	0.194	0.186	0.179	0.172	0.165	-0.153	0.214	0.9993	0.41358
0.55	0.172	0.167	0.161	0.156	0.149	0.143	0.137	0.131	-0.133	0.1733	0.9996	0.273234
0.65	0.152	0.147	0.142	0.137	0.131	0.126	0.12	0.115	-0.119	0.153	0.9997	0.23052
0.79	0.143	0.138	0.134	0.129	0.125	0.12	0.115	0.111	-0.101	0.143	0.9996	0.28476
0.93	0.13	0.126	0.122	0.118	0.113	0.108	0.105	0.0994	-0.0973	0.131	0.995	0.228486
1.01	0.122	0.118	0.115	0.111	0.107	0.103	0.0994	0.0949	-0.0853	0.122	0.9991	0.248826
1.21	0.119	0.115	0.112	0.109	0.105	0.101	0.0972	0.0934	-0.0805	0.119	0.998	0.26103
1.79	0.0949	0.0919	0.0896	0.0865	0.0836	0.0806	0.078	0.075	-0.0627	0.095	0.9996	0.218994
2.29	0.0795	0.0773	0.0751	0.0729	0.0705	0.068	0.0661	0.0635	-0.0505	0.0797	0.9996	0.197976
3.14	0.0685	0.0664	0.0643	0.0622	0.06	0.0579	0.0553	0.0536	-0.0477	0.0686	0.9995	0.141702
3.25	0.0664	0.0647	0.0619	0.0608	0.059	0.0565	0.0541	0.0507	-0.0486	0.0671	0.995	0.12543
4.79	0.0611	0.0592	0.0573	0.0556	0.0537	0.0516	0.0497	0.0477	-0.0422	0.0612	0.9996	0.12682
7.31	0.059	0.0573	0.0556	0.0539	0.0522	0.0503	0.0486		-0.0383	0.0591	0.9998	0.141024
8.13	0.0563	0.0549	0.0531	0.0516	0.0502	0.048	0.0462		-0.0377	0.0567	0.998	0.12682
9.33	0.053	0.0517	0.0503	0.0481	0.0473	0.0459	0.0443		-0.032	0.053	0.995	0.14238
11.8	0.0463	0.045	0.0442	0.042	0.0419	0.04	0.0389		-0.0271	0.0463	0.987	0.130176
13.9	0.0419	0.0411	0.0402	0.0393	0.0381	0.0372	0.0366		-0.0205	0.042	0.997	0.14577

(2). w/c=0.40

Time	Area Fraction of Aggregates								A	B	| r |	θ
	0	0.0459	0.0922	0.137	0.185	0.229	0.273	0.317				(x10 -4)
0.43	0.458	0.447	0.43	0.416	0.403	0.394	0.369	0.341	-0.364	0.467	0.984	0.702975
0.56	0.334	0.325	0.314	0.302	0.293	0.284	0.27	0.257	-0.244	0.337	0.997	0.634725
0.71	0.255	0.246	0.237	0.228	0.219	0.21	0.211	0.191	-0.201	0.256	0.9997	0.375375
0.96	0.195	0.19	0.183	0.174	0.169	0.164	0.156	0.148	-0.15	0.197	0.997	0.320775
1.25	0.173	0.167	0.161	0.155	0.149	0.143	0.137	0.131	-0.133	0.173	0.9999	0.273
1.75	0.149	0.145	0.139	0.133	0.129	0.123	0.119	0.113	-0.115	0.15	0.999	0.238875
2	0.147	0.143	0.137	0.132	0.127	0.122	0.117	0.111	-0.115	0.148	0.9994	0.225225
2.75	0.139	0.135	0.13	0.125	0.12	0.115	0.11	0.105	-0.11	0.14	0.9999	0.20475
4	0.133	0.129	0.124	0.12	0.115	0.11	0.106	0.101	-0.103	0.134	0.9997	0.211575
5.08	0.115	0.111	0.107	0.103	0.0987	0.0949	0.0911	0.0868	-0.0888	0.1152	0.9999	0.18018
6.33	0.102	0.0987	0.0957	0.0919	0.088	0.0849	0.0818	0.0777	-0.0777	0.103	0.9994	0.172673
8	0.1	0.0972	0.0926	0.0896	0.0865	0.0833	0.0802	0.0762	-0.0742	0.1	0.998	0.176085
13.4	0.0734	0.0712	0.0689	0.0666	0.0644	0.0623	0.0598	0.0574	-0.0504	0.0736	0.9995	0.15834
20.3	0.0651	0.063	0.061	0.0574	0.0574	0.0543	0.0522	0.0454	-0.0464	0.065	0.984	0.126945

(3). w/c=0.50

Time	Area Fraction of Aggregates							A	B	| r |	θ
	0	0.0452	0.0907	0.136	0.181	0.226	0.272				(x10 -4)
0.5	0.4905	0.4713	0.4559	0.4388	0.4244	0.3997	0.3885	-0.375	0.4881	0.995	0.76908
0.67	0.3488	0.3375	0.3248	0.3132	0.2994	0.2859	0.2776	-0.2712	0.3494	0.998	0.53176
0.83	0.2757	0.263	0.254	0.2481	0.2386	0.2232	0.2176	-0.2097	0.2742	0.99	0.4386
1	0.2367	0.229	0.22	0.2156	0.2063	0.1937	0.188	-0.1885	0.2389	0.992	0.34272
1.21	0.2039	0.1965	0.189	0.1853	0.1769	0.1667	0.161	-0.1623	0.2052	0.993	0.29172
1.5	0.1786	0.1709	0.1635	0.1612	0.1543	0.1447	0.1403	-0.1406	0.1785	0.991	0.25772
2	0.1559	0.1478	0.1409	0.14	0.134	0.1259	0.1209	-0.1223	0.1548	0.99	0.221
3	0.1358	0.1292	0.12	0.1162	0.1127	0.109	0.1053	-0.104	0.1324	0.987	0.19312
4	0.1302	0.1217	0.1154	0.1146	0.1098	0.1038	0.0994	-0.1002	0.1271	0.995	0.18292
5	0.1253	0.1186	0.1134	0.1129	0.1066	0.1009	0.0979	-0.0965	0.124	0.988	0.18686

6	0.1259	0.1204	0.1139	0.1135	0.107	0.101	0.0968	-0.1079	0.1263	0.992	0.12512
7	0.1239	0.1182	0.1112	0.1105	0.1062	0.105	0.0963	-0.098	0.1232	0.997	0.17116
8.04	0.1224	0.1169	0.1106	0.1099	0.1028	0.0992	0.0952	-0.0986	0.1218	0.993	0.15749
9	0.1212	0.116	0.1094	0.1065	0.1028	0.0985	0.0942	-0.0957	0.121	0.999	0.1719
10	0.1201	0.115	0.1086	0.1083	0.102	0.0973	0.0934	-0.0984	0.1201	0.994	0.14742
11	0.1181	0.1141	0.1086	0.1083	0.1007	0.0966	0.0928	-0.0984	0.1194	0.988	0.14287
13	0.1171	0.1131	0.1069	0.1066	0.1005	0.0959	0.0921	-0.0957	0.1185	0.994	0.15484
15	0.1139	0.1101	0.1034	0.1008	0.0981	0.0936	0.09	-0.0879	0.1136	0.997	0.17476
17	0.111	0.1074	0.102	0.1014	0.0953	0.091	0.0878	-0.0901	0.1121	0.993	0.1494
18	0.1101	0.1062	0.1014	0.1007	0.0946	0.0905	0.0808	-0.0878	0.1109	0.991	0.15742

2. Silica glass as aggregate

(1). w/c=0.40

Time	Area	Fraction of Aggregates						A	B	| r |	θ
	0	0.0884	0.179	0.267	0.356	0.446	0.526				(x10 -4)
0.5	0.3674	0.3315	0.2857	0.2788	0.2493	0.2193	0.1938	-0.298	0.3522	0.987	0.71815
0.75	0.2292	0.2051	0.1831	0.1743	0.1524	0.1355	0.1209	-0.1895	0.22	0.996	0.40413
1	0.179	0.1494	0.1424	0.1316	0.1111	0.102	0.0906	-0.1415	0.1651	0.989	0.3127
1.5	0.1416	0.1249	0.1132	0.1021	0.0922	0.0812	0.0717	-0.1209	0.1351	0.9998	0.18815
2	0.1216	0.1144	0.1019	0.0932	0.0838	0.0733	0.0643	-0.1124	0.1234	0.999	0.14575
3	0.1182	0.1072	0.0954	0.0901	0.0774	0.0699	0.0624	-0.1018	0.1153	0.995	0.17888
4	0.1123	0.1026	0.0924	0.0872	0.0753	0.0677	0.0599	-0.0974	0.1111	0.997	0.18153
5	0.1066	0.0966	0.0876	0.081	0.0708	0.0638	0.057	-0.0909	0.1043	0.999	0.17755
6	0.0986	0.0927	0.0834	0.0779	0.0676	0.0613	0.0551	-0.086	0.0997	0.997	0.18153
7	0.0974	0.0882	0.0797	0.0737	0.065	0.0585	0.0523	-0.0819	0.095	0.999	0.17358
8	0.0935	0.0862	0.0774	0.0728	0.0634	0.0574	0.0514	-0.0791	0.0927	0.997	0.1802
9	0.0907	0.0825	0.0751	0.0707	0.0608	0.0555	0.0498	-0.0755	0.0892	0.996	0.18153
10	0.0884	0.0809	0.0735	0.0662	0.0595	0.0539	0.049	-0.0731	0.0865	0.998	0.17755
11	0.0866	0.0802	0.0721	0.0667	0.0583	0.053	0.0479	-0.0742	0.0861	0.996	0.15768
12	0.0857	0.0784	0.0716	0.0656	0.0593	0.0532	0.0479	-0.0695	0.0842	0.9998	0.19478
13	0.0832	0.0774	0.0698	0.0646	0.0572	0.0518	0.0468	-0.0697	0.0829	0.998	0.1749
14	0.0824	0.0759	0.0688	0.0617	0.0556	0.051	0.0466	-0.0669	0.0808	0.994	0.18418
15	0.0812	0.0738	0.0677	0.0624	0.0552	0.0503	0.0455	-0.0653	0.0794	0.999	0.18683
16	0.0788	0.0729	0.0671	0.0623	0.0544	0.0498	0.045	-0.0648	0.0787	0.997	0.18418
17	0.0774	0.0723	0.0661	0.0608	0.0534	0.0488	0.0443	-0.0648	0.0777	0.997	0.17093
18	0.0722	0.0714	0.0653	0.0601	0.0528	0.0482	0.0437	-0.0641	0.0768	0.998	0.16828
19	0.076	0.0703	0.0644	0.0591	0.0521	0.0475	0.0429	-0.0633	0.0757	0.998	0.1643
20	0.0757	0.0703	0.0641	0.0584	0.0516	0.0472	0.0429	-0.0632	0.0754	0.997	0.16165

(2). w/c=0.50

Time	Area	Fraction of Aggregates						A	B	| r |	θ
	0	0.0884	0.179	0.267	0.356	0.446	0.526				(x10 -4)
0.5	0.5391	0.4893	0.4384	0.386	0.345	0.2997	0.256	-0.5275	0.5328	0.999	0.07023
0.75	0.3196	0.2817	0.256	0.2311	0.2049	0.1803	0.1546	-0.2887	0.3077	0.9998	0.25175
1	0.2472	0.2208	0.2	0.1799	0.1611	0.1422	0.1232	-0.22	0.2394	0.9999	0.25705
1.5	0.1796	0.1706	0.1548	0.1389	0.1252	0.111	0.0966	-0.1674	0.1848	0.9997	0.23055
2	0.1662	0.151	0.1367	0.1228	0.114	0.0953	0.0857	-0.1507	0.1637	0.9993	0.17225
3	0.1435	0.1326	0.12	0.1071	0.0969	0.0854	0.075	-0.1306	0.1434	9994	0.1696
4	0.1377	0.1271	0.1148	0.1025	0.0922	0.0797	0.0715	-0.1279	0.1377	0.9991	0.12985
5	0.1355	0.1251	0.1128	0.1008	0.0905	0.0777	0.0706	-0.1262	0.1354	0.998	0.1219
6	0.1328	0.123	0.1101	0.0967	0.089	0.0768	0.0712	-0.1193	0.1315	0.993	0.16165
7	0.1313	0.1219	0.11	0.0985	0.0885	0.0761	0.0695	-0.1216	0.1318	0.998	0.13515
8	0.1283	0.1191	0.1077	0.0968	0.0869	0.0747	0.0685	-0.1177	0.1288	0.998	0.14708
9	0.1269	0.1169	0.106	0.0957	0.0559	0.0738	0.0682	-0.1138	0.1264	0.998	0.16695
10	0.1244	0.1147	0.1043	0.0944	0.0847	0.0729	0.0674	-0.1107	0.1241	0.998	0.17755
11	0.1232	0.1136	0.1042	0.0921	0.0835	0.072	0.0668	-0.1089	0.1223	0.997	0.17755
12	0.1209	0.1122	0.1019	0.0923	0.0829	0.0712	0.0663	-0.1077	0.1212	0.997	0.17888
13	0.1196	0.1107	0.1008	0.0914	0.0821	0.0708	0.0656	-0.1056	0.1197	0.998	0.18683
14	0.1193	0.1105	0.1004	0.0909	0.0815	0.0707	0.0644	-0.107	0.1196	0.999	0.16695
15	0.1185	0.1095	0.0997	0.0904	0.0813	0.0704	0.0648	-0.1042	0.1184	0.998	0.18815
16	0.1173	0.1084	0.0987	0.0895	0.0805	0.0695	0.0647	-0.1024	0.117	0.997	0.19345

17	0.1152	0.1068	0.0973	0.0882	0.0796	0.0688	0.0641	-0.1	0.1152	0.997	0.2014
18	0.1139	0.1056	0.0963	0.0874	0.0788	0.0682	0.0635	-0.0986	0.1139	0.998	0.20273
19	0.1149	0.1047	0.0954	0.0866	0.0781	0.0676	0.0628	-0.098	0.113	0.998	0.19875
20	0.1118	0.1038	0.0945	0.0857	0.0773	0.0668	0.0624	-0.0971	0.1119	0.997	0.1961
20.83	0.1118	0.1029	0.0937	0.0852	0.0768	0.0665	0.0618	-0.0962	0.111	0.998	0.1961

II. CEMENT PASTES WITH DIFFERENT W/C RATIOS

Cement : Low alkali portland cement.

Temperature: 20°C.

Unit : ohm-1 m-1.

	W/C Ratio								
	0.25	*0.3*	*0.35*	*0.4*	*0.45*	*0.5*			
Time	*Initial Volumetric Fraction of Cement*						Slope	Intercept	I r I
(hrs.)	*0.559*	*0.514*	*0.476*	*0.442*	*0.414*	*0.388*			
25	0.09354	0.1565	0.2474	0.2951	0.3516	0.3934	-1.79256	1.097861	0.997629
30	0.0845	0.125	0.1969	0.2418	0.2781	0.3048	-1.35167	0.839794	0.995432
40	0.0753	0.1036	0.1478	0.1839	0.207	0.2292	-0.93692	0.597683	0.996606
50	0.0708	0.09194	0.1247	0.1557	0.1738	0.1908	-0.73513	0.479767	0.995701
60	0.0678	0.0854	0.1108	0.1397	0.1544	0.1691	-0.62183	0.413147	0.994594
70	0.0653	0.0806	0.1048	0.1287	0.1409	0.1548	-0.54676	0.369223	0.995151
80	0.0637	0.0793	0.102	0.1223	0.1331	0.146	-0.49817	0.341626	0.996712
100	0.0606	0.0762	0.0943	0.1119	0.1221	0.1349	-0.44184	0.307444	0.998291
120	0.0558	0.0711	0.09056	0.1051	0.1155	0.1293	-0.43213	0.297444	0.998328
145	0.0553	0.0684	0.08832	0.1001	0.1104	0.1236	-0.40173	0.27963	0.997047
168	0.0533	0.0665	0.0853	0.0968	0.1076	0.1218	-0.39926	0.276002	0.996728
192	0.0513	0.0644	0.0815	0.09491	0.1053	0.1193	-0.39789	0.272929	0.997021
240	0.0481	0.0608	0.0776	0.09155	0.1028	0.1176	-0.40648	0.273917	0.995723

III. QUARTZ SAND - WHITE PORTLAND CEMENT SYSTEMS

Units : (I). Electrical conductivity: ohm-1 m-1; (II). Excess interfacial conductance: ohm-1
Temperature : 20°C. W/C = 0.50

1. r=0.561 mm

Time	*Volumetric Fraction of Aggregate*					k	b	|r|	θ
(hrs.)	*0.15*	*0.2*	*0.25*	*0.3*	*0.35*				(x10 -4)
1	0.3604716	0.3471742	0.311142	0.282159	0.2514137	-0.566262	0.4520376	0.993555	0.253593
2	0.3785079	0.3581461	0.3255722	0.2956865	0.2651287	-0.578436	0.4692172	0.999305	0.263231
3	0.3627737	0.3526563	0.3211728	0.2899411	0.2586466	-0.541939	0.4525228	0.988399	0.253865
4	0.3475665	0.3322122	0.3050035	0.2777305	0.2504736	-0.497335	0.4269309	0.99685	0.239508
5	0.3203404	0.3005285	0.2773536	0.2553314	0.2330211	-0.439671	0.3872328	1.001767	0.217238
6	0.2938953	0.2737303	0.2541578	0.2346094	0.215055	-0.393603	0.3526903	1.002041	0.197859
7	0.2607165	0.2444691	0.2278167	0.2096588	0.1918772	-0.344978	0.3131521	1.00174	0.175678
8	0.2317449	0.218354	0.2035646	0.187465	0.1716929	-0.301986	0.2780609	1.001319	0.155992
9	0.207613	0.1958224	0.1805607	0.1690562	0.1566124	-0.257535	0.2463167	1.000994	0.138184
10	0.1939757	0.1847734	0.1725918	0.1604433	0.1482866	-0.231417	0.2298683	1.000578	0.128956
11	0.1885919	0.1784921	0.1670902	0.1563193	0.1453907	-0.21715	0.2214644	1.001912	0.124242
12	0.1820279	0.167562	0.1586139	0.1494585	0.140355	-0.202898	0.2103281	0.99578	0.117994
14	0.1773668	0.1625737	0.1536023	0.1456851	0.1375044	-0.193227	0.2036532	0.990942	0.114249
16	0.1675989	0.1581623	0.1506359	0.1406753	0.1313233	-0.180077	0.1946983	1.001136	0.109226
20	0.1592351	0.1503887	0.1444881	0.1339073	0.1244965	-0.171917	0.1854824	0.997966	0.104056
24	0.1525006	0.1456409	0.1391855	0.1283146	0.1185476	-0.170465	0.179454	0.995005	0.100674
28	0.145465	0.1380705	0.1299512	0.1208925	0.1120687	-0.167941	0.1712749	1.001131	0.096085
32	0.1395311	0.130372	0.1225032	0.1143346	0.106241	-0.165235	0.1639052	1.001693	0.091951
36	0.131422	0.1249885	0.1176228	0.1085349	0.0998775	-0.159085	0.1562605	0.999334	0.087662
40	0.1275921	0.1219104	0.1143879	0.1049281	0.0959527	-0.160522	0.1530848	0.996928	0.085881
44	0.1258524	0.119386	0.1130798	0.1032654	0.094328	-0.158338	0.1507669	0.996556	0.08458
48	0.1235466	0.116682	0.109107	0.1005103	0.092169	-0.157854	0.1478665	1.000909	0.082953
52	0.1200139	0.1142045	0.1070153	0.0980407	0.0895125	-0.154333	0.1443407	0.998088	0.080975
56	0.1178573	0.1110929	0.1047129	0.0957633	0.0874561	-0.152264	0.1414426	0.999275	0.079349
60	0.1167337	0.1087917	0.1041357	0.0948824	0.0867783	-0.14764	0.1391744	0.997016	0.078077
64	0.1161641	0.1071763	0.1030652	0.0939627	0.0861081	-0.146651	0.1379581	0.996201	0.077394
68	0.1156308	0.1064414	0.1027361	0.0934782	0.0856086	-0.146015	0.1372828	0.994731	0.077016
72	0.1146503	0.1050764	0.1021716	0.0926938	0.0848592	-0.14393	0.1358727	0.991414	0.076225
76	0.1126469	0.1033469	0.1001347	0.0912219	0.0837342	-0.139901	0.1331922	0.993295	0.074721
80	0.1119673	0.1027295	0.0997075	0.0906506	0.0831025	-0.139617	0.1325358	0.992432	0.074353
84	0.1113469	0.1023259	0.0993841	0.0902616	0.0826844	-0.138779	0.1318952	0.992063	0.073993
88	0.1113647	0.1021189	0.0992435	0.0901389	0.0825917	-0.139052	0.1318546	0.991768	0.07397
92	0.1114171	0.1016244	0.0990876	0.0900103	0.0825682	-0.138624	0.1315974	0.99001	0.073826
96	0.1109	0.1015261	0.0990068	0.0899896	0.0825969	-0.136286	0.1308753	0.990214	0.073421
100	0.1101805	0.1008877	0.0988109	0.0892318	0.0815283	-0.137921	0.1306081	0.987364	0.073271
104	0.110156	0.1003717	0.0986395	0.0891625	0.0816217	-0.136556	0.1301292	0.985565	0.073002
108	0.1096534	0.1001385	0.0979745	0.0886478	0.0811118	-0.137148	0.1297922	0.988122	0.072813
112	0.1102592	0.1003668	0.0980835	0.0889815	0.0815841	-0.137471	0.1302228	0.988701	0.073055
116	0.1096956	0.0996932	0.0980615	0.0888827	0.0815906	-0.134041	0.129095	0.985032	0.072422
120	0.109283	0.0978636	0.0980412	0.0883238	0.0810801	-0.131891	0.1278911	0.970837	0.071747
124	0.1093558	0.0981147	0.0980364	0.0884021	0.0811568	-0.132221	0.1280685	0.973087	0.071846
128	0.1090991	0.0979507	0.0980021	0.0882209	0.0808978	-0.132265	0.1279003	0.972231	0.071752
132	0.1090137	0.0976131	0.0977673	0.0879629	0.0806482	-0.132762	0.1277916	0.971167	0.071691
136	0.1086481	0.0973297	0.0976451	0.087862	0.0806035	-0.131114	0.1271961	0.969798	0.071357
140	0.1080657	0.0967597	0.0969667	0.087311	0.0801209	-0.130676	0.1265139	0.970609	0.070974
144	0.1083494	0.0969561	0.0971934	0.0875065	0.0803007	-0.131094	0.1268348	0.970297	0.071154

2. r=0.356 mm

Time	*Volumetric Fraction of Aggregate*					k	b	|r|	θ
(hrs.)	*0.15*	*0.2*	*0.25*	*0.3*	*0.35*				(x10 -4)
1	0.3848227	0.3508317	0.3259893	0.2932815	0.2622626	-0.605341	0.4747727	0.999133	0.169019
2	0.3801125	0.3456666	0.3196102	0.2921454	0.2593597	-0.590054	0.4668922	0.998879	0.166214
3	0.3760962	0.3456135	0.3115987	0.2913176	0.258456	-0.579153	0.4614045	0.99756	0.16426
4	0.3600124	0.330124	0.2998896	0.2796821	0.2489336	-0.545199	0.4400281	0.998055	0.15665
5	0.342514	0.3160848	0.2856465	0.2648358	0.2400576	-0.512324	0.4179087	0.998287	0.148776
6	0.3220981	0.295632	0.2701243	0.249321	0.2271235	-0.472521	0.3909899	0.998707	0.139192
7	0.306214	0.281254	0.2586514	0.2380975	0.2164708	-0.445286	0.371459	0.999323	0.132239
8	0.2810215	0.2621301	0.235161	0.2184671	0.2006742	-0.408715	0.3416695	0.996593	0.121634
9	0.260124	0.2450124	0.221013	0.2015879	0.1866066	-0.380919	0.3180985	0.99697	0.113243
10	0.2430154	0.2245632	0.2065421	0.1869032	0.1733408	-0.354018	0.2953775	0.998519	0.105154
11	0.2301241	0.2101421	0.191254	0.176241	0.1641165	-0.331833	0.2773337	0.994964	0.098731
12	0.2133198	0.195621	0.1774337	0.1656868	0.1510214	-0.309062	0.257882	0.996759	0.091806
14	0.2108621	0.1963289	0.1758829	0.162014	0.1504865	-0.310132	0.2566479	0.99543	0.091367
16	0.2095632	0.1908096	0.1720376	0.1618585	0.1472813	-0.30703	0.2530675	0.993883	0.090092
20	0.195621	0.1792773	0.1602918	0.1511789	0.1376969	-0.287893	0.2367865	0.993335	0.084296
24	0.1828608	0.1693316	0.1499743	0.1413837	0.128705	-0.272519	0.2225808	0.993193	0.079239
28	0.1742568	0.1618295	0.142694	0.1346705	0.1223965	-0.261759	0.2126093	0.992597	0.075689
32	0.1663363	0.1537309	0.1382451	0.1283511	0.1159089	-0.252469	0.2036318	0.997981	0.072493
36	0.1594041	0.1486086	0.1332451	0.1230142	0.1116741	-0.242109	0.1957164	0.997961	0.069675
40	0.1556242	0.1442524	0.1284213	0.1202339	0.1084018	-0.236927	0.1906184	0.996064	0.06786
44	0.1515214	0.1407512	0.1253425	0.1171575	0.1055858	-0.23093	0.1858042	0.996409	0.066146
48	0.1481866	0.1381569	0.121277	0.1146255	0.103179	-0.227093	0.1818583	0.992693	0.064742
52	0.1450214	0.1355033	0.118786	0.1125174	0.1010468	-0.22187	0.1780426	0.992251	0.063383
56	0.1420321	0.1325134	0.1161452	0.1099801	0.0988858	-0.217652	0.1743243	0.992189	0.062059
60	0.138214	0.1308559	0.1142855	0.1077908	0.0963759	-0.213482	0.170875	0.991804	0.060832
64	0.136241	0.1299324	0.1130676	0.1065865	0.0952197	-0.210777	0.1689037	0.990262	0.06013
68	0.1351201	0.1280124	0.1113454	0.1060124	0.0937402	-0.20952	0.167226	0.989828	0.059532
72	0.1340124	0.1275622	0.1111344	0.104521	0.0935182	-0.208059	0.1661644	0.991035	0.059155
76	0.1334201	0.1260545	0.1107226	0.1035012	0.0928638	-0.207332	0.1651454	0.993946	0.058792
80	0.1323245	0.1248264	0.1085899	0.1024321	0.0921891	-0.20533	0.163405	0.99101	0.058172
84	0.1308712	0.1228145	0.10626	0.1010058	0.0910076	-0.203072	0.1611598	0.988704	0.057373
88	0.1293061	0.1214359	0.1056146	0.0999275	0.0895394	-0.202084	0.1596856	0.991111	0.056848
92	0.1294614	0.121721	0.1051847	0.0995301	0.0898905	-0.202665	0.1598238	0.989011	0.056897
96	0.1292384	0.1214422	0.1054795	0.1000252	0.089139	-0.203231	0.1598727	0.990829	0.056915
100	0.1278452	0.121021	0.1041045	0.0987066	0.0887528	-0.200998	0.1583356	0.987692	0.056367
104	0.1280322	0.120652	0.1037355	0.0988888	0.088378	-0.202143	0.158473	0.987503	0.056416
108	0.1274686	0.1195937	0.1030309	0.098196	0.0879663	-0.200804	0.1574522	0.987953	0.056053
112	0.12672	0.1193404	0.1024317	0.0976012	0.0873675	-0.200888	0.1569142	0.987154	0.055861
116	0.1256426	0.1187021	0.1014969	0.096718	0.086819	-0.199263	0.1556914	0.9856	0.055426
120	0.1252161	0.1186231	0.1016495	0.0968282	0.0861797	-0.199735	0.1556331	0.986884	0.055405
124	0.1250214	0.1184228	0.1017771	0.0967872	0.0860471	-0.199169	0.1554033	0.987867	0.055324
128	0.1250012	0.1183215	0.1012774	0.0965731	0.0860589	-0.199266	0.155263	0.986442	0.055274
132	0.1249121	0.1182496	0.1012305	0.0964732	0.0860262	-0.199096	0.1551524	0.986521	0.055234
136	0.1249012	0.1179214	0.1016245	0.0963971	0.0860124	-0.198604	0.1550223	0.988941	0.055188
140	0.1248621	0.1176521	0.1005701	0.0961583	0.0858832	-0.198903	0.154751	0.985768	0.055091
144	0.1248235	0.117621	0.1002198	0.0960713	0.0859867	-0.198447	0.1545561	0.984233	0.055022

3. r=0.136 mm

Time	*Volumetric Fraction of Aggregate*					k	b	|r|	θ
(hrs.)	*0.15*	*0.2*	*0.25*	*0.3*	*0.35*				(x10 -4)
1	0.3895256	0.3476772	0.3205277	0.2751542	0.2590238	-0.667053	0.4851449	0.991469	0.06598
2	0.3984934	0.3542551	0.3240142	0.286292	0.2636597	-0.675261	0.4941581	0.99482	0.067206
3	0.3943221	0.3518385	0.3212553	0.2845913	0.2620471	-0.663594	0.4887095	0.995358	0.066464
4	0.3807401	0.3411937	0.3088312	0.2753655	0.25352	-0.640537	0.4720643	0.995531	0.064201
5	0.3608727	0.3311694	0.2952592	0.267209	0.2407269	-0.608504	0.4511734	0.998568	0.06136
6	0.3400515	0.3140743	0.2804775	0.2514723	0.2283552	-0.571989	0.4258835	0.998321	0.05792
7	0.317942	0.2890268	0.262878	0.2353531	0.2135146	-0.525057	0.3950072	0.998964	0.053721
8	0.2913115	0.2703493	0.2439359	0.2195235	0.1955999	-0.484498	0.3652684	0.999508	0.049677
9	0.2729758	0.2525145	0.2247067	0.2109887	0.1823491	-0.445558	0.3400965	0.995749	0.046253
10	0.2586122	0.2329427	0.210213	0.1948875	0.1729506	-0.418757	0.3186103	0.996619	0.043331
11	0.2459789	0.2272627	0.20317	0.181768	0.1686557	-0.400282	0.3054377	0.99596	0.04154
12	0.22903	0.2068428	0.1869041	0.1656852	0.1570611	-0.370191	0.2816524	0.990966	0.038305
14	0.2259799	0.2073217	0.1878989	0.1667985	0.154266	-0.367902	0.2804285	0.997281	0.038138
16	0.2213753	0.2029759	0.1833586	0.1625757	0.1514008	-0.360698	0.2745118	0.996032	0.037334
20	0.2081	0.1885421	0.1717496	0.153207	0.1411506	-0.338468	0.2571668	0.997175	0.034975
24	0.1939755	0.1760811	0.1592154	0.1417086	0.1315962	-0.318262	0.2400809	0.99582	0.032651
28	0.1835947	0.1656398	0.1508502	0.1326099	0.1247174	-0.301569	0.2268746	0.993258	0.030855
32	0.1767166	0.1570972	0.1439546	0.1270087	0.119517	-0.288976	0.2171027	0.990863	0.029526
36	0.1700163	0.1524372	0.1388024	0.1225877	0.1152029	-0.278953	0.2095475	0.992469	0.028498
40	0.1646493	0.1473145	0.1346276	0.1185324	0.111726	-0.269257	0.2026843	0.991676	0.027565
44	0.1612348	0.1432283	0.1314385	0.1162491	0.1089289	-0.263182	0.1980114	0.991568	0.02693
48	0.1573185	0.1404623	0.1280693	0.1132939	0.1063176	-0.258341	0.1936775	0.992057	0.02634
52	0.1541936	0.1376483	0.1256788	0.110864	0.1043998	-0.252744	0.1897428	0.991409	0.025805
56	0.1509958	0.1341446	0.1226369	0.1081968	0.1021301	-0.247358	0.1854604	0.989954	0.025223
60	0.1479635	0.1320554	0.1208119	0.1070197	0.0998543	-0.242508	0.182168	0.993214	0.024775
64	0.1471575	0.1310161	0.1193003	0.1065525	0.0991357	-0.241014	0.180886	0.992736	0.024601
68	0.1459221	0.1283835	0.118597	0.1044479	0.0984905	-0.237597	0.1785675	0.988182	0.024285
72	0.1465778	0.1282363	0.1191365	0.1050377	0.0984583	-0.238875	0.1792081	0.98794	0.024372
76	0.1443431	0.1279445	0.1175136	0.1033285	0.0974518	-0.236797	0.1773156	0.989925	0.024115
80	0.140313	0.1252494	0.1143692	0.1015268	0.0945057	-0.230674	0.1728614	0.993565	0.023509
84	0.1389338	0.1225523	0.1122934	0.0994799	0.093868	-0.226408	0.1700274	0.988227	0.023124
88	0.1378365	0.1213451	0.1114228	0.0989842	0.0928317	-0.224741	0.1686693	0.989041	0.022939
92	0.1378839	0.1217769	0.1116741	0.0988383	0.0929044	-0.225795	0.1690644	0.98955	0.022993
96	0.1370567	0.1230459	0.1111936	0.0987154	0.0926727	-0.226197	0.1690861	0.992289	0.022996
100	0.135903	0.1207747	0.1098258	0.0974757	0.0918298	-0.222891	0.1668845	0.989949	0.022696
104	0.1356876	0.1212726	0.109782	0.0972314	0.0916534	-0.224219	0.1671802	0.990812	0.022737
108	0.1358791	0.1206505	0.1096746	0.0976307	0.0913727	-0.224065	0.1670579	0.991082	0.02272
112	0.1345266	0.1198165	0.1083797	0.0966506	0.0903458	-0.223055	0.1657076	0.991592	0.022536
116	0.1335043	0.1184278	0.1074603	0.0960458	0.0894979	-0.220789	0.1641846	0.991432	0.022329
120	0.1331659	0.1180832	0.1077276	0.0950954	0.0896279	-0.220128	0.1637719	0.989843	0.022273
124	0.1343086	0.1199373	0.109431	0.0962194	0.0903658	-0.223207	0.1658542	0.992129	0.022556
128	0.1341442	0.1194605	0.108866	0.0963105	0.0901593	-0.222239	0.1653479	0.992077	0.022487
132	0.134404	0.1193263	0.1086404	0.0960921	0.090123	-0.223592	0.1656152	0.991053	0.022524
136	0.133568	0.1187418	0.1077977	0.0954493	0.0894694	-0.22298	0.1647501	0.991264	0.022406
140	0.1330192	0.117746	0.1076853	0.0954408	0.0887734	-0.221593	0.1639313	0.99218	0.022295
144	0.1330822	0.1186909	0.1076843	0.0964057	0.0883789	-0.223384	0.1646944	0.995295	0.022398

4. r=0.099 mm

Time	*Volumetric Fraction of Aggregate*					k	b	|r|	θ
(hrs.)	*0.15*	*0.2*	*0.25*	*0.3*	*0.35*				(x10 -4)
1	0.3706196	0.3441315	0.3072902	0.2706555	0.2485037	-0.635416	0.4670941	0.996672	0.046242
2	0.386479	0.3477251	0.3227654	0.2847735	0.2592813	-0.634694	0.4788784	0.997412	0.047409
3	0.3822816	0.3452911	0.3117746	0.2782351	0.2546175	-0.644768	0.4756321	0.997233	0.047088
4	0.3604192	0.3271449	0.2918241	0.2625807	0.2406571	-0.608177	0.4485694	0.996311	0.044408
5	0.3378185	0.3033845	0.2656187	0.2396467	0.2269033	-0.571136	0.4174584	0.985159	0.041328
6	0.3153992	0.2802269	0.2448849	0.2217458	0.2095246	-0.540461	0.3894715	0.982912	0.038558
7	0.2863826	0.2554798	0.222266	0.2004747	0.1918798	-0.488022	0.3533019	0.979613	0.034977
8	0.2571337	0.2284831	0.2009575	0.1849677	0.1737024	-0.420756	0.3142378	0.98254	0.03111
9	0.2379575	0.2144883	0.1918632	0.1748701	0.1627868	-0.379919	0.2913729	0.991827	0.028846
10	0.2182136	0.1996313	0.1837403	0.1670489	0.1514427	-0.332248	0.2670774	0.999535	0.026441
11	0.2134061	0.1964691	0.1815115	0.1620053	0.1502713	-0.321467	0.2610994	0.997901	0.025849
12	0.2125889	0.1991221	0.1813702	0.1598863	0.1495649	-0.330567	0.2631484	0.995046	0.026052
14	0.2111429	0.1940191	0.1756954	0.1570954	0.1488826	-0.322889	0.2580893	0.99302	0.025551
16	0.2036885	0.1845753	0.1686563	0.1509311	0.1423312	-0.312717	0.2482158	0.993212	0.024573
20	0.1873804	0.1692469	0.1556188	0.1392111	0.1298613	-0.290148	0.2288007	0.995175	0.022651
24	0.1729655	0.1554421	0.1446524	0.1281099	0.1192065	-0.2697	0.2115004	0.994796	0.020939
28	0.1621503	0.1451667	0.1366769	0.1206212	0.1117971	-0.250504	0.1979085	0.993926	0.019593
32	0.1538915	0.1375145	0.1298609	0.1149863	0.1063034	-0.235409	0.1873636	0.993666	0.018549
36	0.149629	0.133167	0.1249961	0.1109618	0.103231	-0.230002	0.1818976	0.99256	0.018008
40	0.1453718	0.1297346	0.1220002	0.1085065	0.1002804	-0.222822	0.1768841	0.993905	0.017512
44	0.1432071	0.1285466	0.1210293	0.1071306	0.0992364	-0.218715	0.1745088	0.994455	0.017276
48	0.1402603	0.1265172	0.1181993	0.1052875	0.0964817	-0.217574	0.1717427	0.996984	0.017003
52	0.1365064	0.1218071	0.1150687	0.1021955	0.0940517	-0.209042	0.1661865	0.993914	0.016452
56	0.1340383	0.1194823	0.1124341	0.1004085	0.0924271	-0.204592	0.1629061	0.994044	0.016128
60	0.1328734	0.1189467	0.1119243	0.0991311	0.0916706	-0.204442	0.1620199	0.994313	0.01604
64	0.1320752	0.1182551	0.1108642	0.0984812	0.090835	-0.204509	0.1612293	0.994997	0.015962
68	0.1326222	0.11803	0.1114879	0.0985049	0.0907068	-0.206712	0.1619483	0.993413	0.016033
72	0.1305593	0.1169635	0.1106098	0.0977782	0.089477	-0.2027	0.1597525	0.994842	0.015815
76	0.1298475	0.1155039	0.1083081	0.0976332	0.0885911	-0.200767	0.1581684	0.994974	0.015659
80	0.1282844	0.1148817	0.107726	0.0966669	0.0877429	-0.198596	0.1567093	0.996339	0.015514
84	0.127448	0.1140914	0.1077822	0.0964263	0.0874505	-0.19532	0.1554698	0.995518	0.015392
88	0.1276841	0.1137712	0.1076734	0.0962263	0.0873594	-0.196389	0.1556401	0.994495	0.015408
92	0.1276981	0.1137077	0.1068785	0.0963891	0.0872288	-0.196514	0.1555091	0.995094	0.015395
96	0.126819	0.1139233	0.1069118	0.0960388	0.0870417	-0.194878	0.1548665	0.996783	0.015332
100	0.126066	0.1128277	0.1060387	0.0950824	0.0863926	-0.194184	0.1538275	0.995973	0.015229
104	0.1258066	0.1124408	0.1051923	0.0948364	0.086149	-0.193839	0.1533448	0.995995	0.015181
108	0.1256467	0.1120215	0.1049778	0.0942717	0.0859414	-0.19432	0.1531519	0.995275	0.015162
112	0.1256163	0.1121981	0.1049413	0.094457	0.085775	-0.194847	0.1533093	0.995991	0.015178
116	0.1259805	0.1129707	0.1061768	0.0954106	0.0860274	-0.194933	0.1540463	0.996567	0.015251
120	0.1252619	0.1122587	0.1057622	0.094911	0.0858907	-0.192181	0.152862	0.996087	0.015133
124	0.1250003	0.1124211	0.1058377	0.0949237	0.0857741	-0.1919	0.1527663	0.996704	0.015124
128	0.1246354	0.1121059	0.1015094	0.0946356	0.0855922	-0.191113	0.151474	0.994194	0.014996
132	0.1246697	0.1116358	0.1014242	0.0944915	0.085558	-0.190735	0.1512397	0.993355	0.014973
136	0.12494	0.1117281	0.1053845	0.0941114	0.0852324	-0.194064	0.1527952	0.995662	0.015127
140	0.124049	0.1107081	0.1043442	0.0934133	0.0848217	-0.191499	0.151342	0.995261	0.014983
144	0.1238196	0.1114669	0.104583	0.0940797	0.0851506	-0.189451	0.1511826	0.997129	0.014967

IV. LIMESTONE PARTICLE - WHITE PORTLAND CEMENT SYSTEMS

Units : (i). Electrical conductivity: ohm-1 m-1; (ii). Excess interfacial conductance: ohm-1
Temperature : 20°C.

1. W/C = 0.40

(1). r=0.561 mm

Time	*Volumetric Fraction of Aggregate*			k	b	Irl	θ
(hrs.)	*0.15*	*0.25*	*0.35*				(x10 -4)
1	0.364944027	0.286255898	0.236117113	-0.64413	0.456806	0.991914	0.048742
2	0.38758945	0.305538861	0.252745727	-0.67422	0.483846	0.992245	0.061173
3	0.38321306	0.305478187	0.249734804	-0.66739	0.479657	0.995506	0.061818
4	0.364100366	0.301521541	0.237704238	-0.63198	0.459104	0.999984	0.067255
5	0.345288051	0.28602294	0.225640435	-0.59824	0.43521	0.999985	0.064765
6	0.322677589	0.268635316	0.212142566	-0.55268	0.405987	0.999918	0.066816
7	0.295308604	0.245738135	0.194316569	-0.50496	0.371361	0.999944	0.061803
8	0.263213308	0.226558971	0.174364032	-0.44425	0.33244	0.99494	0.064571
9	0.240057206	0.201488445	0.161334447	-0.39361	0.299363	0.999932	0.065779
11	0.204440485	0.170244053	0.138917388	-0.32762	0.253105	0.99968	0.061756
15	0.201460205	0.165598058	0.137143118	-0.32159	0.248463	0.997797	0.06065
19	0.186186313	0.155115809	0.126531904	-0.29827	0.230513	0.999711	0.056363
23	0.169202137	0.139462902	0.114575963	-0.27313	0.209363	0.998688	0.048551
27	0.157123662	0.126557014	0.106119445	-0.25502	0.193689	0.993491	0.042141
31	0.146927887	0.11932494	0.098746056	-0.24091	0.181894	0.996477	0.037892
35	0.139415186	0.114555457	0.093212277	-0.23101	0.173481	0.999036	0.034659
39	0.132801311	0.107577957	0.088839828	-0.21981	0.164692	0.996393	0.032313
43	0.127175687	0.104918609	0.084700071	-0.21238	0.158693	0.999616	0.030451
47	0.12345712	0.10195586	0.082089465	-0.20684	0.15421	0.99974	0.029046
51	0.117004788	0.096541585	0.077744612	-0.1963	0.146172	0.9997	0.027243
55	0.114530656	0.094686215	0.075873733	-0.19328	0.143351	0.999881	0.025801
59	0.110593334	0.091667779	0.073220744	-0.18686	0.138543	0.999973	0.024863
63	0.108271373	0.087579855	0.071846685	-0.18212	0.134763	0.996926	0.023759
67	0.107809341	0.088756662	0.071360989	-0.18224	0.134869	0.999656	0.023807
71	0.106702314	0.088458097	0.070590121	-0.18056	0.133724	0.999982	0.023763
75	0.105366405	0.086568035	0.069671422	-0.17847	0.131821	0.999527	0.022851
79	0.103878675	0.084678219	0.068803256	-0.17538	0.129631	0.998505	0.022629
83	0.102698431	0.083110863	0.068039554	-0.17329	0.12794	0.997182	0.02209
87	0.101536975	0.083955761	0.067105845	-0.17216	0.127238	0.999925	0.022193
91	0.101134758	0.081635984	0.067160093	-0.16987	0.125779	0.996377	0.022303
95	0.100661261	0.082919371	0.066671095	-0.16995	0.125905	0.999678	0.022436
99	0.098913841	0.07902693	0.065794672	-0.1656	0.122644	0.993338	0.021799
103	0.098752943	0.081063637	0.065389761	-0.16682	0.123439	0.999392	0.021767
107	0.096060271	0.080032245	0.06337556	-0.16342	0.120679	0.999938	0.020879
111	0.095800203	0.078651576	0.063396634	-0.16202	0.119787	0.999431	0.02096
115	0.095570649	0.078010369	0.063196948	-0.16187	0.119393	0.998802	0.020436
119	0.095322743	0.079281889	0.062903085	-0.1621	0.119694	0.999982	0.020698
123	0.0948081	0.077924399	0.062614663	-0.16097	0.118691	0.999602	0.020255
127	0.094350768	0.077526038	0.062447578	-0.15952	0.117987	0.999501	0.020725

131	0.092478341	0.075985519	0.061158634	-0.1566	0.11569	0.999529	0.020099
135	0.092140886	0.076679096	0.06068545	-0.15728	0.115821	0.999952	0.019526
139	0.091472772	0.075780352	0.060351604	-0.15561	0.11477	0.999988	0.019638

(2). r= 0.273 mm

Time	*Volumetric Fraction of Aggregate*			k	b	I r I	θ
(hrs.)	*0.15*	*0.25*	*0.35*				(x10 -4)
1	0.356144981	0.297936891	0.220610236	-0.67767	0.460982	0.9967	0.012558
2	0.378244407	0.315445299	0.234367384	-0.71939	0.489199	0.997321	0.013116
3	0.367067776	0.307973046	0.22680375	-0.70132	0.475945	0.995897	0.011463
4	0.35260922	0.296537467	0.219115747	-0.66747	0.456288	0.995764	0.015437
5	0.343184755	0.284776552	0.214068425	-0.64558	0.442072	0.998491	0.015949
6	0.31436577	0.265183264	0.196956492	-0.58705	0.405597	0.995644	0.019427
7	0.282730073	0.239760912	0.17892981	-0.519	0.363557	0.995101	0.023964
8	0.253278063	0.215606651	0.161144224	-0.46067	0.325177	0.99451	0.024658
9	0.226036789	0.19029246	0.144745627	-0.40646	0.288639	0.997585	0.024117
11	0.207346975	0.17256104	0.134728806	-0.36309	0.262318	0.999707	0.027652
15	0.19422623	0.164243156	0.12780415	-0.33211	0.245119	0.998429	0.032367
19	0.181832982	0.156596345	0.118901757	-0.31466	0.231108	0.993532	0.029125
23	0.172509105	0.146637794	0.112888847	-0.2981	0.218537	0.997103	0.027031
27	0.15861988	0.136374386	0.10305868	-0.27781	0.202136	0.993449	0.023112
31	0.148655429	0.127988752	0.09637988	-0.26138	0.189686	0.992777	0.021067
35	0.13957171	0.117335488	0.090305404	-0.24633	0.17732	0.998426	0.017881
39	0.132420913	0.111423107	0.085433599	-0.23494	0.168493	0.998124	0.016201
43	0.128134461	0.107975849	0.082160765	-0.22987	0.163557	0.997486	0.014076
47	0.124245819	0.104519192	0.079349139	-0.22448	0.158826	0.997559	0.012517
51	0.119780069	0.101415662	0.07 3548329	-0.21616	0.153288	0.99625	0.012533
55	0.116008708	0.098356759	0.073953745	-0.21027	0.148675	0.995733	0.011591
59	0.113010527	0.096762952	0.071834993	-0.20588	0.145339	0.992674	0.011039
63	0.111006371	0.094566128	0.07075462	-0.20126	0.142424	0.994457	0.011263
67	0.109831115	0.093024556	0.069948246	-0.19941	0.140788	0.995906	0.010709
71	0.107946742	0.090904878	0.068873904	-0.19536	0.138083	0.997294	0.010702
75	0.106666781	0.089229906	0.068109594	-0.19279	0.136199	0.998482	0.010476
79	0.104263437	0.086523898	0.066656812	-0.18803	0.132823	0.999467	0.010193
83	0.103353098	0.086527028	0.0661499	-0.18602	0.131847	0.998485	0.010697
87	0.10275378	0.086035192	0.065514004	-0.1862	0.131317	0.998267	0.009807
91	0.101930494	0.085193396	0.06516338	-0.18384	0.130055	0.998666	0.010234
95	0.101410249	0.08515681	0.064687031	-0.18362	0.129655	0.99781	0.009889
99	0.100977641	0.085083957	0.064306469	-0.18336	0.129295	0.997057	0.009634
103	0.100679752	0.083953944	0.06398814	-0.18346	0.128738	0.998703	0.008781
107	0.099373568	0.082868211	0.063211636	-0.18081	0.12702	0.998737	0.008846
111	0.098196006	0.082073996	0.06235833	-0.17919	0.125673	0.998328	0.008483
115	0.097463626	0.081580143	0.062127411	-0.17668	0.124561	0.998304	0.009246
119	0.096798892	0.080301773	0.061876535	-0.17461	0.123312	0.999492	0.009424
123	0.096360749	0.080877001	0.061473597	-0.17444	0.123179	0.997903	0.009403
127	0.096137207	0.079649301	0.061319372	-0.17409	0.122558	0.999534	0.00887
131	0.095505842	0.079137947	0.060805047	-0.1735	0.121859	0.999466	0.008449
135	0.09525153	0.078371878	0.060548787	-0.17351	0.121436	0.999877	0.007862
139	0.095189066	0.077807261	0.060453589	-0.17368	0.121236	1	0.007441

(3). r= 0.199 mm

Time	*Volumetric Fraction of Aggregate*			k	b	|r|	θ
(hrs.)	*0.15*	*0.25*	*0.35*				(x10 -4)
1	0.359034069	0.298703958	0.235174429	-0.6193	0.452462	0.999889	0.039399
2	0.371297072	0.31254607	0.247191171	-0.62053	0.465477	0.999528	0.051532
3	0.361239758	0.306802737	0.242012785	-0.59613	0.452385	0.998746	0.054687
4	0.348334603	0.293812018	0.233607346	-0.57364	0.435327	0.999591	0.052638
5	0.327144341	0.276287542	0.220619128	-0.53263	0.40784	0.99966	0.052492
6	0.305868921	0.259484306	0.206460131	-0.49704	0.381532	0.999257	0.049919
7	0.27907992	0.237557291	0.188297577	-0.45391	0.348456	0.998792	0.045619
8	0.253823569	0.21362503	0.171795663	-0.41014	0.315616	0.999934	0.041979
9	0.221434368	0.185880479	0.150047468	-0.35693	0.275021	0.999997	0.036879
11	0.199911339	0.168539543	0.134713235	-0.32599	0.24922	0.999764	0.031732
15	0.187666049	0.160893839	0.123994499	-0.31836	0.237108	0.99581	0.024745
19	0.177576548	0.148072171	0.115176152	-0.312	0.224942	0.999508	0.016856
23	0.167861844	0.143926933	0.105375728	-0.31243	0.217162	0.991004	0.008831
27	0.158153806	0.129398392	0.096612285	-0.30771	0.204982	0.999286	-0.00016
31	0.149148097	0.121410506	0.08925741	-0.29945	0.194802	0.999095	-0.00481
35	0.141109262	0.113923514	0.083187824	-0.28961	0.185142	0.999375	-0.00789
39	0.133820498	0.109271116	0.07828572	-0.27767	0.176544	0.997769	-0.00853
43	0.127475583	0.102596965	0.074404479	-0.26536	0.167831	0.999351	-0.00903
47	0.122188689	0.100702912	0.07091921	-0.25635	0.162024	0.995663	-0.00883
51	0.118070784	0.09484801	0.068579292	-0.24746	0.155697	0.999369	-0.00923
55	0.113734127	0.093099812	0.065712568	-0.24011	0.150876	0.99672	-0.00915
59	0.112319922	0.089774052	0.065163444	-0.23578	0.148031	0.999681	-0.00911
63	0.109660389	0.087417917	0.063621357	-0.2302	0.144449	0.99981	-0.00897
67	0.108817274	0.087094473	0.062809718	-0.23004	0.14375	0.999484	-0.00956
71	0.108185731	0.086606258	0.0623207	-0.22933	0.143036	0.99942	-0.0098
75	0.106346583	0.084751305	0.06126393	-0.22541	0.140474	0.999707	-0.00975
79	0.105341004	0.083555874	0.060519422	-0.22411	0.139166	0.99987	-0.01019
83	0.103657729	0.083287598	0.059349276	-0.22154	0.137484	0.998921	-0.01016
87	0.102764784	0.080784101	0.058977607	-0.21894	0.135576	0.999997	-0.01033
91	0.102420612	0.081119853	0.058635887	-0.21892	0.135456	0.999878	-0.01044
95	0.102282232	0.080659337	0.058502258	-0.2189	0.135206	0.999975	-0.01067
99	0.101424199	0.079707629	0.05782393	-0.218	0.134152	0.999998	-0.01113
103	0.100277594	0.079448642	0.057101693	-0.21588	0.132913	0.999794	-0.01095
107	0.098436916	0.077813555	0.05613031	-0.21153	0.130344	0.999895	-0.01063
111	0.09780475	0.077685697	0.055607848	-0.21098	0.129779	0.999641	-0.01082
115	0.097278592	0.077329002	0.055434674	-0.20922	0.128986	0.99964	-0.01044
119	0.097221407	0.077078355	0.055319471	-0.20951	0.128917	0.999752	-0.0107
123	0.09714001	0.076732733	0.055133705	-0.21003	0.128843	0.999866	-0.01112
127	0.096787832	0.075731326	0.055005861	-0.20891	0.128069	0.99999	-0.01115
131	0.095449412	0.074098318	0.054187172	-0.20631	0.126156	0.999797	-0.01133
135	0.093904121	0.073158285	0.053579011	-0.20163	0.123954	0.999861	-0.01041
139	0.093185658	0.072846021	0.053013642	-0.20086	0.12323	0.999973	-0.01062

2. W/C = 0.50

(1). r=0.506 mm

Time	*Volumetric Fraction of Aggregate*					k	b	|r|	θ
(hrs.)	*0.1*	*0.15*	*0.25*	*0.3*	*0.35*				(x10 -4)
1	0.396162	0.360046	0.309176	0.268033	0.243028	-0.6092	0.455404	0.997581	0.124659
2	0.409604	0.376719	0.31677	0.277189	0.251885	-0.6377	0.473104	0.998993	0.121368
3	0.396204	0.36361	0.313324	0.268085	0.241937	-0.61699	0.458539	0.996452	0.119452
4	0.385244	0.344927	0.29303	0.258297	0.233506	-0.598	0.44054	0.997653	0.105945
5	0.353262	0.317151	0.270646	0.240379	0.212422	-0.54805	0.404823	0.998118	0.09983
6	0.32639	0.297657	0.250414	0.219889	0.199208	-0.51018	0.376053	0.999037	0.09091
7	0.278356	0.254173	0.215694	0.187712	0.169478	-0.43556	0.321261	0.998576	0.07815
8	0.258976	0.232758	0.198849	0.173236	0.156652	-0.40432	0.297088	0.997541	0.069679
9	0.257928	0.231771	0.196944	0.172438	0.155985	-0.40336	0.295786	0.997875	0.068004
10	0.235986	0.213082	0.181134	0.157158	0.143749	-0.36863	0.271007	0.997505	0.063891
12	0.223563	0.201376	0.17048	0.148781	0.135571	-0.35071	0.256617	0.997818	0.057715
14	0.211476	0.193069	0.165325	0.141119	0.128371	-0.33367	0.244617	0.996763	0.056084
16	0.197992	0.184395	0.152569	0.133682	0.119765	-0.31883	0.231011	0.999167	0.046701
20	0.182936	0.16889	0.143064	0.122531	0.110404	-0.29316	0.212992	0.997549	0.044405
24	0.172307	0.15752	0.133507	0.113542	0.103665	-0.27776	0.199993	0.99701	0.037496
28	0.162669	0.148318	0.125483	0.108265	0.096714	-0.26322	0.18883	0.998379	0.033778
32	0.154767	0.142336	0.120934	0.103152	0.092	-0.2518	0.180551	0.997205	0.032096
36	0.149825	0.137737	0.117262	0.099439	0.088631	-0.24546	0.175034	0.99661	0.028832
40	0.144494	0.131786	0.110284	0.094336	0.086233	-0.23651	0.167824	0.997769	0.02568
44	0.141064	0.130345	0.107858	0.092922	0.084238	-0.23246	0.16475	0.998498	0.024741
48	0.138598	0.127247	0.106577	0.092808	0.080926	-0.22917	0.161979	0.998769	0.023271
52	0.138411	0.127152	0.106671	0.091972	0.080766	-0.23029	0.16196	0.99853	0.021344
56	0.137217	0.126866	0.106384	0.091668	0.079934	-0.22909	0.161106	0.998019	0.021191
60	0.135367	0.1256	0.105414	0.089639	0.07955	-0.22597	0.159087	0.997206	0.021354
64	0.134126	0.124377	0.103478	0.08898	0.078742	-0.22417	0.1575	0.998396	0.020373
68	0.133614	0.122451	0.102293	0.087814	0.078048	-0.22343	0.156232	0.998662	0.018423
72	0.132577	0.120884	0.103857	0.086278	0.077467	-0.22077	0.154989	0.994371	0.019762
76	0.13257	0.120692	0.101429	0.086824	0.076786	-0.22253	0.154843	0.998329	0.016414
80	0.131488	0.121222	0.100705	0.086975	0.076225	-0.2219	0.154361	0.998896	0.016254
84	0.131052	0.120693	0.101228	0.08662	0.075712	-0.22137	0.153975	0.997903	0.016185
88	0.130853	0.121069	0.102271	0.086376	0.075519	-0.22192	0.154258	0.99612	0.015976
92	0.132003	0.120796	0.099845	0.086591	0.076192	-0.22379	0.154556	0.999471	0.013574
96	0.129699	0.121099	0.102842	0.08638	0.074614	-0.22074	0.153697	0.993562	0.01654
100	0.128245	0.120518	0.100879	0.08456	0.074478	-0.21951	0.152224	0.994685	0.014881
104	0.12791	0.1201	0.100175	0.085075	0.073564	-0.21976	0.151911	0.99556	0.013665
108	0.127802	0.119448	0.098552	0.084922	0.073453	-0.21954	0.15133	0.997741	0.012573
112	0.127592	0.119084	0.098033	0.084706	0.0735	-0.21869	0.150881	0.998209	0.012876
116	0.12745	0.118568	0.097706	0.084403	0.073607	-0.21764	0.150405	0.998556	0.013431
120	0.127182	0.11865	0.097861	0.084072	0.073607	-0.21746	0.150289	0.998076	0.013456
124	0.127155	0.118619	0.097831	0.084015	0.073607	-0.21742	0.150252	0.998073	0.013423
128	0.127129	0.118554	0.097863	0.083722	0.073491	-0.21801	0.150293	0.99788	0.012537
132	0.126296	0.118518	0.098327	0.083047	0.073091	-0.21743	0.149864	0.99612	0.01243
136	0.124687	0.118232	0.097638	0.08198	0.072019	-0.21707	0.148838	0.994389	0.01043
140	0.125223	0.11492	0.096966	0.08161	0.071793	-0.21408	0.147341	0.996681	0.011692

(2). r=0.136 mm

Time	*Volumetric Fraction of Aggregate*				k	b	| r |	θ
(hrs.)	*0.05*	*0.15*	*0.25*	*0.35*				(x10 -4)
1	0.477543	0.410475	0.318661	0.244009	-0.79242	0.521155	0.998376	-0.00484
2	0.494258	0.401912	0.334879	0.245688	-0.81274	0.531733	0.998261	-0.00687
3	0.485539	0.396905	0.329935	0.236958	-0.81271	0.524877	0.998213	-0.01151
4	0.468799	0.394261	0.323529	0.226562	-0.79744	0.512777	0.997324	-0.01282
5	0.446931	0.366612	0.303651	0.213356	-0.76369	0.485375	0.997868	-0.01615
6	0.433062	0.351038	0.283578	0.200113	-0.76631	0.470209	0.999196	-0.02765
7	0.404446	0.323655	0.263187	0.184423	-0.72054	0.438035	0.998547	-0.02878
8	0.369832	0.299018	0.242079	0.168623	-0.66057	0.402001	0.998903	-0.0261
9	0.340097	0.273692	0.219754	0.15407	-0.61202	0.369307	0.999215	-0.02632
10	0.307128	0.248752	0.19895	0.142375	-0.54406	0.333114	0.999575	-0.02012
12	0.261487	0.209064	0.167618	0.118183	-0.47136	0.283359	0.999091	-0.021
14	0.231122	0.187189	0.150839	0.105068	-0.41451	0.251457	0.999111	-0.01692
16	0.218632	0.176994	0.141565	0.098697	-0.39523	0.238019	0.99938	-0.01732
20	0.224448	0.184618	0.147066	0.100617	-0.40904	0.245996	0.998974	-0.01816
24	0.212456	0.175802	0.137555	0.097057	-0.38444	0.232606	0.999749	-0.01611
28	0.199017	0.162854	0.126751	0.093141	-0.35373	0.216187	0.999846	-0.01335
32	0.183155	0.149539	0.115051	0.084921	-0.32919	0.199005	0.999594	-0.01391
36	0.170359	0.14142	0.108295	0.079365	-0.30611	0.186081	0.999626	-0.01223
40	0.160224	0.134414	0.102378	0.07495	-0.28786	0.175563	0.999214	-0.01111
44	0.154581	0.129438	0.098124	0.071901	-0.27936	0.169382	0.999151	-0.01146
48	0.149234	0.124038	0.094564	0.068745	-0.27094	0.163334	0.999559	-0.01176
52	0.143693	0.120624	0.091496	0.066195	-0.26162	0.157826	0.999105	-0.01128
56	0.139337	0.116725	0.08808	0.06311	-0.25733	0.153278	0.99908	-0.01243
60	0.137001	0.116954	0.086482	0.062096	-0.25519	0.151671	0.997196	-0.01255
64	0.134111	0.114027	0.08461	0.060523	-0.25018	0.148354	0.997651	-0.01254
68	0.13243	0.114595	0.083156	0.059422	-0.25046	0.147494	0.995032	-0.01325
72	0.130835	0.113302	0.082331	0.058639	-0.24756	0.145789	0.99499	-0.01309
76	0.129221	0.111926	0.081058	0.057814	-0.24509	0.144023	0.994828	-0.01317
80	0.128037	0.110523	0.079818	0.056998	-0.24382	0.142608	0.995116	-0.01356
84	0.128115	0.110042	0.079366	0.056562	-0.24533	0.142588	0.995617	-0.01426
88	0.12755	0.109479	0.078977	0.056477	-0.24372	0.141865	0.995687	-0.01402
92	0.126522	0.108445	0.07853	0.056007	-0.24146	0.140668	0.996006	-0.01381
96	0.126214	0.108168	0.078645	0.055809	-0.24074	0.140356	0.996185	-0.01369
100	0.125107	0.107178	0.078254	0.055577	-0.23751	0.139032	0.996385	-0.01313
104	0.124925	0.106756	0.078262	0.05508	-0.23803	0.138861	0.99675	-0.01348
108	0.123844	0.105836	0.077494	0.054619	-0.23602	0.137652	0.996713	-0.01339
112	0.124324	0.105887	0.076589	0.054121	-0.23991	0.138212	0.996593	-0.01477
116	0.123321	0.105308	0.075624	0.053671	-0.23863	0.137208	0.996037	-0.01488
120	0.121289	0.104796	0.076022	0.053116	-0.23329	0.135465	0.995122	-0.01364
124	0.120677	0.101721	0.075724	0.05191	-0.2323	0.133967	0.998123	-0.01421
128	0.118367	0.098504	0.074252	0.050054	-0.22919	0.131132	0.998919	-0.01473
132	0.119331	0.099339	0.074348	0.049784	-0.23363	0.132427	0.998775	-0.01586
136	0.11903	0.098789	0.073972	0.049449	-0.23356	0.132022	0.998944	-0.01611
140	0.119087	0.098449	0.073638	0.049188	-0.23451	0.131992	0.999153	-0.01656

(3). r=0.099 mm

Time	*Volumetric*	*Fraction*	*of*	*Aggregate*	k	b	| r |	θ
(hrs.)	*0.05*	*0.15*	*0.25*	*0.35*				(x10 -4)
1	0.479187	0.402736	0.340037	0.260209	-0.71963	0.514469	0.999026	0.017183
2	0.474067	0.405147	0.339822	0.260621	-0.70566	0.511047	0.999164	0.020099
3	0.466612	0.402054	0.334369	0.255629	-0.70064	0.504793	0.998913	0.018663
4	0.451019	0.393668	0.319655	0.246693	-0.68699	0.490157	0.998381	0.015921
5	0.426942	0.373016	0.307359	0.232022	-0.65042	0.464918	0.997297	0.015497
6	0.422667	0.351409	0.292467	0.219939	-0.66713	0.455046	0.999238	0.005096
7	0.395619	0.330879	0.273562	0.203381	-0.63403	0.427666	0.999305	0.002464
8	0.36489	0.305062	0.255435	0.188147	-0.57986	0.394355	0.998436	0.003853
9	0.337852	0.27886	0.231439	0.170733	-0.54878	0.364476	0.998952	-0.00068
10	0.311537	0.257125	0.212063	0.155363	-0.51358	0.336739	0.999116	-0.0028
12	0.266657	0.213273	0.177555	0.133946	-0.43385	0.284628	0.997009	-0.00228
14	0.243532	0.196294	0.161198	0.123467	-0.39529	0.260181	0.997862	-0.00166
16	0.225021	0.181982	0.150242	0.112639	-0.36889	0.241248	0.998379	-0.00231
20	0.237639	0.19077	0.156912	0.118186	-0.39222	0.254321	0.99789	-0.00354
24	0.215044	0.174994	0.143872	0.106481	-0.35681	0.23146	0.998956	-0.00317
28	0.197191	0.163435	0.132417	0.097111	-0.33126	0.21379	0.999721	-0.00349
32	0.179846	0.149872	0.119769	0.088692	-0.30356	0.195258	0.999963	-0.00352
36	0.170073	0.140987	0.112117	0.083558	-0.28841	0.184367	0.999992	-0.00392
40	0.15953	0.132966	0.10574	0.079258	-0.26804	0.172981	0.999986	-0.00283
44	0.154373	0.127213	0.101475	0.076293	-0.25998	0.166834	0.99985	-0.00321
48	0.148264	0.12265	0.097519	0.073484	-0.24947	0.160373	0.999897	-0.00294
52	0.143444	0.118006	0.093827	0.071282	-0.24066	0.154773	0.999638	-0.00281
56	0.139087	0.114295	0.09082	0.068842	-0.23421	0.150103	0.999639	-0.00299
60	0.136182	0.11169	0.088836	0.067661	-0.22842	0.146776	0.999473	-0.00272
64	0.133742	0.10896	0.086702	0.066246	-0.22475	0.143862	0.99907	-0.00295
68	0.131322	0.106689	0.085654	0.065423	-0.21873	0.141018	0.998907	-0.00238
72	0.129762	0.105668	0.084614	0.064731	-0.21615	0.139423	0.999015	-0.00231
76	0.128331	0.104181	0.083397	0.063963	-0.21389	0.137746	0.998743	-0.0024
80	0.125905	0.102533	0.082378	0.06316	-0.20839	0.135172	0.998948	-0.00186
84	0.125812	0.102072	0.081658	0.062739	-0.20963	0.134997	0.998642	-0.00236
88	0.124887	0.101435	0.080854	0.062248	-0.2085	0.134055	0.998643	-0.00245
92	0.1242	0.100032	0.080212	0.061759	-0.20714	0.13298	0.998	-0.00253
96	0.123622	0.099447	0.07999	0.061463	-0.20593	0.132317	0.997957	-0.00246
100	0.123517	0.099386	0.079515	0.061276	-0.20659	0.132242	0.997892	-0.00272
104	0.122988	0.099058	0.079146	0.060985	-0.20592	0.131728	0.997983	-0.00275
108	0.121608	0.097589	0.078264	0.060289	-0.20328	0.130094	0.997663	-0.00269
112	0.12109	0.09733	0.078159	0.060014	-0.2024	0.129628	0.997927	-0.00263
116	0.121049	0.096705	0.077416	0.059682	-0.20339	0.129391	0.997223	-0.00307
120	0.119509	0.096082	0.076964	0.059264	-0.19985	0.127925	0.997848	-0.00263
124	0.120087	0.09638	0.076964	0.059282	-0.20183	0.128545	0.9977	-0.00298
128	0.117425	0.094102	0.075215	0.058171	-0.19665	0.125558	0.997375	-0.00274
132	0.11759	0.094694	0.075868	0.058489	-0.19613	0.125886	0.997939	-0.00241
136	0.117277	0.09397	0.07514	0.058147	-0.19622	0.125378	0.997331	-0.00269
140	0.117184	0.094052	0.074838	0.057948	-0.19692	0.12539	0.997465	-0.00292

V. QUARTZ SAND - C3S SYSTEMS

Units : (i). Electrical conductivity: ohm-1 m-1; (ii). Excess interfacial conductance: ohm-1
Temperature : 20°C .
Aggregate size : r=0.561 mm; W/C=0.50

Time	*Volumetric Fraction of Aggregate*					k	b	|r|	θ
(hrs.)	*0.15*	*0.2*	*0.25*	*0.3*	*0.35*				(x10 -4)
1	0.328778	0.306416	0.284067	0.257378	0.22856	-0.49895	0.405777	0.99821	0.205172
2	0.355336	0.335539	0.309116	0.279066	0.246638	-0.54774	0.442073	0.995928	0.215748
3	0.379212	0.354132	0.333674	0.296244	0.26284	-0.58126	0.470536	0.993744	0.232892
4	0.356747	0.332888	0.310313	0.275503	0.249687	-0.54301	0.440781	0.997176	0.220956
5	0.356941	0.326911	0.30339	0.274226	0.247905	-0.54151	0.437253	0.999479	0.213864
6	0.353404	0.323528	0.300838	0.269156	0.244635	-0.54382	0.434267	0.998978	0.201177
7	0.350005	0.320021	0.294462	0.265997	0.241836	-0.54073	0.429646	0.999421	0.194
8	0.340882	0.313731	0.286931	0.252779	0.237841	-0.53407	0.41995	0.994908	0.179252
9	0.33711	0.303953	0.278037	0.247467	0.229905	-0.54179	0.414743	0.995526	0.150199
10	0.323594	0.29253	0.263919	0.23634	0.220072	-0.52647	0.398908	0.994505	0.134442
12	0.292883	0.258494	0.242665	0.212079	0.197286	-0.47522	0.359485	0.991114	0.119702
14	0.253933	0.222113	0.211252	0.185117	0.170645	-0.40715	0.310399	0.989012	0.109305
16	0.224291	0.199296	0.188345	0.164788	0.152466	-0.35632	0.274916	0.9924	0.10483
20	0.186924	0.166775	0.158084	0.140613	0.126978	-0.29211	0.228901	0.994762	0.095828
24	0.16796	0.148911	0.141189	0.129497	0.113185	-0.25793	0.204631	0.991493	0.091662
28	0.155792	0.139229	0.13235	0.119595	0.105943	-0.23866	0.190248	0.994008	0.087345
32	0.14406	0.129951	0.123508	0.112058	0.099001	-0.21602	0.17572	0.994519	0.088938
36	0.137841	0.124524	0.118744	0.106699	0.094143	-0.21044	0.169001	0.993936	0.08052
40	0.134208	0.122933	0.116819	0.1034	0.093193	-0.20314	0.164896	0.995274	0.082667
44	0.132361	0.120798	0.115348	0.101	0.091363	-0.20359	0.16307	0.993446	0.076706
48	0.12706	0.117229	0.111985	0.097831	0.088775	-0.19194	0.15656	0.992112	0.080228
52	0.124853	0.11479	0.109645	0.096584	0.086393	-0.19025	0.154016	0.99281	0.076244
56	0.118992	0.110276	0.105508	0.092788	0.083312	-0.17769	0.146599	0.991201	0.07892
60	0.116201	0.107591	0.103191	0.089721	0.081903	-0.17293	0.142954	0.989848	0.077606
64	0.113898	0.10559	0.101035	0.087362	0.080405	-0.17043	0.140265	0.989435	0.074743
68	0.112314	0.103871	0.099691	0.086989	0.078938	-0.16727	0.138178	0.990197	0.074793
72	0.112423	0.103899	0.100015	0.085906	0.07932	-0.1684	0.138412	0.986927	0.073346
76	0.109539	0.10138	0.097564	0.084332	0.077644	-0.16168	0.134511	0.987908	0.074969
80	0.108181	0.099188	0.095438	0.083706	0.075948	-0.1599	0.132466	0.991206	0.072562
84	0.106632	0.09787	0.09414	0.081799	0.075365	-0.15721	0.130463	0.990019	0.07197
88	0.104197	0.096507	0.092872	0.079733	0.074296	-0.15315	0.127809	0.986111	0.072109
92	0.103363	0.095315	0.091714	0.078959	0.07321	-0.15332	0.126842	0.98765	0.069084
96	0.103203	0.095622	0.091826	0.078688	0.073437	-0.15293	0.126789	0.986253	0.069655
100	0.10102	0.093465	0.090034	0.076186	0.072084	-0.15031	0.124134	0.981706	0.067126
104	0.099314	0.091777	0.088643	0.075127	0.071217	-0.14569	0.121638	0.981065	0.068756
108	0.098203	0.090978	0.087765	0.074288	0.070549	-0.144	0.120356	0.980483	0.068323
112	0.098258	0.091127	0.087882	0.074113	0.070257	-0.14603	0.120836	0.979888	0.065861
116	0.097696	0.090801	0.087618	0.073778	0.070119	-0.14435	0.12009	0.978497	0.066915
120	0.096742	0.089795	0.086657	0.073087	0.069225	-0.14348	0.118972	0.979599	0.065404
124	0.09557	0.088906	0.086068	0.072429	0.069037	-0.13909	0.117174	0.976464	0.068578
128	0.093246	0.0865	0.083983	0.070547	0.067353	-0.13548	0.114196	0.975347	0.066972
132	0.092126	0.085636	0.083281	0.070164	0.066676	-0.13275	0.112763	0.975483	0.068065
136	0.092368	0.08593	0.083459	0.070113	0.066538	-0.13496	0.113421	0.975403	0.065773
140	0.091946	0.0856	0.083373	0.069903	0.066462	-0.13333	0.112789	0.973245	0.067047
144	0.091015	0.084481	0.082173	0.069066	0.065651	-0.13229	0.111549	0.975249	0.065518
148	0.090598	0.083717	0.081838	0.069061	0.065374	-0.13021	0.110669	0.975536	0.06694
152	0.087984	0.081891	0.079838	0.067168	0.064194	-0.12461	0.107367	0.972761	0.06815

156	0.087881	0.081259	0.079066	0.066915	0.063794	-0.12504	0.107042	0.976957	0.066434
160	0.087663	0.081588	0.079646	0.066827	0.063635	-0.12563	0.10728	0.972186	0.065988
164	0.087514	0.081457	0.079434	0.066518	0.063511	-0.12589	0.10716	0.971799	0.065165
168	0.08648	0.080554	0.078664	0.065909	0.0629	-0.12361	0.105803	0.971079	0.065631
174	0.08567	0.07956	0.077721	0.064521	0.062587	-0.12241	0.104614	0.966462	0.064536
180	0.084173	0.078063	0.076325	0.063254	0.061743	-0.11934	0.102546	0.964393	0.064481
186	0.083086	0.077852	0.075012	0.062987	0.061535	-0.11594	0.101078	0.970268	0.066725
192	0.083012	0.0771	0.074586	0.062631	0.06146	-0.11515	0.100545	0.969654	0.066702
198	0.082234	0.076984	0.074124	0.062538	0.061206	-0.113	0.099668	0.97125	0.068251
204	0.08106	0.076012	0.073865	0.061954	0.059987	-0.11241	0.098678	0.968534	0.066588
210	0.08083	0.075812	0.073652	0.061732	0.059751	-0.11248	0.098474	0.968504	0.065891
216	0.08015	0.075195	0.073521	0.061717	0.059647	-0.10897	0.097287	0.965881	0.069125
222	0.079411	0.074399	0.073106	0.061309	0.058936	-0.10808	0.096452	0.964542	0.06844
228	0.077549	0.072767	0.071481	0.060625	0.057979	-0.10256	0.093721	0.967748	0.071094
234	0.077087	0.072316	0.071046	0.060205	0.057603	-0.10216	0.093191	0.967491	0.070363
240	0.077278	0.072568	0.071255	0.060115	0.057569	-0.10374	0.093693	0.966185	0.068806
246	0.076188	0.071581	0.070413	0.059413	0.056853	-0.10168	0.092309	0.965031	0.068788
252	0.075083	0.070599	0.069491	0.0589	0.056496	-0.09774	0.09055	0.964972	0.071213
258	0.074605	0.070264	0.069254	0.058752	0.056044	-0.09727	0.090101	0.964545	0.070841
264	0.075	0.070322	0.069403	0.058564	0.055944	-0.09974	0.090782	0.964114	0.06813
270	0.073789	0.069409	0.068659	0.057834	0.055504	-0.09629	0.089111	0.959842	0.069895
276	0.072572	0.068231	0.067526	0.057174	0.054937	-0.09266	0.087252	0.960768	0.071475
282	0.072712	0.068063	0.067379	0.056922	0.054517	-0.09506	0.087684	0.962605	0.068187
288	0.072859	0.068426	0.067861	0.056951	0.054795	-0.09521	0.08798	0.95736	0.068749
294	0.072029	0.067445	0.067052	0.056068	0.054051	-0.09466	0.086995	0.955685	0.067
300	0.070597	0.066258	0.065742	0.055559	0.053487	-0.08984	0.084788	0.958848	0.069836
306	0.070719	0.066235	0.065864	0.055356	0.053297	-0.09145	0.085156	0.956855	0.067856
312	0.070762	0.066185	0.065868	0.055321	0.053241	-0.09181	0.085229	0.956791	0.067376
318	0.070267	0.065715	0.065478	0.05502	0.052837	-0.09111	0.084641	0.956497	0.067042
324	0.069244	0.064689	0.064511	0.054234	0.052425	-0.08819	0.083067	0.954931	0.068097
330	0.069093	0.06494	0.064528	0.054344	0.052296	-0.08838	0.083135	0.956318	0.067926
336	0.069355	0.065081	0.064642	0.054463	0.052042	-0.09049	0.083739	0.958873	0.065672

VI. QUARTZ SAND - HIGH ALKALI PORTLAND CEMENT SYSTEMS

Cement : High alkali portland cement.
Units : (I). Electrical conductivity: ohm-1 m-1; (II). Excess interfacial conductance: ohm-1
Temperature : 20°C .
Aggregate size : r=0.561 mm; W/C=0.50

Time	*Volumetric Fraction of Aggregate*					k	b	I r I	θ
(hrs.)	*0.15*	*0.2*	*0.25*	*0.3*	*0.35*				(x10 -4)
1	0.92071	0.85803	0.784377	0.713167	0.659018	-1.33649	1.121184	0.99764	0.645678
2	0.947853	0.884908	0.797532	0.721359	0.671642	-1.43194	1.162644	0.992932	0.583487
3	0.969951	0.906187	0.809907	0.741689	0.68238	-1.47928	1.191843	0.993483	0.576867
4	0.931712	0.870865	0.780085	0.707853	0.658391	-1.41931	1.144608	0.991615	0.556518
5	0.899799	0.841917	0.752844	0.684295	0.63708	-1.36612	1.104717	0.990741	0.544088
6	0.863232	0.808182	0.723749	0.657912	0.613649	-1.29887	1.058062	0.99056	0.538976
7	0.836241	0.783032	0.700124	0.635002	0.593705	-1.26621	1.026172	0.989328	0.510608
8	0.806886	0.756304	0.671918	0.612143	0.570752	-1.23286	0.991815	0.988006	0.476595
9	0.771073	0.725002	0.639805	0.58294	0.547663	-1.17776	0.947737	0.982443	0.455987
10	0.733314	0.690573	0.604902	0.557296	0.519421	-1.12213	0.901632	0.981131	0.430704
12	0.652109	0.615424	0.539427	0.49686	0.466056	-0.98134	0.799311	0.978528	0.406957
14	0.581088	0.54985	0.480031	0.444459	0.417557	-0.86491	0.710824	0.974629	0.376484
16	0.520256	0.493932	0.428751	0.398445	0.376102	-0.76759	0.635394	0.968	0.346892
20	0.421868	0.401303	0.347601	0.324797	0.306471	-0.6146	0.514059	0.965091	0.292627
24	0.371788	0.353093	0.304413	0.285594	0.267022	-0.55406	0.454898	0.966519	0.23989
28	0.326001	0.310813	0.265785	0.245875	0.23541	-0.49224	0.399836	0.952312	0.201055
32	0.299361	0.282713	0.245322	0.226012	0.212025	-0.46274	0.368772	0.973954	0.169077
36	0.270934	0.254499	0.225412	0.20154	0.192541	-0.41949	0.333857	0.976839	0.152026
40	0.250042	0.232542	0.210215	0.189625	0.175215	-0.38514	0.307814	0.995539	0.143201
44	0.225052	0.210461	0.186173	0.177398	0.156989	-0.33838	0.275809	0.986106	0.140878
48	0.210177	0.198169	0.171597	0.164997	0.147581	-0.31673	0.257686	0.973812	0.130529
52	0.1976	0.187906	0.15981	0.154407	0.140421	-0.29571	0.241957	0.957701	0.125707
56	0.1875	0.179851	0.151265	0.144718	0.135967	-0.2764	0.228959	0.939159	0.12537
60	0.176902	0.168436	0.144298	0.138069	0.127367	-0.25887	0.215732	0.960575	0.121037
64	0.168037	0.161084	0.137636	0.13088	0.123729	-0.23764	0.203683	0.947139	0.126946
68	0.159327	0.152313	0.130111	0.125643	0.116082	-0.22632	0.193275	0.952133	0.11892
72	0.151547	0.145251	0.124649	0.119296	0.112056	-0.20987	0.183029	0.950123	0.120929
76	0.144468	0.13862	0.118805	0.114268	0.10711	-0.19813	0.174188	0.947334	0.118085
80	0.139314	0.133016	0.11536	0.111234	0.102763	-0.18977	0.167779	0.961211	0.115755
84	0.133055	0.125743	0.112729	0.107797	0.098105	-0.1757	0.15941	0.986041	0.118593
88	0.129614	0.123571	0.109187	0.104375	0.097101	-0.16844	0.15488	0.973098	0.11945
92	0.124797	0.118202	0.105751	0.101627	0.092562	-0.16209	0.14911	0.982696	0.115146
96	0.120197	0.114682	0.101415	0.097512	0.090384	-0.15359	0.143236	0.971822	0.114562
100	0.11769	0.11256	0.099445	0.09495	0.089186	-0.14924	0.140075	0.968504	0.113839
104	0.114862	0.110102	0.096588	0.092505	0.087067	-0.14638	0.136819	0.961092	0.110055
108	0.112996	0.107971	0.095464	0.091094	0.085414	-0.14408	0.134609	0.97033	0.108143
112	0.110474	0.105695	0.092749	0.089247	0.08319	-0.14203	0.131779	0.964214	0.104043
116	0.108414	0.10394	0.09089	0.087314	0.081942	-0.13914	0.129284	0.959074	0.102458
120	0.106044	0.101916	0.089483	0.084292	0.081228	-0.13452	0.126222	0.952248	0.102507
124	0.103914	0.099832	0.087971	0.082941	0.079809	-0.1302	0.123444	0.955361	0.102782
128	0.102892	0.098718	0.086868	0.081595	0.07852	-0.13173	0.122652	0.956445	0.097698
132	0.102703	0.098841	0.085948	0.081576	0.078226	-0.13244	0.122568	0.946319	0.096146
136	0.100858	0.097265	0.084507	0.080308	0.077322	-0.12806	0.120066	0.940868	0.097319

140	0.097798	0.093849	0.08298	0.078775	0.075082	-0.12101	0.11595	0.961952	0.098947
144	0.096463	0.092704	0.081768	0.07695	0.074249	-0.12036	0.114518	0.954317	0.096141
148	0.093912	0.090138	0.08063	0.076181	0.073082	-0.11123	0.110597	0.966366	0.102217
152	0.092546	0.089204	0.079391	0.075171	0.072706	-0.10743	0.10866	0.95403	0.103906
156	0.091888	0.08816	0.079536	0.074386	0.072081	-0.10677	0.107904	0.966648	0.103002
160	0.090712	0.087037	0.078439	0.073787	0.071089	-0.10499	0.106461	0.969183	0.102288
164	0.089899	0.08671	0.077312	0.073139	0.070932	-0.10301	0.105351	0.952827	0.102879
168	0.088205	0.085788	0.074678	0.071773	0.069844	-0.10147	0.103426	0.919015	0.100357

VII. SILICA FUME COATED AGGREGATE - CEMENT PASTE SYSTEMS

Cement : White portland cement .
Units : (i). Electrical conductivity: ohm-1 m-1; (ii). Excess interfacial conductance: ohm-1
Temperature : 20°C .
Aggregate size : r=0.506 mm for limestone and r=0.561 mm for quartz.
Designing thickness of silica fume coating : 14 um.

1. Limestone Mortars (W/C=0.5)

Time	*Volumetric Fraction of Aggregate*					k	b	I r I	θ
(hrs.)	*0.15*	*0.2*	*0.25*	*0.3*	*0.35*				(x10 -4)
1	0.401216	0.371386	0.340531	0.305925	0.266717	-0.66892	0.504385	0.998328	0.147849
2	0.399503	0.369948	0.339027	0.308522	0.265984	-0.65693	0.500829	0.997189	0.159078
3	0.389864	0.365206	0.333455	0.301501	0.260552	-0.64466	0.491281	0.996141	0.155611
4	0.384282	0.356846	0.32958	0.294945	0.253198	-0.64814	0.485804	0.995334	0.135894
5	0.371017	0.345616	0.319975	0.282265	0.244153	-0.63416	0.471144	0.994658	0.122386
6	0.357236	0.33056	0.305332	0.27171	0.236214	-0.60179	0.450657	0.997068	0.125147
7	0.340341	0.315721	0.287643	0.256215	0.224808	-0.58114	0.430231	0.998711	0.108291
8	0.318616	0.295784	0.27152	0.241847	0.209105	-0.54592	0.403854	0.996908	0.100969
9	0.291224	0.272639	0.250258	0.217221	0.190899	-0.51213	0.372482	0.994839	0.078578
10	0.26479	0.245264	0.223138	0.197153	0.172464	-0.46553	0.336944	0.998483	0.067277
12	0.230296	0.21295	0.190549	0.172125	0.149571	-0.40455	0.292236	0.999116	0.057017
14	0.201285	0.18708	0.171713	0.151238	0.129995	-0.35685	0.257474	0.995742	0.049528
16	0.189783	0.173852	0.157962	0.140756	0.122804	-0.33411	0.240558	0.999612	0.045085
20	0.179858	0.165614	0.151419	0.132138	0.116737	-0.31944	0.229012	0.998392	0.040619
24	0.184804	0.169421	0.154631	0.137767	0.117942	-0.33076	0.235602	0.998198	0.038197
28	0.176334	0.161782	0.146936	0.130243	0.113089	-0.31606	0.224691	0.999265	0.035385
32	0.165923	0.151848	0.137992	0.122134	0.105872	-0.29964	0.211663	0.999299	0.030121
36	0.158664	0.144001	0.13027	0.116788	0.10049	-0.28712	0.201823	0.999482	0.026334
40	0.15105	0.13751	0.125714	0.111359	0.09525	-0.2755	0.193052	0.998468	0.023742
44	0.144108	0.131788	0.120352	0.106734	0.090305	-0.26532	0.184988	0.997403	0.020509
48	0.137859	0.126651	0.115036	0.101275	0.086411	-0.25654	0.177582	0.998016	0.016581
52	0.133114	0.122063	0.110093	0.097412	0.083057	-0.24953	0.171531	0.998749	0.013096
56	0.128656	0.117985	0.106835	0.093662	0.080128	-0.24276	0.166143	0.998498	0.010889
60	0.125364	0.115318	0.104281	0.090942	0.077691	-0.23944	0.16258	0.998005	0.007466
64	0.123209	0.112482	0.101672	0.088428	0.075668	-0.23827	0.15986	0.998787	0.002561
68	0.120719	0.110651	0.099726	0.086311	0.073907	-0.23593	0.157245	0.998426	-0.0001
72	0.118776	0.110247	0.098725	0.085299	0.072496	-0.23502	0.155863	0.996707	-0.00206
76	0.116426	0.105909	0.095559	0.082416	0.070487	-0.23074	0.151845	0.998855	-0.00502
80	0.114243	0.104486	0.093763	0.080761	0.069102	-0.22802	0.149475	0.998646	-0.00641
84	0.11312	0.103125	0.092321	0.079416	0.068057	-0.22767	0.148125	0.999011	-0.00925
88	0.11202	0.102007	0.091571	0.078773	0.067284	-0.22541	0.146684	0.998913	-0.00908
92	0.110982	0.101476	0.090804	0.077928	0.06647	-0.22515	0.145819	0.998566	-0.01082
96	0.110855	0.099728	0.090865	0.077598	0.066218	-0.22281	0.144755	0.998338	-0.00957
100	0.108698	0.099559	0.089099	0.07585	0.065106	-0.22179	0.143109	0.9981	-0.01201
104	0.107474	0.098678	0.088198	0.074992	0.064281	-0.22014	0.14176	0.997787	-0.01265
108	0.106995	0.098117	0.087482	0.074451	0.063851	-0.21991	0.141156	0.998095	-0.01379
112	0.105885	0.097473	0.086668	0.073352	0.062913	-0.22013	0.140291	0.997415	-0.01635
116	0.105541	0.097123	0.086603	0.073396	0.062499	-0.21962	0.139938	0.997289	-0.01639
120	0.105494	0.095164	0.085779	0.072825	0.061949	-0.21886	0.138957	0.998686	-0.01758
124	0.105153	0.09393	0.085172	0.072275	0.061439	-0.21817	0.138135	0.998672	-0.01849
128	0.104741	0.092714	0.084441	0.071513	0.061046	-0.21718	0.137186	0.998402	-0.01923
132	0.103211	0.094787	0.083967	0.071048	0.060404	-0.21871	0.13736	0.997721	-0.02136
136	0.102844	0.094436	0.083645	0.070346	0.059808	-0.22033	0.137297	0.997401	-0.02425

140	0.10316	0.094606	0.083415	0.07043	0.059615	-0.22253	0.137879	0.997867	-0.02651
144	0.102369	0.094062	0.082975	0.070033	0.058796	-0.22235	0.137235	0.997436	-0.02783
148	0.102272	0.093709	0.082551	0.069692	0.058769	-0.22205	0.136911	0.997935	-0.02814
152	0.101318	0.092758	0.080293	0.068413	0.058407	-0.22033	0.135321	0.998411	-0.02927
156	0.10078	0.092125	0.07914	0.06854	0.05781	-0.21905	0.134441	0.998668	-0.02933
160	0.100226	0.091773	0.081003	0.068002	0.057316	-0.21918	0.13446	0.997662	-0.0295
164	0.100498	0.091879	0.081269	0.068004	0.057263	-0.22069	0.134955	0.997576	-0.03079
168	0.100337	0.091967	0.08246	0.068098	0.057285	-0.21994	0.135015	0.995454	-0.02938

2. Quartz Mortars

(1). W/C=0.50

Time	*Volumetric Fraction of Aggregate*					k	b	I r I	θ
(hrs.)	*0.15*	*0.2*	*0.25*	*0.3*	*0.35*				(x10 -4)
1	0.42607	0.390658	0.347895	0.315806	0.276718	-0.74711	0.538207	0.998641	0.112573
2	0.425514	0.388991	0.345434	0.314562	0.274522	-0.75283	0.538011	0.99807	0.101335
3	0.415488	0.384868	0.34059	0.307317	0.269868	-0.73758	0.528021	0.997643	0.101824
4	0.408294	0.37498	0.336146	0.297831	0.261757	-0.74045	0.520914	0.999411	0.076522
5	0.390474	0.362376	0.322016	0.286264	0.252036	-0.70598	0.499127	0.997691	0.079878
6	0.375429	0.349273	0.311238	0.273152	0.241057	-0.68973	0.482462	0.996439	0.063512
7	0.35593	0.328502	0.291093	0.260584	0.228166	-0.64689	0.454578	0.998416	0.065402
8	0.33684	0.307111	0.278424	0.243924	0.214716	-0.61487	0.429921	0.99915	0.056118
9	0.308879	0.282538	0.255191	0.221988	0.195144	-0.57604	0.396758	0.998443	0.035713
10	0.286064	0.260355	0.233827	0.205696	0.179577	-0.53527	0.366921	0.999791	0.028261
12	0.239059	0.219202	0.19564	0.17187	0.15016	-0.45026	0.307751	0.999125	0.021257
14	0.21009	0.193142	0.173547	0.150474	0.132202	-0.39689	0.271113	0.997618	0.018293
16	0.196571	0.179817	0.161233	0.140686	0.123017	-0.37248	0.253384	0.998964	0.01421
20	0.186052	0.169174	0.152445	0.133148	0.116345	-0.35088	0.239153	0.999406	0.014677
24	0.18948	0.172439	0.155762	0.135278	0.118419	-0.35857	0.243918	0.998809	0.013666
28	0.182515	0.167527	0.150162	0.130418	0.114242	-0.34731	0.2358	0.99813	0.01195
32	0.172431	0.157415	0.141665	0.123026	0.107643	-0.32793	0.222418	0.998695	0.010656
36	0.164703	0.149687	0.135228	0.117206	0.102468	-0.3139	0.212334	0.998741	0.008597
40	0.157436	0.143245	0.12814	0.112624	0.097976	-0.29908	0.202654	0.999798	0.009167
44	0.150307	0.137563	0.12319	0.107508	0.09395	-0.28554	0.193888	0.998941	0.009899
48	0.145279	0.132553	0.118398	0.1039	0.090459	-0.27659	0.187265	0.999559	0.008061
52	0.140801	0.128105	0.114416	0.100853	0.08766	-0.26707	0.181134	0.999859	0.008666
56	0.135257	0.123759	0.110324	0.096008	0.084341	-0.25756	0.174489	0.999283	0.007795
60	0.132172	0.121563	0.10753	0.094795	0.082474	-0.25233	0.170789	0.998593	0.007208
64	0.129289	0.118376	0.104916	0.092831	0.080645	-0.24567	0.166628	0.999264	0.007995
68	0.127256	0.11656	0.102744	0.091381	0.079126	-0.24288	0.164133	0.998873	0.006211
72	0.125878	0.114575	0.101569	0.090221	0.078067	-0.23995	0.16205	0.999607	0.005839
76	0.122393	0.111708	0.098366	0.087892	0.075878	-0.23369	0.157671	0.998876	0.005261
80	0.120818	0.110164	0.096673	0.08657	0.074498	-0.23247	0.155861	0.998513	0.002478
84	0.119856	0.108765	0.09547	0.085715	0.073522	-0.23144	0.154525	0.998438	0.000654
88	0.118659	0.107756	0.094638	0.084532	0.072522	-0.231	0.15337	0.998859	-0.00176
92	0.118306	0.107163	0.093887	0.084247	0.072038	-0.2309	0.152853	0.998331	-0.00303
96	0.117661	0.106096	0.0931	0.083599	0.071319	-0.23036	0.151945	0.998287	-0.00457
100	0.116131	0.10505	0.091505	0.082534	0.070221	-0.22867	0.150256	0.997266	-0.00615
104	0.114881	0.104056	0.090745	0.081325	0.069257	-0.22796	0.149042	0.998061	-0.00822
108	0.114592	0.10348	0.089146	0.08122	0.068497	-0.2289	0.148611	0.994569	-0.01118
112	0.113876	0.102786	0.089495	0.080062	0.067871	-0.22947	0.148185	0.99809	-0.01345
116	0.113924	0.102354	0.089157	0.079829	0.067445	-0.23097	0.148284	0.997931	-0.01597
120	0.113761	0.102136	0.088437	0.079635	0.066974	-0.23215	0.148226	0.996733	-0.01835
124	0.112871	0.101289	0.087863	0.0788	0.066297	-0.23127	0.147242	0.997383	-0.01947

128	0.112186	0.10129	0.086944	0.078253	0.065633	-0.23228	0.146932	0.99605	-0.02223
132	0.112072	0.100399	0.086833	0.077951	0.065332	-0.23186	0.146482	0.996954	-0.02269
136	0.111545	0.099996	0.086384	0.077528	0.064948	-0.23132	0.145911	0.996919	-0.02329
140	0.111201	0.100169	0.084856	0.07756	0.064388	-0.23247	0.145752	0.991921	-0.02588
144	0.111091	0.099485	0.085799	0.077071	0.064426	-0.23149	0.145447	0.996623	-0.02491
148	0.110538	0.09923	0.085364	0.076661	0.064074	-0.23099	0.144922	0.996513	-0.02545
152	0.10961	0.098789	0.084799	0.075878	0.063472	-0.23037	0.144103	0.996776	-0.02659
156	0.109449	0.096926	0.084505	0.075469	0.062998	-0.22872	0.143049	0.997276	-0.02645
160	0.109211	0.097482	0.084598	0.075247	0.062941	-0.22955	0.143284	0.998098	-0.02735
164	0.108822	0.096378	0.084028	0.074835	0.062438	-0.22862	0.142455	0.997628	-0.02793
168	0.108713	0.094707	0.083381	0.07461	0.061944	-0.22727	0.141488	0.994735	-0.02812

(2). W/C=0.40

Time	*Volumetric Fraction of Aggregate*					k	b	|r|	θ
(hrs.)	*0.05*	*0.1*	*0.15*	*0.2*	*0.25*				(x10 -4)
1	0.435312	0.412577	0.385719	0.352717	0.32962	-0.54249	0.464562	0.998122	0.288648
2	0.439375	0.415081	0.387286	0.354218	0.329839	-0.55987	0.469141	0.998694	0.268977
3	0.401268	0.378904	0.356457	0.323931	0.303271	-0.50193	0.428056	0.997467	0.262082
4	0.380796	0.356646	0.33805	0.303259	0.280539	-0.5078	0.408028	0.995939	0.194933
5	0.356634	0.333045	0.310678	0.278487	0.259724	-0.49676	0.382227	0.99744	0.143213
6	0.324913	0.307792	0.284967	0.256543	0.234261	-0.4651	0.351461	0.996865	0.116102
7	0.286058	0.267723	0.245335	0.228071	0.205977	-0.39962	0.306576	0.999287	0.112649
8	0.256192	0.245093	0.225	0.20232	0.189449	-0.35252	0.276489	0.993853	0.116342
9	0.233441	0.224305	0.201905	0.184331	0.174262	-0.31666	0.251149	0.990725	0.112311
10	0.221974	0.207133	0.196517	0.176714	0.163739	-0.29378	0.237282	0.996503	0.116208
12	0.213921	0.200092	0.1851	0.170536	0.16006	-0.27456	0.227125	0.998293	0.123664
14	0.210125	0.197012	0.181548	0.166587	0.156852	-0.27394	0.223516	0.997463	0.114692
16	0.218688	0.204604	0.19094	0.174755	0.161573	-0.28816	0.233336	0.999584	0.115651
20	0.196933	0.185641	0.175339	0.160495	0.14595	-0.25422	0.211005	0.996826	0.116471
24	0.186827	0.173775	0.160937	0.14864	0.137403	-0.24796	0.198711	0.999572	0.09369
28	0.173178	0.160992	0.149711	0.138256	0.126452	-0.23238	0.184574	0.999928	0.083186
32	0.163253	0.154124	0.14122	0.130676	0.117717	-0.22904	0.175754	0.998519	0.064682
36	0.156808	0.146066	0.135096	0.1236	0.112977	-0.22026	0.167948	0.999931	0.059213
40	0.151753	0.13986	0.12852	0.116671	0.108008	-0.22136	0.162166	0.998556	0.040938
44	0.145237	0.133261	0.123281	0.112659	0.103465	-0.20829	0.154824	0.999043	0.044777
48	0.141828	0.128644	0.118486	0.107893	0.100733	-0.20588	0.150399	0.995121	0.036871
52	0.135197	0.123659	0.113893	0.104306	0.096166	-0.19483	0.143869	0.998107	0.039217
56	0.130127	0.120584	0.111399	0.101377	0.092754	-0.18791	0.139434	0.999802	0.039729
60	0.127358	0.118822	0.10941	0.098997	0.090058	-0.18885	0.137256	0.999506	0.031861
64	0.126217	0.116932	0.107961	0.097269	0.088531	-0.18547	0.134742	0.997536	0.031124
68	0.125402	0.115448	0.106485	0.095732	0.087521	-0.18501	0.133275	0.99499	0.02786
72	0.122617	0.11432	0.105334	0.094567	0.08626	-0.18493	0.13236	0.999049	0.025444
76	0.121203	0.11295	0.104398	0.093029	0.085045	-0.18447	0.130996	0.99835	0.022477
80	0.119585	0.112239	0.10319	0.091281	0.083966	-0.18439	0.129453	0.997668	0.018302
84	0.118359	0.110708	0.102075	0.090855	0.08205	-0.18494	0.12855	0.997966	0.014746
88	0.118006	0.109564	0.100519	0.090153	0.08135	-0.18469	0.127971	0.997886	0.013595
92	0.118136	0.108795	0.100095	0.088985	0.081322	-0.18687	0.127498	0.998866	0.008177
96	0.117292	0.107933	0.099528	0.088361	0.080376	-0.18681	0.12672	0.998953	0.006116
100	0.116145	0.10674	0.098854	0.088188	0.078791	-0.18652	0.125721	0.999111	0.003854
104	0.115627	0.108624	0.098069	0.087478	0.078542	-0.19063	0.126263	0.997891	-0.00231
108	0.114711	0.107346	0.097227	0.085558	0.078207	-0.18959	0.125049	0.996965	-0.00378
112	0.114428	0.106255	0.096544	0.085481	0.077589	-0.1889	0.12396	0.997654	-0.00554
116	0.113088	0.105846	0.095413	0.085587	0.07618	-0.18815	0.123188	0.998111	-0.00629
120	0.112797	0.105305	0.094324	0.085066	0.076057	-0.18744	0.12244	0.996252	-0.00707

124	0.112185	0.104827	0.094254	0.08368	0.075531	-0.18891	0.122654	0.997373	-0.00922
128	0.111849	0.104656	0.094054	0.083986	0.075022	-0.18865	0.122479	0.997391	-0.00922
132	0.111086	0.103242	0.093988	0.08227	0.074517	-0.18822	0.121254	0.997715	-0.01186
136	0.11034	0.103041	0.093415	0.082249	0.074104	-0.18653	0.120755	0.996917	-0.01009
140	0.109977	0.103556	0.092474	0.082048	0.073871	-0.18744	0.120502	0.996853	-0.01251
144	0.10926	0.102409	0.092554	0.080657	0.07371	-0.1857	0.119573	0.995849	-0.01186
148	0.10851	0.101498	0.092541	0.08035	0.072519	-0.18626	0.119022	0.996103	-0.01445
152	0.108242	0.101544	0.091644	0.079979	0.072319	-0.18683	0.11877	0.996333	-0.01622
156	0.10806	0.099759	0.090815	0.079254	0.072118	-0.18478	0.117854	0.996957	-0.01495
160	0.107283	0.099173	0.090527	0.079187	0.07125	-0.18411	0.117249	0.997111	-0.0154
164	0.106753	0.098691	0.089792	0.078406	0.070984	-0.18364	0.116097	0.998278	-0.01776
168	0.106	0.098549	0.089795	0.078166	0.070806	-0.18154	0.115526	0.998031	-0.01543

VIII. QUARTZ SAND - CEMENT BLENDED WITH SILICA FUME SYSTEMS

Cement : White portland cement .
Units : (i). Electrical conductivity: ohm-1 m-1; (ii). Excess interfacial conductance: ohm-1
Temperature : 20°C ; W/C=0.50
Aggregate size : r=0.561 mm.
Amount of SF : Equivalent to that resulting in 14 um thick SF layer on aggregate surfaces .

Time	*Volumetric Fraction of Aggregate*					k	b	|r|	θ
(hrs.)	*0.2*	*0.25*	*0.3*	*0.35*	*0.4*				(x10 -4)
0.25	0.309335	0.279235	0.25589	0.228671	0.202421	-0.52878	0.413745	0.999362	0.171732
1	0.352386	0.321545	0.293026	0.26438	0.235765	-0.58082	0.467665	0.999867	0.225675
2	0.346721	0.31605	0.293054	0.263861	0.236218	-0.54639	0.455098	0.999203	0.254799
3	0.345698	0.315114	0.290303	0.262439	0.235339	-0.54679	0.453814	0.99955	0.250459
4	0.335023	0.307452	0.284972	0.257475	0.231233	-0.51511	0.437765	0.999509	0.26467
5	0.325669	0.298435	0.278155	0.249643	0.22319	-0.5075	0.427269	0.998685	0.249462
6	0.320052	0.286424	0.267201	0.240193	0.215131	-0.51215	0.419445	0.99685	0.218824
7	0.306831	0.269797	0.253705	0.230483	0.209043	-0.46978	0.394907	0.990044	0.229218
8	0.280405	0.256465	0.239206	0.21378	0.190396	-0.44541	0.369672	0.998314	0.204021
9	0.273114	0.235725	0.218808	0.202957	0.186839	-0.41064	0.346679	0.976017	0.204547
10	0.250477	0.219332	0.201	0.187861	0.173424	-0.37115	0.317764	0.979662	0.197276
12	0.221263	0.191663	0.174088	0.167616	0.158369	-0.29967	0.272501	0.949169	0.20398
14	0.206331	0.182533	0.16597	0.158931	0.149511	-0.27448	0.255	0.966345	0.201993
16	0.203342	0.187071	0.170582	0.15949	0.147048	-0.28034	0.257607	0.995813	0.19836
20	0.195017	0.174107	0.164824	0.152196	0.140405	-0.26227	0.24399	0.989297	0.193953
24	0.179711	0.16367	0.153482	0.141988	0.130821	-0.23892	0.225612	0.996317	0.186053
28	0.168263	0.15616	0.145592	0.133357	0.121539	-0.2325	0.214733	0.999742	0.167546
32	0.160782	0.148657	0.139631	0.126916	0.115123	-0.22612	0.206058	0.998669	0.155146
36	0.155071	0.143468	0.13267	0.120989	0.109529	-0.22713	0.200484	0.999924	0.137628
40	0.149251	0.139211	0.127452	0.116808	0.105885	-0.21827	0.193203	0.999764	0.133767
44	0.145314	0.134578	0.123433	0.113031	0.102444	-0.21457	0.188132	0.999929	0.126458
48	0.139331	0.130507	0.118201	0.108568	0.098268	-0.20813	0.181414	0.998901	0.119663
52	0.13652	0.126676	0.116476	0.106088	0.095747	-0.20427	0.177582	0.999937	0.116137
56	0.132395	0.123198	0.112771	0.102989	0.093045	-0.19782	0.172225	0.999843	0.113172
60	0.130069	0.120143	0.110336	0.100777	0.091157	-0.19438	0.16881	0.999964	0.110025
64	0.12757	0.11808	0.10844	0.099026	0.089555	-0.19017	0.165584	0.999992	0.108854
68	0.125361	0.116394	0.105932	0.09683	0.087388	-0.19102	0.163687	0.999723	0.101935
72	0.12289	0.114699	0.105547	0.095633	0.08591	-0.18605	0.160752	0.999217	0.102989
76	0.120349	0.112175	0.103512	0.093891	0.084509	-0.17993	0.156866	0.999362	0.103542
80	0.119992	0.111029	0.102204	0.092582	0.083159	-0.18423	0.157062	0.999822	0.096051
84	0.118074	0.109054	0.100779	0.091366	0.082238	-0.17872	0.153918	0.999779	0.097534
88	0.117717	0.10869	0.100115	0.09066	0.081425	-0.18123	0.15409	0.999854	0.093326
92	0.115854	0.107375	0.098893	0.089577	0.080469	-0.17714	0.151575	0.999733	0.093921
96	0.115309	0.106497	0.098379	0.089	0.079936	-0.17649	0.15077	0.999695	0.092879
100	0.113592	0.104911	0.097094	0.08789	0.079032	-0.17228	0.148189	0.999638	0.093502
104	0.113447	0.104837	0.09727	0.087674	0.078586	-0.17377	0.148494	0.999157	0.091574
108	0.112374	0.102594	0.095928	0.086359	0.077516	-0.1719	0.146525	0.998475	0.089543
112	0.113016	0.102196	0.095276	0.085828	0.077013	-0.17675	0.147691	0.998148	0.08375
116	0.11031	0.101861	0.094943	0.085031	0.075868	-0.17143	0.145031	0.998112	0.08624
120	0.110247	0.101533	0.095401	0.084719	0.075175	-0.17391	0.145589	0.996012	0.083159
124	0.109406	0.100333	0.093875	0.083542	0.074178	-0.17449	0.144614	0.997364	0.079344
128	0.109063	0.099093	0.093783	0.083293	0.074099	-0.17145	0.143303	0.995461	0.081344
132	0.108478	0.09797	0.0923	0.08217	0.073156	-0.17289	0.142681	0.996425	0.076919
136	0.107328	0.096765	0.090953	0.08081	0.07175	-0.17422	0.141787	0.99665	0.071923

140	0.107619	0.097098	0.090386	0.080109	0.070723	-0.18156	0.143656	0.997947	0.063433
144	0.106106	0.096918	0.09078	0.079718	0.069888	-0.17927	0.142464	0.995805	0.064372
148	0.105478	0.095938	0.089986	0.079055	0.069038	-0.17821	0.141427	0.995951	0.063457
152	0.105507	0.094642	0.089252	0.0782	0.068563	-0.18066	0.14143	0.995049	0.058882
156	0.10573	0.093885	0.087952	0.077314	0.067852	-0.18465	0.141943	0.995914	0.052845
160	0.10372	0.0929	0.087623	0.076617	0.067044	-0.17927	0.139361	0.994854	0.055678

IX. OPAL - HIGH ALKALI PORTLAND CEMENT SYSTEMS

Cement : High alkali portland cement .
Units : (i). Electrical conductivity: ohm-1 m-1; (ii). Excess interfacial conductance: ohm-1
Temperature : 20°C ; W/C=0.50
Aggregate size : r=0.199 mm.

Time	*Volumetric Fraction of Aggregate*					k	b	|r|	θ
(hrs.)	*0.188*	*0.247*	*0.304*	*0.36*	*0.414*				(x10 -4)
1	0.696684	0.567306	0.438531	0.346732	0.250199	-1.97279	1.056858	0.997725	-0.25705
2	0.720634	0.5998	0.452859	0.347437	0.258102	-2.08586	1.106948	0.997174	-0.28221
3	0.772523	0.632308	0.476221	0.365957	0.270259	-2.25197	1.184898	0.996639	-0.31483
4	0.767319	0.62429	0.476135	0.381713	0.281072	-2.15328	1.15769	0.99611	-0.27644
5	0.732553	0.590852	0.453302	0.355939	0.274548	-2.04038	1.098858	0.994624	-0.26009
6	0.686787	0.569764	0.430518	0.342252	0.260903	-1.91261	1.036802	0.995631	-0.23708
7	0.656745	0.54681	0.422708	0.328709	0.252323	-1.81945	0.992024	0.997273	-0.21984
8	0.630539	0.514379	0.397098	0.317162	0.241053	-1.73012	0.943581	0.995966	-0.20878
9	0.609357	0.500907	0.378599	0.305639	0.233318	-1.67915	0.913676	0.994652	-0.20473
10	0.58899	0.471176	0.361622	0.290236	0.222115	-1.62181	0.877586	0.993558	-0.2026
12	0.529478	0.424943	0.320703	0.260814	0.200209	-1.45882	0.78867	0.992109	-0.18296
14	0.469301	0.390785	0.293976	0.239459	0.181555	-1.28801	0.704768	0.994988	-0.15314
16	0.419394	0.351354	0.261684	0.216954	0.165229	-1.13907	0.627605	0.99364	-0.13111
20	0.343562	0.287904	0.214131	0.177367	0.138161	-0.92411	0.51186	0.992522	-0.10369
24	0.286438	0.239863	0.179478	0.148076	0.114595	-0.77183	0.427246	0.993476	-0.08687
28	0.254512	0.210527	0.161105	0.131662	0.102875	-0.67737	0.377108	0.994393	-0.0741
32	0.230607	0.19211	0.147724	0.119254	0.092021	-0.62026	0.344035	0.996081	-0.06913
36	0.213741	0.175384	0.135512	0.110639	0.084829	-0.57172	0.317024	0.995348	-0.0638
40	0.200831	0.162689	0.125922	0.103337	0.078979	-0.53724	0.29692	0.994326	-0.06093
44	0.186738	0.153634	0.118074	0.096907	0.074544	-0.49827	0.276755	0.99486	-0.05515
48	0.176626	0.146498	0.110765	0.090808	0.070106	-0.47632	0.263094	0.994141	-0.05418
52	0.16957	0.141148	0.105848	0.086916	0.067867	-0.4567	0.252467	0.993101	-0.05174
56	0.162866	0.132578	0.102193	0.083287	0.064863	-0.43488	0.240753	0.993928	-0.04892
60	0.157953	0.127545	0.099734	0.081295	0.063356	-0.41743	0.232291	0.993996	-0.04577
64	0.153268	0.123426	0.096537	0.079073	0.061749	-0.40319	0.224815	0.993407	-0.04376
68	0.146504	0.120867	0.093477	0.077652	0.060601	-0.38115	0.215156	0.994295	-0.03875
72	0.141488	0.112955	0.089693	0.073905	0.058352	-0.36412	0.20546	0.992308	-0.0371
76	0.134973	0.110156	0.085946	0.071496	0.057041	-0.34493	0.196293	0.992656	-0.03349
80	0.130028	0.105042	0.084803	0.069555	0.055213	-0.32819	0.18824	0.994443	-0.0304
84	0.12542	0.101824	0.081542	0.068349	0.054742	-0.31001	0.180184	0.993003	-0.02636
88	0.121857	0.098881	0.078718	0.066105	0.052715	-0.30332	0.175441	0.992756	-0.02664
92	0.116881	0.097152	0.076302	0.064371	0.052177	-0.28756	0.168391	0.993129	-0.0232
96	0.112496	0.09405	0.073596	0.062654	0.050346	-0.27601	0.162149	0.993348	-0.02175
100	0.110097	0.089146	0.072031	0.060776	0.049056	-0.26681	0.156956	0.992247	-0.02081
104	0.106653	0.086958	0.070939	0.059212	0.048267	-0.25625	0.151946	0.993654	-0.01879
108	0.104168	0.084828	0.069308	0.05801	0.047369	-0.24898	0.148079	0.993309	-0.01782
112	0.101334	0.083238	0.067967	0.056545	0.047073	-0.23977	0.143786	0.993369	-0.01598
116	0.100479	0.081522	0.06673	0.056049	0.045893	-0.23878	0.142388	0.99251	-0.01671
120	0.096065	0.081112	0.06533	0.055356	0.04484	-0.2272	0.137292	0.996022	-0.0141
124	0.094275	0.078595	0.063652	0.054036	0.044274	-0.22082	0.133785	0.994533	-0.01336
128	0.092222	0.076844	0.062738	0.05327	0.043714	-0.21377	0.130444	0.99487	-0.01201
132	0.090935	0.075439	0.061877	0.052515	0.043144	-0.21009	0.128354	0.994602	-0.01165
136	0.088795	0.074014	0.06077	0.051539	0.042663	-0.20341	0.125107	0.994766	-0.01044
140	0.087115	0.073097	0.059927	0.050916	0.042258	-0.19835	0.122683	0.995121	-0.0095
144	0.084568	0.073762	0.057931	0.050382	0.041385	-0.19446	0.120449	0.99347	-0.00914

148	0.083598	0.070848	0.057454	0.049358	0.041163	-0.18854	0.117537	0.994383	-0.00812
152	0.082269	0.07022	0.057024	0.048754	0.040529	-0.18599	0.116041	0.995552	-0.00792
156	0.081229	0.068575	0.056502	0.048311	0.040062	-0.18185	0.113962	0.995749	-0.00723
160	0.079978	0.067827	0.055763	0.047847	0.039805	-0.17782	0.112051	0.995657	-0.00646
164	0.078064	0.067709	0.054386	0.047259	0.039047	-0.1745	0.110098	0.995089	-0.00621
168	0.076985	0.066928	0.053638	0.04659	0.038626	-0.17198	0.108593	0.99482	-0.00603
172	0.075589	0.065643	0.052698	0.045921	0.038104	-0.16779	0.106365	0.994685	-0.00547
176	0.076106	0.064086	0.052912	0.045447	0.03785	-0.16867	0.106319	0.99509	-0.00609
180	0.074837	0.063072	0.052538	0.045086	0.037724	-0.16345	0.104112	0.995466	-0.00483
184	0.072712	0.062316	0.051792	0.044546	0.037217	-0.15728	0.101309	0.996892	-0.00353
188	0.071411	0.062612	0.050668	0.044229	0.036822	-0.15512	0.100089	0.995492	-0.00331
192	0.070632	0.062138	0.050097	0.043799	0.036518	-0.15336	0.099044	0.995067	-0.00318
196	0.069765	0.061361	0.049421	0.043419	0.03618	-0.15079	0.097659	0.994703	-0.00285
200	0.069343	0.060064	0.049776	0.043026	0.036224	-0.14755	0.096336	0.996794	-0.00202
204	0.068877	0.059569	0.049676	0.042824	0.036032	-0.14605	0.095591	0.997289	-0.00177
208	0.068224	0.059258	0.049298	0.042738	0.03582	-0.14408	0.094666	0.997328	-0.00138
212	0.067317	0.059489	0.048353	0.04246	0.03556	-0.14267	0.093809	0.995444	-0.0013
216	0.067108	0.058077	0.047265	0.042256	0.035693	-0.13942	0.092268	0.992539	-0.00067
220	0.066557	0.058314	0.04692	0.04184	0.035864	-0.13795	0.091646	0.991158	-0.00032
224	0.067217	0.057548	0.046809	0.041581	0.035674	-0.14019	0.092187	0.990659	-0.00127
228	0.06579	0.056922	0.04669	0.041316	0.035482	-0.13513	0.09013	0.992837	4.43E-05
232	0.065369	0.056743	0.046218	0.041245	0.035232	-0.13433	0.089609	0.99213	5.67E-05
236	0.064161	0.056965	0.046092	0.040885	0.034598	-0.13324	0.088859	0.99381	3.1E-05
240	0.06397	0.055102	0.044565	0.040724	0.034619	-0.12959	0.087011	0.988293	0.000612
244	0.063384	0.055873	0.045401	0.04045	0.034398	-0.13006	0.087257	0.993376	0.000547
248	0.063277	0.055193	0.0449	0.040211	0.034634	-0.12812	0.086413	0.991278	0.000993
252	0.062937	0.055491	0.044811	0.040129	0.034587	-0.12774	0.086244	0.99108	0.001081
256	0.062796	0.054822	0.044572	0.040067	0.034522	-0.12642	0.08561	0.990862	0.001325
260	0.062184	0.055564	0.044575	0.04012	0.034055	-0.12704	0.085743	0.991503	0.001042
264	0.061629	0.055286	0.044339	0.039812	0.033679	-0.12644	0.08521	0.991929	0.000911
268	0.061307	0.055042	0.044017	0.039399	0.033253	-0.1271	0.085065	0.991989	0.000328
272	0.061052	0.054135	0.044043	0.039165	0.033523	-0.12408	0.083931	0.993394	0.001203
276	0.061009	0.05392	0.043998	0.039168	0.033245	-0.12453	0.08395	0.994129	0.000927
280	0.060478	0.05337	0.043751	0.03889	0.033045	-0.12287	0.083088	0.994591	0.001168
284	0.060116	0.053141	0.043592	0.038791	0.032878	-0.12194	0.082603	0.994802	0.001303
288	0.059611	0.053592	0.043308	0.038574	0.03243	-0.12288	0.082686	0.993765	0.000763
292	0.059702	0.052997	0.043259	0.038345	0.032504	-0.12232	0.082376	0.994683	0.000823
296	0.059793	0.052542	0.043107	0.038183	0.03231	-0.12283	0.082356	0.995005	0.000465
300	0.059008	0.052536	0.04291	0.038093	0.032107	-0.12088	0.08151	0.99502	0.000917
304	0.05869	0.052149	0.042873	0.038057	0.032223	-0.11873	0.080726	0.995404	0.001565
308	0.0585	0.052089	0.042569	0.037765	0.031939	-0.11947	0.080725	0.994935	0.001071
312	0.058124	0.05272	0.042543	0.037745	0.031581	-0.12051	0.081008	0.99379	0.000666
316	0.057743	0.051837	0.04237	0.037419	0.031526	-0.11839	0.080004	0.9954	0.001072
320	0.057959	0.051439	0.042268	0.037346	0.031559	-0.11849	0.079971	0.995728	0.00097
324	0.057703	0.051346	0.042196	0.037246	0.031448	-0.11798	0.079689	0.995879	0.00103
328	0.057211	0.051033	0.042005	0.037167	0.031308	-0.11631	0.07894	0.996017	0.001393
332	0.057162	0.051932	0.042116	0.037292	0.031243	-0.1177	0.079564	0.994281	0.001094
336	0.057341	0.051941	0.042063	0.037284	0.031201	-0.11852	0.07983	0.994267	0.000813
340	0.057544	0.050361	0.041643	0.037645	0.031225	-0.11578	0.078719	0.994785	0.001524
344	0.057264	0.049966	0.041408	0.036878	0.030132	-0.11929	0.079227	0.996593	-0.0003
348	0.056972	0.05011	0.041895	0.036635	0.029747	-0.12025	0.07946	0.998512	-0.0007
352	0.056716	0.049998	0.041264	0.036535	0.02946	-0.12035	0.079212	0.997243	-0.00101
356	0.05673	0.051114	0.041751	0.03692	0.029692	-0.12082	0.0798	0.996168	-0.00074
360	0.057314	0.051372	0.041661	0.036862	0.029736	-0.12332	0.080705	0.995863	-0.0015
364	0.056343	0.051264	0.041659	0.036729	0.029729	-0.11991	0.079429	0.995283	-0.00051

368	0.056191	0.050412	0.041572	0.036356	0.029606	-0.11898	0.078832	0.997434	-0.00049
372	0.055961	0.050075	0.041359	0.036247	0.029403	-0.11848	0.078463	0.997565	-0.00052
376	0.055788	0.049933	0.041267	0.036153	0.029292	-0.11817	0.078246	0.997611	-0.00053
380	0.055976	0.050947	0.041586	0.036563	0.029683	-0.1185	0.07881	0.995675	-0.00019
384	0.056093	0.05109	0.041883	0.036579	0.029666	-0.11919	0.079128	0.996139	-0.00033
388	0.055997	0.051007	0.041486	0.036327	0.029515	-0.1197	0.079087	0.995516	-0.00071
392	0.055555	0.050103	0.041192	0.035896	0.029383	-0.11778	0.078066	0.997066	-0.00045
396	0.055411	0.049639	0.041104	0.03588	0.029212	-0.11709	0.077679	0.997808	-0.00038
400	0.054975	0.049419	0.040919	0.035719	0.029066	-0.11595	0.077106	0.997648	-0.00019
404	0.055451	0.05061	0.041434	0.036118	0.029443	-0.11767	0.078219	0.995915	-0.00023
408	0.054837	0.050769	0.041383	0.036143	0.029465	-0.11563	0.077508	0.99393	0.000422
412	0.0552	0.049948	0.041281	0.036268	0.029673	-0.11455	0.077138	0.996928	0.000765
416	0.055391	0.049481	0.041661	0.035926	0.029884	-0.11429	0.077053	0.998918	0.000855
420	0.055257	0.049677	0.041638	0.03578	0.029761	-0.11484	0.077173	0.998494	0.00061
424	0.055295	0.049822	0.041489	0.036218	0.029558	-0.11516	0.077323	0.997826	0.000548
428	0.055053	0.051144	0.041444	0.036188	0.030012	-0.11506	0.077586	0.992882	0.000873
432	0.054778	0.051028	0.041316	0.035986	0.029368	-0.11649	0.077746	0.992638	8.4E-05
436	0.054422	0.050582	0.041155	0.035939	0.029372	-0.11451	0.076946	0.993247	0.0006
440	0.054361	0.049973	0.041052	0.035562	0.029263	-0.1143	0.076628	0.995487	0.000429
444	0.054065	0.049399	0.041661	0.035808	0.029175	-0.11207	0.075935	0.997301	0.001213
448	0.054055	0.04989	0.041088	0.035884	0.029154	-0.11285	0.076164	0.994928	0.000923
452	0.054293	0.049336	0.041363	0.035497	0.029241	-0.11312	0.076176	0.997824	0.000759
456	0.054957	0.050405	0.041239	0.035806	0.029154	-0.11712	0.077754	0.995476	-0.00033
460	0.05414	0.050365	0.041129	0.035685	0.029141	-0.11439	0.076705	0.993485	0.000446
464	0.053659	0.049289	0.040838	0.035541	0.02892	-0.11183	0.075489	0.995928	0.000931
468	0.053559	0.049096	0.041382	0.035117	0.029317	-0.11049	0.075128	0.997056	0.001462
472	0.053455	0.048925	0.040836	0.035287	0.028663	-0.11182	0.075269	0.996735	0.00072
476	0.053587	0.048935	0.040801	0.03511	0.028769	-0.11226	0.07541	0.99708	0.000568
480	0.054072	0.050103	0.040961	0.035332	0.028754	-0.11568	0.076849	0.994227	-0.00027
484	0.053562	0.049177	0.041097	0.034805	0.028709	-0.11334	0.075766	0.996521	0.000206
488	0.053372	0.049082	0.040786	0.035384	0.028699	-0.1115	0.075204	0.995916	0.000868
492	0.053416	0.048958	0.04076	0.034838	0.028666	-0.11253	0.07538	0.996649	0.000357
496	0.053905	0.049815	0.041102	0.03553	0.02884	-0.11392	0.07631	0.995023	0.000363
500	0.053983	0.050127	0.041109	0.035341	0.028769	-0.11533	0.076764	0.994104	-0.00012
504	0.053636	0.049868	0.040985	0.035102	0.028971	-0.11336	0.076016	0.99406	0.00044
508	0.05349	0.049734	0.040725	0.034955	0.028765	-0.1136	0.075908	0.993847	0.000176
512	0.052521	0.048654	0.040453	0.034513	0.028531	-0.10986	0.074179	0.995167	0.000933
516	0.052228	0.048293	0.040359	0.034255	0.028339	-0.1093	0.073767	0.995621	0.000895
520	0.052976	0.049443	0.040656	0.035154	0.028538	-0.11168	0.075148	0.993296	0.00069
524	0.052976	0.049324	0.040406	0.034738	0.028382	-0.11278	0.075292	0.993641	0.000106
528	0.052745	0.049135	0.040189	0.034391	0.028124	-0.11316	0.075158	0.993499	-0.00028
532	0.052702	0.04908	0.040167	0.03437	0.028136	-0.1129	0.075055	0.993574	-0.00021
536	0.052073	0.047901	0.039982	0.03401	0.028419	-0.10826	0.073236	0.996263	0.001058
540	0.051936	0.04781	0.039927	0.034	0.028002	-0.10909	0.073344	0.996201	0.000617
544	0.053011	0.049291	0.040722	0.035048	0.02837	-0.11232	0.075275	0.994111	0.000396
548	0.05259	0.04893	0.040174	0.034361	0.027976	-0.11281	0.074943	0.993867	-0.00026
552	0.05266	0.048871	0.039958	0.034166	0.027958	-0.11338	0.075032	0.99408	-0.00055
556	0.052585	0.048814	0.040021	0.034188	0.027998	-0.11283	0.074864	0.994187	-0.00036
560	0.051464	0.047641	0.039706	0.033637	0.027763	-0.10859	0.072902	0.995282	0.000505
564	0.051627	0.047504	0.039734	0.033612	0.027713	-0.10916	0.073068	0.996243	0.000296
568	0.052835	0.049156	0.040666	0.034835	0.028262	-0.11221	0.075106	0.994114	0.000297
572	0.052549	0.048645	0.040159	0.034246	0.028244	-0.11144	0.07449	0.994947	0.000196
576	0.053231	0.049072	0.040421	0.034369	0.028013	-0.1152	0.075882	0.995408	-0.00092
580	0.052355	0.048774	0.040027	0.034442	0.027751	-0.11234	0.074665	0.993474	-0.00023
584	0.051905	0.047937	0.040039	0.033779	0.027759	-0.11043	0.0737	0.995606	7.93E-05

588	0.051894	0.047895	0.040094	0.033752	0.027766	-0.11035	0.073671	0.995729	0.000106
592	0.052826	0.049115	0.040641	0.034743	0.028042	-0.11304	0.075281	0.994141	-8.2E-05
596	0.052677	0.048873	0.040193	0.034155	0.027792	-0.11404	0.075246	0.994382	-0.00078
600	0.05247	0.048748	0.040045	0.033958	0.027702	-0.11375	0.075004	0.994118	-0.00082
604	0.052323	0.048657	0.03991	0.033814	0.027631	-0.11358	0.074835	0.993901	-0.00088
608	0.05121	0.047343	0.03964	0.033337	0.027368	-0.10908	0.072787	0.995437	6.7E-05
612	0.051474	0.047448	0.039723	0.033412	0.027408	-0.10993	0.073159	0.995874	-0.00013
616	0.051518	0.047428	0.039735	0.033384	0.027358	-0.11028	0.073255	0.996043	-0.00026
620	0.051481	0.0474	0.039792	0.033466	0.027396	-0.10981	0.073137	0.996072	-7.3E-05
624	0.052227	0.048469	0.039889	0.033824	0.027459	-0.11349	0.074716	0.99434	-0.00094
628	0.052241	0.047552	0.039692	0.033332	0.027445	-0.11288	0.074211	0.997361	-0.00104
632	0.051525	0.047391	0.039662	0.03336	0.027389	-0.11018	0.073207	0.996189	-0.00025
636	0.051301	0.047276	0.039507	0.033251	0.027293	-0.10971	0.072924	0.995891	-0.00021
640	0.051278	0.047246	0.039558	0.033206	0.027143	-0.11018	0.073027	0.995867	-0.00042
644	0.051082	0.047175	0.039438	0.033183	0.027143	-0.1094	0.072709	0.995538	-0.00022
648	0.052133	0.048407	0.039962	0.033711	0.027389	-0.11349	0.074661	0.994319	-0.00099
652	0.051209	0.047345	0.039364	0.033065	0.027091	-0.11055	0.073066	0.995217	-0.00063
656	0.051379	0.047334	0.0395	0.033116	0.027182	-0.11072	0.073207	0.995824	-0.00061
660	0.051102	0.047131	0.039346	0.032999	0.027047	-0.11006	0.07283	0.995667	-0.00054
664	0.052181	0.048413	0.040099	0.034071	0.027381	-0.11305	0.074637	0.994427	-0.00072
668	0.052048	0.048207	0.039734	0.03353	0.027186	-0.11388	0.074601	0.994663	-0.00131
672	0.051788	0.048245	0.039572	0.033352	0.027042	-0.11384	0.074448	0.993522	-0.00144

X. SPRATT AGGREGATE- HIGH ALKALI PORTLAND CEMENT SYSTEMS

Cement : High alkali portland cement .
Units : (i). Electrical conductivity: ohm-1 m-1; (ii). Excess interfacial conductance: ohm-1
Temperature : 20°C ; W/C=0.50
Aggregate size : r=0.136 mm.

Time	*Volumetric Fraction of Aggregate*					k	b	|r|	θ
(hrs.)	*0.2*	*0.25*	*0.3*	*0.35*	*0.4*				(x10 -4)
0.25	0.946234	0.862776	0.778045	0.694769	0.61113	-1.67643	1.281519	0.999993	0.111452
1	0.995447	0.896159	0.810434	0.709208	0.611857	-1.90826	1.3771	0.999382	0.071349
2	1.060926	0.951797	0.848065	0.738166	0.629808	-2.15174	1.491273	0.999923	0.038612
3	0.980737	0.890858	0.758594	0.67477	0.578835	-2.03978	1.388694	0.994755	0.01961
4	0.957094	0.868191	0.751925	0.666931	0.574119	-1.93442	1.343978	0.997559	0.036968
5	0.928049	0.838252	0.743011	0.653991	0.563416	-1.82706	1.293461	0.999891	0.051288
6	0.894179	0.809431	0.71999	0.635913	0.550495	-1.72177	1.238534	0.999909	0.061666
7	0.840114	0.755177	0.690167	0.602384	0.520294	-1.58487	1.157088	0.99807	0.068346
8	0.805674	0.725832	0.648306	0.568133	0.488621	-1.58361	1.122396	0.999974	0.045326
9	0.770458	0.694877	0.611165	0.536745	0.460002	-1.55808	1.082075	0.999667	0.029479
10	0.725689	0.651491	0.582339	0.507421	0.433945	-1.45512	1.016712	0.999853	0.031711
12	0.65243	0.583584	0.51416	0.445396	0.376467	-1.38023	0.928475	0.999998	0.005661
14	0.581826	0.520512	0.451979	0.391695	0.329349	-1.26754	0.835335	0.999603	-0.00659
16	0.517747	0.465488	0.396647	0.346757	0.292129	-1.13993	0.745733	0.997419	-0.00967
20	0.4179	0.379539	0.315031	0.280406	0.23831	-0.91663	0.601225	0.990182	-0.0067
24	0.362383	0.329687	0.273407	0.244081	0.208016	-0.78868	0.520119	0.989227	-0.00385
28	0.323924	0.295164	0.23742	0.212801	0.1799	-0.74082	0.472089	0.981767	-0.01482
32	0.298552	0.270215	0.218353	0.193377	0.161679	-0.70117	0.438787	0.986495	-0.01949
36	0.284866	0.253473	0.212549	0.182518	0.149764	-0.68232	0.42133	0.997619	-0.02281
40	0.274242	0.239374	0.211622	0.175738	0.141886	-0.6567	0.405581	0.998565	-0.02191
44	0.263115	0.230283	0.198918	0.165877	0.133254	-0.64826	0.392767	0.999937	-0.0268
48	0.253005	0.220761	0.190297	0.157799	0.125809	-0.63471	0.379948	0.999904	-0.02937
52	0.249608	0.216655	0.186005	0.152722	0.120098	-0.6459	0.378789	0.999844	-0.03523
56	0.248798	0.214054	0.186327	0.150581	0.11684	-0.65478	0.379753	0.998597	-0.0386
60	0.243347	0.209246	0.182035	0.146951	0.113835	-0.64264	0.371874	0.998596	-0.03845
64	0.238478	0.204792	0.17695	0.142429	0.109578	-0.64033	0.366543	0.998982	-0.04103
68	0.23364	0.200512	0.172207	0.13839	0.105951	-0.635	0.36064	0.999294	-0.04263
72	0.226445	0.195402	0.162241	0.1315	0.100155	-0.63296	0.353037	0.999863	-0.04688
76	0.219671	0.188504	0.157301	0.126139	0.094967	-0.62355	0.34438	1	-0.0485
80	0.214142	0.183948	0.153189	0.123075	0.0928	-0.60711	0.335564	0.999989	-0.04704
84	0.211049	0.18086	0.151769	0.121423	0.091391	-0.59751	0.330551	0.999959	-0.0461
88	0.207062	0.177139	0.14876	0.118617	0.088914	-0.58964	0.32499	0.999916	-0.04631
92	0.204565	0.174726	0.146937	0.116806	0.087261	-0.58506	0.321576	0.99985	-0.04655
96	0.201034	0.172302	0.141306	0.112898	0.083842	-0.58758	0.318549	0.999818	-0.04975
100	0.195564	0.167845	0.13684	0.10959	0.081401	-0.57316	0.310197	0.999598	-0.0489
104	0.194002	0.165635	0.138	0.109528	0.081266	-0.56315	0.306632	0.999979	-0.04679
108	0.190868	0.163258	0.136508	0.108031	0.08013	-0.55225	0.301318	0.999837	-0.04546
112	0.187452	0.159939	0.133743	0.106042	0.078717	-0.54274	0.295999	0.999928	-0.04476
116	0.182183	0.155958	0.128519	0.102466	0.076067	-0.53145	0.288473	0.999936	-0.04476
120	0.177622	0.151576	0.127448	0.101128	0.075355	-0.50997	0.279615	0.999827	-0.04105
124	0.168886	0.145394	0.12055	0.097252	0.073567	-0.47756	0.264397	0.999902	-0.0367
128	0.165667	0.142726	0.11959	0.096677	0.073708	-0.45993	0.257654	0.999998	-0.0333
132	0.163757	0.141495	0.117604	0.095576	0.073081	-0.45454	0.254665	0.999843	-0.03289
136	0.16155	0.140741	0.113974	0.094016	0.072356	-0.45023	0.251596	0.997862	-0.03302
140	0.157298	0.136997	0.110497	0.091082	0.069896	-0.44144	0.245585	0.997594	-0.03312

144	0.154978	0.134852	0.109527	0.090143	0.069274	-0.43224	0.241425	0.998234	-0.03178
148	0.150345	0.130996	0.106855	0.08819	0.068156	-0.41437	0.233218	0.998366	-0.02926
152	0.147074	0.128276	0.10584	0.087563	0.068246	-0.39674	0.226421	0.998971	-0.02589
156	0.144158	0.125689	0.104836	0.086708	0.067899	-0.383	0.220758	0.999526	-0.02351
160	0.140973	0.123112	0.102926	0.085397	0.067203	-0.37051	0.215075	0.999518	-0.02171
164	0.139739	0.121762	0.10189	0.084184	0.065936	-0.37037	0.213813	0.99968	-0.02251
168	0.138077	0.121443	0.100894	0.084818	0.067625	-0.35506	0.209089	0.998515	-0.01878

XI. OBSIDIAN - HIGH ALKALI PORTLAND CEMENT SYSTEMS

Cement : High alkali portland cement .
Units : (i). Electrical conductivity: ohm-1 m-1; (ii). Excess interfacial conductance: ohm-1
Temperature : 20°C ; W/C=0.50
Aggregate size : r=0.21 mm.

Time	*Volumetric Fraction of Aggregate*					k	b	|r|	θ
(hrs.)	*0.2*	*0.25*	*0.3*	*0.35*	*0.4*				(x10 -4)
1	0.970014	0.888802	0.807745	0.726845	0.64532	-1.62269	1.294553	0.999999	0.223397
2	1.042343	0.950093	0.858512	0.767599	0.674012	-1.83831	1.410006	0.99998	0.193686
3	1.058817	0.959437	0.87559	0.807276	0.67683	-1.83227	1.425271	0.989391	0.213947
4	1.043523	0.950895	0.858727	0.767017	0.67347	-1.84797	1.413117	0.999991	0.190195
5	0.994658	0.907401	0.818915	0.729201	0.644401	-1.75743	1.346144	0.999927	0.18325
6	0.955815	0.87309	0.788371	0.701657	0.622921	-1.67444	1.290703	0.999787	0.18313
7	0.937934	0.85946	0.77352	0.680114	0.616571	-1.64414	1.266762	0.996921	0.179201
8	0.897961	0.821983	0.740519	0.653569	0.588561	-1.57443	1.212847	0.998184	0.171391
9	0.864402	0.788158	0.713697	0.641018	0.561209	-1.50706	1.165814	0.99979	0.169165
10	0.819603	0.748015	0.676586	0.605316	0.533409	-1.43018	1.105638	0.999998	0.159798
12	0.744493	0.678013	0.615437	0.556766	0.482477	-1.29056	1.002605	0.99863	0.149343
14	0.660492	0.602644	0.545573	0.489281	0.429877	-1.14918	0.890328	0.999931	0.130417
16	0.601128	0.54941	0.497513	0.445439	0.394077	-1.03615	0.808358	0.999996	0.123473
20	0.473845	0.434011	0.395244	0.357546	0.315576	-0.78601	0.631047	0.999723	0.112393
24	0.401975	0.368787	0.337361	0.307698	0.270986	-0.64613	0.531202	0.998896	0.105468
28	0.360678	0.332058	0.304331	0.277496	0.247093	-0.56346	0.47337	0.999624	0.102614
32	0.327924	0.301639	0.277416	0.255255	0.224845	-0.50509	0.428941	0.997508	0.096829
36	0.305898	0.281582	0.258412	0.236388	0.20978	-0.47486	0.40087	0.999128	0.088512
40	0.288351	0.265095	0.244354	0.226128	0.197842	-0.43997	0.376344	0.995134	0.087184
44	0.279439	0.256551	0.235321	0.21575	0.189544	-0.44118	0.367676	0.997886	0.077231
48	0.264928	0.243112	0.223439	0.205909	0.179809	-0.41488	0.347904	0.996023	0.074882
56	0.249304	0.227468	0.207353	0.188961	0.163681	-0.4195	0.333204	0.997482	0.056213
64	0.226852	0.207537	0.189384	0.172393	0.150753	-0.37468	0.301789	0.99856	0.0546
72	0.208446	0.190713	0.173879	0.157944	0.138414	-0.34567	0.277579	0.998988	0.049492
80	0.190943	0.174814	0.1591	0.143802	0.126842	-0.31843	0.254628	0.999745	0.044461
88	0.176539	0.161955	0.147626	0.133554	0.118459	-0.28912	0.234363	0.999883	0.043696
96	0.163662	0.150135	0.13673	0.123447	0.109676	-0.26932	0.217526	0.999969	0.039878
104	0.151243	0.139195	0.127057	0.114828	0.102961	-0.24186	0.199616	0.999979	0.040293
112	0.143577	0.131923	0.120532	0.109403	0.097225	-0.23045	0.189667	0.999806	0.037836
120	0.136567	0.125505	0.114308	0.102977	0.092184	-0.22258	0.181083	0.999945	0.034329
128	0.127532	0.117529	0.107514	0.097488	0.087509	-0.20018	0.167568	0.999999	0.035821
136	0.123179	0.113368	0.103697	0.094165	0.084076	-0.19482	0.162142	0.999923	0.033877
144	0.119225	0.109829	0.10037	0.090849	0.081577	-0.18855	0.156936	0.999984	0.032796
152	0.112926	0.104492	0.095122	0.084816	0.078254	-0.17804	0.148534	0.995883	0.031332
160	0.109777	0.101293	0.092909	0.084625	0.075942	-0.16867	0.143511	0.999947	0.032615
168	0.106589	0.09854	0.090422	0.082235	0.074323	-0.16168	0.138925	0.999973	0.032698
176	0.102586	0.094929	0.087227	0.079481	0.071913	-0.15359	0.133303	0.999987	0.032458
184	0.1005	0.092958	0.085445	0.077962	0.070361	-0.15055	0.13061	0.999994	0.031757
192	0.099063	0.091538	0.083905	0.076163	0.068857	-0.15157	0.129377	0.999923	0.029745
200	0.095066	0.088041	0.081046	0.074082	0.066997	-0.1402	0.123105	0.999993	0.031124
208	0.093174	0.086131	0.079066	0.071977	0.06498	-0.14109	0.121392	0.999996	0.0287
216	0.092699	0.085737	0.078741	0.071714	0.064816	-0.13958	0.120615	0.999992	0.02894
224	0.089232	0.082646	0.075998	0.069288	0.062826	-0.13234	0.1157	0.999967	0.028847
232	0.087507	0.081028	0.074531	0.068014	0.061573	-0.12977	0.11346	0.999997	0.028297
240	0.08748	0.080868	0.074271	0.06769	0.061047	-0.13209	0.113898	0.999998	0.027131
248	0.084362	0.078204	0.071988	0.065712	0.059672	-0.12374	0.109111	0.999966	0.027946

256	0.084012	0.077341	0.071039	0.065106	0.057697	-0.12973	0.109958	0.998789	0.024644
264	0.083675	0.077474	0.071197	0.064843	0.058795	-0.12478	0.108631	0.999943	0.026716
272	0.081283	0.075501	0.069507	0.063301	0.057943	-0.11776	0.104835	0.999513	0.027645
280	0.080156	0.07436	0.068528	0.062659	0.056937	-0.11628	0.103411	0.999985	0.027187
288	0.080031	0.074203	0.068332	0.062417	0.056678	-0.11698	0.103427	0.999979	0.02671
296	0.077527	0.072003	0.066321	0.060482	0.055271	-0.11206	0.09994	0.999705	0.026492
304	0.075892	0.070426	0.064989	0.059578	0.054058	-0.10903	0.097698	0.99999	0.026261
312	0.077185	0.071621	0.066002	0.06033	0.054874	-0.11182	0.099549	0.999965	0.026251
320	0.073984	0.068831	0.063581	0.058234	0.053274	-0.10403	0.094791	0.999871	0.026707
328	0.073181	0.067995	0.062789	0.057563	0.052416	-0.10392	0.093965	0.999995	0.025918
336	0.074667	0.069312	0.063889	0.058398	0.05318	-0.10778	0.096222	0.99994	0.02559
344	0.070761	0.065835	0.061401	0.057457	0.05155	-0.0936	0.089481	0.9959	0.028435
352	0.069115	0.064466	0.059898	0.055412	0.0506	-0.09217	0.087548	0.999882	0.027409
360	0.072484	0.067162	0.061817	0.056449	0.051172	-0.10667	0.093818	0.999993	0.023839
368	0.068905	0.064301	0.059725	0.055177	0.050517	-0.0918	0.087266	0.999986	0.027368
376	0.068359	0.063709	0.059097	0.054522	0.049798	-0.09262	0.086882	0.999976	0.026394
384	0.070447	0.065409	0.060492	0.055697	0.050416	-0.09955	0.090357	0.999777	0.02519
392	0.067405	0.062815	0.05829	0.053831	0.049109	-0.09115	0.085635	0.999922	0.026111
400	0.066543	0.062095	0.057676	0.053287	0.04878	-0.08867	0.084277	0.999983	0.026422
408	0.069018	0.064192	0.059355	0.054506	0.049702	-0.09663	0.088345	0.999998	0.025118
416	0.065878	0.061502	0.057041	0.052493	0.048289	-0.08837	0.083552	0.999859	0.025869
424	0.065204	0.060824	0.056516	0.05228	0.047754	-0.08689	0.082582	0.999895	0.02589
432	0.06736	0.062663	0.058013	0.053409	0.04862	-0.09346	0.086053	0.999963	0.02493

XII. P.C. CLINKER - HIGH ALKALI PORTLAND CEMENT SYSTEMS

Cement : High alkali portland cement .
Units : (i). Electrical conductivity: ohm-1 m-1; (ii). Excess interfacial conductance: ohm-1
Temperature : 20°C ; W/C=0.50
Aggregate size : r=0.199 mm.

Time	*Volumetric Fraction of Aggregate*					k	b	Irl	θ
(hrs.)	*0.2*	*0.25*	*0.3*	*0.35*	*0.4*				(x10 -4)
0.25	1.515439	1.386567	1.230026	1.045816	0.972281	-2.85414	2.086267	0.986194	0.124786
1	1.360963	1.268675	1.171201	1.068541	0.986624	-1.89763	1.740489	0.998882	0.323275
2	1.359755	1.271309	1.180395	1.087012	1.003504	-1.7936	1.718475	0.999716	0.355465
3	1.369145	1.279562	1.187263	1.092246	1.008099	-1.81682	1.732908	0.999665	0.353847
4	1.375568	1.286674	1.189048	1.082688	1.01126	-1.8652	1.748609	0.996728	0.343495
5	1.349669	1.25308	1.147176	1.031956	0.953997	-2.02494	1.754657	0.996841	0.275195
6	1.256103	1.166827	1.072019	0.97168	0.893467	-1.84084	1.62427	0.998648	0.269991
7	1.209167	1.129423	1.045655	0.957863	0.886167	-1.63512	1.53619	0.999093	0.303356
8	1.114892	1.035606	0.963653	0.899033	0.805081	-1.51239	1.41737	0.996492	0.278195
9	1.099564	1.013213	0.936449	0.869271	0.763746	-1.63116	1.425796	0.994858	0.230084
10	1.008748	0.937745	0.868893	0.802189	0.726888	-1.39855	1.288458	0.999646	0.242142
12	0.888683	0.82463	0.765714	0.711933	0.637608	-1.22969	1.134621	0.997393	0.214082
14	0.794687	0.742846	0.69455	0.649801	0.590867	-1.00137	0.99496	0.998124	0.22262
16	0.715532	0.672172	0.630954	0.591879	0.544234	-0.84577	0.884687	0.999039	0.218169
20	0.609273	0.563895	0.522501	0.485091	0.431744	-0.86773	0.782819	0.996852	0.138947
24	0.467911	0.439257	0.413542	0.390768	0.356233	-0.54369	0.57665	0.995643	0.145649
28	0.415292	0.381057	0.351408	0.326343	0.282939	-0.63884	0.54306	0.992363	0.079673
32	0.360878	0.329917	0.300713	0.273266	0.238792	-0.60165	0.481207	0.998724	0.054474
36	0.324944	0.295588	0.265992	0.236158	0.207279	-0.58952	0.442849	0.999975	0.033887
40	0.298923	0.270021	0.240511	0.210395	0.182706	-0.58412	0.415747	0.999838	0.017908
44	0.282247	0.253637	0.22344	0.191657	0.16622	-0.58806	0.39986	0.99891	0.005315
48	0.258853	0.231318	0.203096	0.174188	0.148026	-0.55757	0.370366	0.999773	-0.00091
52	0.246356	0.219588	0.190757	0.159863	0.137221	-0.55599	0.357553	0.997942	-0.00891
56	0.235181	0.209199	0.180714	0.149726	0.128752	-0.54466	0.344113	0.996846	-0.01292
60	0.224194	0.199247	0.171576	0.14118	0.121682	-0.52618	0.32943	0.996003	-0.01452
64	0.212915	0.189103	0.162448	0.13295	0.114824	-0.50467	0.313849	0.995274	-0.01537
68	0.201874	0.179428	0.154466	0.126988	0.109575	-0.47407	0.296689	0.995801	-0.01317
72	0.190431	0.16947	0.14531	0.117953	0.103388	-0.45121	0.280672	0.992548	-0.01369
76	0.179687	0.159071	0.137215	0.114118	0.095983	-0.42472	0.264631	0.998723	-0.01259
80	0.178661	0.15794	0.134704	0.108953	0.093263	-0.43957	0.266574	0.995125	-0.018
84	0.174628	0.154109	0.13116	0.105781	0.090122	-0.43468	0.261564	0.995345	-0.01919
88	0.174062	0.153494	0.129172	0.101096	0.088036	-0.4489	0.263841	0.989673	-0.02409
92	0.173743	0.152775	0.127806	0.098835	0.085872	-0.45936	0.265615	0.988806	-0.02763
96	0.173669	0.15249	0.127336	0.098209	0.084978	-0.46333	0.266334	0.989144	-0.02893
100	0.174294	0.152401	0.125848	0.094634	0.082062	-0.48446	0.271187	0.986402	-0.03522
104	0.169417	0.148171	0.121732	0.090099	0.079241	-0.47685	0.264786	0.982666	-0.03612
108	0.168615	0.147145	0.120508	0.088703	0.077568	-0.48108	0.26483	0.98313	-0.038
112	0.164561	0.1438	0.118341	0.088184	0.076819	-0.4622	0.257002	0.984855	-0.03477
116	0.164415	0.142985	0.1171	0.08676	0.074239	-0.47315	0.259046	0.986963	-0.03835
120	0.161214	0.140228	0.114831	0.085022	0.072859	-0.46383	0.253981	0.986702	-0.03756
124	0.155133	0.135162	0.110352	0.080701	0.070411	-0.44781	0.244695	0.982924	-0.03662
128	0.152648	0.133116	0.108628	0.079184	0.069563	-0.44021	0.24069	0.981516	-0.03589
132	0.149745	0.130497	0.106978	0.07919	0.068483	-0.42766	0.235277	0.985371	-0.03388
136	0.14325	0.125108	0.103084	0.07718	0.0668	-0.40166	0.223582	0.986282	-0.03005
140	0.137441	0.120107	0.099968	0.077021	0.0653	-0.37474	0.212388	0.991693	-0.02546
144	0.135882	0.118098	0.09946	0.07997	0.063892	-0.36422	0.208726	0.999178	-0.02318

148	0.131399	0.115096	0.09438	0.069251	0.061775	-0.37019	0.205436	0.97934	-0.02812
152	0.130136	0.114098	0.093078	0.067073	0.061003	-0.37058	0.204252	0.973931	-0.02911
156	0.128439	0.112003	0.093046	0.071568	0.060175	-0.35392	0.199224	0.992474	-0.02497
160	0.126752	0.110992	0.092319	0.070733	0.060801	-0.34432	0.195616	0.98943	-0.02307
164	0.127152	0.110964	0.091853	0.069817	0.059477	-0.35299	0.197751	0.989863	-0.02555
168	0.124923	0.108157	0.089799	0.06985	0.056267	-0.35123	0.195169	0.996933	-0.02651

XIII. SILICA FUME - SATURATED Ca(OH)2 SOLUTION SYSTEMS

Unit : ohm-1 m-1.
Temperature : 18°C .

Time	*Initial volumetric fraction of silica fume*				
(hrs.)	*0.152*	*0.175*	*0.205*	*0.249*	*0.317*
0.5	0.505096	0.315071	0.265669	0.275453	0.302318
1	0.463861	0.27904	0.2523	0.274495	0.298575
2	0.426027	0.244418	0.240505	0.273695	0.295327
3	0.39028	0.227919	0.238	0.271504	0.296449
4	0.355131	0.214263	0.23438	0.268046	0.291937
5	0.319904	0.208002	0.232186	0.269166	0.293292
6	0.291154	0.204559	0.2283	0.265214	0.293885
7	0.263049	0.201231	0.228582	0.263555	0.284439
8	0.244003	0.199027	0.23182	0.26205	0.285992
9	0.225758	0.194665	0.227899	0.257588	0.286725
10	0.214819	0.194689	0.230847	0.260352	0.287758
12	0.196815	0.19155	0.227264	0.256163	0.283702
14	0.186125	0.189511	0.21881	0.256871	0.283788
16	0.179894	0.189443	0.224988	0.257784	0.281095
18	0.173513	0.18855	0.219376	0.256877	0.281209
20	0.171987	0.185449	0.216226	0.252513	0.281632
22	0.16901	0.184691	0.214874	0.251551	0.28232
24	0.167617	0.185461	0.216815	0.249085	0.280781
28	0.16404	0.184316	0.211123	0.246746	0.277693
32	0.162544	0.182313	0.211305	0.242615	0.271796
36	0.161043	0.180758	0.208686	0.244917	0.270041
40	0.162805	0.181201	0.209037	0.24243	0.272306
44	0.160133	0.180992	0.204622	0.239363	0.270881
48	0.158695	0.181492	0.200653	0.238143	0.271416
52	0.155262	0.179737	0.198958	0.236445	0.268332
56	0.153188	0.178127	0.198567	0.233767	0.26858
60	0.153919	0.180379	0.198794	0.232914	0.263069
64	0.157986	0.180382	0.198672	0.234723	0.263552
68	0.155399	0.182847	0.195957	0.236219	0.268487
72	0.154443	0.180963	0.193592	0.232907	0.264638
76	0.151985	0.179558	0.191779	0.233828	0.261598
80	0.15004	0.179717	0.188719	0.227958	0.263578
84	0.151468	0.179624	0.191021	0.229099	0.260605
88	0.151399	0.179513	0.191228	0.229542	0.264513
92	0.152478	0.17946	0.192368	0.232252	0.262537
96	0.153464	0.182486	0.189018	0.236158	0.268244
100	0.150702	0.180608	0.184272	0.232153	0.262663
104	0.149894	0.182084	0.186374	0.232093	0.259118
108	0.151359	0.182586	0.187771	0.230945	0.260441
112	0.150979	0.182449	0.187681	0.233664	0.263069

116	0.151808	0.185186	0.188851	0.238138	0.26037
120	0.153821	0.18623	0.186978	0.239175	0.265598
124	0.15009	0.182705	0.180452	0.23571	0.262089
128	0.151066	0.183303	0.184121	0.233406	0.258679
132	0.152322	0.184187	0.184628	0.236349	0.262556
136	0.151992	0.188338	0.183616	0.234676	0.260706
140	0.151682	0.186813	0.18104	0.237228	0.262186
144	0.150714	0.185341	0.17918	0.231749	0.258886
148	0.15052	0.183023	0.17627	0.227537	0.257032
152	0.149113	0.184695	0.17566	0.226598	0.257482
156	0.149611	0.185517	0.174288	0.228695	0.256016
160	0.150924	0.186693	0.175637	0.229911	0.258386
164	0.149017	0.184747	0.17533	0.228281	0.255184
168	0.149216	0.185896	0.174769	0.226647	0.256672

APPENDIX B

SULPHATE EXPANSION DATA

I. SF COATED AND UNCOATED AGGREGATE - PORTLAND CEMENT SYSTEMS

Cement : White portland cement.
Aggregate : Quartz sand, r=0.561 mm.
W/C=0.50 , and aggregate/cement ratio = 1.44 (volumetric fraction of aggregate : 0.40).
Designing thickness of SF layer on aggregate surface: 10 um.
Temperature : room temperature (around 20°C).
All the specimen were cured in water for 28 days at 20°C before corrosion.

Corrosion time (days)	EXPANSION (%) in 5% sodium sulphate solution		EXPANSION (%) in 10% sodium sulphate solution	
	Uncoated	Coated	Uncoated	Coated
0	0	0	0	0
2	2.43E-06	0	0.038994	0
4	0.015601	0	0.062393	0
8	0.046797	0.007899	0.054595	0
11	0.085791	0.007899	0.085789	0.007904
14	0.109187	0.007899	0.116985	0.007904
17	0.22617	0.063196	0.187178	0.021128
21	0.452343	0.078995	0.335365	0.102741
25	1.34924	0.189587	0.701936	0.308207
30		0.48976		

II. EFFECTS OF IONIC CONCENTRATION AND TEMPERATURE ON SULPHATE EXPANSION

Cement : White portland cement.
Aggregate : Quartz sand, r=0.561 mm.
W/C=0.50 , and aggregate/cement ratio = 2.
Steam-curing for 8 days at 20°C before immersion in 5% Na2SO4 solution.
All the specimen were removed from Na2SO4 solution at 18 days corrosion and placed in CH, NH, BH solutions and H2O.
CH - Calcium Hydroxide Solution ; NH - Sodium Hydroxide Solution;
BH - Barium Hydroxide Solution.

Corrosion time (days)	CH	NH	BH	H2O
0	0	0	0	0
3	0.0477	0.04271	0.04234	0.0367
5	0.0795	0.08542	0.08996	0.07339
7	0.09539	0.10682	0.11641	0.08388
11	0.18551	0.19753	0.21166	0.17301
14	0.25441	0.24022	0.26458	0.22029
18	0.51412	0.54469	0.58737	0.44072
20	0.65723	0.52331	0.69313	0.46696
21	0.72613	0.52331	0.85711	0.5876
24	0.76858	0.48589	1.20638	0.72407
28	0.98064	0.52328	1.64036	0.84467
31	1.07075	0.50725	1.88382	0.95476
41	1.33581	0.53924	2.11151	1.36408

	Temperature (°C)		
4	23	38	64
0	0	0	0
0.01567	0.03166	0.0452	0.07832
0.0235	0.05538	0.0795	0.11747
0.03133	0.0712	0.1054	0.15666
0.047	0.11866	0.1943	0.31334
0.05483	0.21359	0.4112	0.611
0.08617	0.47465	1.0541	1.7151

III. SF ADDITION TO CEMENT PASTE ON SULPHATE EXPANSION

Cement : White portland cement.
Aggregate : Quartz sand, r=0.561 mm.
Aggregate/cement ratio = 1.44 (volumetric fraction of aggregate : 0.40).
Amount of SF : 7% by cement weight.
Temperature : room temperature (around 20°C).
The specimen were cured in water for 28 days at 20°C before corrosion.
5% Sodium sulphate solution.

Corrosion time (days)	EXPANSION OF MORTAR BAR (%) w/c=0.50 without SF	w/c=0.55 with 7% SF
0	0	0
2	2.43E-06	0
4	0.015601	0.00765
8	0.046797	0.023575
11	0.085791	0.03929
14	0.109187	0.00786
17	0.22617	0.047144
21	0.452343	0.062858
25	1.34924	0.04715
30		0.110009
36		0.133584